AMINE FUNCTIONALIZED MCM-41 FOR CO_2 CAPTURE

A Thesis

Submitted in Partial Fulfillment of the Requirements for the Degree of

DOCTOR OF PHILOSOPHY

by

L.Sravanthi

DEPARTMENT OF CHEMICAL ENGINEERING

INDIAN INSTITUTE OF TECHNOLOGY GUWAHATI

ASSAM, INDIA-781039

SEPTEMBER 2014

Dedication

To
My Grand Parents,
My Parents,
My Teachers
&
The Almighty

Department of Chemical Engineering
Indian Institute of Technology Guwahati
Guwahati 781039 (INDIA)

CERTIFICATE

It is certified that the work described in this thesis entitled ***"Amine Functionalized MCM-41 for CO_2 Capture"*** by **L.Sravanthi** for the award of degree of ***Doctor of Philosophy*** is an authentic record of the results obtained from the research work carried out under my supervision in the Department of Chemical Engineering, Indian Institute of Technology Guwahati, India. This work has not been submitted elsewhere for the award of any degree.

(Dr. Aloke Kumar Ghoshal)
Professor
Department of Chemical Engineering
Indian Institute of Technology Guwahati
Assam 781039

ACKNOWLEDGEMENTS

First of all, I would like to express my sincere thanks to my thesis supervisor, Professor. Aloke Kumar Ghoshal, for providing me an opportunity to work under his guidance. I am extremely grateful to Prof. Ghoshal for his support, freedom and encouragement throughout my doctoral work. Sir has always made available himself for discussions besides his busy schedules. Through his actions, he has shown me how research should be carried out and trained me to live as a professional researcher. It has been a great privilege working under his guidance and learn from his research expertise. Thank you sir, for all your help, advices and support.

I sincerely thank my doctoral committee members, for being kind enough to extend their help at various phases of my research work. I am thankful to my committee members, Dr. Sasidhar Gumma, Prof. Bishnupada Mandal and Dr. Pranab Kumar Ghosh for their suggestions and advices during my review seminars. I thank, Dr. Sasidhar, for his willingness to lend his help in rectifying the problems I faced during adsorption measurements, whenever I approached him. I am thankful to Professor. Bishnupada Mandal for being very kind and allowing me to avail the research facilities in his laboratory. I am thankful to Dr. G. Pugazhenthi, Prof. Prabir Kumar Saha, Prof. Pallab Ghosh, Dr. Mahuya De, Dr. Nanda Kishore and all other faculty members for their advices and help during my doctoral work.

Special thanks to my dear brother and co-author, Mayur Tikmani for his concern and consistent enquiries about the progress of my work. Our work together has once again made me to realise the importance of collaborative research and the power of minds united in amicable relationship is immense. Thank you Mayur, for your patience in clearing my doubts, concern and good wishes. I would gratefully acknowledge two of my co-authors, Aakansha Mishra and Satyannarayana Edubilli for their kind help for completion of my doctoral work. I would never forget the sincere help rendered by Satya at the beginning stage of my doctoral work. Thanks a lot Satya, for helping me despite your illness. I am

thankful to all my co-research fellows Manna, Sanjib, Kamal, Rupak, Kishant, Abhik, Prashant, Prudhvi, Sahu, Ashim, Samarpita, Abhjit, Sonauk, Vinoth, Atanu, Patrali, Pradip, Mudit, Nitun, Venu and Manish Kumar Sinha for their help in several forms during my doctoral work. I am indebted to my institute for providing me with analytical facilities for characterization of materials, funding for my work, hostel facilities, scholarship and access to avail learning resources. I am also thankful to all the technical staffs Mr. Harsha, Mr. Kaustav, Ms. Ritumoni, Mr. Lukumoni, Mr. Prasun, Mr. Debojit .... and non-technical staffs Mr. Kalyan, Mr. Bhagya Bora ... of my department. I am thankful to Mr. Animes Roy for delivering the chemicals, glass wares and other accessories ordered, on time. I am also grateful to Ms. Champa Chakradhour, for her assistance in house-hold works for the past two years, through which I could manage both family and research. Thank you Champa, for showering your affection and care for me as well as your Ravi bhaiya. We miss you.

I will forever be thankful to my school teacher Ms. Parimala and her family members. I still fondly think of the days she carried me to school in her bi-cycle. Herself and my aunt, Ms.Shantha Kumari had put forth constructive efforts to develop my academic skills. I take this opportunity to express my gratefulness to all my school, under-graduate and post-graduate teachers as well as friends and well-wishers for extending their support and help at every important walk of my life. Thank you all and I am always indebted to you for all the good deeds you have done for me.

Blessed to have wonderful grandparents, parents, siblings, in-laws and husband. Words cannot describe the limits of appreciation for our relationship. My grandfather, Mr. Ramakrishna Reddy has been the impetus for me to learn the prominence of hard work. My grandmother Mrs. Janaki Reddy, a person with positive disposition always remains as an example for me to follow for her discipline and courage. My Mother Mrs. Sujana Loganathan, a great role model of strength and character, has taught me always to strive hard for my personal best and I am proud to be her daughter. Happy to have wonderful sisters Ms. Sandhiya and Indhu providing me immense support at all the up's and down's

of my life. Great to have wonderful in-laws, Mr & Mrs. Gnananandam, showering unconditional love and supporting me with every possible way to see the completion of my doctoral work. My husband Ravi has been the reason for what I am today and central part for completion of this long dissertation journey. The days we worked together for both of our doctoral degree at IIT Guwahati in the past four years are always memorable. It's painful; I deeply miss my beloved father Mr. Loganathan and my son, who are not with me today to share this joy. I believe my dad's advices, blessings, complete love and his presence in my surname drive me with positive energy always to move forward in life. I do miss my dearest companions namely Rubotherm magnetic suspension balance, surface area analyzer, thermo gravimetric analyzer…… my research lab, this green campus and every precious thing I used for my doctoral work hereafter.

Above all, I owe it all to the Almighty "Lord Shri Ram" for granting me with wisdom, courage, health, and being all in all to undertake this research task and enabling me to its completion.

Sravanthi Loganathan

ABSTRACT

The doctoral work mainly focuses on developing novel MCM-41 that will allow enhanced amine loading and demonstrate effective CO_2 capture characteristics. At first, the influence of controlled addition of aqueous ammonia on the structural properties of MCM-41 has been investigated. It was found that pH of the reaction mixture played key role in affecting the pore size of MCM-41. The synthesis of MCM-41 under mild alkaline pH condition (~7.75) resulted in a mesoporous material with pore size of ~30 nm and pore volume of ~2.5 cc/g in comparison to conventional MCM-41 which contains pore size of ~3 nm and pore volume of ~1 cc/g. The CO_2 adsorption measurements were carried out on conventional MCM-41 (MCM-41-3) and MCM-41 with enlarged pore size (MCM-41-30) at four different temperatures (30, 45, 60 and 75 °C) and pressure conditions ranging from 0-25 bar. The outcome of the study indicated that the adsorption capacities of both the samples ranging from low pressures to 5 bar are similar to each other. However, little lower adsorption capacity is exhibited by MCM-41-3 than MCM-41-30 starting from 10 bar pressure. It has been inferred that the significant difference was reflected, owing to the fact that sample MCM-41-30 possessed enlarged pore size and higher pore volume.

In order to investigate the influence of pore size and pore volume on the amine tethering, two different MCM-41 supports discussed above are selected. Mono amine tethering on the MCM-41-3 as well as MCM-41-30 was carried out under dry conditions to screen the best support. MCM-41-30 series exhibited a higher CO_2 adsorption capacity than MCM-41-3, irrespective of the amount of monoamino silane added. In case of MCM-41-3 series, CO_2 adsorption capacity, amine loading, amine efficiency decreased with respect to amount of amino silane added in the reaction mixture. These results revealed the importance of selecting mesoporous supports with enlarged pore size and pore volume for amino silane tethering. MCM-41-30 series exhibited a

maximum CO_2 adsorption capacity, amine loading, amine efficiency for 9 mmol of amino silane (both mono and tri) addition in the reaction mixture. Further increase in amine concentration affected grafting efficiency and hence amine loading as well as CO_2 adsorption capacity exhibited downturn. In order to increase the amine loading and further enhance the CO_2 uptake in the important low pressure regime (0.1-0.2 bar), wet grafting process was followed for amino silane tethering on MCM-41-30 support. Based on the dry grafting experiments, the optimum amount of amino silane that can be grafted per gram of support was determined as 9 mmol for both the amino compounds. Further, the effect of addition of water for optimization of the adsorbent composition and influence of temperature for optimizing efficient synthesis conditions for tethering of mono and tri amino silane compounds were investigated. Addition of water in the reaction mixture showed profound impact on the CO_2 adsorption characteristics of mono and tri amine tethered MCM-41-30 samples. The adsorbents exhibited a maximum adsorption capacity of ~1.2 and ~2.1 mmol/g (75 °C, 0.2 bar) respectively, which indicated that MCM-41-30 support developed herein, served as a promising support for amine tethering application and demonstrated effective CO_2 capture characteristics .

Key Words

CO_2 capture, MCM-41, Amino silane, Adsorption capacity, Grafting, Mesoporous silica.

CONTENTS

LIST OF ABBREVIATIONS

AF-PE-MCM-41	Amine functionalized pore-expanded MCM-41
BET	Brunauer, Emmet and Teller
BJH	Barret, Joyner and Halenda
Btu	British thermal units
C	Calcined
COP	Conference of the parties
CUMs	Co-ordinatively unsaturated metal sites
CS	Concentration swing
DEA	Diethanol amine
DLS	Dynamic light scattering
DMDA	Dimethyl decyl amine
DOE	Department of Energy
DP	N-[3-(trimethoxysilyl) propyl] ethylenediamine
DRIFTS	Diffuse reflectance infrared Fourier transform spectroscopy
EDX	Energy-dispersive X-ray
EU	European union
FESEM	Field emission scanning electron microscopy
FTIR	Fourier transform infrared
HAS	Hyperbranched amino silica
HMS	Hexagonal mesoporous silica
IEO	International energy outlook
INR	Indian Rupees
IUPAC	International union of pure and applied chemistry
MEA	Monoethanol amine
MOFs	Metal organic frameworks
MSB	Magnetic suspension balance

NASA	National aeronautics and space administration
NETL	National energy thermal laboratory
NOAA	National oceanic and atmospheric administration
OECD	Organization for economic cooperation and development
OMMs	Ordered mesoporous materials
PEI	Polyethylene imine
PE-MCM-41	Pore-expanded MCM-41
ppm	Parts per million
PS	Pressure swing
SEM	Scanning electron microscopy
TEOS	Tetraethyl ortho silicate
TEPA	Tetraethylene pentamine
TGA	Thermogravimetric analysis
TP	N-[3-(trimethoxysilyl) propyl] ethylenetriamine
TVS	Temperature vacuum swing
UC	Uncalcined
UNFCCC	United nations framework convention on climate change
USD	US Dollars
VS	Vacuum swing
XRD	X-ray diffraction

LIST OF NOMENCLATURE

a	Unit cell parameter (nm)
b	Affinity constant (bar^{-1})
c	Pore geometry constant
d	Mesopore diameter (nm)
d_{100}	Interplanar spacing (nm)
D_c/r_P^2	Diffusion time constant (s^{-1})
k_{id}	Intraparticle diffusion rate constant (mmol/g. $s^{0.5}$)
k_f	First order rate constant (s^{-1})
k_s	Second order rate constant (g/mmol. s)
n	Measure of surface heterogeneity in Sips model
N	Number of data points
n_s	Maximum adsorption capacity in Toth model (mmol/g)
P	Pressure (bar)
q_e	Equilibrium adsorption capacity (mmol/g)
q_m	Maximum adsorption capacity (mmol/g)
q_t	Adsorption capacity at time "t" (mmol/g)
R	Universal gas constant (J/mol. K)
R^2	Regression co-efficient
t	Measure of surface heterogeneity in Toth model
T	Temperature (°C)
V_p	Mesopore volume (cc/g)
W	Pore wall thickness (nm)

LIST OF GREEK LETTERS

θ	Theta (degree)
ρ_s	Pore wall density (g/cc)

LIST OF FIGURES

LIST OF TABLES

CHAPTER 1

INTRODUCTION

The chapter provides a brief outline on World's energy consumption spectrum and its impact on the global warming issue. An overview of absorption and adsorption technologies for post-combustion CO_2 capture from coal-fired power plants is discussed. The advantages of adsorption over other absorption and subsequently the importance of amine tethered mesoporous silica adsorbents for CO_2 capture is discussed. Thereafter, the chapter presents the outline of objectives of the doctoral work followed by organization of the thesis.

1.1. Introduction

In the recent years, World's energy consumption has been increasing at a rapid rate due to economic development and population growth. The International Energy Outlook report released in July 2013 (IEO2013) projects that there will be 56% rise in the world energy consumption by 2040 **[1]**. It has been projected that total world energy use rises from 524 quadrillion British thermal units (Btu) in 2010 to 630 quadrillion Btu in 2020 and to 820 quadrillion Btu in 2040, which corresponds to an increase of 16% and 36% respectively (Figure 1.1). It has been predicted that much of the growth in energy consumption may occur in countries that are not included in Organization for Economic Cooperation and Development (OECD) **[1]**. At present, there prevails huge variation in the economic performance of various countries world-wide. For OECD countries, the pace of economic growth varies but is relatively slow when compared to emerging economies like non-OECD nations. This is because, the demand for energy consumption in non-OECD nations are driven by strong as well as long-term economic growth. Therefore, energy consumption in non-OECD countries is predicted to rise by 90 percent, whereas, the increase is only 17% for OECD nations **[1]**.

The significant increase in the energy consuming spectrum for non-OECD nations conveys the fact that world's energy resources will also be utilized effectively in order to meet the growing energy demand. At present, the energy demand for electricity generation is met by several resources such as coal, natural gas, nuclear energy, hydrothermal energy etc. (Figure 1.2). Currently, coal remains as the major source for the generation of electricity world-wide **[1]**. However, environmental impact created by carbon dioxide (CO_2) emissions due to burning of coal has driven government policies in favor of renewable energy resources for electricity generation. Efforts of replacing conventional carbon-based resources with renewable energy for electricity generation will only be implemented over time and still, it would be unrealistic to envision a future world without burning coal. Indeed,

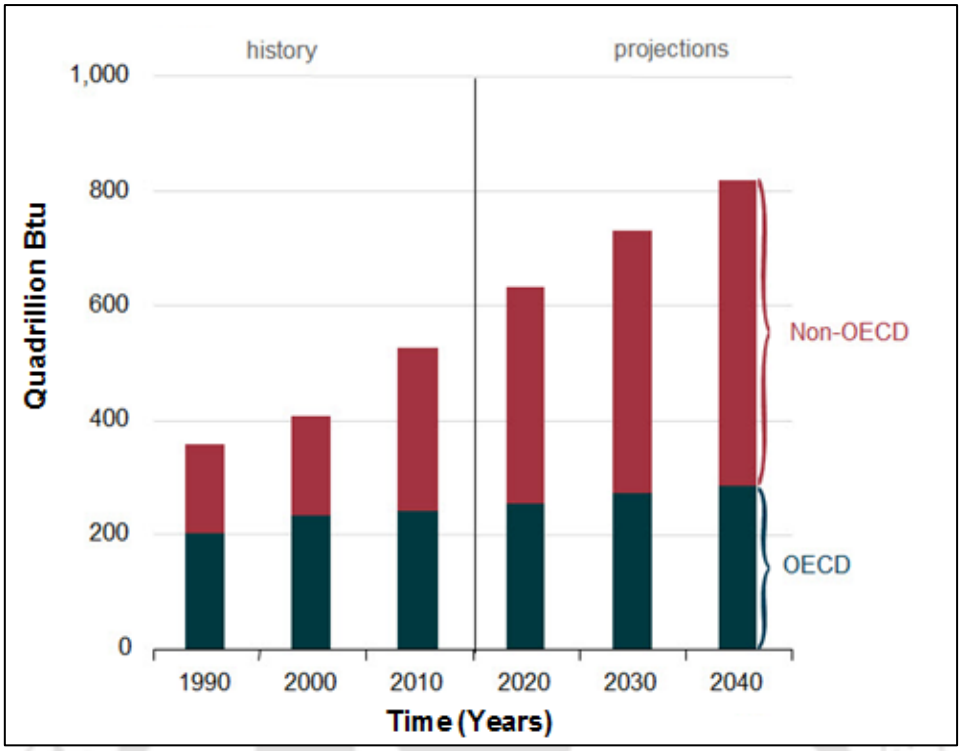

Figure 1.1. History and projections for world's energy consumption **[1]**

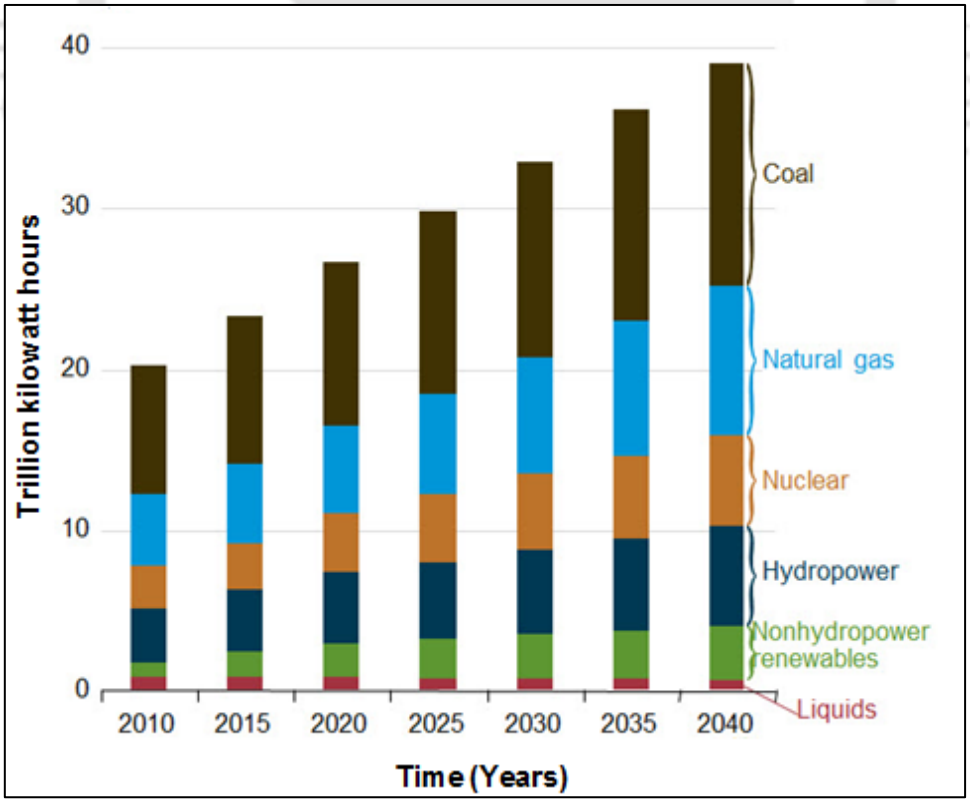

Figure 1.2. Contribution of various sources towards global electricity generation **[1]**

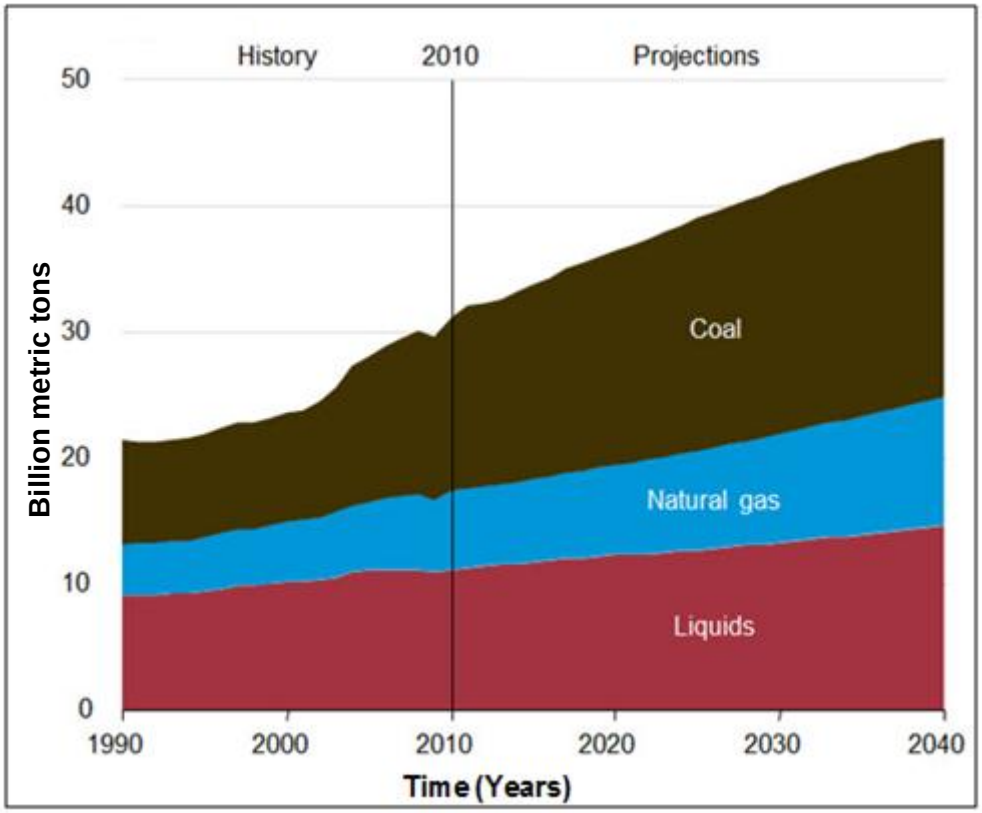

Figure 1.3. Global CO_2 emissions by various energy resources **[1]**

World's coal consumption is set to rise even if the sources of energy are diversified (Figure 1.2). The global CO_2 emissions by different energy resources are presented in Figure 1.3. It can be noticed from Figure 1.3. that World's energy related CO_2 emissions tend to rise by 45.5 billion metric tons in 2040 out of which coal contributes a major share. With continued economic growth, heavy reliance on coal for global electricity generation is expected in future. This underlines the fact that, as along as coal consumption is inevitable for power generation, CO_2 emission could not be avoided as well.

In order to adequately address the global warming crisis, nations worldwide already took initiation to create and enforce policies for urgent reduction in greenhouse gas emissions. As a part of this, governments agreed at the United Nations Framework Convention on Climate Change (UNFCCC) Conference of the Parties in Cancun, Mexico in 2010 (COP-16) that the average global temperature increase, compared with pre-industrial levels, must be

held below 2 °C, by reducing the greenhouse gas emissions **[2, 3]**. In addition to this, a deadline was set at COP-18 in Doha, Qatar in 2012 for agreeing and enacting a new global climate agreement to come into effect in 2020 **[2, 3]**. There is broad international acceptance that stabilizing the atmospheric concentration of carbon dioxide (CO_2) at below 450 parts per million (ppm) is a near 50% chance of achieving the 2 °C target, so that worst impacts of climate change could be avoided. However, the 450 ppm threshold is drawing ever closer, as the global greenhouse gas emissions already started to rise at a rapid pace. The CO_2 levels in the atmosphere reached 400 ppm in May 2013, having jumped by 2.7 ppm in 2012 with the five top emitters being China (29%), the United States (16%), the European Union (EU27) (11%), India (6%), and the Russian Federation (5%) **[4]**. This jump is considered as the second highest rise as per the records of National Oceanic and Atmospheric Administration (NOAA) Earth System Research Laboratory **[2, 3]**. According to National Aeronautics and Space Administration (NASA) Global Land-Ocean Temperature Index, average global temperatures have already increased around 0.8 °C. Without additional action, a further increase in long-term temperature of 2.8 °C to 4.5 °C appears to be in prospect, with most of the increase occurring in this century **[2, 3]**. If global increases in CO_2 emissions continue at this rapid pace, it is anticipated that within the next two decades global CO_2 cumulative emissions will reach levels that will make it impossible to meet a critical, internationally agreed-upon target established in international climate negotiations to hold the increase in global temperature below 2 °C. Already we experience the deadly effects of climate change in the form of rising seas, wild fires, extreme weather of all kinds, and passing 400 ppm is an ominous sign of what comes next. This underlines the importance of immediate action required well before 2020, in order to keep open a realistic opportunity for an efficient and effective mitigation of global warming problem.

As discussed earlier, coal based energy sector is by far the largest anthropogenic source of greenhouse gas emissions globally, accounting for more than one-third of CO_2 emissions approximately. Unfortunately, huge change in the energy consuming spectrum cannot be

expected at least for next few decades, as coal will remain as the dominant source. As immediate halt in the CO_2 rise is impossible, capture and sequestration of CO_2 from coal-fired power plants is deemed as an appropriate solution to tackle the climatic issues driven by CO_2 emission.

1.2. An overview of absorption and adsorption

The flue gas released from coal-fired power plants typically contains 10-15% CO_2, 70-80% N_2, 3-4% O_2, 8-10% H_2O, with trace amounts of SOx, and NOx **[4]**. Two primary capture technologies proposed for CO_2 removal includes (i) absorption and (ii) adsorption.

1.2.1. Absorption

Amine absorption is the dominant technology followed worldwide in industries, towards removal of acidic gases such as CO_2. In physical absorption process, the CO_2 is basically dissolved in a liquid solvent, and involves no chemical reaction. The CO_2 molecules bind with the solvent either by van der Waal's or by electrostatic force of interaction **[5]**. The common physical absorbents used for CO_2 absorption include polyethylene glycol, dimethyl ether, N-methyl-2-pyrolidone, methanol, polyethylene glycol, and propylene carbonate **[5]**. Physical absorption process is only effective for high CO_2 partial pressure conditions.

At present, commercial operations for CO_2 capture from flue gas involves a chemical absorption process, in which monoethanol amine (MEA) is generally used as the sorbent **[6-9]**. The process is based on temperature dependent acid-base reaction, CO_2 which is acidic in nature, reacts with basic solution at temperature conditions of ~ 40-60 °C **[6-9]**. After the reaction, the solution is directed to a regeneration system, wherein, the solvent is subjected to high temperature conditions in order to liberate (desorb) the gaseous CO_2. In several industries, amine absorption processes such as UCARSOL and Flour Econamine are in practice over decades for removal of CO_2 from various gas streams **[10]**. The commercial implementation of amine absorption process suffers from severe shortcomings such as requirement of energy-intensive and expensive stripping process, low absorption-desorption

rate, absorption tower corrosion issues, enormous solvent loss, and amine degradation **[6-9]**.

At present, research efforts related to absorption are aimed at development of technological concepts for reducing the heat of regeneration or development of solvents that can be regenerated by minimal energy. Fluor's Econamine FG+ is an example of one such technological concept developed, through which reduced regeneration energy is achieved by increasing the solvent concentration **[4]**. In addition to this, the use of catalysts in order to fasten the reaction kinetics and rate of absorption is also being investigated **[4]**. As degradation of solvent used in the absorption process imparts disposal as well as replacement cost, exploration of inexpensive solvents which offer best performance still remains as a major challenge to be addressed.

1.2.2. Adsorption

In the longer term, adsorption by porous solid materials have been explored as potentially lower cost option and promising alternative to conventional amine solutions for CO_2 capture. Among numerous traits suitable for CO_2 separation, adsorption serves as an attractive method to complement or replace the current technologies, in terms of its flexibility, simplicity of its design, low energy requirement and also easy operation as well as maintenance **[11]**. However, practically suitable adsorbents for CO_2 capture from flue gas should possess the following attributes if indeed to be competitive with absorption technology.

(i) High CO_2 equilibrium capacity: Information about equilibrium adsorption capacities plays important role in evaluating the potential of any adsorbent for carbon capture applications. An adsorbent developed is expected to exhibit a minimum CO_2 adsorption capacity of ~2-4 mmol/g at conditions relevant to flue gas, if in fact to be considered as potential for the said application.

(ii) Fast kinetics: As adsorption kinetics is known to affect the working capacity in a dynamic process, an appropriate CO_2 adsorbent is also expected to possess high rate of adsorption. Similarly, fast desorption kinetics is favourable for quick completion of cycle.

(iii) High CO_2 selectivity: An ideal adsorbent for flue gas separation is expected not to show affinity to adsorb any other gas or impurities or moisture present in the feed gas in order to overcome adverse impact on the process economics.

(iv) Mild conditions for regeneration: The adsorbent should also be regenerated under mild operating conditions. Regeneration of adsorbents can be achieved through temperature swing or vacuum swing or a combination of both. However, the mode of regeneration can be chosen based on the structural and chemical properties of the adsorbent. Lower the regeneration energy, greater will be profit for trade-offs.

(v) Stability: In a practical process, adsorbent is expected to possess excellent stability when subjected to extensive adsorption-desorption cycles. As the lifespan of adsorbents decides the time required for replacement and shows profound impact in terms of economics, it is of prime importance in assessing the potential of an adsorbent.

(vi) Low cost: Apart from the scale of material required to capture CO_2, another challenge lies in the quantification of commercial-scale cost savings for imparting any change in the adsorbent properties.

The widely investigated physical sorbents include zeolites **[12-15]**, activated carbons **[16-18]**, metal organic frameworks (MOFs) **[19-25]**, and mesoporous silica **[26, 27]**. As these sorbents mainly rely on physical adsorption, inherent research activities have been focused on increasing the surface area of these materials in order to achieve enhanced adsorption capacity **[12-27]**. As certain factors such as high cost, poor accessibility to active sites located within the pore wall surface, low selectivity towards CO_2 and regeneration trouble limit their widespread applications, the researchers are still impelled to focus on novel

adsorbents in order to alleviate the high energy cost for regeneration and equipment corrosion problems that are associated with the use of amine absorption.

After the breakthrough discovery of the M41S family of mesoporous silicas, the area of ordered mesoporous materials (OMMs) underwent dramatic growth. These unique materials exhibit large surface areas, considerable surface silanol groups, narrow pore size distributions, and a variety of tunable pore systems in terms of pore sizes (typically 3-10 nm), pore volume (typically 0.5–1.5 cm^3/g) and pore connectivity **[26-28]**. These characteristics make them to serve as potential substrates for amine functionalization. Amine tethered mesoporous silica materials (called as organic-inorganic hybrid sorbents) have recently emerged as a promising class of solids that can effectively adsorb CO_2 from humid streams. Unlike amine impregnation, covalently tethering of amino silane moieties on the mesoporous silica supports overcomes amine leaching and offers high regenerability when subjected to continuous adsorption/desorption cycles **[29, 30]**. However, amine loading is affected by pore size, pore volume, surface area, the availability of accessible silanol groups, and the length of alkyl chain groups of silane compounds **[29, 30]**. For example, amine tethering on MCM-41 supports which possess pore size of only ~3-4 nm and pore volume of ~0.8-1.0 cc/g resulted in diffusion limitations, thereby limiting their practical application for CO_2 capture process **[29, 30]**. In the recent years, mesoporous supports with enlarged pore size and pore volumes have received considerable attention for the art of amine tethering process. At present, three conventional methods have been used to enlarge the pore size of mesoporous materials: (1) increasing the chain length of surfactants (n = 6-16) **[31]** or using copolymer as templates **[32]** (2) post-synthesis hydrothermal treatment **[33]** (3) the use of expanders (e.g. alkanes **[34]**, amines **[35]** and trimethylbenzene **[36]**). Recent studies revealed that the amine tethering on MCM-41 with enlarged pore diameter resulted in increased equilibrium CO_2 adsorption capacity and faster CO_2 adsorption kinetics (explained in detail in Chapter 2). In view of this, an effort has been undertaken in this doctoral work to

develop novel MCM-41 that will allow enhanced amine loading and demonstrate effective CO_2 capture characteristics.

1.3. Objectives of the present work

The objectives of the doctoral thesis are framed as follows:

- Synthesis and characterization of novel MCM-41 for amine tethering.
- Synthesis and characterization of amine-tethered MCM-41 adsorbent.
- Estimation of equilibrium adsorption capacities relevant to flue gas conditions for the synthesized adsorbents.
- Performance analysis of the synthesized adsorbents for post-combustion CO_2 capture.

1.4. Organization of thesis

The doctoral thesis is organized in nine chapters as follows:

Chapter 1: Introduction

The chapter provides a brief outline on World's energy consumption spectrum and its impact on the global warming issue. An overview of absorption and adsorption technologies for post-combustion CO_2 capture from coal-fired power plants is discussed. The advantages of adsorption over other absorption and subsequently the importance of amine tethered mesoporous silica adsorbents for CO_2 capture is discussed. Thereafter, the chapter presents the outline of objectives of the doctoral work followed by organization of the thesis.

Chapter 2: Literature Review

This chapter outlines the history of various adsorbents reported so far for carbon capture application. The adsorbents for CO_2 capture are categorized into two types based on the adsorption mechanism involved, i.e., physisorbents and chemisorbents. The merits and de-merits of zeolites, activated carbon, metal-organic frameworks, amine impregnated and amine tethered mesoporous silica adsorbents for CO_2 capture are discussed in this chapter.

Chapter 3: Synthesis and Characterization of novel MCM-41

This chapter presents the strategies used for development of novel MCM-41 support. The detailed experimental method used for synthesis of the same is discussed. Several characterization techniques used to examine the structural, thermal, morphological and CO_2 adsorption characteristics of the synthesized samples are discussed.

Chapter 4: Surface Heterogeneity for CO_2 Capture on MCM-41.

The chapter provides a new insight into details of role of surface characteristics of MCM-41 on CO_2 adsorption phenomenon. Infrared spectroscopy analysis is carried out in order to get an insight into various surface functionalities that can exist on MCM-41. Thereafter, an approach based on isotherm modelling is provided to derive the information about the various prevailing characteristics of such silica surface and quantitatively determine the individual contribution of surface groups of silica to the overall adsorption capacity. A patch-wise topography hypothesis is proposed for CO_2 adsorption on porous silica and the same is validated for N_2 adsorption. Theory for Langmuir, Sips, Toth and Langmuir dual-site models are also discussed.

Chapter 5: Mechanistic Investigation of CO_2 Adsorption Kinetics on MCM-41.

The chapter enlightens the mechanistic steps that control the diffusion of CO_2 uptake kinetics on MCM-41. The actual rate-controlling step for CO_2 uptake kinetics on MCM-41 under wide range of pressure (0.1-11 bar) and temperature conditions (30, 45, 60, 75 °C) is discussed. Kinetic models such as Pseudo-first order, Pseudo-second order, Interparticle diffusion, Intraparticle diffusion and Boyd's models are considered for the study and discussion about the theory for the same is also provided.

Chapter 6: Synthesis, Characterization and CO_2 Adsorption Studies for Amine Tethered MCM-41.

The chapter highlights the importance for selection of suitable support for amine tethering. The optimization of synthesis procedure for fine tuning of the adsorbent's composition for its

better CO_2 capture performance is discussed. Several characterization techniques used for structural, thermal, organic loading analyses and CO_2 adsorption performance of amine tethered MCM-41 is discussed.

Chapter 7: Evaluation of Amine Tethered MCM-41 based on Post Combustion CO_2 Capture Metrics.

The chapter elucidates the performance of amine tethered MCM-41 in terms of post combustion CO_2 capture metrics such as (i) CO_2 adsorption capacity (ii) Amine efficiency (iii) Operating window (iv) CO_2 adsorption kinetics (v) Selectivity (vi) Cyclic adsorption-desorption studies and (vii) Cost. Comparative analysis of the same with other adsorbents such as activated carbon, zeolites, metal organic frameworks, amine impregnated and amine tethered mesoporous silica adsorbents is highlighted to rank the performance of MCM-41 for the said application.

Chapter 8: Modeling of CO_2 Adsorption on Amine Tethered MCM-41: Equilibrium and Kinetic studies.

The chapter elucidates the investigation of experimental equilibrium and kinetic data by several isotherm and kinetic models. The theory for both isotherm (Langmuir and Langmuir dual-site models) and kinetic models (Pseudo first order, Pseudo second order, Double-exponential models) are discussed.

Chapter 9: Conclusions and Future Directions.

The chapter elucidates the major inferences drawn from the doctoral work and an outlook for future studies.

1.5. References

[1] The International Energy Outlook Report, **2013**.

[2] Thompson, S. L.; and Schneider, S. H.; Carbon dioxide and Climate: Ice and Ocean, *Nature*, **1981**, 290, 9-10.

[3] Steinacher, M.; Joos, F.; and Stocker, T. F. Allowable Carbon Emissions Lowered by Multiple Climate Targets, *Nature*, **2013**, 499, 197-201.

[4] Espinal, L.; Poster, D. L.; Wong-Ng, W.; Allen, A. J.; and Green, M. L.; Measurement, Standards, and Data Needs for CO_2 Capture Materials: A Critical Review, Environ. Sci. Technol., **2013**, 47, 11960-11975.

[5] Peng, Y.; Zhao, B.; and Li, L.; Advance in Post-combustion CO_2 Capture with Alkaline Solution: A Brief Review, *Energy Procedia*, **2012**, 14, 1515-1522.

[6] Veltman, K.; Singh, B.; and Hertwich, E.G. Human and Environmental Impact Assessment of Post combustion CO_2 Capture Focusing on Emissions from Amine-Based Scrubbing Solvents to Air, *Environ. Sci. Technol.* **2010**, 44, 1496-1502.

[7] Ma, X.; Wang, X.; and Song, C. "Molecular Basket" Sorbents for Separation of CO_2 and H_2S from Various Gas Streams, *J. Am. Chem .Soc*. **2009**, 131, 5777-5783.

[8] Meisen, P.; and Lim, A. Solubility of CO_2 in 2-amino-2-methyl- 1-propanol solutions, *J. Chem. Eng. Data* .**1991**, 36, 130-133.

[9] Veawab, Tontiwachwuthikul, A.; and Chakma, P. Corrosion Behavior of Carbon Steel in the CO_2 Absorption Process Using Aqueous Amine Solutions, *Ind. Eng. Chem. Res*. **1999**, 38, 3917-3924.

[10] Wang, X.; Schwartz, V.; Clark, J.C.; Ma, X.; Overbury, S.H.; Xu, X.; and Song, Infrared Study of CO_2 Sorption over "Molecular Basket" Sorbent Consisting of Polyethylenimine-Modified Mesoporous Molecular Sieve, *J. Phys. Chem.* **2009**, 113, 7260-7268.

[11] Sravanthi, L.; Tikmani, M.; and Ghoshal, A. K. Novel Pore-Expanded MCM-41 for CO_2 Capture: Synthesis and Characterization, *Langmuir* **2013**, 29, 3491-3499.

[12] Siriwardane, R.V.; Shen, M.S.; Fisher, E.P.; and Poston, J.A. Adsorption of CO_2 on Molecular Sieves and Activated Carbon, *Energy & Fuels.* **2001,** 15, 279-284.

[13] Calleja, G.; Pau, J.; and Calles, J.A. Pure and Multicomponent Adsorption Equilibrium of Carbon Dioxide, Ethylene, and Propane on ZSM-5 Zeolites with Different Si/Al Ratios, *J. Chem. Eng. Data.* **1998,** 43, 994-1003.

[14] Rutherford, S.W.; and Do, D.D. Adsorption Dynamics of Carbon dioxide on a Carbon Molecular Sieve 5A, *Carbon.* **2008**, 38, 1339-1350.

[15] Takamura, Y.; Narita, S.; Aoki, J.; Hironaka, S.; Uchida, S.; Evaluation of Dual-Bed Pressure Swing Adsorption for CO_2 Recovery from Boiler Exhaust Gas, *Sep. Purif. Technol*. **2001**, 24, 519–528.

[16] Wilson, R.J.; and Danner, R.P. Adsorption of Synthesis Gas-Mixture Components on Activated Carbon, *J. Chem. Eng. Data*. **1983,** 28, 19-23.

[17] Kapoor, A.; and Yang, R.T. Kinetic Separation of Methane-Carbon dioxide Mixture by Adsorption on Molecular sieve Carbon, *Chem. Eng. Sci.* **1989**, 44, 1723-1733.

[18] Siriwardane, R.V.; Shen, M.S.; Fisher, E.P.; and Poston, J.A. Adsorption of CO_2 on Molecular Sieves and Activated Carbon, *Energy & Fuels.* **2001,** 15, 279-284.

[19] Karra, J.R.; and Walton, K.S. Molecular Simulations and Experimental Studies of CO_2, CO, and N_2 Adsorption in Metal-Organic Frameworks, *J. Phys. Chem. C.* **2010,** 114, 15735–15740.

[20] Yazaydın, A.O.; Benin, A.I.; Faheem, S.A.; Jakubczak, P.; Low, J.J.; Willis, R.R.; and Snurr, R.Q. Enhanced CO_2 Adsorption in Metal-Organic Frameworks via Occupation of Open-Metal Sites by Coordinated Water Molecules, *Chem. Mater.* **2009,** 21, 1425–1430.

[21] Walton, K.S.; Millward, A.R.; Dubbeldam, D.; Frost, H.; Low, J.J.; Yaghi, O.M.; and Snurr, R.Q. Understanding Inflections and Steps in Carbon Dioxide Adsorption Isotherms in Metal Organic Frameworks, *J. Am. Chem. Soc.* **2008**,130, 406-407.

[22] Yazaydın, A.O.; Snurr, R.Q.; Park, T.H.; Koh, K.; Liu, J.; Levan, M.D.; Benin, A.I.; Jakubczak, P.; Lanuza, M.; Galloway, D.B.; Low, J.J.; and Willis, R.R. Screening of Metal-Organic Frameworks for Carbon Dioxide Capture from Flue Gas Using a Combined Experimental and Modeling Approach, *J. Am. Chem. Soc.* **2009**, 131, 18198–18199.

[23] Herm, J.R.; Swisher, J.R.; Smit, B.; Krishna, R.; and Long, J.R. Metal Organic Frameworks as Adsorbents for hydrogen Purification and Precombustion Carbon Dioxide Capture, *J. Am. Chem. Soc.* **2011**, 133, 5664–5667.

[24] Millward, A.R.; and Yaghi, O.M. Metal-Organic Frameworks with Exceptionally High Capacity for Storage of Carbon Dioxide at Room Temperature, *J. Am. Chem. Soc.* **2005**, 127, 17998-17999.

[25] Omar, J.; Ricard, G.; and Maldonado, A.J.H. Cu_2 (pyrazine-2, 3-dicarboxylate)$_2$ (4,4′-bipyridine) Porous Coordination Sorbents: Activation Temperature, Textural Properties, and CO_2 Adsorption at Low Pressure Range, *J. Phys. Chem. C*. **2010**, 114, 1827–1834.

[26] Beck, J.S.; Vartuli, J.C.; Roth, W.J.; Leonowicz, M.E.; Kresge, C.T.; Schmitt, K.D.; Chu, C.T.W.; Olson, D.W.; Sheppard, E.W.; McCullen, S.B.; Higgins, J.B.; and Schlenkert, J.L.; A New Family of Mesoporous Molecular Sieves Prepared with Liquid Crystal Templates *J. Am. Chem. Soc*. **1992**, 114, 10834-10843.

[27] Sayari, A.; and Yang, Y. Expanding the Pore Size of MCM-41 Silicas: Use of Amines as Expanders in Direct Synthesis and Post synthesis Procedures, *J. Phys. Chem. B.* **1999,** 103, 3651-3658.

[28] Sayari, A.; and Hamoudi, S. Periodic Mesoporous Silica-Based Organic-Inorganic Nanocomposite Materials, *Chem. Mater.* **2001,** 13, 3151-3168.

[29] Sayari, A.; Belmabkhouta, Y.; and Guerrerob, R.S. Flue gas treatment via CO_2 adsorption, *Chem. Eng. J.* **2011**, 171, 760-764.

[30] Choi, S.; Drese, J. H.; and Jones, C. W. Adsorbent Materials for Carbon dioxide Capture from Large Anthropogenic Point Sources, *ChemSusChem.* 10.1002/cssc.200900036.

[31] Liu, L.; Zhang, G.Y.; Dong, J.X. Large Pore Mesoporous MCM-41 Templated from Cetyltriethylammonium Bromide, *Chinese Chemical Letters*. **2004**, 15, 737-740.

[32] Zhao, D.; Huo, Q.; Feng, J.; Chmelka, B.F.; and Stucky, G.D. Nonionic Triblock and Star Diblock Copolymer and Oligomeric Surfactant Syntheses of Highly Ordered, Hydrothermally Stable, Mesoporous Silica Structures, *J. Am. Chem. Soc.* **1998**, *120,* 6024-6036.

[33] Corma, A.; Kan, Q.; Navarro, M.T.; Pariente, J.P.; and Rey, F. Synthesis of MCM-41 with Different Pore Diameters without Addition of Auxiliary Organics, *Chem. Mater.* **1997**, 9, 2123–2126.

[34] Blin, J.L.; and Su, B.L. Tailoring Pore Size of Ordered Mesoporous Silicas Using One or Two Organic Auxiliaries as Expanders, *Langmuir.* **2002,** 18, 5303-5308.

[35] Sayari, A.; Yong, Y.; Kruk, M.; and Jaroniec, M. Expanding the Pore Size of MCM-41 Silicas: Use of Amines as Expanders in Direct Synthesis and Post synthesis Procedures, *J. Phys. Chem. B*. **1999**, 103, 3651–3658.

[36] Jiang, D.; Gao, J.; Yang, J.; Su, W.; Yang, Q.; and Li, C. Mesoporous Ethane-Silicas Functionalized with Trans-(1R,2R)-diaminocyclohexane: Relation between Structure and Catalytic Properties in Asymmetric Transfer Hydrogenation, *Microporous Mesoporous Mater*. **2007**, 105, 204–210.

CHAPTER 2

LITERATURE REVIEW

This chapter outlines the history of various adsorbents reported so far for carbon capture application. The adsorbents for CO_2 capture are categorized into two types based on the adsorption mechanism involved, i.e., physisorbents and chemisorbents. The merits and de-merits of zeolites, activated carbon, metal-organic frameworks, amine impregnated and amine tethered mesoporous silica adsorbents for CO_2 capture are discussed in this chapter.

2.1. Introduction

A wide variety of solid adsorbents have been reported in the literature for CO_2 capture application **[1-4]**. Those adsorbents include zeolites, activated carbons, metal-organic frameworks, amine impregnated and amine tethered mesoporous silica etc. Based on the interaction mechanism between adsorbent and CO_2, adsorbents are classified into two types (i) physisorbents and (ii) chemisorbents. Zeolites, activated carbons and metal-organic framework sorbents fall under the category of physisorbents as they interact with CO_2 via physisorptive mechanism **[1-4]**. Amine impregnated and amine tethered mesoporous silica materials are included in the category of chemisorbents as they interact with CO_2 via chemisorptive mechanism **[1-4]**.

2.2. Physisorbents

For physisorbents such as zeolites, activated carbons and metal organic frameworks, selective adsorption of CO_2 over other gas components in the flue gas takes place via van der Waals force of attraction between CO_2 and surface of the respective adsorbent **[1-4]**. Apart from this, the adsorption may also be favoured by interactions between the quadrupole of CO_2 and ionic as well as polar sites of the solid adsorbent surface **[1-4]**.

2.2.1. Zeolites

Zeolites are a class of porous crystalline aluminosilicate frameworks, which consists of SiO_4 and AlO_4 tetrahedrons arranged in a regular fashion through shared oxygen atoms. The presence of aluminium atoms introduces negative charges in the framework, which is then compensated or balanced by exchangeable alkali cations such as Na^+, K^+, Ca^{2+} and Mg^{2+}) in the pore space throughout the zeolite structure. These structural characteristics favour the zeolites to adsorb acidic gas molecules such as CO_2. Zeolites possess open crystal lattices consisting of pores with molecular dimensions, through which gas molecules penetrate. The adsorption and gas separation characteristics of zeolites are highly dependent on the size, charge density, and distribution of these cations in the porous structure **[1-4]**.

Huesca et al. reported CO_2 adsorption capacities of three natural zeolites, including erionite (ERI), mordenite (MOR), and clinoptilolite (HEU) at 17 °C. The CO_2 adsorption capacity of corresponding adsorbents is reported to be ~1.4, ~1.6 and ~2.7 mmol/g (at 17 °C and 0.1 bar) **[5]**. Harlick et al. investigated the CO_2 adsorption capacity of zeolite adsorbents such as 13X and HY-5. The CO_2 adsorption capacities of those adsorbents were reported to be 1.2 mmol/g (HY-5) and 4.5 mmol/g (13X) (at 22 °C and 1 bar) respectively. The variation in the adsorption capacity was concluded to be due to the different Si/Al ratios of the adsorbents and the effect of type of charge balancing cations **[6]**. Walton et al. investigated the effect of substitution of Na cations by Rb, Cs, K and Li on the CO_2 adsorption capacity. It was found that the adsorption capacity at 0.1 bar followed the sequence Li ≈ Na > K > Rb > Cs for X zeolites. The adsorption capacities of the respective adsorbents were predicted to be ~5.5, ~4.5, ~4, ~3.7 and ~2.8 mmol/g **[7]**. Michelena et al. made an investigation on predicting the CO_2 adsorption capacity of NaY zeolite at 0 °C and pressure condition close to 0.1 bar. The NaY zeolite exhibited a maximum of 5 mmol/g of CO_2 adsorption capacity (at 0 °C and 0.1 bar) **[8]**. Cavenati et al. presented the CO_2 adsorption isotherms on zeolite 13X at 20, 35, and 50 °C. It was found that CO_2 uptake dramatically reduced from 4.5 mmol/g (at 20 °C and 0.1 bar) to 2.1 mmol/g (at 50 °C and 0.1 bar) with increase in the operating temperature **[9]**. These results indicate that zeolites exhibit better CO_2 uptake performance under mild operating conditions.

In terms of CO_2 adsorption kinetics, zeolites are ranked as the fastest adsorbents reaching the maximum equilibrium capacity in order of minutes **[1-4]**. However, for practical CO_2 applications, performance of zeolite based adsorbents in the presence of moisture is a challenge issue. Rege et al. reported that adsorption of CO_2 on type X zeolites is not favoured in the presence of moisture **[10]**. Gallei et al. carried out a study on investigating the effect of moisture on the CO_2 adsorption capacity of zeolite CaY and NiY. It was found that the presence of moisture in the feed gas limited the adsorption of CO_2 due to competitive adsorption of H_2O on the active sites of the adsorbents, thereby causing

substantial decrease in CO_2 uptake **[11]**. Ruthven et al. made an effort to study the effect of H_2O on the CO_2 adsorption using X (FAU) zeolites such as NaLSX, LiLSX, and CaX. It was found that the CO_2 adsorption capacity was drastically reduced (almost negligible) with increase in H_2O concentration of 12-15% at a given partial pressure of 0.05 bar and at 25 °C **[12]**. Although zeolites have been shown to exhibit promising results for separating CO_2 at mild temperatures (<30 °C), their selectivity for CO_2 over other gases (N_2, CH_4, H_2O, etc.) is another issue with zeolite based adsorbents **[1-4]**. The substantial decrease of CO_2 adsorption capacity of zeolite adsorbents at elevated temperatures limits their application for post-combustion CO_2 capture applications.

2.2.2. Activated Carbons

Activated carbons are regarded as another fascinating group of adsorbents for CO_2 capture applications because of their low cost and high thermal stability **[1-4]**. As activated carbons can be produced via carbonization and activation from cheap raw materials such as coal and other biomass sources, these adsorbents find commercial applications **[1-4]**. Variations in the surface area, pore size distribution and pore structure of the activated carbons prepared from several sources lead to difference in adsorption capacity of sorbents **[1-4]**. Do et al. reported the CO_2 adsorption capacity of Ajax activated carbon to be ~0.8 and ~0.1 mmol/g at 25 °C and 100 °C respectively (0.2 bar) **[13]**. Yang et al. reported the CO_2 adsorption equilibrium measurements on commercialized adsorbent i.e. BPL activated carbon. The CO_2 uptake capacity of the adsorbent was reported to be ~0.8 mmol/g (at 25 °C and 0.2 bar) **[14]**. Na et al. investigated the CO_2 adsorption capacity of a proprietary activated carbon at five different temperatures. The adsorption capacity of the same was reported to be ~0.9, ~0.7, ~0.5, ~0.3 and ~0.1 mmol/g at 15, 25, 35, 45 and 55 °C (0.2 bar) respectively **[15]**. Like zeolites, the adsorption capacity of activated carbons also dramatically drops down for even a small rise in temperature.

Cho et al. made a comparative analysis on CO_2 adsorption capacities for BPL activated carbon and zeolite 13X. It was found that BPL activated carbon exhibited 2.5 mmol/g (15 °C and 1 bar) of CO_2 adsorption capacity which was comparatively lower than zeolite 13X (~4.5 mmol/g) **[16]**. Cho et al. reported that the mild adsorption capacity of activated carbon is beneficial in terms of regeneration, where less energy is required than zeolite 13X. The heat of adsorption values for activated carbon and zeolite 13X were calculated to be 36 kJ/mol and 30 KJ/mol respectively **[16]**. It has been shown in their study, that zeolite 13X have a stronger physical interaction with CO_2 in comparison to activated carbon, thereby making the regeneration process highly energy intensive. The advantage of regeneration energy makes activated carbon to be competitive for CO_2 capture, in spite of its lower adsorption capacity than zeolite 13X at ambient conditions. The adsorption kinetics of CO_2 is considered to be comparable to zeolites, in which maximum equilibration capacity can be reached in scale of minutes **[17]**. However, presence of moisture in the feed gas was shown to adversely affect the CO_2 capture capacity due to partial oxidation of carbon surfaces **[18]**. Hence, carbonaceous materials seem to be attractive for CO_2 removal only at low temperature and in the absence of moisture. These limitations make activated carbon materials unsuitable for low pressure and high temperature CO_2 capture application like flue gas treatment.

2.2.3. Metal-Organic Frameworks

Metal-organic frameworks (MOFs) are emerging class of porous materials, which have attracted growing interest among the scientific community in the recent years for carbon capture applications. MOFs are porous crystalline materials composed of metal ions linked by organic spacers. The pore size and chemical potential of adsorbing surfaces of these materials can be tuned easily by readily incorporating various organic linkers in the framework. These properties make MOF based adsorbents to be attractive materials for carbon capture applications. Therefore, both experimental and theoretical studies on CO_2 adsorption properties on MOF based adsorbents were reported extensively **[1-4]**.

Finsy et al. investigated the feasibility of MIL-53 adsorbent for CO_2 capture application and obtained an adsorption capacity of ~0.5 mmol/g (30 °C, 0.1 bar) **[19]**. Banerjee et al. carried out CO_2 adsorption measurements on ZIF-78 and obtained an uptake of ~0.8 mmol/g (25 °C, 0.1 bar) **[20]**. Yang et al. reported the CO_2 adsorption capacity of Cu-BTC to be ~0.5 mmol/g (25 °C, 0.1 bar). In addition to this, the same group measured N_2 adsorption capacity of Cu-BTC and was reported to be ~0.2 mmol/g (25 °C, 0.9 bar) **[21]**. Bastin et al. reported CO_2 adsorption capacity of MOF-508 to be ~0.1 mmol/g (50 °C, and 0.1 bar). MOF-508 also showed preferential adsorption of N_2 with an adsorption capacity of ~0.6 mmol/g (50 °C, 0.9 bar) **[22]**. The selectivity of CO_2 over N_2 for Cu-BTC and MOF-58 was predicted to be only ~15 and ~2 respectively, which drives an issue of CO_2 separation in mixture of gases containing N_2 for these adsorbents **[21, 22]**. In addition, it becomes important to notice that all these adsorbents exhibit unfavourable adsorption isotherm properties at low pressure regime, a disadvantage for CO_2 separation from flue gas.

Yazaydin et al. studied the CO_2 adsorption characteristics on Ni/DOBDC and CO/DOBDC adsorbents and reported the uptake capacity to be ~2.7 and ~2.8 mmol/g respectively (23 °C, 0.1 bar) **[23]**. Mason at al. investigated the CO_2 adsorption capacity of Mg/DOBDC (or Mg-MOF-74) and reported CO_2 adsorption capacity of the same to be 6 mmol/g (21 °C and 0.2 bar). Mg-MOF-74 was reported to exhibit highest adsorption capacity among majority of the MOFs reported in the literature (at ambient temperature conditions). However, its adsorption capacity was found to substantially decrease with respect to rise in temperature i.e ~2.4 mmol/g (75 °C and 0.2 bar) **[24]**. The presence of co-ordinatively unsaturated metal sites (CUMs) in Mg-MOF was shown to enhance selectivity of CO_2 over N_2 due to strong interaction between CO_2 and Mg metal centre. However, the presence of moisture in the feed gas was reported to affect the CO_2 adsorption properties of Mg-MOF adversely. Yu et al. investigated the effect of water on CO_2 adsorption in Mg-MOF-74 and the study confirmed that the CO_2 adsorption capacity exhibited downturn i.e. ~3 mmol/g (21 °C, 0.2

bar) **[25]**. Therefore, for indeed Mg-MOF-74 to be a potential adsorbent for flue gas treatment, the co-adsorption issue of CO_2 with water is an urgent problem to be resolved.

Interestingly, water-stable MOFs such as ZIF-8 and ZIF-69 were also reported for CO_2 capture application **[26, 27]**. Van et al. examined the CO_2 adsorption properties on Ni-MOF74 and HKUST-1 under humid conditions **[28]**. In case of Ni-MOF74 material, dry CO_2 adsorption capacity of ~3.28 mmol/g was obtained under low pressure condition relevant to flue gas (25 °C, 0.1 bar). Presence of water vapour in the feed gas was observed to show impact on CO_2 adsorption capacity, but not as higher as zeolite 5A and NaX type zeolites. In addition to this, the research group also investigated the effect of moisture on the stability of the MOF. It was observed that HKUST-1 adsorbent started to degrade substantially over 7 runs and Ni-MOF74 adsorbent showed stability up to 10 runs **[28]**. The heats of adsorption values for interaction of CO_2 with majority of the MOFs are generally low (~30 to 45 kJ/mol) and are comparable to that of physical adsorbents such as zeolites and activated carbons **[1-4]**. On the whole, MOFs can be promising materials for CO_2 removal provided that key properties for flue gas treatment such as stability, multi-cycle applicability and competitive sorption are addressed adequately.

2.4. Chemisorbents

Inspired by amine absorption technology, silica supported amine materials have emerged as a promising class of adsorbents effective for CO_2 capture from flue gas. Adsorption of CO_2 on amine functionalized adsorbents takes place via acid-base interactions between amine groups within the pores or on external surface of silica and CO_2. For reaction of primary and secondary amines with CO_2, zwitterion mechanism was proposed by Caplow **[29]**, which includes two steps. In the first step, lone pair present in the amine attacks the carbon atom in CO_2 and forms the zwitterion complex. In the second step, free base is then donated by another primary amine in order to deprotonate the unstable zwitterion complex and form carbamate. Therefore, under dry conditions of adsorption, maximum amine efficiency of

amine functionalized adsorbent is 0.5 mol CO_2 per mol N. Under humid conditions, H_2O serves as a base for deprotonation reaction; thereby leading to maximum amine efficiency of 1.0 mol CO_2 per mol N. Secondary as well as sterically hindered amines (primary amine attached to tertiary carbon atom, secondary amine attached to secondary or tertiary carbon atom) also follow similar mechanism for CO_2 adsorption **[30]**.

As tertiary amines lack free proton required for deprotonation step, they do not react directly with CO_2. The mechanism for interaction of tertiary amines with CO_2 was first proposed by Donaldson **[31]**, which involves the base-catalyzed hydration of CO_2. In the first step, dissociation of water molecule takes place to form the quaternary cationic species and In OH^-. the second step, hydroxide ion interacts with CO_2 to form the bicarbonate anion. Third step involves the association of ionic species i.e. protonated amine and bicarbonate anion. As CO_2 adsorption by tertiary amines requires water, amine functionalized silica sorbents based on tertiary amines are not considered as an attractive option for CO_2 capture under dry conditions **[1-4]**.

2.4.1. Classification of Amine Functionalized Silica Adsorbents

Amine functionalized silica adsorbents have been classified into three types based on the methodology followed for functionalization of amine on the porous silica support.

2.4.1.1. Class I Adsorbents

Class I type of amine functionalized silica sorbents are prepared by physically loading of monomeric or pre-synthesized polymeric amine species into the porous support by impregnation technique **[1-4]**. Song and his research group are the first to design class I adsorbents and introduce the same for carbon capture applications. Song et al. impregnated polyethyleneimine (PEI) onto mesoporous material MCM-41 for CO_2 adsorption and coined the term “molecular basket” for the resultant composite adsorbent. The CO_2 adsorption capacity of PEI-impregnated MCM-41 was found to increase with respect to loading. For PEI loading of 75 wt%, CO_2 adsorption capacity of ~3.02 mmol/g was reported for PEI-

impregnated MCM-41 under a stream of 100% CO_2 (75 °C, 1 bar). The optimum amount of PEI that can be loaded in MCM-41 was found to be 50 wt% based on the amine efficiency of the composite adsorbent. The 50 wt% PEI loaded MCM-41 exhibited an adsorption capacity of ~2.0 mmol/g under a stream of 15%CO_2/air mixture. Unlike other adsorbents discussed earlier in the physisorbents section, PEI-impregnated MCM-41 composite showed an interesting behaviour that the CO_2 adsorption capacity increased with respect to temperature (25 to 75 °C). The enhancement in the adsorption capacity observed with rise in temperature was concluded to be due to the occurrence of a bulk-like state of PEI inside the mesopores. Further, it was mentioned that when PEI is present in bulky state, amine groups are not readily accessible for CO_2 at low temperature, resulting in a diffusion-limited process **[32]**. Ever since, the basic design involved in the synthesis of class I adsorbents was adopted by several researchers and similar behaviour of the composite sorbent with temperature was reported **[33-35]**. Thereafter, the concept of diffusion-limited process for CO_2 adsorption process on PEI impregnated silica adsorbent has been widely accepted by the scientific community. The same adsorbent designed by Song et al. showed positive effect for CO_2 adsorption capacity in terms of moisture. In a mixture of 10%H_2O/13%CO_2/air, the adsorbent exhibited a CO_2 uptake capacity of ~2.8 mmol/g at 75 °C in comparison to ~2.0 mmol/g under dry conditions, which in turn supported the bicarbonate formation mechanism in the presence of moisture **[33]**.

The type of silica support structure used in the impregnation process has been shown to affect the CO_2 adsorption properties. Ahn et al. investigated the CO_2 adsorption characteristics of PEI (50 wt %) impregnated using five different silica supports. Interestingly, it was observed that all the supports used in the study for impregnation process exhibited variation in the CO_2 uptake capacity. Further, it was concluded that the adsorption capacity was dependent on the pore diameter of the silica support used for impregnation process. It was observed that CO_2 uptake capacity increased in the order of KIT-6>SBA-15~SBA-16>MCM-48>MCM-41, which corresponds to the order of average pore diameter of the bare

support (6.5, 5.5, 4.1, 3.1 and 2.8 nm respectively). Similar trend for the time required for each PEI impregnated adsorbent to reach 90% of its equilibrium capacity was noticed **[34]**. In a separate contribution, Song et al. impregnated PEI in SBA-15 mesoporous silica and reported a CO_2 adsorption capacity of ~3.18 mmol/g under 15% CO_2/air, which was around 37% higher in comparison to PEI impregnated MCM-41 at 75 °C. It was further confirmed from this study, that the CO_2 adsorption properties of aminated adsorbents are influenced by the pore size and pore volume of the silica support used for impregnation **[36]**.

Yue et al. investigated the effect of as-synthesized silica support (without removing the organic template by calcination) for amine impregnation process and subsequently the CO_2 adsorption characteristics. An adsorption capacity of ~3.2 mmol/g for SBA-15 sample impregnated with 50 wt% tetraethylene pentamine (TEPA) was obtained (75 °C, 0.1 bar), which was 10% higher than the TEPA loaded in supports prepared by calcination. The approach proposed by Yue et al. provided an added advantage by excluding the removal of organic template step during synthesis of silica supports. It was mentioned that the reason for enhancement in the adsorption capacity for as-synthesized supports is attributed to the interaction of TEPA with polymeric template leading to uniform distribution of TEPA inside the pores **[37]**.

Sayari et al. impregnated diethanolamine (DEA) on a variety of supports such as conventional MCM-41 and pore-expanded MCM-41 (PE-MCM-41) and compared the CO_2 adsorption capacities of those adsorbents as well as stability to a benchmark adsorbent, zeolite13X. PE-MCM-41 synthesized by post-synthesis hydrothermal treatment (pore size: ~10 nm) exhibited an adsorption capacity of ~3 mmol/g (25 °C, 0.1 bar). The adsorption capacity obtained for DEA impregnated PE-MCM-41 was comparable to the CO_2 adsorption uptake reported for zeolite 13X (~2.8 mmol/g) under similar experimental conditions **[38]**.

In contrast to physisorbents, amine impregnated adsorbents were shown to express positive effect towards CO_2 adsorption capacity in the presence of moisture in the feed gas. In a

study reported by Song et al., it was noticed that PEI impregnated adsorbent exhibited much longer breakthrough time for CO_2 adsorption under humid conditions when compared dry conditions. An enhancement in the CO_2 adsorption capacity of around ~30% was noticed under humid conditions **[36]**.

As class I adsorbents can be synthesized via simplest route, it seems that these adsorbents may be an attractive option for large scale carbon capture applications. However, it becomes important to be addressed here, that amine impregnated adsorbents are more sensitive to temperature conditions used in regeneration process. Any solid sorbent developed for carbon capture application should exhibit recycle stability when subjected to multiple adsorption/desorption cycles. Zhu et al. reported a loss of ~4% in the CO_2 adsorption capacity, when TEPA impregnated SBA-15 was subjected to seven continuous adsorption-desorption cycles **[39]**. Similarly, loss in the adsorption capacity of ~9% and ~50% were also reported for TEPA and PEI impregnated MCM-41 and SBA-15 respectively after 4-6 adsorption-desorption cycles **[34, 39]**. Even though, amine impregnated silica sorbents are evidenced to exhibit high adsorption capacity (~3-4 mmol/g) at conditions relevant to flue gas, recycle stability or durability issue associated with these adsorbents limits their application for post-combustion CO_2 capture.

2.4.1.2. Class II adsorbents

Class II type of silica supported adsorbents are prepared by covalently tethering the amine groups to the surface hydroxyl group of mesoporous silica via silane chemistry **[1-4]**. Leal et al. was the first to put forth the concept of synthesizing amine-grafted sorbents for CO_2 capture. (3-aminopropyl) triethoxysilane (AP) tethered silica gel synthesized by their research group provided a CO_2 adsorption capacity of ~0.41 mmol/g (23 °C, 1 bar) **[40]**. Despite, the adsorption capacity was comparatively lower than zeolites, activated carbons, metal-organic frameworks and amine impregnated adsorbents, the novel concept proposed

by Leal et al. paved the way for the scientific community to further broaden the research in the area of amine tethered mesoporous silica adsorbents for carbon capture application.

Huang et al. made a comparative investigation on the performance of AP grafted MCM-48 and xerogel towards CO_2 adsorption. The CO_2 adsorption capacity of AP grafted MCM-48 was reported to be 59% higher than AP grafted xerogel. AP-MCM-48 and AP-xerogel showed an adsorption capacity of ~1.42 mmol/g and ~0.58 mmol/g respectively (~20 °C, 0.1 bar). It was inferred that the variation in the adsorption capacity was attributed to the amine loading capacity of both the support materials. AP-MCM-48 exhibited amine loading of ~2.3 mmol(N)/g, which was 26% higher than AP-xerogel (~1.7 mmol/g), thereby leading to improved efficiency for CO_2 adsorption **[41]**.

Knowles et al. explored the suitability of amorphous silica gel and hexagonal mesoporous silica (HMS) for amine tethering. AP-HMS exhibited a higher adsorption capacity of 1.59 mmol/g (20 °C, 0.9 bar) in comparison to AP-silica gel (~0.68 mmol/g) under the similar conditions. Amine loading was also observed to be 52% higher in the case of AP-HMS, as compared with AP-silica gel. It was concluded that the variations in the adsorption capacities as well as loadings are due to the difference in surface areas of HMS (1198 m^2/g) compared to amorphous silica (567 m^2/g) **[42]**.

Knofel et al. grafted N-[3- (trimethoxysilyl)propyl] ethylenediamine (DP) on SBA-16 silica based on the assumption that the occurrence of two amine groups per carbon chain may lead to enhanced amine efficiency. Incorporation of diamine into SBA-16 silica support provided an adsorption capacity of ~1.4 mmol/g (27 °C, 1 bar). The amine efficiency of AP functionalized silica adsorbents was found to be higher than DP functionalization **[43]**.

Wang et al. pursued the effect of ethanol extraction for removal of surfactant with the aim to improve efficiency of amine functionalization and adsorption properties. The aminated SBA-15 synthesized after removal of surfactant by solvent extraction performed better than the sample prepared by grafting on calcined SBA-15. Amine grafted as-synthesized SBA-15

sample yielded an adsorption capacity of ~0.5 mmol/g (65 °C, 0.1 bar) with an amine efficiency of ~0.44, which is close to stoichiometric ratio of 0.5. It was inferred from this study, that extraction of structure directing agent by ethanol extraction process could preserve the surface silanol groups leading to improvement in the grafting efficiency as well as adsorption capacity **[44]**.

Zelenak et al. investigated the effect of pore size on the performance of amine-functionalized adsorbents for CO_2 capture. In their study, AP was tethered onto two different mesoporous silica supports i.e. MCM-41 and SBA-15 with a pore size of 3.3 nm and 7.1 nm respectively. The AP functionalized SBA-15 exhibited an adsorption capacity of ~1.54 mmol/g, whereas, the CO_2 uptake of AP-MCM-41 was only ~0.57 mmol/g (20 °C, 0.1 bar). It was concluded from the study that variation in the adsorption capacity exhibited by the two adsorbents was attributed to the pore size and amine surface density. The mesoporous silica support SBA-15 with larger pore size was reported to possess higher amine surface density (2.4 (N)/nm^2)) in comparison to AP-MCM-41 having amine density of only 1.1 (N)/nm^2 **[45]**.

Hiyoshi et al. made a comparative investigation on the adsorption characteristics of AP, DP and TP (N-[3-(trimethoxysilyl)propyl] diethylenetriamine) grafted SBA-15. The study demonstrated that higher amine density resulted through tri amine bearing species led to synthesis of best performing adsorbent. TP-SBA-15 had been reported with CO_2 adsorption capacity of ~1.58 and ~1.80 mmol/g respectively under dry and humid streams. Moreover, the adsorbent was also reported to be stable for more than 50 adsorption-desorption cycles when subjected to regeneration at 100 °C **[46]**.

Sayari et al. have made noteworthy contributions to the CO_2 capture research by amine tethered mesoporous silica adsorbents. Sayari demonstrated the favourable influence of using materials with enlarged pore diameter and pore volume in comparison to conventional MCM-41 silica. In their study, the application of pore expansion or swelling agents for the enlarging the pore-size of MCM-41 through post-synthesis hydrothermal treatment was

introduced for the first time. The MCM-41 generated with enlarged pore diameter was named as “pore-expanded MCM-41 (PE-MCM-41) by their research group. The PE-MCM-41 exhibited a pore size of ~10 nm and pore volume of ~2.5 cc/g, which is significantly higher in comparison to conventional MCM-41 with pore size and pore volume of ~3 nm and 0.8 cc/g respectively. Sayari et al. compared the performance of TP grafted on conventional MCM-41 and PE-MCM-41. It was observed that TP-PE-MCM-41 exhibited a 50% higher adsorption capacity in comparison to TP-MCM-41, irrespective of amine loadings. In addition to this, TP-PE-MCM-41 outperformed TP-MCM-41 in terms of CO_2 adsorption kinetics, thus indicating the importance of pore size and pore volume to be selected for amine tethering process **[47]**.

In a separate contribution, Sayari’s group explored the effect of water on grafting efficiency and further optimized the temperature conditions suitable for grafting reactions with the aim to enhance amine loading and CO_2 adsorption capacity. The study indicated that addition of water in the grafting reaction could help in hydroxylation of silica surface, thereby, amine loading was also noticed to be enhanced. Enhancement in the amine loading and adsorption capacity of ~ 30% and ~70% was observed for TP-PE-MCM-41 under wet grafting conditions in comparison to conventional dry grafting procedure. The study indicated the fact that combination of pore expansion and optimized grafting conditions could improve the adsorption capacity as well as rate of adsorption dramatically. The same group also explored the effect of moisture on the CO_2 adsorption performance of TP-PE-MCM-41. In the presence of 5%CO_2/27% moisture/N_2, the adsorption capacity for TP-PE-MCM-41 increased by ~10% in comparison to dry conditions. The work provided evidence that TP-PE-MCM-41 outperformed benchmark adsorbent zeolite 13X in terms of adsorption capacity as well as kinetics **[48]**. Later contributions of Sayari et al. on TP-PE-MCM-41 demonstrated that in addition to enhanced CO_2 adsorption capacity, the novel adsorbent could exhibit high selectivity towards CO_2 over N_2. The adsorbent also exhibited a stable adsorption capacity of ~1.6 mmol/g (50 °C, 0.1 bar) over 100 adsorption-desorption cycles when regenerated at 90

°C under vacuum **[49]**. This provides a clear illustration that covalently tethered amine sorbents indeed possess potential to be used for multicycle adsorption/desorption process. Apart from this, amine tethered adsorbents show a clear advantage of overcoming amine leaching issue addressed for amine impregnated silica materials.

2.4.1.3. Class III adsorbents

Class III type of silica supported adsorbents are prepared by polymerization of reactive monomers inside the open space available in the mesoporous supports. In this method, the open space present in the mesoporous silica support serves as galleries for the polymerization reaction. In addition to this, these galleries in turn constrain the polymerization process resulting in low-molecular weight polymers **[1-4]**.

The concept of step-wise polymerization of melamine dendrons on mesoporous silica SBA-15 was introduced by Chaffee et al. for synthesis of CO_2 adsorbents characterized by amine loading. The melamine functionalized SBA-15 exhibited the highest amine loading of ~7.49 mmol(N)/g. However, as the reaction involved a series of steps in synthesizing higher generation dendrimers, the adsorbent was reported to lose its structural properties due to space confinement of pores and hence, negative impact on the CO_2 adsorption properties were noticed **[50]**.

In a later contribution, Jones et al. proposed an innovative approach for amine polymerization inside the pore channels of SBA-15. In their research work, ring opening polymerization of aziridine was carried out inside the pores of SBA-15 and a covalently tethered hyperbranched aminosilica (HAS) had been synthesized. The novel HAS adsorbent exhibited a CO_2 adsorption capacity of ~3.11 mmol/g (25 °C, 0.1 bar). In addition, the adsorbent was characterized with an amine loading of ~7.0 mmol(N)/g and promising in terms of amine efficiency (0.44), which is close to theoretical value of 0.5. At conditions relevant to flue gas, the HAS adsorbent exhibited a stable adsorption capacity of ~1.98 mmol/g (75 °C, 0.1 bar) for 12 adsorption-desorption cycles, when regenerated at 130 °C

[51]. In a separate contribution, the same group made an effort in enhancing the loading of hyberbranched amine and successfully demonstrated a better adsorption capacity of ~4 mmol/g (75 °C, 0.1 bar) in the presence of humid conditions **[52]**.

2.5. Conclusions

In the summary, physical adsorbents such as zeolites, activated carbons and MOFs were found to be highly applicable for carbon capture at low temperature and high pressure conditions. In addition, preferential adsorption of water vapour and N_2 on physisorbents has been shown to affect the CO_2 adsorption properties detrimentally. In contrast, significant progress in the development of amine functionalized mesoporous silica adsorbents for flue gas treatment has been achieved via optimization of synthesis conditions and selection of supports with preferable structural properties.

A number of advantages which are common to class II and class III adsorbents i.e. silica supports that exhibit high silanol density, high surface area, large pore size and pore volume have been demonstrated to provide beneficial effects for covalently tethering the amine moieties by either silane chemistry or ring-opening polymerization technique. As mentioned earlier, despite class II and class III adsorbents exhibit less equilibrium adsorption capacity in comparison to class I adsorbents, they are shown to exhibit faster adsorption-desorption kinetics as well as multicycle stability over several hundreds of cycles. On the whole, amine grafted mesoporous silica adsorbents have been shown to exhibit promising results in terms of CO_2 adsorption capacity, selectivity, fast adsorption kinetics, multicycle stability if designed properly. Therefore, an alternative carbon capture technology based on amine tethered solid sorbents can be expected in the near future.

2.6. References

[1] Choi, S.; Drese, J. H.; and Jones, C. W. Adsorbent Materials for Carbon dioxide Capture from Large Anthropogenic Point Sources, *ChemSusChem.* 10.1002/cssc.200900036.

[2] Sayari, A.; Belmabkhout, Y.; and Guerrero, R.S. Flue Gas Treatment via CO_2 Adsorption, *Chem. Eng. J*. **2011**, 171, 760-764.

[3] Wang, Q.; Luo, J. L.; Zhong, Z.; and Borgana, A. CO_2 Capture by Solid Adsorbents and Their Applications: Current Status and New Trends, *Energy Environ. Sci.* **2011**, 4, 42-45.

[4] Samanta, A.; Zhao, A.; Shimizu, G. K. H.; Sarkar, P.; and Gupta, R. Post-Combustion CO_2 Capture Using Solid Sorbents: A Review, *Ind. Eng. Chem. Res.* **2012**, 51, 1438–1463.

[5] Huesca, H. R.; Diaz, L.; and Armenta, A. G. Adsorption Equilibria and Kinetics of CO_2, CH_4 and N_2 in Natural Zeolites, *Sep. Purif. Technol.* **1999**, 15, 163-173.

[6] Harlick, P.; and Tezel, F. H. An Experimental Adsorbent Screening Study for CO_2 Removal from N_2, *Microporous Mesoporous Mate*r. **2004**, 76, 71-79.

[7] Walton, K. S.; Abney, M. B.; and LeVan, M. D. CO_2 Adsorption in Y and X Zeolites Modified by Alkali Metal Cation Exchange, *Micropor. Mesopor. Mater.* **2006**, 91, 78–84.

[8] Michelena, J. A.; Peeters, G.; Vansant, E. F.; and De Bievre, P. The Adsorption of Carbon monoxide and Carbon dioxide in Calcium-Exchanged Zeolite Y, *Recl. Trav. Chim. Pays Bas.* **1977**, 96, 121-124.

[9] Cavenati, S.; Grande, C.A.; and Rodrigues, A.E. Adsorption Equilibrium of Methane, Carbon Dioxide and Nitrogen on Zeolite 13X at High Pressures, *J Chem Eng Data*. **2004**, 49, 1095-1101.

[10] Rege, S.U.; and Yang, R.T. A Novel FTIR Method for Studying Mixed Gas Adsorption at Low Concentrations: H_2O and CO_2 on Zeolite and ɣ-Alumina, *Chem. Eng. Sci.* **2001**, 56, 3781-3796.

[11] Gallei, E.; and Stumpf, G. Infrared Spectroscopic Studies of the Adsorption of Carbon dioxide and the Co-Adsorption of Carbon dioxide and Water on CaY and NiY Zeolites, *J. Colloid Interface Sci.* **1976**, 55, 415-420.

[12] Brandani, F.; and Ruthven, D.M. The Effect of Water on the Adsorption of CO_2 and C_3H_8 on Type X Zeolites, *Ind. Eng. Chem. Res.* **2004**, 43, 8339-8344.

[13] Do, D. D.; and Wang, K. A New Model for the Description of Adsorption Kinetics in Heterogeneous Activated Carbon*, Carbon* **1998**, 36, 1539-1554.

[14] Kikkinides, E. S.; Yang, R. T.; and Cho, S. H. Concentration and Recovery of Carbon dioxide From Flue Gas by Pressure Swing Adsorption, *Ind. Eng. Chem. Res.* **1993**, 32, 2714-2720.

[15] Na, B. K.; Koo, K. K.; Eum, H. M.; Lee, H.; and Song, H. K. CO_2 Recovery from Flue Gas by PSA Process using Activated Carbon, *Korean J. Chem. Eng.* **2001**, 18, 220-227.

[16] Chue, K. T.; Kim, J. N.; Yoo, Y. J.; Cho, S. H.; and Yang, R. T. Comparison of Activated Carbon and Zeolite 13X for CO_2 Recovery from Flue Gas by Pressure Swing Adsorption, *Ind. Eng. Chem. Res.* **1995**, 34, 591-598.

[17] Ding, L. P.; Bhatia, S. K.; and Liu, F. Kinetics of Adsorption on Activated Carbon: Application of Heterogeneous Vacancy Solution Theory, *Chem. Eng. Sci.* **2002**, 57, 3909-3928.

[18] Adams, L. B.; Hall, C. R.; Holmes, R. J.; and Newton, R. A. An Examination of How Exposure to Humid Air Can Result in Changes in the Adsorption Properties of Activated Carbons, *Carbon* **1988**, 26, 451-459.

[19] Finsy, V.; Ma, L.; Alaert, L.; De Vos, D. E.; Baron, C. V.; and Denayer, J.F.M. Separation of CO_2 Mixtures With the MIL-53(Al) Metal-Organic Framework, *Microporous Mesoporous Mater.* **2009**, 120, 221-227.

[20] Banerjee, R.; Furukawa, H.; Britt, D.; Kobler, C.; Keeffe, M.; and Yaghi, O. M. Control of Pore Size and Functionality in Isoreticular Zeolitic Imidazolate Frameworks and their Carbon dioxide Selective Capture Properties, *J. Am. Chem. Soc.* **2009**, 131, 3875-3877.

[21] Yang, Q.; Xue, C.; Zhong, C.; and Chen, J. F. Molecular Simulation of Separation of CO_2 from Flue Gas in Cu-BTC Metal-Organic Framework, *AIChE J.* **2007**, 53, 2832–2840.

[22] Bastin, L.; Barcia, P. S.; Hurtado, E. J.; Silva, J. A. C.; Rodrigues, A. E.; and Chen, B. A Microporous Metal-Organic Framework for Separation of CO_2/N_2 and CO_2/CH_4 by Fixed-Bed Adsorption, *J. Phys. Chem. C* **2008**,112, 1575-1581.

[23] Yazaydin, A. O.; Snurr, R. Q.; Park, T. H.; Koh, K.; Liu, J.; LeVan, M. D.; Benin, A. I.; Jakubczak, P.; Lanuza, M.; Galloway, D.B.; Low, J. J.; and Willis, R. R. Screening of Metal-Organic Frameworks for Carbon dioxide Capture from Flue Gas Using a Combined Experimental and Modeling Approach, *J. Am. Chem. Soc.* **2009**, 131, 18198-18199.

[24] Mason, J. A.; Sumida, K.; Herm, Z. R.; Krishna, R.; and Long, J. R. Evaluating Metal-Organic Frameworks for Post-Combustion Carbon dioxide Capture via Temperature Swing Adsorption, *Energy Environ. Sci.,* **2011**, 4, 3030-3040.

[25] Yu, J.; and Balbuena, P. B. Water Effects on Post-combustion CO_2 Capture in Mg-MOF-74, *J. Phys. Chem. C* **2013**, 117, 3383-3388.

[26] Liu, Y.; Hu, E.; Khan, E. A.; and Lai, Z. Synthesis and Characterization of ZIF-69 Membranes and Separation for CO_2/CO Mixture. *J. Membr. Sci.* **2010**, 353, 36-40.

[27] Park, K. S.; Ni, Z.; Cote, A. P.; Choi, J. Y.; Huang, R. D.; Uribe-Romo, F. J.; Chae, H. K.; Keeffe, M.; and Yaghi, O. M. Exceptional Chemical and Thermal Stability of Zeolitic Imidazolate Frameworks. *Proc. Natl. Acad. Sci. U.S.A.* **2006**, 103, 10186-10191.

[28] Liu, J.; Wang, Y.; Benin, A. I.; Jakubczak, P.; Willis, R. R.; and LeVan, M. D. CO_2/H_2O Adsorption Equilibrium and Rates on Metal Organic Frameworks: HKUST-1 and Ni/DOBDC. *Langmuir* **2010**, 26, 14301-14307.

[29] Caplow, M.; Kinetics of Carbamate Formation and Breakdown, *J. Am. Chem. Soc.* **1968**, 90, 6795-6803.

[30] Sartori, G.; and Savage, D. W. Sterically Hindered Amines for CO_2 Removal from Gases, *Ind. Eng. Chem. Fundam.,* **1983**, 22, 239-249.

[31] Donaldson, T. L.; and Nguyen, Y. N.; Carbon Dioxide Reaction Kinetics and Transport in Aqueous Amine Membranes, *Ind. Eng. Chem. Fundam.,* **1980**, 19, 260-266.

[32] Xu, X. C.; Song, C. S.; Andresen, J. M.; Miller, B. G.; and Scaroni, A. W. Novel Polyethylenimine-Modified Mesoporous Molecular Sieve of MCM-41 Type as High-Capacity Adsorbent for CO_2 Capture, *Energy Fuels* **2002**, 16, 1463-1469..

[33] Xu, X.; Song, C.; Miller, B.G.; and Scaroni, A.W. Influence of Moisture on CO_2 Separation from Gas Mixture by a Nanoporous Adsorbent Based on Polyethylenimine-Modified Molecular Sieve MCM-41, *Ind. Eng. Chem. Res.* **2005**, 44, 8113-8119.

[34] Son, W. J.; Choi, J. S.; and Ahn, W. S. Adsorptive Removal of Carbon dioxide using Polyethylenimine-Loaded Mesoporous Materials, *Microporous Mesoporous Mater.* **2008**, 113, 31-40.

[35] Chen, C.; Yang, S. T.; Ahn, W. S.; and Ryoo, R. Amine-Impregnated Silica Monolith with a Hierarchical Pore Structure: Enhancement of CO_2 Capture Capacity, *Chem. Commun.* **2009**, 24, 3627-3629.

[36] Ma, X.; Wang, X.; and Song, C. “Molecular Basket” Sorbent for Separation of CO_2 and H_2S from Various Gas Streams, *J. Am. Chem. Soc.* **2009**, 131, 5777-5783.

[37] Yue, M. B.; Sun, L. B.; Cao, Y.; Wang, Z. J.; Wang, Y.; Yu, Q.; and Zhu, J. H. Promoting the CO_2 Adsorption in the Amine-Containing SBA-15 by Hydroxyl Group, *Micropor. Mesopor. Mater.* **2008**, 114, 74-81.

[38] Franchi, R. S.; Harlick, P. J. E.; and Sayari, A. Applications of Pore-Expanded Mesoporous Silica. 2. Development of a High-Capacity, Water-Tolerant Adsorbent for CO_2, *Ind. Eng. Chem. Res.* **2005**, 44, 8007-8013.

[39] Yue, M. B.; Chun, Y.; Cao, Y.; Dong, X.; and Zhu, J. H. Novel CO_2-Capturer Derived from the As-prepared SBA-15 Occluded by Template, *Adv. Funct. Mater.* **2006**, 16, 1717-1722.

[40] Leal, O.; Bolivar, C.; Ovalles, C.; Garcia, J. J.; and Espidel, Y. Reversible Adsorption of Carbon dioxide on Amine Surface-Bonded Silica Gel, *Inorg. Chim. Acta* **1995**, 240, 183-189.

[41] Huang, H. Y.; Yang, R. T.; Chinn, D.; and Munson, C. L. Amine-Grafted MCM-48 and Silica Xerogel as Superior Sorbents for Acidic Gas Removal from Natural Gas, *Ind. Eng. Chem. Res.* **2003**, 42, 2427-2433.

[42] Knowles, G. P.; Graham, J. V.; Delaney, S. W.; and Chaffee, A. L. Aminopropyl Functionalized Mesoporous Silica as CO_2 Adsorbents, *Fuel Process. Technol.* **2005**, 86, 1435-1448.

[43] Knofel, C.; Descarpenteries, J.; Benzaouia, A.; Zelenak, V.; Mornet, S.; Llewellyn, P.L.; and Hornebecq, V. Functionalized Micro-/Mesoporous Silica for the Adsorption of Carbon dioxide, *Microporous Mesoporous Mater.* **2007**, 99, 79-85.

[44] Wang, L.; Ma, L.; Wang, A.; Liu, Q.; and Zhang, T. CO_2 Adsorption on SBA-15 Modified by Amino Silane, *Chin. J. Catal.* **2007**, 28, 805-810.

[45] Zelenak, V.; Badanicova, M.; Halamova, D.; Cejka, J.; Zukal, A.; Murafa, N.; and Goerigk, G. Amine-Modified Ordered Mesoporous Silica: Effect of Pore Size on Carbon dioxide Capture, *Chem. Eng. J.* **2008**, 144, 336-342.

[46] Hiyoshi, N.; Yogo, K.; and Yashima, T. Adsorption Characteristics of Carbon dioxide on Organically Functionalized SBA-15, *Microporous Mesoporous Mater.* **2005**, 84, 357-365.

[47] Belmabkhout, Y.; and Sayari, A. Effect of Pore Expansion and Amine Functionalization of Mesoporous Silica on CO_2 Adsorption Over a Wide Range of Conditions, *Adsorption* **2009**, 15, 318-328.

[48] Serna-Guerrero, R.; and Sayari, A. Modeling Adsorption of CO_2 on Amine Functionalized Mesoporous Silica. 2: Kinetics and Breakthrough Curves, *Chem. Eng. J.* **2001**, 161, 182-190.

[49] Serna-Guerrero, R.; Belmabkhout, Y.; and Sayari, A. Further Investigations of CO_2 Capture using Triamine-Grafted Pore-Expanded Mesoporous Silica, *Chem. Eng. J.* **2010**, 158, 513-519.

[50] Liang, Z.; Fadhel, B.; Schneider, C. J.; and Chaffee, A. L. Stepwise Growth of Melamine-Based Dendrimers into Mesopores and their CO_2 Adsorption Properties *Microporous Mesoporous Mater.* **2008**, 111, 536-543.

[51] Hicks, J. C.; Drese, J. D.; Fauth, D. J.; Gray, M. L.; Qi, G.; and Jones, C. W. Designing Adsorbents for CO_2 Capture from Flue Gas-Hyperbranched Aminosilicas Capable of Capturing CO_2 Reversibly, *J. Am. Chem. Soc.* **2008**, 130, 2902-2903.

[52] Drese, J. H.; Choi, S.; Lively, R. P.; Koros, W. J.; Fauth, D. J.; Gray, M. L. and Jones, C. W. Synthesis-Structure-Property Relationships for Hyperbranched Aminosilica CO_2 Adsorbents, *Adv. Func. Mater.* **2009**, 19, 3821-3832.

CHAPTER 3

SYNTHESIS AND CHARACTERIZATION OF MCM-41

This chapter presents the strategies used for development of novel MCM-41 support. The detailed experimental method used for synthesis of the same is discussed. Several characterization techniques used to examine the structural, thermal, morphological and CO_2 adsorption characteristics of the synthesized samples are discussed. This part of work has been published in ***Langmuir*** *29 (2013) 3491-3499.*

3.1. Introduction

Several synthesis strategies are discussed in literature in order to control the pore size of MCM-41. Changing the size of the hydrocarbon chain in alkyltrimethylammonium salts afforded MCM-41 with pores in the range of 2 to 4.5 nm **[1]**. Further increase in the pore size of around ~10 nm is achieved by addition of organic molecules such as dimethyl decylamine (DMDA) as expander agent during post-synthesis hydrothermal treatment **[2, 3]**. The detailed literature survey on amine functionalized mesoporous materials presented in Chapter 2 well documents the fact that pore-expanded supports serve as promising materials for amine loading. This underlines the urge for development of novel supports that will allow enhanced amine loading and demonstrate effective CO_2 capture characteristics. In view of this, an effort has been made in the present work to develop a novel strategy for controlling the pore size and pore volume of the bare support. This chapter describes the effect of aqueous ammonia in tuning the pore structural characteristics of MCM-41 directly during the synthesis by adjusting the composition of the reaction mixture. Based on the characterization results, mechanism for pore expansion process is also described.

3.2. Experimental section

3.2.1. Materials

All chemicals such as cetrimide (tetra decyl trimethyl ammonium bromide), 25% aqueous ammonia and tetraethyl orthosilicate (TEOS) were obtained from Merck and used as supplied. Cetrimide was used as the structure directing agent, 25% aqueous ammonia was used as the mineralizing agent and TEOS was used as the templating agent. CO_2 gas used for adsorption equilibrium measurements is 99% pure and is supplied by Assam Air Products, Guwahati, India.

3.2.2. Synthesis of MCM-41

Cetrimide (2 g) was weighed and added to a 250 mL beaker filled with 120 mL water. The cetrimide-water mixture was stirred for 30 minutes using a magnetic stirrer. Ensuring that cetrimide was homogeneously dispersed, 10 mL of TEOS was added, stirred for 5 minutes followed by the addition of 8 mL of 25% aqueous ammonia and again stirred for 5 min. The gel-mixture was then stirred for 12 hours. The beaker containing the gel-mixture was kept air-tight throughout the reaction period to prevent loss of aqueous ammonia. The as-synthesized white precipitate was filtered, washed with ethanol and distilled water. The obtained white product was subjected for drying around 12 hours to remove moisture. Calcination of the synthesized sample was carried out at 550 °C for 5 hours. In order to study the effect of aqueous ammonia on the synthesis of MCM 41, the same experiment was repeated with different quantities of 25% aqueous ammonia ranging from 1 mL to 9 mL, whereas rest of the procedure followed during synthesis remains unchanged. Accordingly, the samples were named as 1C, 3C, 5C, 7C, and 9C, where “numeric values” refer to the amount (in mL) of 25% aqueous ammonia added during synthesis and “C” refers to the calcined sample. Preceding the 12 hours stirring step in synthesis protocol, the mixture was stirred for 5 mins to make a note of initial pH of the mixture. After completion of the reaction, again the pH check was made and was noted down as final pH of the sol-gel mixture. Quick reference for the synthesis protocol is summarized in Table: 3.1.

Table 3.1. Experimental protocol for synthesis of samples 1C-9C

Sample name	CTAB (g)	Water (mL)	Stirring time (min)	TEOS (mL)	Stirring time (min)	Aq. ammonia (mL)	Stirring time (min)	pH initial	Stirring time (hrs)	pH final
1C	2	120	30	10	5	1	5	9.19	12	7.75
3C	2	120	30	10	5	3	5	9.50	12	9.29
5C	2	120	30	10	5	5	5	9.84	12	9.58
7C	2	120	30	10	5	7	5	9.97	12	9.93
9C	2	120	30	10	5	9	5	10.04	12	10.02

3.2.3. Material characterization

Thermo gravimetric analysis (TGA) was performed on a Mettler Toledo thermo gravimetric analyzer (TGA/SDTA 851® model). The measurements were carried out under nitrogen atmosphere with a heating rate of 10 °C/min. Nitrogen physisorption measurements were conducted on a Beckman Coulter surface area analyzer (COULTER SA 3100 model). The different MCM-41 materials were degassed at 105 °C for 4 hours prior to N_2 adsorption-desorption measurements. The specific surface area was calculated by BET (Brunauer, Emmett, and Teller) model. Pore size distribution was obtained through the BJH (Barrett, Joyner and Halenda) approach, and the total pore volume was estimated at a relative pressure of 0.99, assuming that full surface saturation has been achieved with nitrogen. X-ray diffraction (XRD) patterns of MCM-41 samples were carried out under air atmosphere at room temperature on a Bruker A8 advance instrument using Cu Kα (λ= 0.154 nm) radiation operating at 40 kV and 40 mA. The diffraction data were recorded in the 2θ range of 1 - 10° with a scanning rate of 0.02° (s^{-1}) and 0.5 s step size. FT-IR spectra were recorded between 4,000 and 450 (cm^{-1}) region using spectroscopic quality KBr powder with a Shimadzu IR affinity-1 model spectrometer. The morphologies of the synthesized samples were monitored by field emission scanning electron microscopy (FESEM) using a Zeiss Sigma model. EDX spectra are pictoriated by scanning electron microscopy (SEM) (Make: Zeiss Model: LEO1430VP). The amine content of the sample 1C was analyzed by an elemental analyser (Make: EuroEA Model: 3000). Dynamic light scattering (DLS) measurements for micelle size was carried out by particle size analyzer (Make: Beckman Coulter Model: DelsaTM Nano).

3.2.4. Calculation methods

The XRD (1 0 0) interplanar spacing, $d_{1\,0\,0}$ was calculated by equation 1.

$$d_{1\,0\,0} = \frac{1.5406}{2\sin\theta} \quad (1)$$

where, θ is the scanning diffraction angle corresponding to peak at (1 0 0) plane position. The pore center distance in hexagonal geometry, a (unit cell parameter), was then determined from equation 2

$$a = \frac{2}{\sqrt{3}} d_{100} \quad (2)$$

The primary mesopore diameter, d, was determined from the d_{100} X-ray spacing and the specific primary mesopore volume V_p of the ordered honeycomb structure by equation 3.

$$d = c\, d_{100} \left(\frac{\rho_s V_p}{1+\rho_s V_p}\right)^{\frac{1}{2}} \quad (3)$$

In the equation, c is a constant representing characteristics of the pore geometry (equal to 1.2125 for spherical as well as hexagonal pores), and ρ_s is the pore wall density (assumed to be 2.2 g/cc for silica with amorphous pore walls). The pore wall thickness, W, was estimated by equation 4.

$$W = a - d \quad (4)$$

3.2.5. CO_2 adsorption measurements

Adsorption equilibrium measurements of pure CO_2 for MCM 41 samples at four different temperatures (30 °C, 45 °C, 60 °C, 75 °C) were performed in the pressure range of 0-25 bar, using Rubotherm balance composed mainly of a magnetic suspension balance (MSB) and a network of valves, mass flow meters, temperature and pressure sensors. For performing adsorption experiment, the adsorbent was weighed and placed in a basket suspended by a permanent magnet through electromagnet. Prior to each adsorption equilibrium measurements, activation of the sample was done, with the aim to remove away any pre-adsorbed gas; by heating it at 110 °C under vacuum (and then a purge flow of helium).The out gassed adsorbent was exposed to pure CO_2 at constant temperature. The change in weight of the adsorbent sample with respect to pressure and temperature was measured continuously until the thermodynamic equilibrium was reached. Correction for the buoyancy effect was made to determine the excess adsorbed amount. The necessary buoyancy volume (volume of the suspension system and volume of the adsorbent) was obtained from

helium measurements at 30 °C in the pressure range of 0-25 bar, based on the assumption that helium penetrates in all open pores of the materials without being adsorbed. The temperature during adsorption measurements was held constant by using a thermostatic circulating fluid.

3.3. Results and discussion

3.3.1. Proposed mechanism for pore-expansion

When cetrimide is dissolved in water above its critical micelle concentration, hexagonal arrangement of cylindrical micelles of the surfactant is ordered in the reaction medium through “Liquid crystal templating mechanism” **[4]**. In the nucleation process of synthesis of MCM 41, aqueous ammonia acts as the mineralizing agent and upon its addition in the reaction mixture, hydrolysis of inorganic siliceous source takes place followed by the production of small silicate oxy-anions. These silicate oxy-anions diffuse towards the surface of the cylindrical micelles as a result of electrostatic attractions. As the quaternary ammonium hydrophilic parts (in cetrimide) bestow overall positive charge (N^+) on the surface of the micelles, silicate oxy-anions (SiO^-) tend to arrange themselves around these micelles by electrostatic interactions (N^+ SiO^-). Therefore the concentration of silicate oxy-anions at the surface of the micelles rapidly increases. And then, the silicate oxy-anions start to condense with each other, thereby forming a monolayer of amorphous silica in the form of siloxane bridges around the micelles.

The proposed mechanism for pore expansion process is described in Figure 3.1. The amount of aqueous ammonia added during the synthesis is found to play a key role in the pore expansion process. It is important to have a look at the variation in the pH condition of the reaction mixture during initial and final stage of the synthesis (Table 3.1). When 1 mL of aqueous ammonia is used for the synthesis, pH is observed to change from 9.19 to 7.75, while in the other cases, significant difference in the initial and final pH condition is not observed. This is due to the utilization of maximum amount of ammonia for hydrolysis and

condensation reaction of the silica source in the case of 1C. In rest of the cases, apart from ammonia being used as the mineralizing agent, there still remains sufficient ammonia to maintain the pH condition. This remaining aqueous ammonia is also found to show some pronounced effect in reducing the size of the micelle. This reduction in size of the micelle is due to the fact that there exhibits a shrinkage phenomenon of hydrophobic chain of the surfactant molecules when exposed to higher alkaline conditions. Also subsequent reduction in the aggregation number of the surfactant monomer to form the micelle structure at higher pH conditions leads to reduction in size of the micelle which in turn results in the reduced pore size of the bare support after calcination **[5]**.

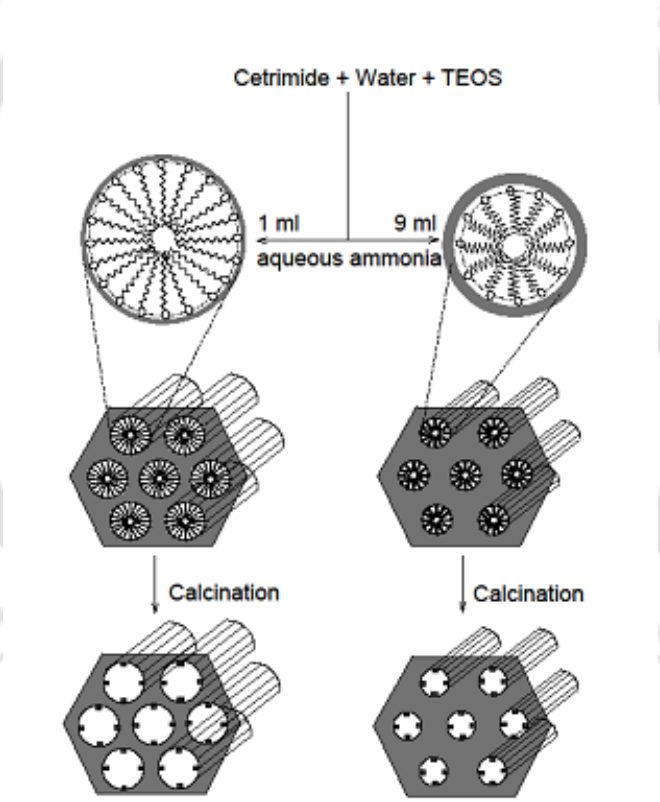

Figure 3.1. Proposed mechanism for pore-expansion process

3.3.2. N_2 adsorption-desorption analysis

The nitrogen adsorption/desorption isotherms and pore size distributions of the prepared MCM-41 samples are shown in Figure 3.2(a) and 3.2(b) respectively. The isotherms

observed for the different MCM-41 samples depict a typical type IV adsorption-desorption isotherm and exhibit remarkably sharp capillary condensation steps, which is the characteristic feature of the mesoporous material. As the amount of aqueous ammonia used for the synthesis is increased, the position of the capillary condensation step gradually shifts from the relative pressure of 0.75 to lower pressure range of about 0.16, indicating a systematic decrease in pore size. The adsorption isotherm for the larger pore size MCM-41 (1C) features a narrow type 1 hysteresis loop with parallel adsorption and desorption branches **[6, 7]**, whereas adsorption isotherms for samples with lower pore size (3C, 5C, 7C, 9C) were all found to be reversible as the adsorption curve almost coincided with the desorption curve. This indicates the more pronounced effect of capillary condensation in case of 1C suggesting larger pore size and pore volume. The total adsorbed amounts are significantly increased with increasing pore size, suggesting that the pore volumes are larger for larger size pores. The pore size distributions calculated through BJH method depicted in Figure 3.2(b) indicates that the synthesized MCM-41 samples contain only the mesopores not micropores **[8]**. All the MCM-41 samples maintain the same pattern of narrow pore size distribution exhibiting the average pore diameter under the range of 3.5-4 nm, except for sample 1C. The average pore diameter for sample 1C, is centered at 30 nm, which indicates the increase in pore size (particle size of the range 25-40 nm has been detected by DLS). We also tested the reproducibility of the properties of the synthesized samples and the uncertainity in the obtained results was estimated to be within 1%. N_2 adsorption-desorption isotherm pattern, surface area (1045 m^2/g) and pore volume (2.59 cc/g) are highly comparable with the recently reported surface area (1254 m^2/g) and pore volume (2.44 cc/g) of the adsorbent PE-MCM-41 synthesized through the most expensive swelling agents by post synthesis hydrothermal restructuring **[9]**. Hence, it can be observed that in the present case also remarkable increase in pore size and pore volume has been achieved without much decrease in the surface area. The BET surface areas of the samples, total pore volume and the average mesopore diameter calculated from the nitrogen adsorption data in the relative pressure range of 0.01–1, are summarized in Table 3.2.

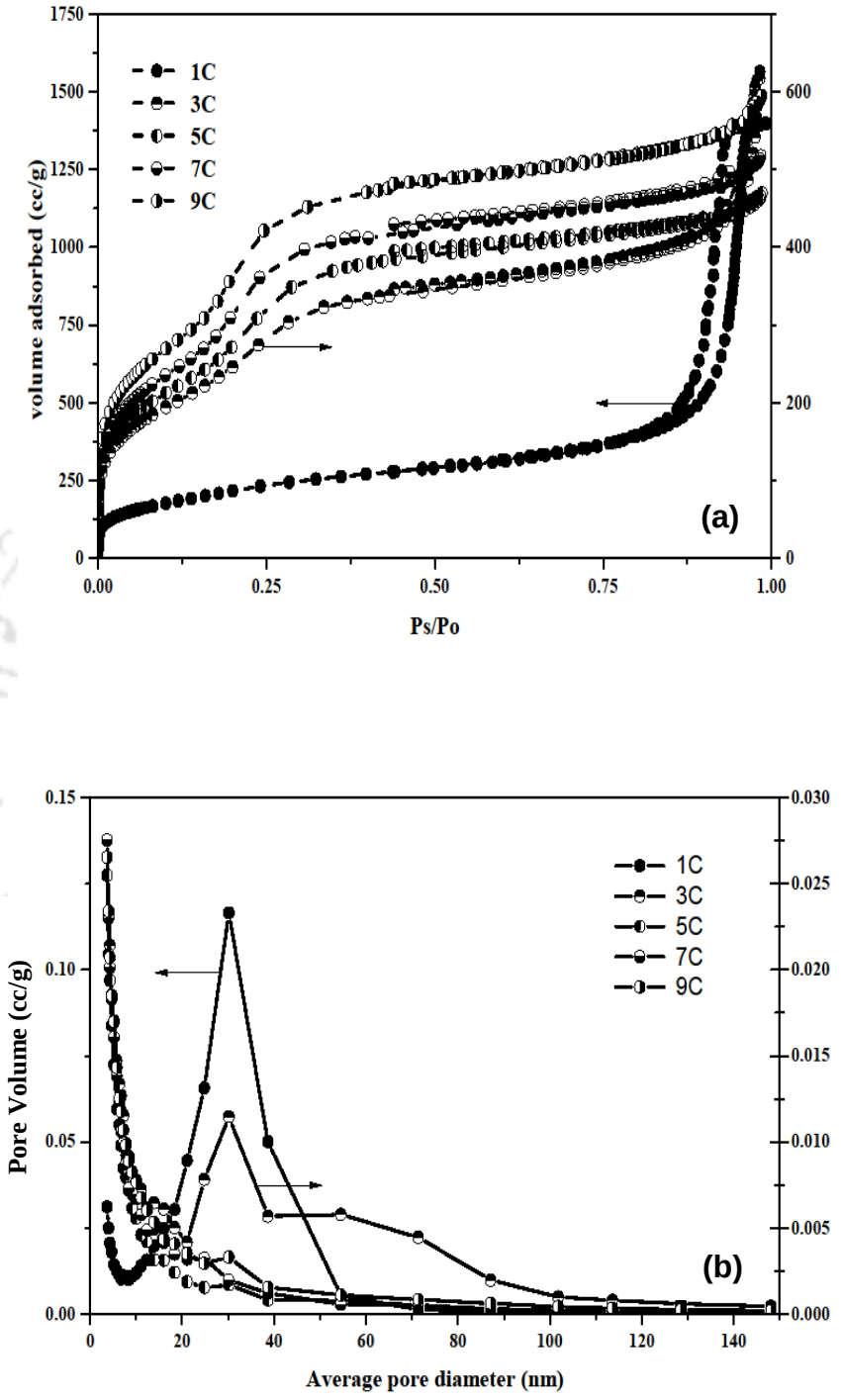

Figure 3.2 (a) Nitrogen adsorption-desorption isotherms of samples 1C-9C, (b) BJH pore size distribution profile for samples 1C-9C.

Table 3.2. Structural properties of samples 1C-9C

S:NO	Sample name	Surface area (m^2/g)	Pore volume (cc/g)	Pore diameter (BET) (nm)	Interplanar spacing d_{100} (nm)	Pore center distance a (nm)	Primary mesopore diameter (XRD) d_p (nm)	Pore wall thickness w (nm)
1	1C	1045.21	2.5882	30	4.902#	5.660#	5.484 #	0.176#
2	3C	1065.15	0.9666		4.572	5.279	4.573	0.705
3	5C	1103.78	0.7932	3.5-4	3.803	4.391	3.678	0.713
4	7C	1130.47	0.7914		3.433	3.964	3.319	0.645
5	9C	1204.13	0.7902		3.232	3.732	3.123	0.608

Weak peak on XRD spectrum, d_{100}, d_p, w is inaccurate.

3.3.3. XRD analysis

XRD spectra for all the MCM-41 samples are displayed in Figure 3.3. Only one low-angle peak for d_{100} plane corresponding to the mesophase is observed in the samples 1C, 3C and 5C. This might be due to the fact that, since the materials are not crystalline at the atomic level, no reflections at higher angles are observed **[10]**. Whereas, the XRD patterns for samples 7C and 9C are reflected with very sharp intense diffractograms and at least three well pronounced peaks (1 0 0), (1 1 0), and (2 0 0) indicating the presence of well resolved hexagonally arranged pore geometry and high structural ordering of the MCM-41 materials. The quality of the samples, as evaluated from the width and intensity of the main peaks, increases with the amount of aqueous ammonia added during formation of MCM 41. Hence, it is clear that the samples 1C, 3C and 5C seem to have a pore system less ordered than 7C and 9C. Despite of the fact, sample 1C possesses poorly ordered structure; it exhibited higher CO_2 adsorption capacity at higher pressure conditions, when compared to the sample 9C. This is due to the broader pore size distribution and higher pore volume observed in BET analysis.` It is important to be taken in to consideration that PE-MCM 41 synthesized by Sayari and co-workers also exhibited less intense (1 0 0) peak and poor structural order, inspite of its better CO_2 adsorption performance than conventional MCM-41. It is mentioned that, the reason for this unusual behavior might be due to the increase in pore size after expansion **[9]**. The gradual shift in main peak (1 0 0) from left to right i.e.to higher diffraction

angles observed in the whole XRD spectra reveals that pore size is decreased with increase in amount of aqueous ammonia added during synthesis. The reason for this shift as discussed earlier is due to the shrinkage phenomenon of the micelles at higher alkaline pH conditions. The values of the XRD unit cell parameters are listed in Table 3.2. In general, structural disordering limits the application of XRD to detect the accurate d_{100} spacing value **[3]**. Due to this fact, the pore diameter calculated for sample 1C from XRD is much smaller than that of BET.

The interplanar spacing d_{100} and the primary mesopore diameter tend to decrease with respect to increase in the amount of aqueous ammonia added during the synthesis of different MCM 41 samples **[11]**. This decreasing trend observed here (Table 3.2) is in good agreement with the results obtained from BET analysis, which proves that pore size is decreased enormously at higher alkaline pH conditions. This decrease is similar to that of the experimental results reported in literature **[12-14]**. Pore center distance (*a*) also exhibits downturn behavior, which in turn suggests that pore size is gradually shifted towards lower values. When 1 mL aqueous ammonia is added in the reaction mixture, precipitation of silica took place after 6 hours. This indicates the slow rate of hydrolysis and polycondensation resulting in the formation of thinner layer of amorphous solid silica phase around the micelles **[15]**. For rest of the samples, higher degree of hydrolysis and polycondensation occurs resulting in increased values of wall thickness. Besides sample 1C, all others exhibit almost similar structural characteristics (Table 3.2). Instead of analyzing all the samples possessing similar characteristics, we have chosen sample 1C and 9C for all further analysis.

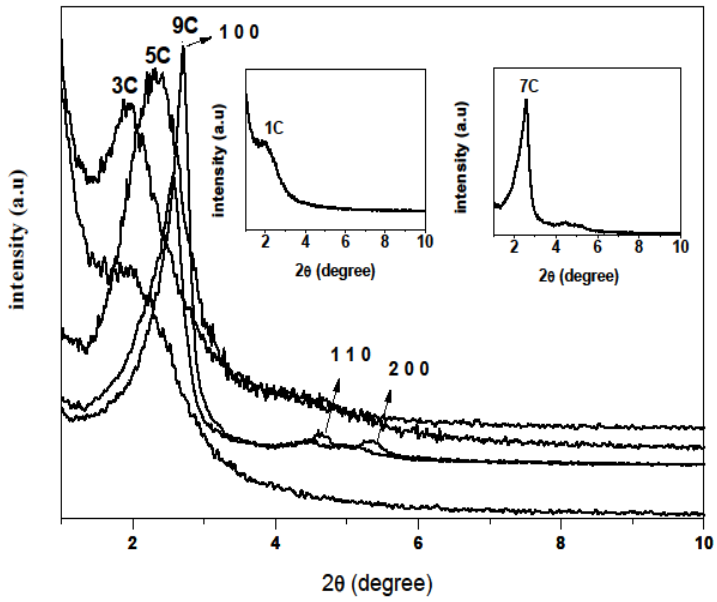

Figure 3.3. X-ray diffractograms for samples 1C-9C.

3.3.4. Thermo-gravimetric analysis

Thermo gravimetric analysis of the samples 1C, 9C, 1UC, 9UC (where "UC" refers to uncalcined sample) and the surfactant cetrimide are shown in Figure 3.4. It can be observed from the TGA profile of cetrimide that almost all the weight loss occurs between 200 and 300 °C. This is due to the decomposition of hydrocarbon chain present in the surfactant. Maximum weight loss in the above mentioned temperature range corresponds to decomposition of about 95% of the surfactant. Also, it can be noticed that complete degradation of the surfactant takes place at around 550 °C. Hence, calcination temperature was maintained at 550 °C in the present work for complete removal of the surfactant from the synthesized samples. The as-synthesized MCM-41 sample shows the weight loss in three distinct regions. The removal of water molecules physisorbed on the external surface of the materials causes the first region of weight loss (4-5%) between 50 °C and 100 °C. The

second region of weight loss (36%) between 200 °C and 550 °C is attributed to the breaking of the hydrocarbon chain in the surfactant and loss of water that is generated from the condensation of adjacent silanol groups **[16]**. The third region of weight loss (2%) between 550 °C and 900 °C is possibly due to degradation of germinal and vicinal silanol groups present in the samples 1UC and 9UC **[17]**. MCM-41 calcined at 550 °C shows two regions of weight loss and only about 2% of weight loss is observed after 100 °C, which indicates that the surfactant is completely removed from the MCM-41.

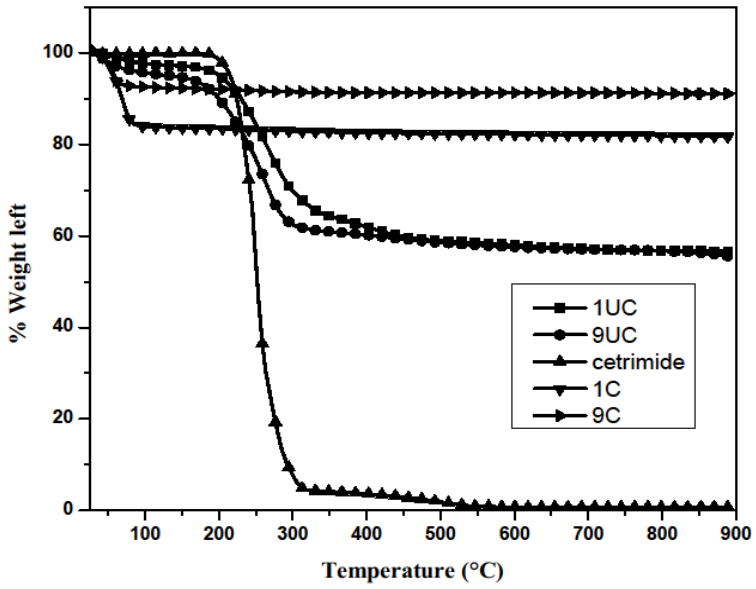

Figure 3.4. Thermo gravimetric analysis

3.3.5. FTIR and EDX analysis

Figure 3.5(a&b) shows the FTIR spectra of the as-synthesized and calcined samples of MCM-41. The as-synthesized sample shows two very sharp intense bands at 2,924 and 2,852 (cm^{-1}) that are due to the C-H stretching of the hydrocarbon chain of the surfactant molecules (Fig.3.5(a)). The corresponding bending vibration mode is observed at 1,477 (cm^{-1}). In the hydroxyl region (3,600-3,200 (cm^{-1})), a broad band is seen around 3,143 (cm^{-1}), which is attributed to surface silanols and adsorbed water molecules. The absorption bands close to 1,735 (cm^{-1}) are due to the bending vibration of adsorbed water molecules. The

asymmetric stretching vibrations of Si-O-Si are observed by the absorption bands at 1,066 and 1,228 (cm^{-1}). The band at 952 (cm^{-1}) is attributed to Si-OH vibrations. The absorption peaks around 460 to 795 (cm^{-1}) are mainly due to bending vibration of Si-O-Si bonds and the band at 795 (cm^{-1}) may also correspond to free silica **[16]**. The spectrum of the sample calcined at 550 °C also shows the similar bands and the bond stretching properties. All the bands belonging to the organic groups disappeared for the sample calcined at 550 °C (Fig.3.5(b)), which proves that surfactant has been removed completely from the samples during the process of calcination. The FTIR results discussed so far, are in good agreement with EDX spectra shown in Figure 3.6. Fig.3.6(a, b) shows the EDX spectra of uncalcined samples 1UC and 9UC respectively. Existence of C and Br peaks are indicative of the presence of the surfactant. However, there is no existence of C and Br with corresponding calcined samples 1C and 9C as shown in Fig.3.6(c, d). This further proves that the surfactant was totally removed during calcination.

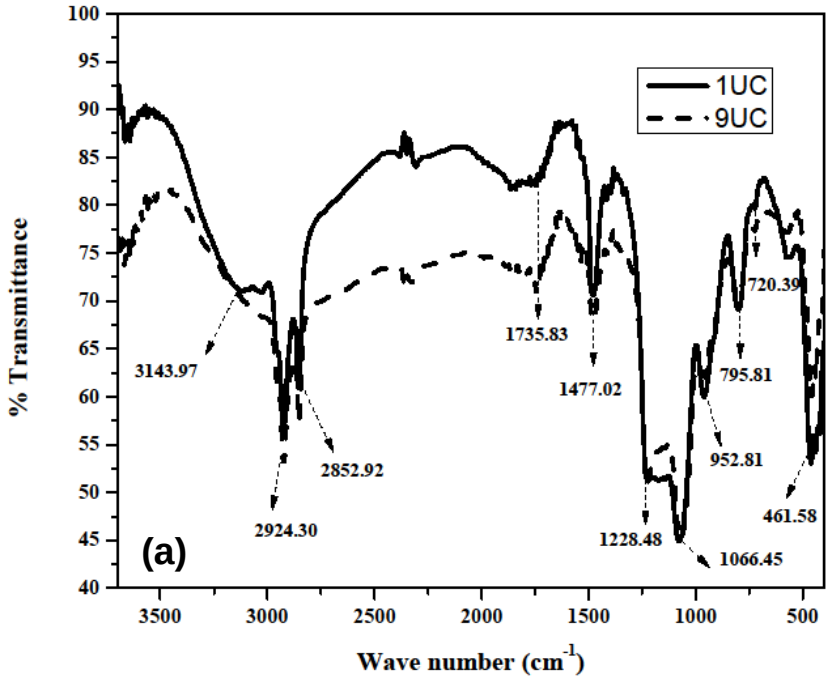

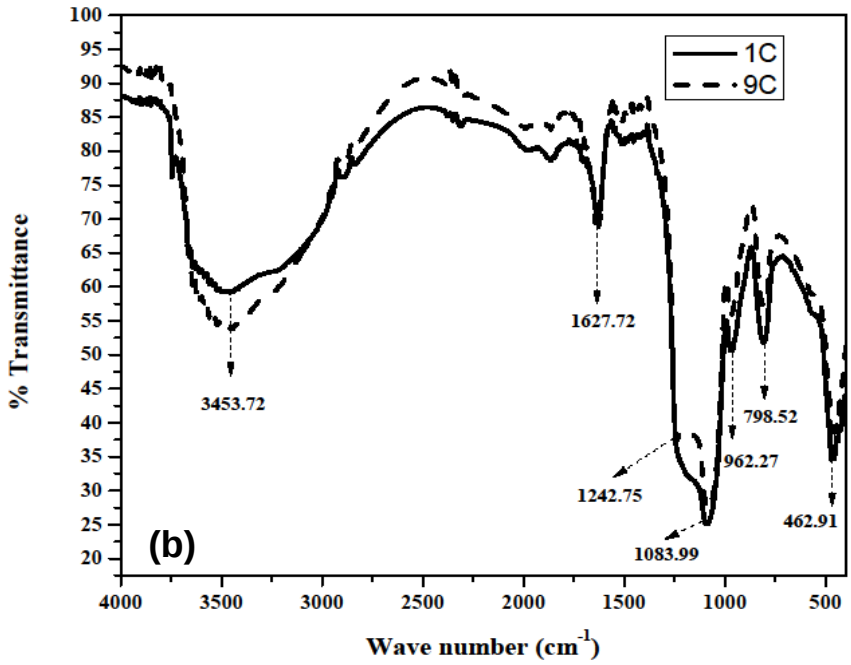

Figure 3.5. FTIR spectra for (a) as-synthesized samples 1UC and 9UC, (b) calcined samples 1C and 9C

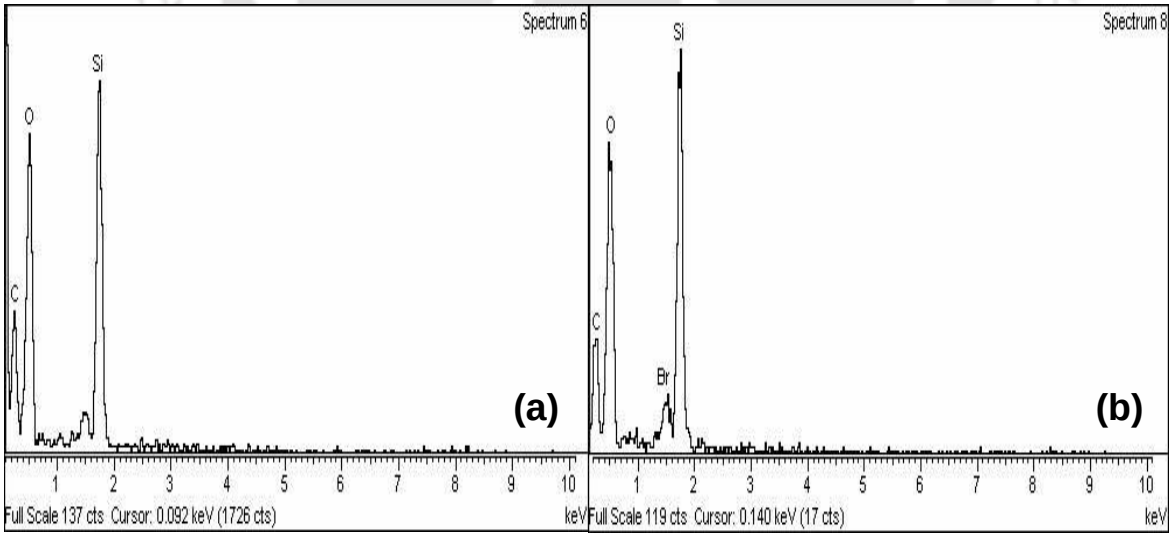

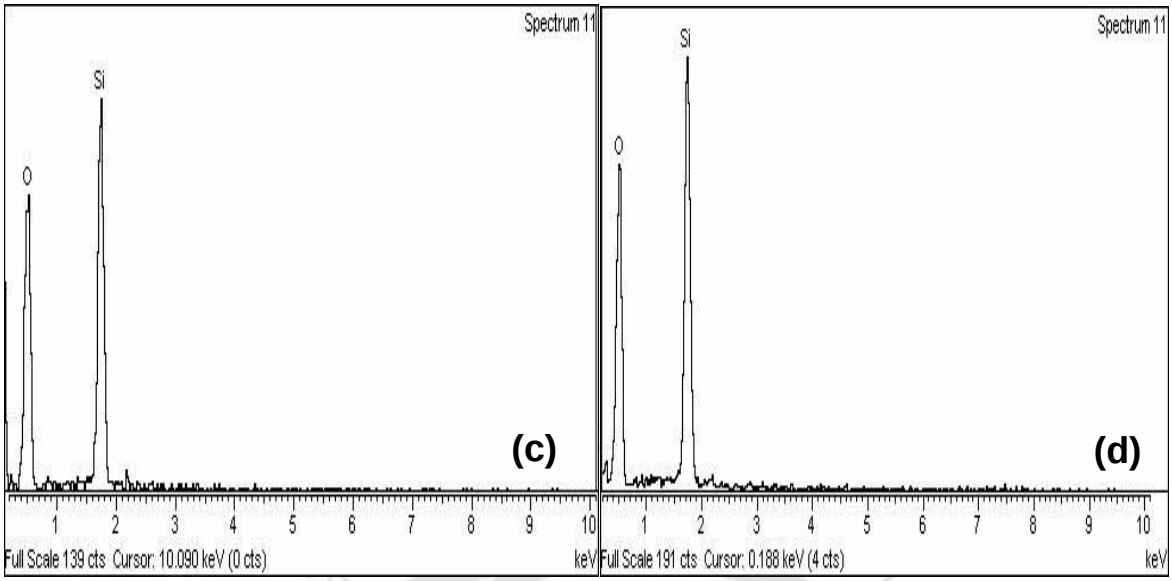

Figure 3.6. EDX spectra for (a) uncalcined sample 1UC, (b) uncalcined sample 9UC, (c) calcined sample 1C and (d) calcined sample 9C.

3.3.6. FE-SEM analysis

The morphology of samples 1C and 9C which are depicted by FE-SEM micrographs (Figure 3.7) reveals that the particles are spherical in shape **[18]**.

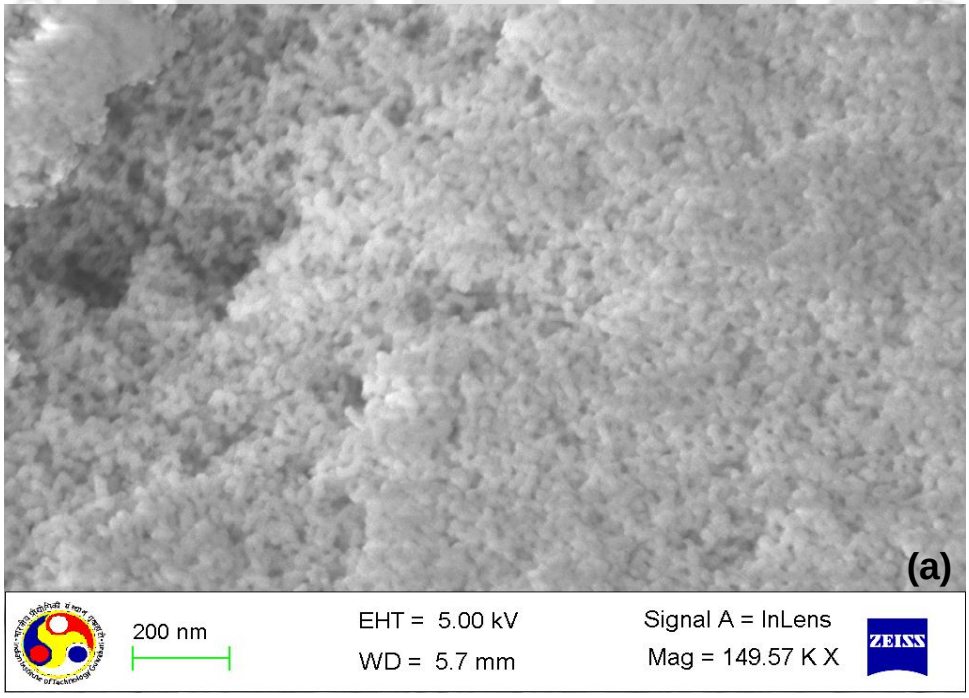

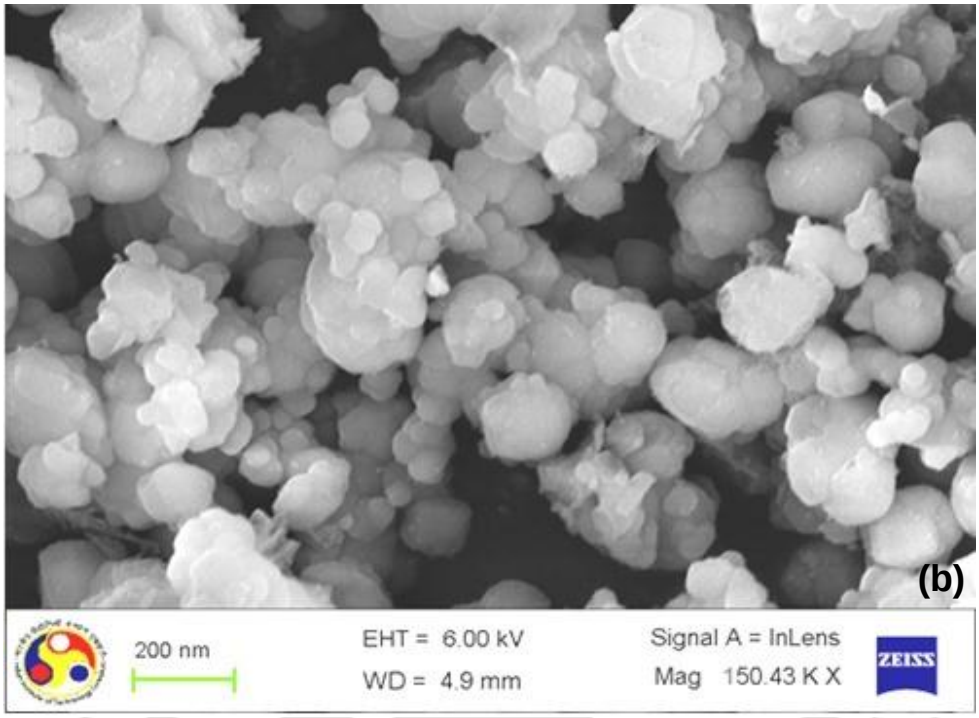

Figure 3.7. FESEM micrographs for (a) sample 1C and (b) sample 9C.

3.3.7. CO_2 adsorption analysis

The adsorption capacity measurements of CO_2 on to samples 1C and 9C were obtained at four different temperatures (30, 45, 60, 75 °C) and pressures ranging from 0-25 bar and the same is shown in Figure 3.8. The isotherms were found to be of Type I according to the IUPAC classification for adsorption isotherms. The adsorption-desorption isotherm curves coincided with each other, indicating that CO_2 adsorption-desorption process is reversible in nature when only physisorption occurs. The adsorption capacities (~2 mmol/g) of samples 1C and 9C ranging from low pressures to 5 bar are similar to each other. Hence it is further confirmed, that long range ordering of pores did not play any role in terms of adsorption capacities up to certain low pressure conditions irrespective of temperatures **[19]**. However, little lower adsorption capacity is exhibited by sample 9C than 1C starting from 10 bar pressure. This significant difference might have been reflected, owing to the fact that sample 1C possesses higher pore volume indicating more multi-layered adsorption when compared to sample 9C. However, the adsorption capacities of both the samples tend to decrease with respect to increase in temperature confirming that CO_2 adsorption is exothermic in nature.

The CO_2 adsorption equilibrium capacity (0.6 mmol/g, 1 bar, 30 °C) of large pore size sample 1C is again valid for great comparison with the literature data (~0.6-0.7 mmol/g, 1 bar, 25 °C) reported for both PE-MCM 41 and MCM-41 (with different pore size) by Sayari **[20]** and Seaton group **[21]** respectively**.** We also compared the adsorption capacity of sample 1C with a large number of well-known benchmark industrial adsorbents such as NoritAC, 13X and rapidly evolving hybrid materials such as IRMOFs **[22]**. The maximum adsorption capacity of these adsorbents is about 10, 7.1 and 20.5 mmol/g respectively at a pressure of ~20 bar. The adsorption capacity of sample 1C is ~5.1 mmol/g at 20 bar. Even though, sample 1C exhibited the lowest adsorption capacity, CO_2 adsorption capacity kept increasing with respect to pressure due to capillary condensation in the space available within the mesopores. Hence, sample 1C can also be possibly utilized for CO_2 capture under high pressure conditions.

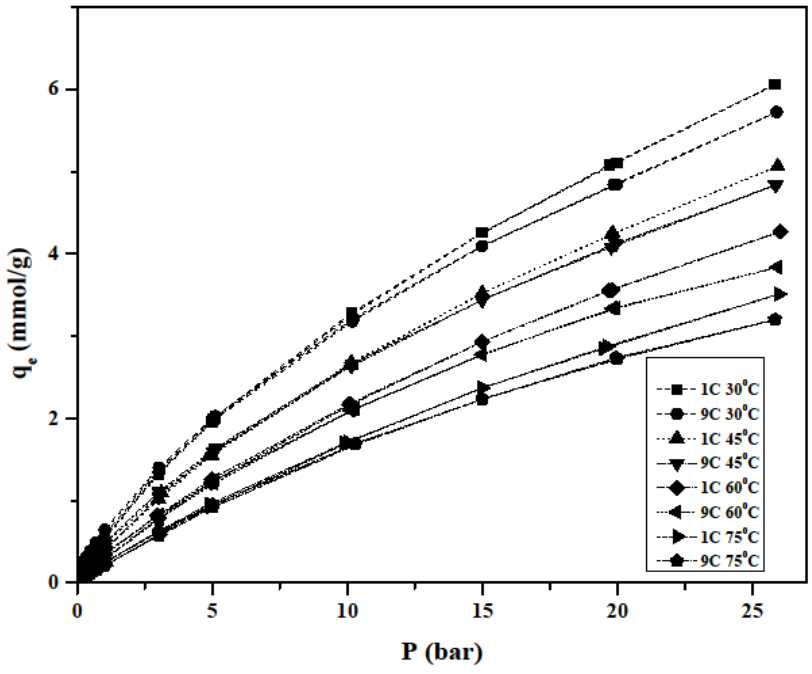

Figure 3.8. CO_2 adsorption-desorption isotherms of samples 1C and 9C

3.4. Conclusions

A suitable experimental strategy to fabricate larger pore size MCM-41 without using any swelling agent is developed. It was found that pH plays very important role in governing the pore size of MCM-41 by creating potential impact on the micelle behaviour. This is reflected from the average pore size (30 nm) of sample 1C. Therefore, MCM-41 prepared with 30 nm can act as a promising support material for amine tethering process and demonstrate effective CO_2 adsorption characteristics.

3.5. References

[1] Liu, L.; Zhang, G.Y.; Dong, J.X. Large Pore Mesoporous MCM-41 Templated from Cetyltriethylammonium Bromide, *Chinese Chemical Letters*. **2004**, 15, 737-740.

[2] Blin, J.L.; and Su, B.L. Tailoring Pore Size of Ordered Mesoporous Silicas Using One or Two Organic Auxiliaries as Expanders, *Langmuir.* **2002,** 18, 5303-5308.

[3] Sayari, A.; Yong, Y.; Kruk, M.; and Jaroniec, M. Expanding the Pore Size of MCM-41 Silicas: Use of Amines as Expanders in Direct Synthesis and Post synthesis Procedures, *J. Phys. Chem. B*. **1999**, 103, 3651–3658.

[4] Vartuli, J.C.; Kresge, C.T.; Leonowicz, M.E.; Chu, A.S.; McCullen, S.B.; Johnson, I.D.; and Sheppardt, E.W. Synthesis of Mesoporous Materials: Liquid-Crystal Templating versus Intercalation of Layered Silicates, *Chem. Mater*. **1994,** 6, 2070-2077.

[5] Ghosh, P.; Colloid and Interface Science, Kindley Edition, India.

[6] Kruk, M.; Jaroniec, M.; and Sayari, A. Application of Large Pore MCM-41 Molecular Sieves to Improve Pore Size Analysis Using Nitrogen Adsorption Measurements, *Langmuir*. **1997**, 13, 6267-6273.

[7] Huo, Q.; Margoleses, D.I.; and Stucky, G.D. Surfactant Control of Phases in the Synthesis of Mesoporous Silica-Based Materials, *Chem. Mater.* **1996**, 8, 1147-1160.

[8] Saha, B.; and Ghoshal, A.K. Model-free Kinetics Analysis of Decomposition of Polypropylene Over Al-MCM-41, *Thermochimica Acta*. **2007**, 460**,** 77-84.

[9] Gorji, A.H.; Belmabkhout, Y.; and Sayari, A. Polyethylenimine-Impregnated Mesoporous Silica: Effect of Amine Loading and Surface Alkyl Chains on CO_2 Adsorption, *Langmuir*. **2011**, 27, 12411–12416.

[10] Huang, L.; Huang, Q.; Xiao, H.; and Eic, M. Effect of Cationic Template on the Adsorption of Aromatic Compounds in MCM-41, *Microporous and Mesoporous Mater*. **2007**, 98, 330-338.

[11] Qiao, S.Z.; Bhatia, S.Z.; and Zhao, X.S. Prediction of Multilayer Adsorption and Capillary Condensation Phenomena in Cylindrical Mesopores, *Microporous and Mesoporous Mater.* **2003**, 65, 287–298.

[12] Kruk, M.; Jaroniec, M.; and Sayari, A. Adsorption Study of Surface and Structural Properties of MCM-41 Materials of Different Pore Sizes, *J. Phys. Chem. B*. **1997**, 101, 583-589.

[13] Feuston, B.P.; and Higgins, J.B. Model Structures for MCM-41 Materials: A Molecular Dynamics Simulation, *J. Phys. Chem.* **1994**, 98, 4459-4462.

[14] Kruk, M.; Jaroniec, M.; Sakamoto, Y.; Terasaki, O.; Ryoo, R.; and Ko, C.H. Determination of Pore Size and Pore Wall Structure of MCM-41 by Using Nitrogen Adsorption, Transmission Electron Microscopy, and X-ray Diffraction, *J. Phys. Chem. B*. **2000**, 104, 292-301.

[15] Blin, J.L.; Otjacques, C.; Su, H.B. Kinetic Study of MCM-41 Synthesis, *International Journal of Inorganic Materials*. **2001**, 3, 75-86.

[16] Monash, P.; and Pugazhenthi, G.; Investigation of Equilibrium and Kinetic Parameters of Methylene Blue Adsorption onto MCM-41, *Korean J. Chem. Eng*. **2010**, 27, 1184-1191.

[17] Kim, J.M.; Chang, S.M.; Kong, S.M.; Kim, K.S.; Kim, J.; and Kim, W. Control of Hydroxyl Group Content in Silica Particle Synthesized by the Sol-Precipitation Process, *Ceramics International.* **2009**, 35, 1015-1019.

[18] Mortera, R.; Onida, B.; Fiorilli, S.; Cauda, V.; Brovarone, C.V.; Baino, F.; Verne, E.; and Garrone, E. Synthesis and Characterization of MCM-41 spheres inside bioactive glass-ceramic scaffold, *Chem. Eng. J*. **2008**, 137, 54-61.

[19] Jiang, D.; Gao, J.; Yang, J.; Su, W.; Yang, Q.; and Li, C. Mesoporous Ethane-Silicas Functionalized with Trans-(1R,2R)-diaminocyclohexane: Relation between Structure and Catalytic Properties in Asymmetric Transfer Hydrogenation, *Microporous Mesoporous Mater*. **2007**, 105, 204–210.

[20] Serna-Guerrero, R.; Belmabkhout, Y.; and Sayari, A. A Semi-Empirical Equilibrium Model for CO_2 Adsorption on Amine-Functionalized Mesoporous Silica, *Chem. Eng. J*. **2010**,161, 173–181.

[21] He, Y.; and Seaton, N.A. Heats of Adsorption and Adsorption Heterogeneity for Methane, Ethane, and Carbon Dioxide in MCM-41**,** *Langmuir.* **2006,** *22,* 1150-1155.

[22] Belmabkhout, Y.; Guerrero, R.; and Sayari, A. Adsorption of CO_2 from Dry Gases on MCM-41 Silica at Ambient Temperature and High Pressure: Pure CO_2 Adsorption, *Chem. Eng. Sci.* **2009**, 64, 3721-3728.

CHAPTER 4

SURFACE HETEROGENEITY FOR CO_2 CAPTURE ON MCM-41

The chapter provides a new insight into details of role of surface characteristics of MCM-41 on CO_2 adsorption phenomenon. Infrared spectroscopy analysis is carried out in order to get an insight into various surface functionalities that can exist on MCM-41. Thereafter, an approach based on isotherm modelling is provided to derive the information about the various prevailing characteristics of such silica surface and quantitatively determine the individual contribution of surface groups of silica to the overall adsorption capacity. A patch-wise topography hypothesis is proposed for CO_2 adsorption on porous silica and the same is validated for N_2 adsorption. Theory for Langmuir, Sips, Toth and Langmuir dual-site models are also discussed.

4.1. Introduction

For porous silica prepared under ideal conditions, it is expected that (SiO_4) tetrahedra are stacked in an ordered design which is repeated regularly, so that a regular distribution of the hydroxyls at the silica surface is expected **[1]**. However, in reality, porous silica materials are quite heterogeneous due to irregular packing and incomplete condensation during the synthesis process **[2]**. Surface defects which are mainly borne out by incomplete condensation polymerization results in the existence of multiple sites on the silica surface, which could be exposed ions, oxygen vacancies, silanol groups, and siloxane linkages **[3-5]**. The heterogeneity phenomenon influences the adsorption characteristics of porous materials **[6-9]**. This part of work provides a new insight into details of role of surface characteristics of MCM-41 on adsorption phenomenon by using CO_2. For this study, we have considered the silica surface of our pore-expanded material (MCM-41) (surface area: 1045 m^2/g, pore volume: 2.58 cc/g and average pore size: 30 nm). DRIFTS analysis is carried out in order to get an insight into various surface functionalities that can exist on MCM-41. Based on the outcome, an approach is provided to derive the information about the various prevailing characteristics of such silica surface and quantitatively determine the individual contribution of surface groups of silica to the overall adsorption capacity. For this study, CO_2 adsorption isotherm data obtained for MCM-41 (1C) at four different temperatures (30, 45, 60, 75 °C) and pressures ranging from 0-25 bar (shown in Figure 3.8) were used.

4.2. Experimental section

4.2.1. Materials

The details of materials used for synthesis of MCM-41 have been described in section 3.2.1. N_2 gas used for adsorption equilibrium measurements is 99% pure and was supplied by M/S Assam Air Products, Guwahati, India.

4.2.2. Synthesis of MCM-41

The synthesis procedure for MCM-41 has been described in section 3.2.2.

4.2.3. Material characterization

DRIFT spectra were recorded in the mid IR region (4000−450 cm^{-1}) using Shimadzu IR Affinity-1 model spectrometer with a resolution of 40 scans per run.

4.2.4. CO_2 and N_2 adsorption measurements

Both CO_2 and N_2 adsorption measurements were conducted by the similar procedure described in section 3.2.5.

4.2.5. Determination of isotherm model parameters

Recently several authors suggested that transformation of the isotherm models in to their linearized form apparently generate real problems and errors arising from the complexities, leading to the violation of theories behind the isotherms **[10]**. So isotherm parameter sets were determined by nonlinear regression using an iterative method with the aid of Matlab *version 7*. This provides a mathematically rigorous method for determining isotherm parameters using the original form of the isotherm equation.

4.3. Theory

4.3.1. Mathematical models of adsorption isotherms

A wide variety of equilibrium isotherm models (Langmuir, Freundlich, Brunauer-Emmett-Teller, Redlich-Peterson, Dubinin-Radushkevich, Temkin, Toth, Koble-Corrigan, Sips, Khan, Hill, Flory-Huggins and Radke-Prausnitz isotherm), have been formulated till date to describe the experimental sorption data **[11,12]**. Among the existing theoretical adsorption models, Langmuir is the simplest one to describe the adsorption on homogeneous surface. However, as mentioned earlier in the main text, practical adsorbents are not ideally homogeneous. Hence, in order to obtain a deeper insight into the nature of the surface, models which strongly describe surface heterogeneity such as Sips, Toth and Langmuir-multi site models were also selected to fit the equilibrium CO_2 and N_2 adsorption data **[13-20]**. The purpose of this work is to determine the individual contribution of surface groups of

silica to the overall adsorption capacity. In view of this, the simple isotherm models which take care of both surface heterogeneity and can quantitatively determine the adsorption capacity of different surface sites are considered. Despite, other isotherm models such as Freundlich or D-R isotherm models too accounts for surface heterogeneity, it is not possible to obtain information about individual adsorption capacity of different surface functionalities by these models. Based on this rationale, Langmuir-multi site model is given paramount importance in the present study.

Langmuir Equation is given by:

$$q_e = q_m \frac{bP}{1+bP} \tag{1}$$

where, q_m and b are Langmuir parameters representing maximum adsorption capacity and adsorption affinity respectively. q_e is the adsorption uptake at equilibrium and P is the pressure of the adsorbate **[21, 32]**.

Sips Equation is given by:

$$q_e = q_m \frac{bP^{1/n}}{1+bP^{1/n}} \tag{2}$$

where, n is a measure of the surface heterogeneity **[13]**.

Toth Equation is given by:

$$q_e = \frac{n_s bP}{\left(1+(bP)^t\right)^{1/t}} \tag{3}$$

where, n_s and t are the characteristic parameter of the Toth model representing maximum adsorption capacity and surface heterogeneity respectively **[23]**.

Langmuir-multi site model is given by:

$$q_e \equiv \sum_{j=1}^{N} q_{m,j} \frac{b_j P}{1+b_j P} \quad (4)$$

where, $q_{m,j}$ and b_j represent the saturation capacity and affinity constant of site *j* **[18, 19]**.

4.3.2. Error calculation

To estimate the accuracy of the fit of the proposed model, an error function based on the normalized standard deviation was calculated using a method reported in the literature

$$\Delta q(\%) = \sqrt{\frac{\sum\left[\left(q_{\exp} - q_{model}\right)/q_{\exp}\right]^2}{N-1}} \text{ X } 100\% \quad (5)$$

Where, Δq (%) is the normalized standard deviation, q_{exp} and q_{model} are the experimental and calculated amounts of CO_2 adsorbed, and *N* is the number of data points available in uptake curve **[22]**.

4.3.3. Heat of adsorption

Heat of adsorption shows the enthalpy change before and after the adsorption process. Therefore, it is a measure of the strength of interaction between the adsorbent and the adsorbate.

Adsorption data at different temperatures allowed the calculation of the isosteric heat of adsorption (ΔH_{iso}) using the Clausius–Clapeyron equation **[24, 25]**.

$$\Delta H_{iso} = R \frac{dlnp}{d(1/T)}\Big|_{q_e} \quad (6)$$

Where *p* is pressure at constant equilibrium uptake, R is the universal gas constant and T is temperature.

4.4. Results & discussion

4.4.1. DRIFTS Analysis

Prior to recording the DRIFT spectra, MCM-41 is dehydrated at 150 °C in order to remove the physisorbed moisture. The spectrum is presented in two sections in Figure 4.1: (a) 4000-3000 cm^{-1} (hydroxyl region) and (b) 1500-700 cm^{-1} (siloxane region) to provide clarity for identifying different surface functionalities. The isolated silanol group, which is not H-bonded, shows a narrow absorption band at about 3731 cm^{-1} **[9]**. The broad absorption band observed thereafter in the hydroxyl region corresponds to the vicinal silanol groups, which are H-bonded **[9, 26, 27]**. The absorption band at 3598 and 3547 cm^{-1} is resulted from the superposition of hydrogen bonded OH groups **[9]**. However, it is difficult to distinguish the germinal silanols due to its overlapped peak position with that of isolated silanols. This is because, it is reported that the IR bands corresponding to OH stretch of geminal silanol groups differ by only 2 cm^{-1} to that of isolated silanol **[27]**. The absorption band observed in the 1300-1000 cm^{-1} region is assigned to the asymmetric stretching modes of Si-O-Si vibrational moiety **[28]**. The band identified at 828 cm^{-1} is attributed to the symmetric stretching vibration of Si-O-Si bridges **[29, 30]**. The bands observed at 968 and 775 cm^{-1} is due to the presence of dangling $Si\text{-}O^-$ groups and free silica in the surface of MCM-41 **[31, 32]**. Therefore, in accordance with the literature, incomplete condensation polymerization reaction during the synthesis of MCM-41 results in the existence of multiple sites on the silica surface, which are exposed ions, oxygen vacancies, silanol groups, and siloxane linkages and the schematic representation of the same is shown in Figure 4.2.

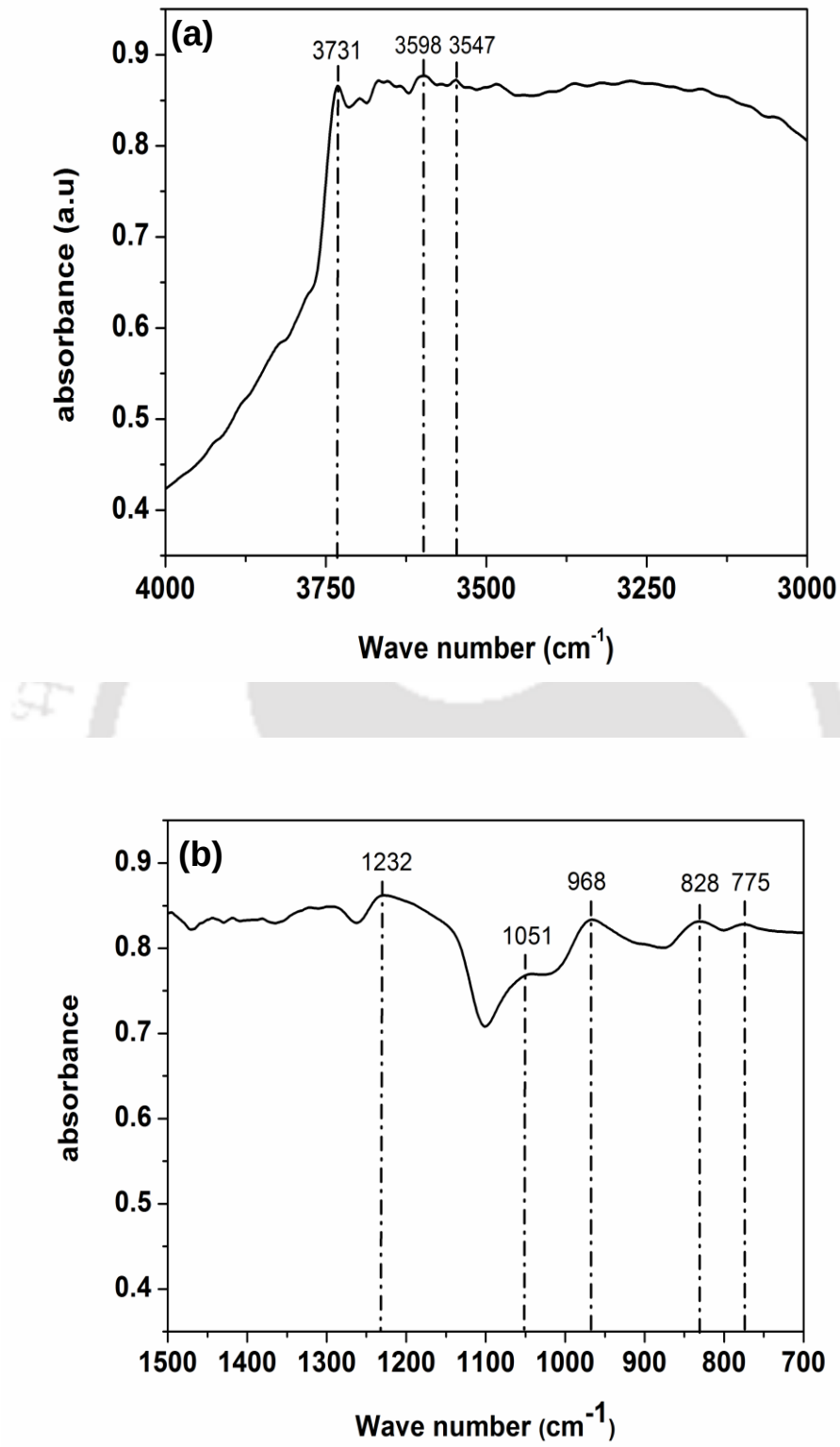

Figure 4.1. DRIFT spectra for MCM-41 in (a) hydroxyl region

(b) siloxane region

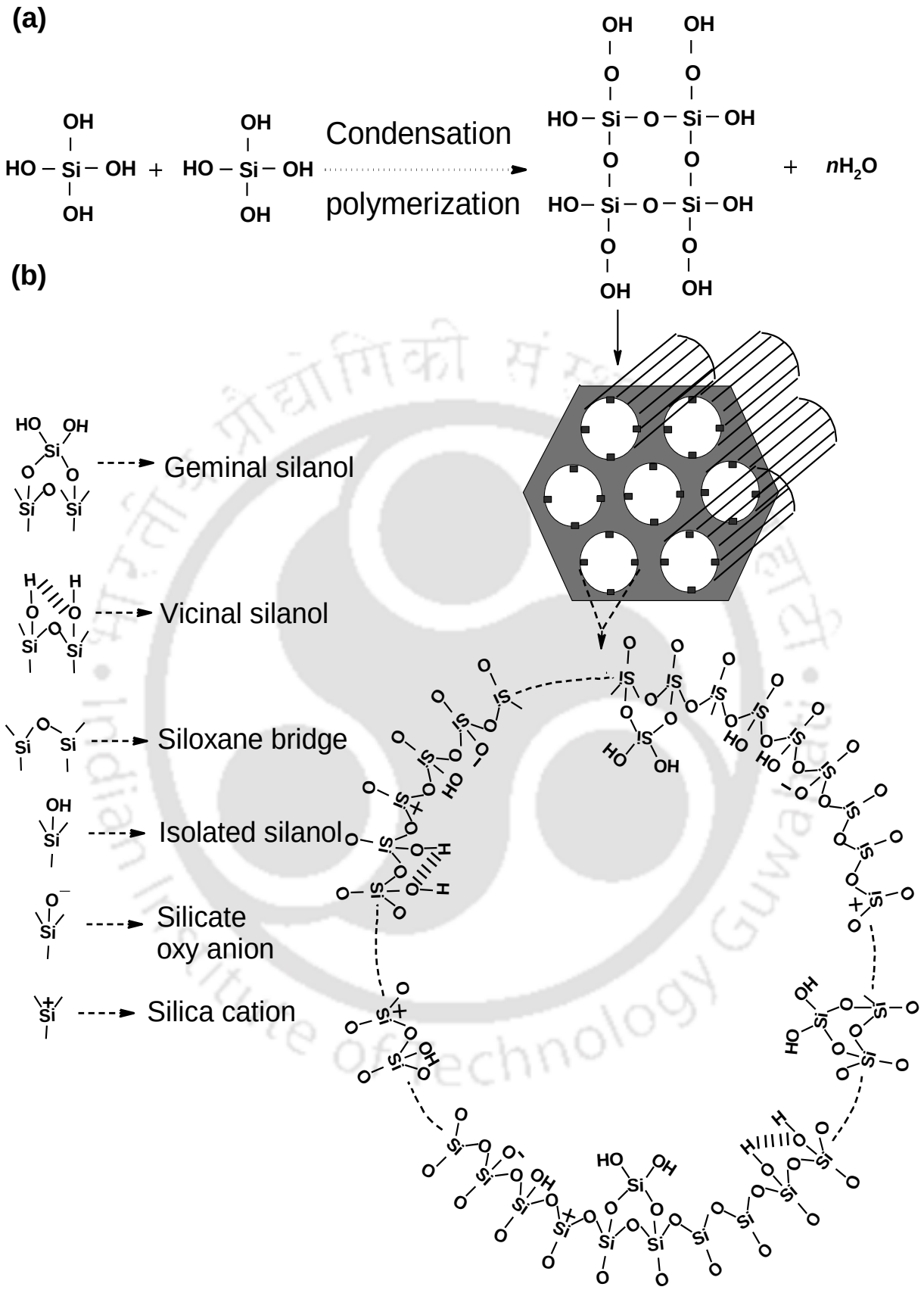

Figure 4.2. (a) Sol-gel reaction (b) Hypothetical cross-section of MCM-41.

4.4.2. Comparison of CO_2 adsorption isotherms

To understand the surface characteristics of MCM-41, the experimental CO_2 equilibrium data were fitted to Langmuir, Sips, Toth and Langmuir multi-site isotherm models which do provide information about nature of the surface **[33]**. Fig. 4.3 (a-d) shows a typical comparison of experimental adsorption data with the predicted values by different models (Langmuir, Sips, Toth and Langmuir multi-site) for CO_2 adsorption on MCM-41 at 30-75 °C and the corresponding model parameters are provided in Table 4.1. Error, Δq (%) for different isotherms are presented in Table 4.2. Among the four models, it is observed that Toth and Langmuir multi-site isotherm models adequately described the adsorption data throughout the entire range of pressure and temperature analyzed followed by Sips and Langmuir. The Langmuir adsorption model deviated to accurately describe the adsorption data, primarily because it fails to account for the surface roughness of the adsorbate and multi-layered adsorption phenomenon **[34]**. Sips model showed deviation mainly in small pressure regime due to the fact that, this model doesn't provide the correct Henry law limit **[35]**. In contrast, Toth and Langmuir multi-site models which better describe the surface heterogeneity fitted CO_2 adsorption equilibrium data well indicating that MCM-41 is heterogeneous in nature. This fact is further corroborated with the information provided by the model parameters.

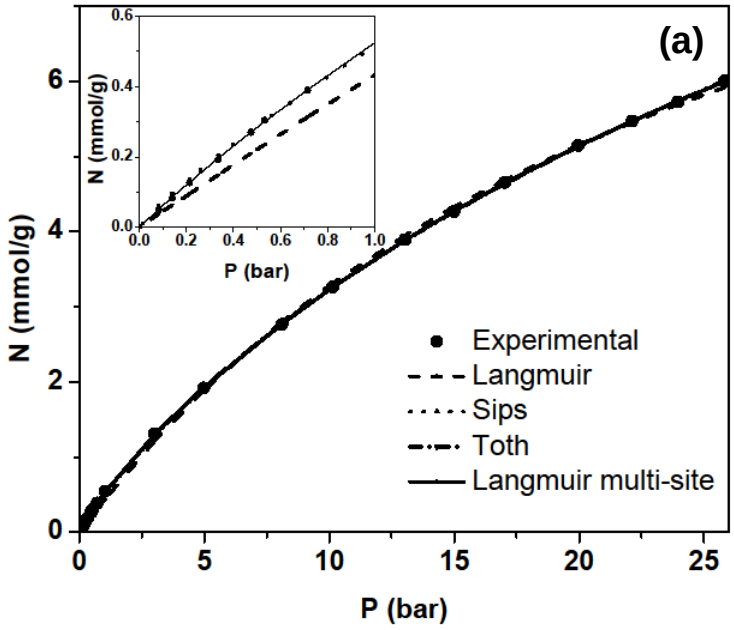

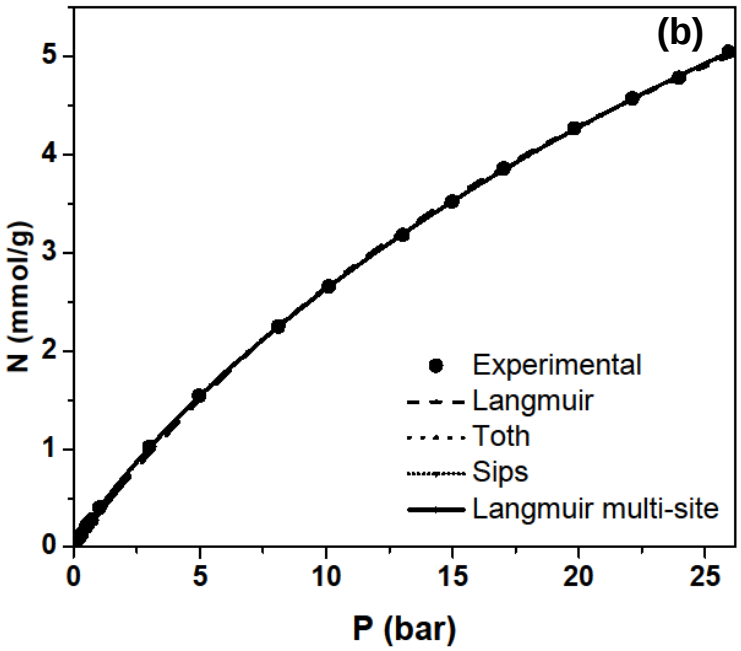

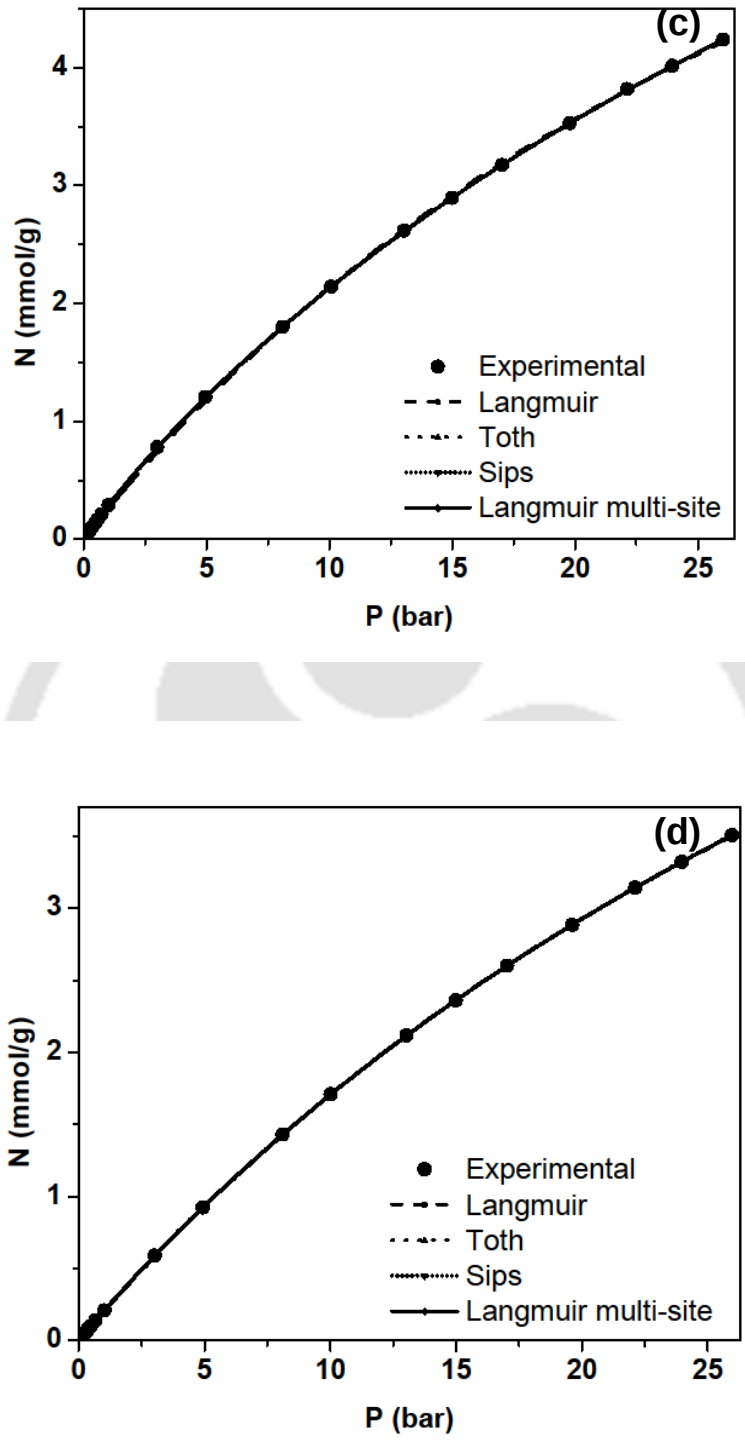

Figure 4.3. Comparison of different isotherm models with experimental data generated for adsorption of CO_2 on MCM-41 (a) 30 °C (b) 45 °C (c) 60 °C and (d) 75 °C.

Table 4.1. CO_2 isotherm model parameters for MCM-41

	Langmuir		Sips				Toth		Langmuir multi-site			
Temperature (°C)	q_m	b	q_m	B	n	n_s	b	t	$q_{m,A}$	b_A	$q_{m,B}$	b_B
30	12.03	0.0375	18.10	0.0295	1.153	15.20	0.0318	0.831	14.56	0.0232	0.589	0.499
45	11.22	0.0310	15.31	0.0262	1.111	13.32	0.0275	0.870	13.36	0.0200	0.533	0.321
60	10.74	0.0249	13.37	0.0220	1.070	11.91	0.0231	0.922	12.42	0.0176	0.385	0.230
75	10.22	0.0200	10.76	0.0195	1.014	10.62	0.0194	0.974	10.58	0.0166	0.075	0.196

Table 4.2. Error (%) across different isotherm models for CO_2 adsorption on MCM-41

Temperature (°C)	Langmuir	Sips	Toth	Langmuir multi- site
30	14.6	8.01	4.29	2.45
45	12.3	6.26	4.10	2.53
60	7.23	3.76	3.57	1.36
75	1.50	1.84	1.34	1.00

4.4.3. Analysis of CO_2 model parameters

It is clear from Table 4.1, that all the model parameters are function of temperature. q_m and n_s decreased with increase in temperature because adsorption of CO_2 is an exothermic process and desorption becomes prominent with the rise in temperature. The temperature dependency of b by van't Hoff equation **[36]** suggests that, b should decrease with increase in temperature which is further confirmed by our present result. The values of b lying in the range of (0.02-0.04) bar^{-1} revealed that MCM-41 interacts with CO_2 through physisorption process **[33, 37]**. Moreover the value of t<1 (Toth parameter) indicated that the surface of MCM-41 is not uniformly homogeneous in nature. This is also reflected from the value of n>1 (sips parameter) **[37, 38]**. Moreover, the respective model parameters also rightly show decreasing trend with increasing temperature. Thus, the inference of model parameters also corroborated the statement that MCM-41 is heterogeneous in nature. Error, Δq (%) for all the isotherms is presented in Table 4.2. The statistical analysis supports that Langmuir multi-site model fitted excellently the experimental data at all regimes of pressure and temperature.

4.4.4. Interaction of CO_2 with surface functional groups of porous silica

To have further insight into the heterogeneous nature of the surface, all the possible types of the surface functionalities of MCM-41, with which the CO_2 molecules can interact are considered. Fig. 4.2(b) shows the hypothetical cross section of a pore in MCM-41 that helps to visualize different kinds of surface groups that can be exposed to the external environment. Si atoms in the silica framework architecture are mostly bound to four bridging oxygen atoms. This siloxane linkage can interact with CO_2 through dispersive forces (in the form of dipole-quadrupole interaction) **[9]**. On the other hand, silicon at the surface can bind to one or two hydroxyl groups to complete its valence, according to which, its binding to the bulk involves two or three Si-O-Si bridges. A single or terminal Si-OH group is called an isolated silanol, when the distance to the closest Si-OH groups is more than ~3.3 Å, so that they cannot be involved in establishing mutual H-bond interactions **[3, 39-42]**. The isolated

silanol groups are then free to establish H-bond interactions with CO_2 molecules as both H-bond donors and acceptors. Pairs of silanol belonging to tetrahedra that share a common oxygen vertex are normally called vicinals. The two silicon atoms of vicinals are separated by a single oxygen so that the two hydroxyl groups are separated by less than 3 Å, despite that, due to local geometrical constraints, only a weakly adduct mutual H-bond can form **[39-42]**. So, these silanol groups (vicinals) will not be readily available for H-bonding with CO_2 as in case of isolated silanol groups. The two OH groups linked to the same surface silicon atom to give the Si-$(OH)_2$ moiety are called geminals. Even though they are very close the two geminal OH are oriented in such a way that they cannot be involved in mutual hydrogen bonds **[34-38]**. Thus, the geminal OH groups are also likely to form H-bonding with CO_2. Apart from this, it is also anticipated that relatively low concentration of surface-associated Si^+ ions could link with CO_2 through an ion quadrupole interaction **[21]**. Existence of surface associated O^- ions on the silica surface as evidenced by DRIFTS spectra is possible but not interacting with CO_2 **[43]**.

4.4.5. Patch-wise topography hypothesis

In reality, it is expected that the five different surface groups (siloxane linkage dipole, isolated silanol, vicinal, geminal, Si^+ ion and O^- ion) are randomly distributed on the periphery of the pore. To figure out the potential surface groups that are responsible for surface heterogeneity, we considered a patch-wise topography hypothesis **[11]** for MCM-41 as shown in Fig. 4.4(a). Based on the type of interaction between CO_2 and surface groups, there would be a definite distribution of energy across the periphery. Hence, all sites that might possess the same energy to adsorb CO_2 are grouped together in one patch and it is assumed that there is no interaction between the patches. Each patch is then considered to be homogeneous and now every patch follows the usual Langmuir assumption. Langmuir multi-site model is applied to the experimental CO_2 equilibrium data to find out the total number of patches on the whole contributing towards surface heterogeneity of MCM-41. The model parameters evaluated at all temperatures (Table 4.1) shows that only first two terms

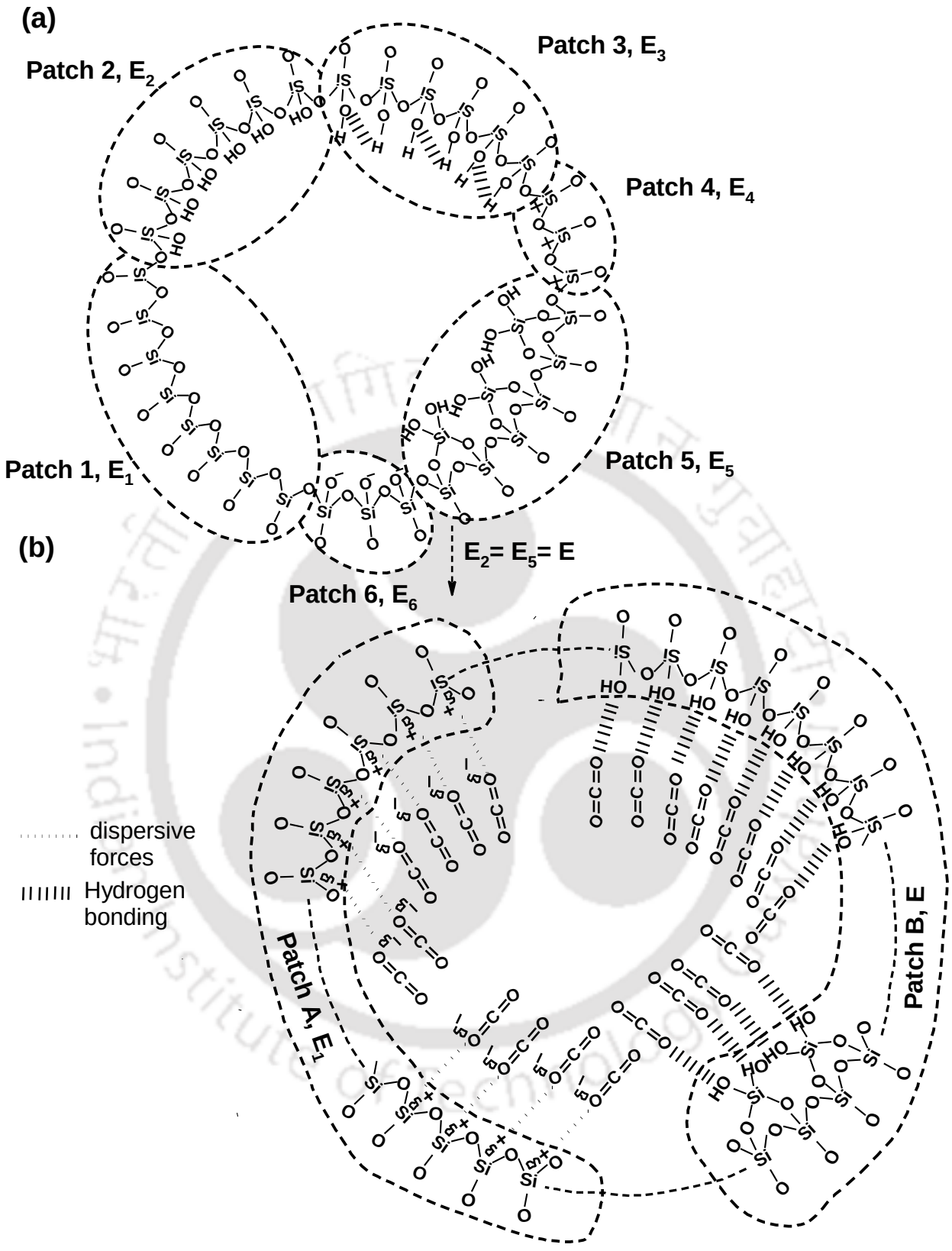

Figure 4.4. Patch wise topography for MCM-41

of the summation are retained and others become vanishingly small. Through this, it indicated that surface heterogeneity of MCM-41 is principally governed by only two patches. Hence, it is clear that there prevails a possibility of negligible interaction of CO_2 with some of the patches.

4.4.6. Heat of adsorption

The energy distribution among the two different patches is analyzed using the temperature dependent form of b_j (Langmuir multisite parameter)

$$b_j = b_{0,j} \exp\left(\frac{H_{ads,j}}{RT_o}\left(1-\frac{T_0}{T}\right)\right) \tag{7}$$

Here subscript 0 refers to the parameters obtained under a reference temperature T_0 **[33]**

The two different values of heat of adsorption (7.75 kJ/mol and 22.19 kJ/mol) obtained clearly indicated the presence of two distinct patches. The heat of adsorption value obtained for patch A (7.75 kJ/mol) indicated that the interaction of CO_2 with patch A is due to dispersive forces **[9]**. The moderate value (22.19 kJ/mol) of heat of adsorption for the other patch rules out the existence of ion-quadrupole interaction for which the heat of adsorption is quite high (~45 kJ/mol) **[44]**. Hence, it is clear that CO_2 molecules interacting with the hydrogen included in the surface hydroxyl groups contributes to 22.19 kJ/mol. The thermal stability of the surface hydroxyl species on silica is strongly temperature dependent. The vicinal silanols have been shown to be dehydroxylated in the temperature range of 450-600 °C **[45]**. Hence, during the calcination process these vicinal groups will get removed as water through dehydroxylation process. However, even if vicinal groups exist on the surface due to incomplete dehydroxylation, these groups are not likely to interact with CO_2 as they are mutually hydrogen bonded with each other already. Now, the functional group on the silica surface could be principally the freely vibrating hydroxyl groups (isolated and geminal silanol groups). These freely vibrating hydroxyl groups are monoenergetic, i.e., the reactivity

of all the OH groups is the same **[46]**. Since these free OH groups are monoenergetic, the heat of adsorption associated with the physisorption process is essentially the same irrespective of whether the OH group belongs to isolated or geminal silanols **[46]**. Hence, the isolated and geminal silanols are grouped together in the same patch, now termed as Patch B (Fig. 4.4(b)). Although the surface ions are also expected to be present on the silica surface, the contribution of these ions towards surface heterogeneity is expected to be almost negligible due to their relatively lower concentration. Finally, it can be concluded that heterogeneous nature of MCM-41 is dominated by the presence of two distinct patches (Patch A: siloxane bridges and Patch B: isolated and geminal silanols), which is further corroborated by the estimated heat of adsorption by Clasius-Clapeyron equation.

The adsorption isotherms of CO_2 obtained at different temperatures ranging from 30 to 75 °C were used for the calculation of isosteric heat of adsorption for MCM-41 based on the Clasius-Clapeyron equation. ΔH_{iso} as a function of loading is portrayed in Fig. 4.5. The value of ΔH_{iso} at zero loading is found to be ~21 kJ/mol and is comparable to the reported typical values (20 kJ/mol) for MCM-41 silica **[37]**. The obtained amount of heat of adsorption is much smaller than 40 kJ/mol, typical heat of adsorption for chemisorptions **[47, 48]**. This indicated that the process of CO_2 adsorption on MCM-41 is governed by physisorption. From the Fig. 4.5, it can be inferred that the isosteric heat of adsorption, is a function of loading of adsorbate and it decreases non-linearly with increase in saturation adsorption capacity. This can be explained by the fact that at low surface coverage CO_2 molecules will be adsorbed on the sites having the highest energy. This results in a strong interaction between the CO_2 molecules and adsorbent surfaces accompanied by high isosteric heat of adsorption. The H-bonding between the silanol group and CO_2 is the dominating factor as also can be seen from the sharp fall of ΔH_{iso} till about 20% of total loading (Fig. 4.5). However, as the surface coverage is increased, sites of lower energies are progressively filled resulting in weaker interaction between CO_2 molecules and adsorbent which in turn leads to a decrease in heat of adsorption **[49, 50]**. The downturn behavior in the isosteric heat of adsorption clearly

indicated the distribution of energies across the adsorption sites. The value of ΔH_{iso} around ~21 kJ/mol, at zero loading strongly supports the predominant contribution of surface OH group towards CO_2 adsorption through hydrogen bonding, at low surface coverage.

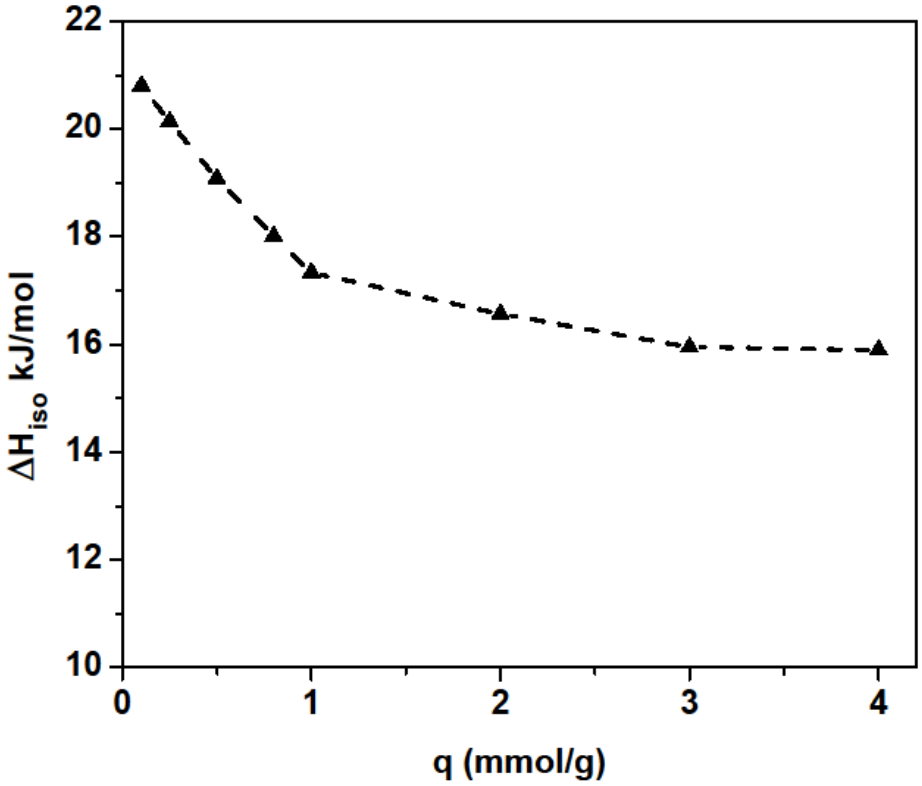

Figure 4.5. Isosteric heat of adsorption for MCM-41 as a function of loading

4.4.7. Surface heterogeneity transformation behavior

In addition to this, we also explored the effect of temperature on the surface heterogeneity of MCM-41. It is to be noted here, that the term surface heterogeneity transformation refers to the change in interaction behaviour of CO_2 with surface functionalities of the adsorbent with respect to temperature and not the change in surface characteristics. Fig. 4.6 shows a plot of relative contribution of each patch (patch A and patch B) to the amount adsorbed as a function of pressure at different temperatures. The figure clearly indicates that the contribution from patch B is decreasing and making the surface to behave apparently

homogeneous as the temperature increases. This is also quite evident from the decreasing trend of $q_{m,B}$ and finally reaching towards zero at 75 °C (Table 4.1). This is because, at low temperature all the sites don't have the same energy, and rather there is a distribution of energies. At higher temperature (~75 °C) the adsorbing sites of MCM-41 become energetically uniform resulting in an almost homogenous surface. At higher temperature, H-bonding becomes less effective which has been explained later in further details and adsorption is mainly due to patch A. Curiously Δq(%) for Langmuir isotherm also decreases from 15% at 30 °C to 3% at 75 °C (Table 4.2). This further supports that with the rise in temperature surface tends to behave apparently homogeneous which is also reflected, as explained earlier, from the value of *t* (Toth parameter) and *n* (Sips parameter) reaching towards unity with the increase in temperature **[33, 37, 38]**.

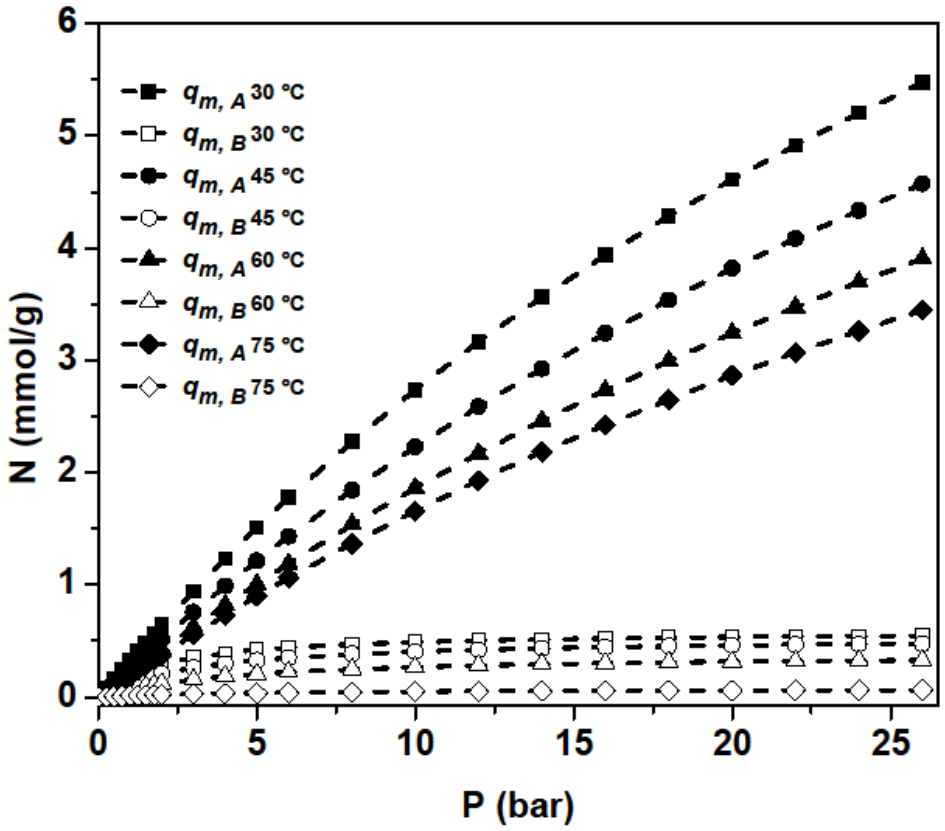

Figure 4.6. Plot of relative contribution of Patch A and Patch B to the amount adsorbed.

4.4.8. Validation of patch-wise topography hypothesis

To further provide validation of the proposed hypothesis, nitrogen adsorption on MCM-41 is considered. Because nitrogen is a quadrupolar molecule like CO_2 and also interacts with the surface functional (OH) groups of the adsorbent in a similar fashion **[47]**, N_2 gas is selected as an adsorbate for validation of our hypothesis. The adsorption isotherms of N_2 on MCM-41 are shown in Fig. 4.7. From Fig. 4.1(a-d) and Fig. 4.7, it can be observed that amount of CO_2 adsorbed is preferentially higher than that of N_2. This is due to the larger quadrupole moment (13.71×10^{-40} Coloumb.m^2) exhibited by CO_2 which in turn strengthens the adsorbate-adsorbent interaction in comparison with N_2 (4.91×10^{-40} Coloumb.m^2) **[51-54]**. The experimental N_2 equilibrium adsorption data is fitted using Langmuir multi-site model to find

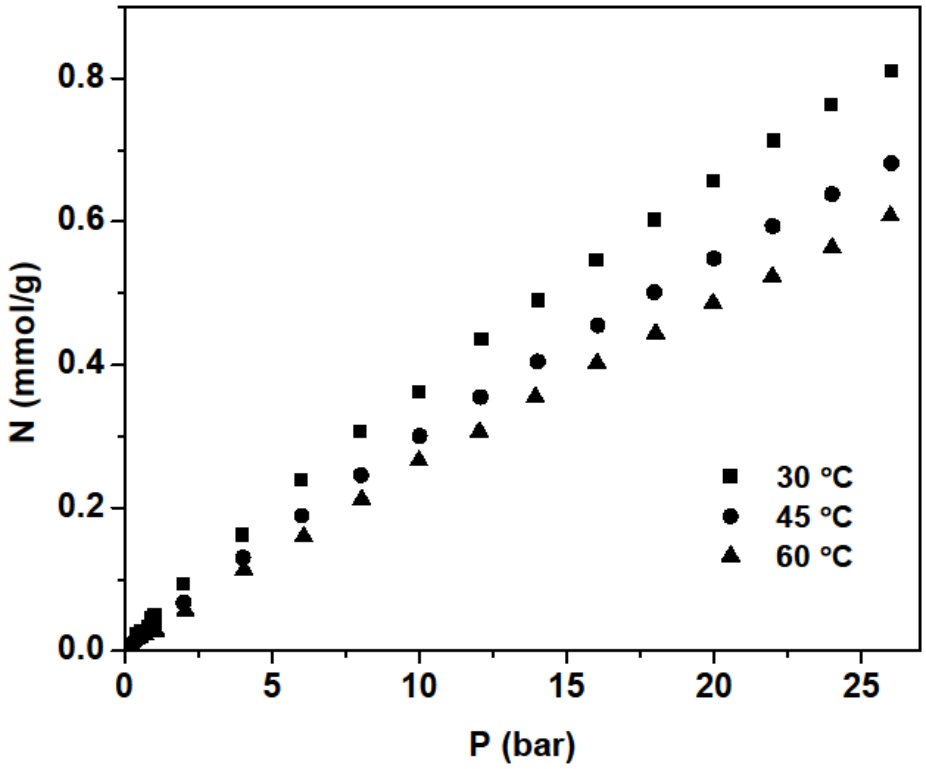

Figure 4.7. N_2 adsorption isotherms of MCM-41

out the relative contribution of each patch available in the adsorbent to the adsorption capacity. The model parameters are listed in Table 4.3 and it can be seen that q_m and b exhibits downturn for patch A and B as the temperature increases. The lower values of model parameters q_m and b observed for N_2 when compared to CO_2 adsorption further provides evidence that N_2 exhibits a weaker interaction with both Si-O-Si (dispersive forces) and Si-OH (H-bonding). Due to relatively weaker H-bond strength between Si-OH and N_2 than CO_2, H-bonding breaks at even lower temperature in the case of N_2 when compared to CO_2. The heat of adsorption value is calculated for the patch A (5.54 kJ/mol) and B (17.96 kJ/mol) by eq. 7. The lower heat of adsorption value (17.96 kJ/mol) obtained for patch B for N_2 adsorption when compared to (22.19 kJ/mol) for CO_2 adsorption further helps in understanding that H-bond strength between Si-OH and N_2 becomes much weaker. As a result, even at 60 °C, only one term in Langmuir multi-site model (Table 4.3) is retained, which is due to dispersive forces (Patch A). It is also clear that the surface hydroxyl groups are no longer effective for adsorption of N_2 at 60 °C, which has been observed at 75 °C for CO_2.

Table 4.3. Langmuir multi-site model parameters for N_2 adsorption on MCM-41

S:No	Temperature (°C)	$q_{m,A}$	b_A	$q_{m,B}$	b_B
1	30	4.008	0.009199	0.03752	0.4181
2	45	3.811	0.008157	0.01599	0.2987
3	60	3.718	0.007549	--	--

4.5. Conclusions

DRIFTS analysis speculated the prevalence of various functionalities on the surface of MCM-41. Different isotherm models (Langmuir, Sips, and Toth) applied to the experimental equilibrium adsorption data provided an insight to understand the nature of the surface. From the Toth and Sips model parameter (t and n), it was inferred that MCM-41 is heterogeneous in nature. Patch-wise topography hypothesis for MCM-41 enlightened the

potential surface groups that contribute to the overall CO_2 adsorption capacity. Langmuir multi-site model was applied to determine the individual contribution of each type of surface group towards the overall adsorption capacity and it was found that the CO_2 adsorption on MCM-41 is principally governed by two potential surface groups (Si-OH and Si-O-Si linkages). Based on the decreasing trend observed in the Langmuir multi–site model parameters with the rise in temperature, it was observed that adsorbent surface becomes apparently more homogeneous as the temperature increases progressively. The downturn exhibited in the heat of adsorption values again confirmed the heterogeneous nature of MCM-41. The temperature-dependent form of the *b* (Langmuir multi-site parameter) allowed calculation of the heat of adsorption values associated with both the surface groups. From the heat of adsorption values, it was concluded CO_2 molecules interact with only silanol groups (hydrogen bonding) and Si-O-Si linkage (dispersive forces).

4.6. References

[1] Li, I.; Bandara, J.; and Shultz, M. J. Time Evolution Studies of the H_2O/Quartz Interface Using Sum Frequency Generation, Atomic Force Microscopy, and Molecular Dynamics, *Langmuir* **2004**, 20, 10474-10480.

[2] Zhou, F.; and Head, J. D.; Role of Si=O in the Photoluminescence of Porous Silicon, *J. Phys. Chem. B* **2000**, 104, 9981-9986.

[3] Rimola, A.; Costa, D.; Sodupe, M.; Lambert, J.; and Ugliengo, P. Silica Surface Features and Their Role in the Adsorption of Biomolecules: Computational Modeling and Experiments, *Chem. Rev.* **2012**, dx.doi.org/10.1021/cr3003054.

[4] Maciel, G. E.; and Sindorf, D. W. Silicon- ^{29} Nuclear Magnetic Resonance Study of the Surface of Silica Gel by Cross Polarization and Magic-Angle Spinning, *J. Am. Chem. Soc.* **1980**, 102, 7606-7607.

[5] Riikonen, J.; Salomaki, M.; Wonderen, J. V.; Kemell, M.; Xu, W.; Korhonen, O.; Ritala, M.; MacMillan, F.; Salonen, J.; and Lehto, V. Surface Chemistry, Reactivity, and Pore Structure of Porous Silicon Oxidized by Various Methods*, Langmuir* **2012**, 28,10573-10583.

[6] Kitaura, R.; Kitagawa, S.; Kubota, Y.; Kobayashi, T.C.; Kindo, K.; Mita, Y.; Matsuo, A.; Kobayashi, M.; Chang, H.C.; Ozawa, T.C.; Suzuki, M.; Sakata M.; and Takata, M. Formation of One-Dimensional Array of Oxygen in a Microporous Metal-Organic Solid, *Science* **2002**, 298, 2358-2361.

[7] Matsuda, R.; Kitaura, R.; Kitagawa, S.; Kubota, Y.; Belosludov, R. V.; Kobayashi, T. C.; Sakamoto, H.; Chiba, T.; Takata, M.; Kawazoe, Y.; and Mita, Y. Highly Controlled Acetylene Accomodation in a Metal-Organic Microporous Material, *Nature* **2005**, 436, 238-241.

[8] Vaidhyanathan, R.; Iremonger, S. S.; Shimizu, G. K. H.; Boyd, P. G.; Alavi, S.; and Woo, T. K. Direct Observation and Quantification of CO_2 Binding within an Amine-functionalized Nanoporous Solid, *Science* **2010**, 330, 650-652.

[9] Roque-Malherbe, R.; Polanco-Estrella, R.; and Marquez-Linares, F. Study of the Interaction between Silica Surfaces and the Carbon Dioxide Molecule, *J. Phys. Chem. C* **2010**, 114, 17773-17787.

[10] Parimal, S.; Prasad, M.; and Bhaskar, U. Prediction of Equilibrium Sorption Isotherm: Comparison of Linear and Nonlinear Methods, *Ind. Eng. Chem. Res.* **2010**, 49, 2882-2888.

[11] Campbell, C. T.; and Sellers, J. R. V. Enthalpies and Entropies of Adsorption on Well-Defined Oxide Surfaces, *Chem.Rev.* **2012**, dx.doi.org/10.1021/cr300329s.

[12] Duran, C.; Ozdes, D.; Gundogdu, A.; and Senturk, H. B. Kinetics and Isotherm Analysis of Basic Dyes Adsorption onto Almond Shell (*Prunus dulcis*) as a Low Cost Adsorbent, *J. Chem. Eng. Data* **2011**, 56, 2136-2147.

[13] Peterson, A. W.; Wolf, L. K.; and Georgiadis, R. M. Hybridization of Mismatched or Partially Matched DNA at Surfaces, *J. Am. Chem. Soc.* **2002**, 124,14601-14607.

[14] Stoermer, R. L.; Cederquist, K. B.; McFarland, S. K.; Sha, M. Y.; Penn, S. G.; and Keating, C. D. Coupling Molecular Beacons to Barcoded Metal Nanowires for Multiplexed, Sealed Chamber DNA Bioassays, *J. Am. Chem. Soc.* **2006**,128, 16892-16903.

[15] Browne, K. A. Sequence-Specific, Self-Reporting Hairpin Inversion Probes, *J. Am. Chem. Soc.* **2005**, 127, 1989-1994.

[16] Yang, W.; Greenaway, A.; Lin, X.; Matsuda, R.; Blake, A. J.; Wilson, C.; Lewis, W.; Hubberstey, P.; Kitagawa, S.; Champness, N. R.; and Schroder, M. Exceptional Thermal Stability in a Supramolecular Organic Framework: Porosity and Gas Storage, *J. Am. Chem. Soc.* **2010**, 132, 14457-14469.

[17] Hao, G. P.; Li, W. C.; Qian, D.; Wang, G. H.; Zhang, W. P.; Zhang, T.; Wang, A. Q.; Schuth, F.; Bongard, H. J.; and Lu, A. H. structurally Designed Synthesis of Mechanically Stable Poly(benzoxaine-co-resol)-Based Porous Carbon Monoliths and Their Application as High Performance CO_2 Capture Sorbents, *J. Am. Chem. Soc.* **2011**, 133, 11378-11388.

[18] Hudson, M. R.; Queen, W. L.; Mason, J. A.; Fickel, D. W.; Lobo, R. F.; and Brown, C. M. Unconventional, Highly Selective CO_2 Adsorption in Zeolite SSZ-13, *J. Am. Chem. Soc.* **2012**, 134,1970-1973.

[19] Sumida, K.; Stuck, D.; Mino, L.; Chai, J. D.; Bloch, E. D.; Zarvorotynska, O.; Murray, L. J.; Dinca, M.; Chavan, S.; Bordiga, S.; Head-Gordon, M.; and Long, J. R. Impact of Metal and Anion Substitutions on the Hydrogen Storage properties of M-BTT Metal-Organic Frameworks, *J. Am. Chem. Soc.* **2013**, 135, 1083-1091.

[20] Nijem, N.; Thissen, P.; Yao, Y.; Longo, R. C.; Roondenko, K.; Wu, H.; Zhao, Y.; Cho, K.; Li, J.; Langreth, D. C.; and Chabal, Y. J. Understanding the Preferential Adsorption of

CO_2 over N_2 in a Flexible Metal-Organic Framework, *J. Am. Chem. Soc.* **2011**,133, 12849-12857.

[21] Haldoupis, E.; Nair, S.; and Sholl, D. Finding MOFs for Highly Selective CO_2/N_2 Adsorption Using Materials Screening Based on Efficient Assignment of Atomic Point Charges, *J. Am. Chem. Soc.* **2012**,134, 4313-4323.

[22] Serna-Guerrero, R.; and Sayari, A. Modeling Adsorption of CO_2 on Amine-functionalized Mesoporous Silica. 2. Kinetics and Breakthrough Curves, *Chem. Eng. J* **2010**, 161,182-190.

[23] Brunelli, N. A.; Didas, S. A.; Venkatasubbaih, K.; and Jones, C. W. Tuning Cooperativity by Controlling the Linker Length of Silica Supported Amines in Catalysis and CO_2 Capture, *J. Am. Chem. Soc.* **2012**,134,13950-13953.

[24] Pan, H.; Ritter, J. A.; and Balbuena, P. B. Examination of the Approximations Used in Determining the Isosteric Heat of Adsorption from the Clasius-Clapeyron Equation, *Langmuir* **1998**,14, 6323-6327.

[25] McDonald, T. M.; Lee, W. R.; Mason, J. A.; Wiers, B. M.; Hong, C. S.; and Long, J. R. Capture of Carbon Dioxide from Air and Flue Gas in the Alkylamine Appended Metal-Organic Framework mmen-Mg_2(dobpdc), *J. Am. Chem. Soc.* **2012**,134,7056-7065.

[26] Anedda, A.; Carbonaro, C. M.; Clemente, F.; Corpino, R.; and Ricci, P. C. Raman Investigation of Surface OH-Species in Porous Silica, *J. Phys. Chem. B* **2003**,107, 13661-13664.

[27] Takeia, T.; Katoa, K.; Meguroa, A.; and Chikazawa, M. Infrared Spectra of Geminal and Novel Triple Hydroxyl Groups on Silica Surface, *Colloids Surf., A.* **1998**,150, 77-84.

[28] Pires, J.; Pinto, M.; Estell, J.; and Echeverria, J. C. Characterization of the Hydrophobicity of Mesoporous Silica and Clays with Silica Pillars by Water Adsorption and DRIFT, *J. Colloid Interface Sci.* **2008**,317, 206-213.

[29] Morey, M. S.; Brien, S. O.; Schwarz, S.; and Stucky, G. D. Hydrothermal and Post Synthesis Surface Modification of Cubic, MCM-48, and Ultra Large Pore SBA-15 Mesoporous Silica with Titanium, *Chem. Mater*. **2000**, 12, 898-911.

[30] Frost, R. L.; Cejka, J.; Weier, M. L.; Martens, W.; and Kloprogge, J. T. A Raman and Infrared Spectroscopic Study of the Uranyl Silicates- Weeksite, Soddyite and Haiweeite, *Spectrochim. Acta.* **2006**, 63, 305-312.

[31] Fidalgo, A.; and Ilharco, L. M. Chemical Tailoring of Porous Silica Xerogels: Local Structure by Vibrational Spectroscopy, *Chem. Eur. J.* **2004**,10, 392-398.

[32] Monash, P.; and Pugazhenthi, G. Investigation of Equilibrium and Kinetic Parameters of Methylene Blue Adsorption onto MCM-41, *Korean J. Chem. Eng*. **2010**, 27, 1184-1191.

[33] Do, D. D. Adsorption Analysis: Equilibria and Kinetics, Imperial College Press, London, **1998**.

[34] Rudzinski, W.; Lee, S. L.; Yan, C. C. S.; and Panczyk, T. A Fractal Approach to Adsorption on Heterogeneous Solid Surfaces. 1. The Relationship between Geometric and Energetic Surface Heterogeneities, *J. Phys. Chem. B* **2001**, 105, 10847-10856.

[35] Basha, S.; and Jha, B. Estimation of Isotherm Parameters for Biosorption of Cd(II) and Pb(II) Brown Seaweed, *Lobophora variegate*, *J. Chem. Eng, Data* **2008**, 53, 449-455.

[36] Ruthven, D.M. Principles of Adsorption and Adsorption Processes, Wiley, New York, **1984**.

[37] Serna-Guerrero, R.; Belmabkhout, Y.; and Sayari, A. Modeling CO_2 Adsorption on Amine-functionalized Mesoporous Silica: 1. A Semi-empirical Equilibrium Model, *Chem. Eng. J.* **2010**, 161,173-181.

[38] Stoermer, R. L.; Cederquist, K. B.; McFarland, S. K.; Sha, M. Y.; Penn, S. G.; and Keating, C. D. Coupling Molecular Beacons to Barcoded Metal Nanowires for Multiplexed, Sealed Chamber DNA Bioassays, *J. Am. Chem. Soc.* **2006**,128, 16892-16903.

[39] Dijkstra, T. W.; Duchateau, R.; Van Santen, R. A.; Meetsma, A.; and Yap, G. P. A. Silsesquioxane Models for Geminal Silica Surface Silanol Sites. A Spectroscopic Investigation of Different Types of Silanols, *J. Am. Chem. Soc.* **2002**, 124, 9856-9864.

[40] Liu, C. C.; and Maciel, G. E. The Fumed Silica Surface: A Study by NMR, *J. Am. Chem. Soc.* **1996**, 118, 5103-5119.

[41] Merle, N.; Trebosc, J.; Baudouin, A.; Rosal, I. D.; Maron, L.; Szeto, K.; Genelot, M.; Mortreux, A.; Taoufik, M.; Delevoye, L.; and Gauvin, R. M. ^{17}O NMR Gives Unprecedented Insights into the structure of Supported Catalysts and Their Interaction with the Silica Carrier, *J. Am. Chem. Soc.* **2012**,134, 9263-9275.

[42] Fleischman, S. D.; and Scott, S. L. Evidence for the Pairwise Disposition of Grafting Sites on Highly Dehydroxylated Silicas via Their Reactions with $Ga(CH_3)_3$, *J. Am. Chem. Soc.* **2011**,133, 4847-4855.

[43] Zhang, H.; Dunphy, D. R.; Jiang, X.; Meng, H.; Sun, B.; Tarn, D.; Xue, M.; Wang, X.; Lin, S.; Ji, Z.; Li, R.; Garcia, F. L.; Yang, J.; Kirk, M. L.; Xia, T.; Zink, J. I.; Nel, A.; and Brinker, C. J. Processing Pathway Dependence of Amorphous Silica Nanoparticle Toxicity: Colloidal vs Pyrolytic, *J. Am. Chem. Soc.* **2012**,134, 15790-15804.

[44] Huang, Y. Y. Quadrupole Interaction of Carbon Dioxide on Silica-Alumina Surface, *J. Phys. Chem*. **1973**,77,103-106.

[45] Sneh, O.; and George, S. M.; Thermal Stability of Hydroxyl Groups on a Well-Defined Silica Surface, *J. Phys. Chem.* **1995**, 99,4639-4647.

[46] Hair, M. L.; and Hertl, W. Reactivity of Boria-Silica Surface Hydroxyl Groups, *J. Phys. Chem.* **1973**, 77, 1965-1969.

[47] Hoang, T. K. A.; Webb, M. I.; Mai, H. V.; Hamaed, A.; Walsby, C. J.; Trudeau, M.; and Antonelli, D. M. Design and Synthesis of Vanadium Hydrazide Gels for Kubas-Type Hydrogen Adsorption: A New Class of Hydrogen Storage Materials, *J. Am. Chem. Soc.* **2010**, 132, 11792-11798.

[48] Soubeyrand-Lenoir, E.; Vagner, C.; Yoon, J. W.; Bazin, P.; Ragon, F.; Hwang, Y. K.; Serre, C.; Chang, J. S.; and Llewellyn, P. L. How Water Fosters a Remarkable 5-Fold Increase in Low-Pressure CO_2 Uptake within Mesoporous MIL-100(Fe), *J. Am. Chem. Soc.* **2012**, 134, 10174-10181.

[49] Jiang, J.; and Sandler, S. I. Separation of CO_2 and N_2 by Adsorption in C_{168} Schwarzite: A Combination of Quantum Mechanics and Molecular Simulation Study, *J. Am. Chem. Soc.* **2005**, 127,11989-11997.

[50] Sillar, K.; and Sauer, J. Ab Initio Prediction of Adsorption Isotherms for Small Molecules in Metal-Organic Frameworks: The Effect of Lateral Interactions for Methane/CPO-27-Mg, *J. Am. Chem. Soc.* **2012**, 134, 18354-18365.

[51] Bae, Y. S.; Farha, O. K.; Hupp, J. T; and Snurr, R. Q. Enhancement of CO_2/N_2 selectivity in a metal-organic framework by cavity modification, *J. Mater. Chem.* **2009**, 19, 2131-2134.

[52] Wilcox, J. Carbon Capture, Springer, London, **2012**.

[53] Garcia-Perez, E.; Parra, J. B.; Ania, C. O.; Garcia-Sanchez, A.; Baten, J. M. V.; Krishna, R.; Dubbeldam, D.; and Calero, S. A. Computational Study of CO_2, N_2, and CH_4 adsorption in Zeolites, *Adsorption* **2007**,13, 469-476.

[54] Aguilar-Armenta, G.; Hernandez-Ramirez, G.; Flores-Loyola, E.; Ugarte-Castaneda, A.; Silva-Gonzalez, R.; Tabares-Munoz, C.; Jimenez-Lopez, A.; and Rodriguez-Castellon, E. Adsorption Kinetics of CO_2, O_2, N_2, and CH_4 in Cation-Exchanged Clinoptilolite, *J. Phys. Chem. B* **2001**,105,1313-1319.

CHAPTER 5

MECHANISTIC INVESTIGATION OF CO_2 ADSORPTION KINETICS ON MCM-41

The chapter examines the individual mechanistic steps that control the diffusion of CO_2 uptake kinetics on MCM-41. The actual rate-controlling step for CO_2 uptake kinetics on MCM-41 under wide range of pressure (0.1-11 bar) and temperature conditions (30, 45, 60, 75 °C) is discussed. Kinetic models such as Pseudo-first order, Pseudo-second order, Interparticle diffusion, Intraparticle diffusion and Boyd's models are considered for the study and discussion about the theory for the same is also provided. This part of work has been published in ***Chemical Engineering Journal*** *256 (2014) 1-8.*

5.1. Introduction

The design of an appropriate adsorption process requires development of model that can describe the dynamics of adsorption in fixed bed with selected adsorbent. Since, the kinetic parameters provide information for designing and modeling the adsorption process, a wide number of literatures described the kinetics of CO_2 adsorption on activated carbons **[1-3]**, zeolites **[4-6]** and metal-organic frameworks **[7-9]**. Sayari et al. described the kinetics of CO_2 adsorption on amine functionalized pore-expanded MCM-41(AF-PE-MCM 41) developed by their research group **[10, 11]**. Several models such as Pseudo-first order, Pseudo-second order and Avrami models are used to predict the kinetic behaviour of CO_2 adsorption on AF-PE-MCM-41 under ambient pressure conditions and at different temperature conditions (30, 40, 55, 70 °C). However, individual mechanistic steps that control the diffusion of CO_2 uptake kinetics on AF-PE-MCM 41 are not taken into consideration in their study. In addition to this, kinetics of gas adsorption on mesoporous silica adsorbents before amine functionalization under wide range of pressure and temperature conditions has not been investigated so far. Hence, this part of work is devoted to the detailed kinetic analysis of CO_2 adsorption on MCM-41. A total of 52 adsorption uptake runs are carried out on MCM-41 over a dynamic pressure regime (0.1 to 11 bar) at four different temperatures (30, 45, 60, 75 °C) using a gravimetric analyzer.

In the present study, the two of the most popular models such as Lagergren's pseudo-first order and pseudo-second order kinetic models are fitted to experimental kinetic data. The type of interaction between CO_2 and MCM-41 as well as adsorption rate behavior of CO_2 on MCM-41 with respect to pressure and temperature is predicted from the best fitted model. In order to understand better the rate-controlling step for CO_2 adsorption kinetics on MCM-41**,** five main mechanisms of mass transport that are expected to occur are taken in to account and the same is depicted in Fig. 5.1. These include (a) molecular diffusion from the bulk CO_2 phase to a film layer surrounding MCM-41 (external diffusion) (b) diffusion from the film to surface of MCM-41 (film diffusion) (c) intraparticle diffusion i.e. migration inside the pores

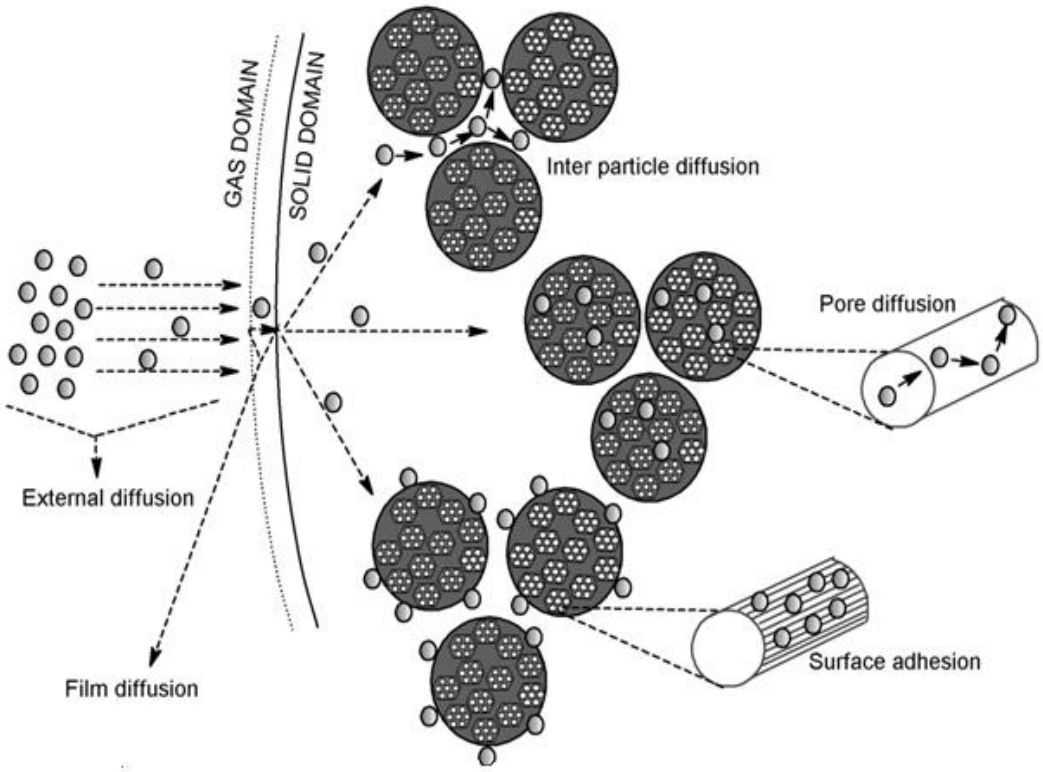

Figure 5.1. Schematic representation of CO_2 diffusion mechanism

of MCM-41 (pore diffusion) (d) inter particle diffusion and (e) surface adhesion, which can occur by chemical or physical interaction with adsorption sites (surface reaction). However, based on the well-established fact that (a) and (e) transport steps are usually vary fast for an adsorption process, it is considered that kinetic process of CO_2 uptake on MCM-41 must have been controlled by CO_2 film diffusion or intraparticle diffusion or inter particle diffusion or combination of all three mechanisms. To figure out the actual rate-controlling step or relative contribution from (b), (c), (d) the experimental CO_2 uptake data is further analyzed by diffusion models such as interparticle diffusion, intraparticle diffusion and Boyd's models that describe the actual mass transfer mechanisms in porous materials.

5.2. Experimental section

5.2.1. Materials

The details of materials used for synthesis of MCM-41 have been described in section 3.2.1.

5.2.2. Synthesis of MCM-41

The synthesis procedure for MCM-41 has been described in section 3.2.2.

5.2.3. Material characterization

The details about characterization of MCM-41 have been elaborated in section 3.2.3.

5.2.4. CO_2 kinetic measurements

Adsorption kinetic measurements of pure CO_2 on MCM-41 at four different temperatures (30, 45, 60, and 75 °C) were performed in the pressure range of 0.1-11 bar, using a Rubotherm balance (Model: Prazisionsmeßtechnik GmbH Origin: Germany) composed mainly of a magnetic suspension balance (MSB). When the kinetic experiment was performed, the adsorbent was weighed and placed in a basket suspended by a permanent magnet through an electromagnet. Prior to adsorption kinetic measurements, the sample was activated with the aim of removing any pre-adsorbed gas and moisture by heating it at 110 °C under vacuum (and then purging with helium) for 2 hours. The outgassed adsorbent was exposed to pure CO_2 at constant temperature. The desired temperature throughout the experiment was maintained with the help of circulating water bath (model: RW-2025G make: Lab companion). Thermocouple was connected to the suspension balance to read the temperature during the experiments. The desired pressure for each kinetic run was set using pressure transducer (model: 627D18TBC1B (up to 1000 Torr) and 627B24TBC1B (up to 20,000 Torr) make:mKs). The change in weight of the adsorbent sample with respect to pressure and temperature was measured continuously until thermodynamic equilibrium was reached. Each test was performed thrice in order to determine uncertainty in the

experiments. As the kinetic measurements were carried out using high precision balance, negligible standard deviation (~0.0004 to 0.0006) in the results was obtained for every pressure and temperature condition analyzed.

5.2.5. Determination of kinetic model parameters

The kinetic model parameters were determined by a similar method explained in section 4.2.5.

5.3. Theory

5.3.1. Adsorption rate

The kinetics of adsorption of gas onto porous solids is often complex and the mechanism of adsorption depends on the physical and chemical properties of the adsorbent as well as the mass transport process. A wide variety of kinetic models (for example, pseudo-first order **[12, 13]**, pseudo-second order **[14, 15]**, Elovich equation **[12-16]**, film diffusion model **[17, 18]**, Avrami model **[19, 20]** have been formulated till date describing gas uptake rate on solid sorbents. Among the existing theoretical kinetic models, pseudo-first order and pseudo-second order models are the simplest models that describe the adsorbate-adsorbent interactions and adsorption rate behavior. Hence, these two models are selected to study the adsorption rate behavior of CO_2 on MCM-41 under different pressure and temperature conditions. In these two models, all the adsorption steps such as external diffusion, pore diffusion, and surface adhesion are lumped together and henceforth called as pseudo models **[21]**. It is assumed that the difference between the equilibrium concentration and the average solid phase concentration is the driving force for adsorption.

5.3.1.1. Pseudo-first order model

The pseudo-first order model is based on the assumption that the adsorption rate is proportional to the number of free adsorption sites. The rate expression associated to the process can then be expressed as:

$$\frac{dq}{dt} = k_f \left(q_e - q_t \right) \tag{1}$$

Where q_e and q_t represents the amount of CO_2 adsorbed at equilibrium and at a given point of time respectively. k_f is first order rate constant **[12, 13]**.

After integration of eq (1) with the boundary conditions i.e. $t = 0$, $q_t = 0$, and $t = t_\infty$, $q_t = q_e$,

$$q_t = q_e \left(1 - e^{-k_f t} \right) \tag{2}$$

The k_f values for CO_2 adsorption on MCM-41 under different pressure and temperature conditions are obtained from the eq (2).

5.3.1.2. Pseudo-second order model

Pseudo-first order model signifies reversible interactions with an equilibrium being established between gas and solid surfaces. In contrast, second order kinetic model assumes that the rate-controlling step is most likely to involve chemical interactions leading to binding of gas to the surface by strong covalent bonding **[14, 15]**. To check whether chemisorption is the rate-controlling factor for CO_2 adsorption on MCM-41, pseudo-second order model is also selected to analyze the experimental kinetic data.

The pseudo-second order model is based on the assumption that the adsorption rate is linearly related to the square of the number of unoccupied adsorption sites and thus the kinetic rate law can be expressed as:

$$\frac{dq_t}{dt} = k_s \left(q_e - q_t \right)^2 \tag{3}$$

Where k_s is second order rate constant **[14, 15]**. Integrating and applying boundary conditions $t = 0$, $q_t = 0$, and $t = t_\infty$, $q_t = q_e$, eq (3) becomes

$$q_t = \frac{q_e^2 k_s t}{1 + q_e k_s t} \tag{4}$$

The k_s values for all the pressure and temperature conditions analyzed are obtained from the eq (4).

5.3.2. Error calculation

To estimate the accuracy of the fit of the kinetic models, an error function based on the normalized standard deviation is calculated using a method reported in the literature

$$\Delta q(\%) = \sqrt{\frac{\sum\left[\left(q_{\exp} - q_{model}\right)/q_{\exp}\right]^2}{N-1}} \times 100\% \quad (5)$$

Where, Δq (%) is the normalized standard deviation, q_{exp} and q_{model} are the experimental and calculated amounts of CO_2 adsorbed, and *N* is the number of data points available in each isotherm **[10]**.

5.3.3. Mechanism of adsorption

Since all the steps concerned with the adsorption process are lumped together, pseudo-first and second order models do not provide any idea regarding the actual rate-controlling step and the mechanism of diffusion associated with the CO_2 adsorption on MCM-41. Therefore, in order to have further insight in to the rate-controlling step and elucidate the CO_2 diffusion mechanism, the experimental kinetic data is analyzed by diffusion models such as interparticle diffusion model, intraparticle diffusion model and Boyd's model.

5.3.3.1. Interparticle diffusion model

The model assumes that the interparticle diffusion is the rate-controlling step and according to this model, for most particle shapes, representation as an equivalent sphere is an acceptable approximation and therefore transport may be described by a diffusion equation, written in spherical coordinate with the assumption of constant diffusivity as **[10, 22]**

$$\frac{\partial q}{\partial t} = D_c\left(\frac{\partial^2 q}{\partial r^2} + \frac{2}{r}\frac{\partial q}{\partial r}\right) \quad (6)$$

The appropriate initial and boundary conditions **[17]** for this equation are

$$q(r,0) = q_0^{'},\ q(r_c,t) = q_0,\ \left(\frac{\partial q}{\partial r}\right)_{r=0} = 0$$

The solution of this equation is then given by the expression

$$\frac{q_t}{q_e} = 1 - \frac{6}{\pi^2}\sum_{n=1}^{\infty}\frac{1}{n^2}\exp\left(-\frac{n^2\pi^2 D_c t}{r_p^2}\right) \tag{7}$$

Eq. (7) can be used to obtain the diffusion time constant, D_c/r_P^2 for CO_2 adsorption on MCM-41 from the experimental uptake profile and q_t/q_e is the fractional approach to equilibrium.

This expression (Eq. (7)) converges rapidly in the long time region since the higher terms of the summation become vanishingly small. For fractional uptakes greater than 70%, only the first term may be retained to obtain **[10, 22]**

$$1 - \frac{q_t}{q_e} \approx \frac{6}{\pi^2}\exp\left(-\frac{\pi^2 D_c t}{r_p^2}\right) \tag{8}$$

In the long time region, a plot of ln [1– (q_t/q_e)] versus t should be linear with slope $-\pi^2(D_c/r_P^2)$ and intercept ln $(6/\pi^2)$ **[10, 22].**

It is also possible to obtain the values of diffusivity from the pseudo-first order kinetic model parameter. The particles are assumed to be comprised of spheres with the same size, a diffusivity factor can be calculated as:

$$k_f = 15\frac{D_c}{r_p^2} \tag{9}$$

If interparticle diffusion is the rate-controlling step, then the values of diffusivity calculated by interparticle model and pseudo-first order model are expected to be in good agreement **[10]**. Otherwise, there should be other mechanism of diffusion which governed the CO_2 adsorption on MCM-41.

5.3.3.2. Intraparticle diffusion model

The adsorption of gases onto porous materials may be governed by either the gas phase mass transport or the intraparticle mass transport rate. Weber-Morris proposed that if adsorption process is influenced by intraparticle diffusion, the uptake of CO_2 (q_t) should vary linearly with the square root of time (t) **[23-25]**. The intraparticle diffusion model usually includes three steps. The first one is the external diffusion adsorption or boundary layer diffusion. The second one is the gradual stage of adsorption which is the intraparticle diffusion. The third one is the final equilibrium stage. The model is derived from Fick's second law of diffusion with the following assumptions

(i) The external resistance to mass transfer is only significant for a very short period at the beginning of diffusion.

(ii) The direction of diffusion is radial

(iii) The pore diffusivity is constant and does not change with time

This model represents a simplest approximation of pore diffusion kinetics and is proposed to identify the adsorption mechanism and predict the rate-controlling step. The adsorption capacity is expressed in the following form:

$$q_t = k_{id} t^{1/2} + C \tag{10}$$

Where k_{id} is the intraparticle diffusion rate constant which can be evaluated from the slope of the Weber-Morris plot of q_t versus $t^{1/2}$ and C represents the intercept. The values of intercept give an idea about the boundary layer thickness, i.e., larger the intercept, greater will be the boundary layer effect **[23-25]**.

According to this model, the Weber-Morris plot should give a straight line if diffusion plays a role in the adsorption rate and should pass through the origin if intraparticle diffusion is the sole rate-controlling step or else other processes may control the adsorption rate. Multi-linearity can be observed when different steps with different rate constants are involved in

adsorption mechanism. The slope of the linear portion corresponding to each step indicates the rate of adsorption. The linear portion having the lowest slope corresponds to the rate-controlling step.

5.3.3.3. Boyd's film-diffusion model

The film-diffusion model of Boyd is a single-resistance model that assumes the main resistance to diffusion is in the boundary layer surrounding the adsorbent particle. Hence, this model can also be used to determine the actual rate-controlling step involved in the CO_2 uptake behavior on MCM-41 and is expressed as

$$F = 1 - \frac{6}{\pi^2}\sum_{n=1}^{\infty}\frac{1}{n^2}\exp\left(-n^2 B_t\right) \tag{11}$$

where, F is the fractional attainment of equilibrium, at different times, t, and expressed as

$$F = \frac{q_t}{q_e} \tag{12}$$

where, q_t and q_e are the CO_2 uptake at time "*t*" and at equilibrium, respectively **[23, 26, 27]**. B_t is a function of F.

For $F > 0.85$,

$$B_t = -0.4977 - \ln\left(1 - F\right) \tag{13}$$

and for $F < 0.85$,

$$B_t = \left(\sqrt{\pi} - \sqrt{\pi - \left(\frac{\pi^2 F}{3}\right)}\right)^2 \tag{14}$$

Eqs (11)-(14) can be used in predicting the mechanistic steps involved in the adsorption process, i.e. whether the rate of adsorption of CO_2 takes place via particle diffusion or film diffusion mechanism. This is done by plotting B_t against time, if the plot is linear and passes through the origin then pore diffusion controls the rate of mass transfer. However, if the plot

is nonlinear or linear but does not pass through the origin, then it can be concluded that film-diffusion or chemical reaction also plays major role on the adsorption rate **[23, 26, 27]**.

5.4. Results & discussion

5.4.1. Comparison of kinetic models

Figure. 5.2 shows the experimental CO_2 uptake versus time at 30, 45, 60, 75 °C for wide range of pressures and the corresponding profiles as predicted by pseudo-first and second order models. Table 5.1-5.4 shows the values of the kinetic constants and the characteristic parameters of the kinetic models, along with the associated errors as calculated by eq 5. From Fig. 5.2, it can be seen that pseudo-first order model appears to fit the process accurately throughout the entire range of pressure and temperature. Accordingly, as can be seen from Table 5.1-5.4, the q values ($q_{e,cal}$) calculated from the pseudo-first order model are more consistent with the experimental q values ($q_{e,exp}$) than those calculated by the pseudo-second order model, providing a good agreement between the measured and predicted data throughout the entire range of pressure and temperature analyzed. This is because, pseudo-first order model is applicable under low surface coverage, and hence describes the early stages of adsorption **[10]**. In contrast, pseudo-second order kinetic model deviates to predict the CO_2 uptake on MCM-41, because this model better suits the adsorption process involving chemical interactions **[15]**. The results are in agreement with the earlier reports, where pseudo-first order model is found to describe the CO_2 uptake behavior better on physical adsorbents **[10]**. As the pseudo-first order equation fits well for the whole range of pressure and temperature, it is clear that adsorption of CO_2 on MCM-41 follows simple first order kinetics.

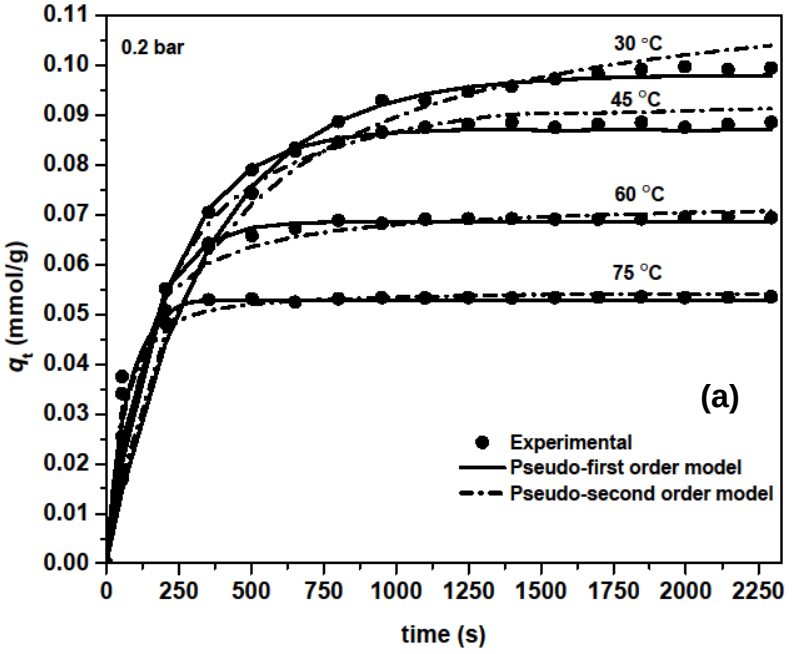

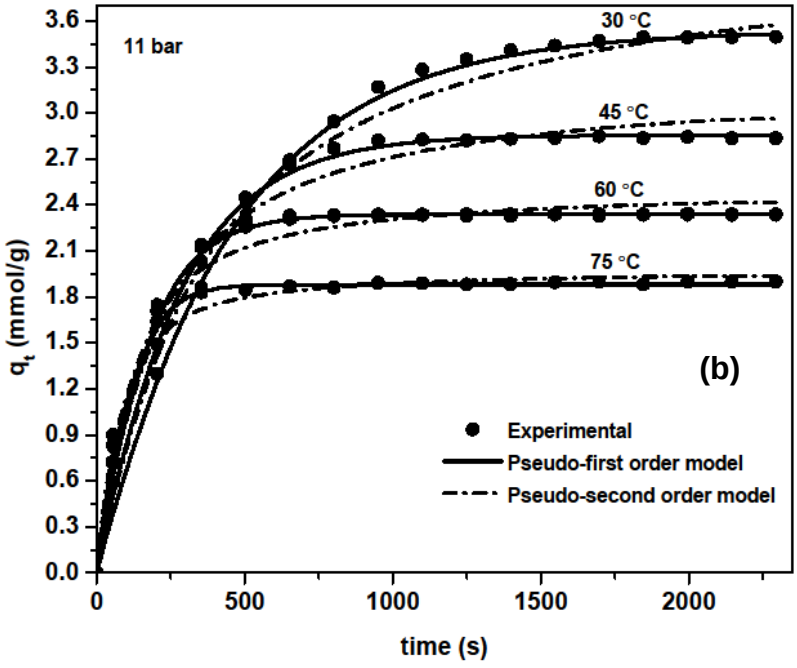

Figure 5.2. Pseudo first-order and pseudo second-order fits (a) 0.2 bar (b) 11 bar

Table 5.1. Kinetic parameters for pseudo-first order and pseudo-second order model at 30 °C.

		Pseudo-first order			Pseudo-second order		
Pressure (bar)	$q_{e,exp}$	$q_{e,cal}$	k_f x 10^{-3}	**Error,** Δq **(%)**	$q_{e,cal}$	k_s x 10^{-3}	**Error,** Δq **(%)**
0.2	0.099	0.098	2.94	4.34	0.118	22.13	7.13
0.3	0.217	0.212	2.89	9.28	0.246	15.21	3.87
0.5	0.302	0.300	2.84	4.90	0.349	10.15	3.61
0.6	0.409	0.403	2.81	2.08	0.470	7.37	6.40
0.8	0.531	0.529	2.80	2.71	0.603	6.22	6.22
1	0.605	0.623	2.79	1.76	0.753	4.15	9.51
3	1.337	1.354	2.63	2.08	1.599	1.96	10.73
5	1.950	1.981	2.48	3.13	2.353	1.24	6.55
7	2.506	2.547	2.27	6.48	3.040	0.87	6.16
9	3.023	3.082	2.22	6.33	3.685	0.68	5.87
11	3.495	3.536	2.22	7.52	4.150	0.65	5.49

Table 5.2. Kinetic parameters for pseudo-first order and pseudo-second order model at 45 °C.

		Pseudo-first order			Pseudo-second order		
Pressure (bar)	$q_{e,exp}$	$q_{e,cal}$	k_f x 10^{-3}	**Error,** Δq **(%)**	$q_{e,cal}$	k_s x 10^{-3}	**Error,** Δq **(%)**
0.2	0.088	0.087	4.78	6.81	0.101	61.78	1.96
0.3	0.135	0.135	4.69	8.48	0.158	37.07	2.80
0.5	0.203	0.202	4.50	5.48	0.240	22.26	4.40
0.6	0.245	0.244	4.46	2.26	0.286	18.32	5.78
0.8	0.328	0.324	4.36	6.93	0.359	18.33	2.41
1	0.398	0.400	4.30	6.11	0.476	10.60	4.31
3	1.041	1.032	4.27	6.06	1.153	5.34	2.74
5	1.556	1.551	4.03	6.21	1.742	3.27	3.50
7	2.096	2.116	3.87	5.89	2.404	2.18	6.50
9	2.444	2.462	3.84	6.87	2.822	1.80	5.49
11	2.834	2.855	3.84	6.68	3.215	1.68	5.15

Table 5.3. Kinetic parameters for pseudo-first order and pseudo-second order model at 60 °C.

		Pseudo-first order			Pseudo-second order		
Pressure (bar)	$q_{e,exp}$	$q_{e,cal}$	k_f x 10^{-3}	Error, Δq (%)	$q_{e,cal}$	k_s x 10^{-3}	Error, Δq (%)
0.2	0.069	0.068	7.90	7.24	0.073	185.52	3.02
0.3	0.127	0.126	7.88	3.40	0.137	89.77	3.14
0.5	0.148	0.146	7.75	6.55	0.160	75.41	2.11
0.6	0.183	0.181	7.60	6.67	0.195	62.39	2.61
0.8	0.248	0.246	7.53	6.33	0.262	48.38	3.13
1	0.299	0.295	7.50	6.27	0.326	34.00	2.12
3	0.778	0.769	7.44	6.89	0.819	15.18	5.16
5	1.231	1.203	7.24	2.77	1.298	8.70	4.59
7	1.730	1.721	7.16	1.98	1.827	6.60	5.89
9	2.030	2.019	7.00	4.01	2.172	5.25	4.44
11	2.335	2.339	6.72	3.81	2.518	4.35	5.53

Table 5.4. Kinetic parameters for pseudo-first order and pseudo-second order model at 75 °C.

		Pseudo-first order			Pseudo-second order		
Pressure (bar)	$q_{e,exp}$	$q_{e,cal}$	k_f x 10^{-3}	Error, Δq (%)	$q_{e,cal}$	k_s x 10^{-3}	Error, Δq (%)
0.2	0.053	0.052	21.4	1.33	0.064	648.6	2.11
0.3	0.077	0.076	20.5	1.66	0.089	417.7	2.01
0.5	0.107	0.107	18.4	1.36	0.133	.113.1	2.35
0.6	0.132	0.134	17.3	1.95	0.160	192.6	3.14
0.8	0.170	0.168	16.9	1.48	0.187	160.7	2.35
1	0.197	0.195	16.8	2.42	0.228	128.9	2.00
3	0.591	0.583	15.7	1.12	0.621	43.9	3.33
5	0.983	0.980	14.2	1.25	1.131	23.2	3.70
7	1.311	1.300	13.5	1.41	1.465	16.6	3.41
9	1.571	1.562	12.8	1.30	1.647	12.9	4.31
11	1.898	1.880	11.7	1.01	2.015	9.7	4.81

5.4.2. Analysis of kinetic model parameter

It can be observed from Table 5.1-5.4 that, pseudo-first order and second order model parameters (k_f and k_s) increase with temperature. This is because, when the temperature progresses molecule's speed (kinetic energy) also increases. So the CO_2 molecules will migrate faster inside the pores which in turn will result in an increase in the rate of diffusion. Hence, there is increase in mass transfer coefficient and the same is reflected in the form of much steeper CO_2 uptake curves (Fig. 5.2) with respect to temperature in the present work. From Fig. 5.2, reduction in the time required to reach equilibrium can be noticed (~ <500 s) for CO_2 uptake on MCM-41 at 60 and 75 °C when compared to (~1000 s) at 30 and 45 °C. Decrease in the time-scaling factor observed, indicates faster kinetics of CO_2 in MCM-41 with respect to rise in temperature. Again, k_f and k_s constantly decreases with increase in pressure which indicates that diffusion is the dominant rate-controlling step for the entire range of pressure. With increase in pressure, repulsive interactions between the neighbouring CO_2 molecules generally lead to an enhancement of wall collisions, causing a decrease in diffusivity. As diffusivity and pressure have an inverse relationship, diffusivity will always decrease with increase in pressure. The variation of k_f with respect to temperature for different pressure condition is also shown in Fig. 5.3. The results obtained in the current work are in good compliance with the literature data, where k values are observed to decrease with increase in pressure in the bulk phase **[28]**. However, the k values are not affected by a large amount with increase in pressure. This might be attributed to the possible fact that the pores of MCM-41 are not partially saturated or blocked even at high CO_2 loadings that can lead to sluggish kinetic behaviour which usually occurs in micro porous materials like zeolites **[29]** and activated carbons **[3]**. However, as mentioned earlier, these models do not provide information about the actual rate-controlling step for CO_2 adsorption on MCM-41.

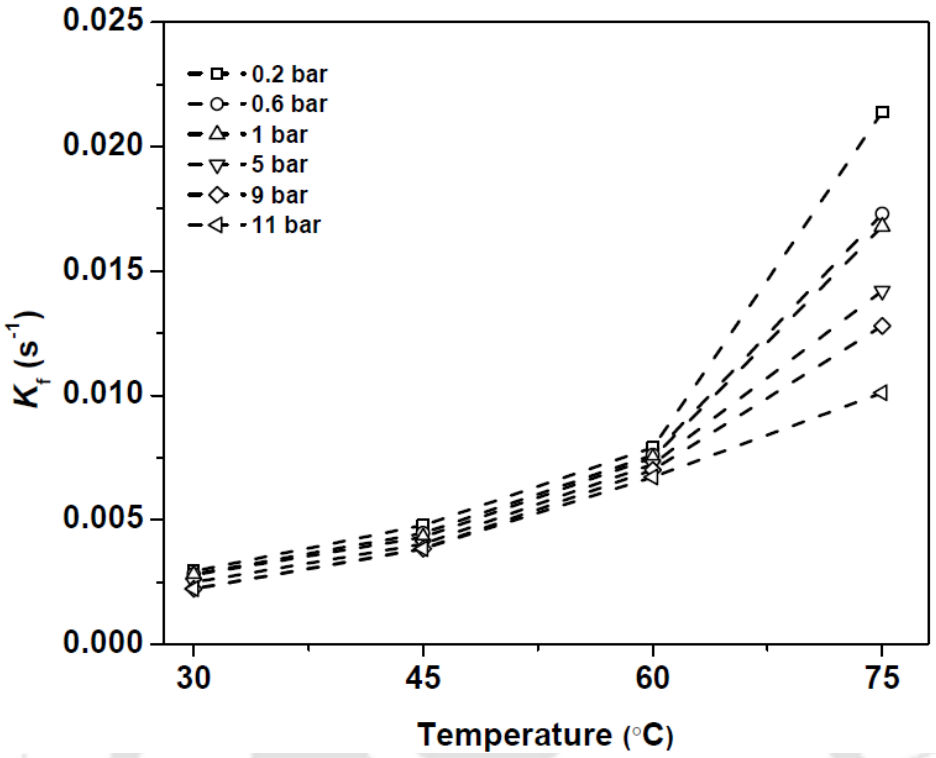

Figure 5.3. Variation of pseudo-first order rate constant (k_f) with temperature for different pressure conditions

Hence, interparticle diffusion model is applied to adsorption kinetic data to investigate whether interparticle diffusion controls the CO_2 uptake kinetics on MCM-41. It can be seen from Table 5.5, that the R^2 (regression co-efficient which determines how well the data points fit any model) values obtained the plots i.e. ln [1– (q_t /q_e)] vs t (not shown here) lie in the range of 0.98-0.99 irrespective of temperature and pressure conditions analyzed. This indicates that the interparticle model fits the experimental data well. Even though, R^2 values seem to reproduce quite well the experimental data, rigorous evaluation is required in order to choose the more reliable diffusion mechanism. It can be noticed from Table 5.5, that the intercept of the linear plots obtained from the fitting of the experimental data in most of the cases is not very close to −0.4977 (ln6/π^2). This suggests that the rate of CO_2 adsorption on MCM-41 is not governed by interparticle diffusion. The diffusion time constant or diffusivity factor is calculated from the slope of a linear plot of ln (1-q_e/q_t) versus t at a given pressure. Only data points with (q_e/q_t) greater than 70% and less than 99% are used for estimating the

diffusion time constants. Interparticle diffusion model is further used to corroborate the values of D_c/r_p^2 calculated from the pseudo-first order model. The diffusion time constant values calculated from pseudo first order model and interparticle model are found to be in poor agreement (Table 5.6). The difference in the value again reflects the violation the assumption of interparticle diffusion as rate-controlling step.

Table 5.5. Interparticle diffusion model

	30 °C			45 °C			60 °C			75 °C		
Pressure (bar)	**slope**	**intercept**	**R^2**	**slope**	**intercept**	**R^2**	**Slope**	**intercept**	**R^2**	**slope**	**intercept**	**R^2**
0.2	-0.0023	-0.1015	0.9952	-0.0037	-0.1179	0.9911	-0.0026	-0.6039	0.9902	-0.0041	-0.5882	0.9908
0.3	-0.0022	-0.1155	0.9920	-0.0043	-0.0409	0.9962	-0.0030	-0.3968	0.9912	-0.0032	-0.5574	0.9890
0.5	-0.0024	-0.168	0.9940	-0.0038	-0.1365	0.9909	-0.0042	-0.3284	0.9905	-0.0049	-0.4604	0.9908
0.6	-0.0021	-0.1864	0.9936	-0.0033	-0.1571	0.9907	-0.0047	-0.1534	0.9926	-0.0055	-0.2892	0.9919
0.8	-0.0023	-0.1902	0.9930	-0.0020	-0.4491	0.9827	-0.0021	-0.4905	0.9902	-0.0058	-0.4441	0.9884
1	-0.0028	-0.0055	0.9940	-0.0031	-0.1431	0.9918	-0.0039	-0.3939	0.9874	-0.0043	-0.2956	0.9850
3	-0.0025	-0.2252	0.9924	-0.0029	-0.2624	0.9900	-0.0031	-0.3215	0.9910	-0.0036	-0.5648	0.9877
5	-0.0031	-0.1231	0.9915	-0.0029	-0.2161	0.9931	-0.0027	-0.4312	0.9906	-0.0046	-0.6994	0.9847
7	-0.0028	-0.0853	0.9926	-0.0038	-0.1835	0.9907	-0.0025	-0.5417	0.9906	-0.0030	-0.5871	0.9907
9	-0.0028	-0.0044	0.9898	-0.0036	-0.1276	0.9912	-0.0032	-0.4856	0.9887	-0.0046	-0.4387	0.9930
11	-0.0025	-0.0313	0.9939	-0.0037	-0.0975	0.9914	-0.0045	-0.4459	0.9921	-0.004	-0.528	0.9910

Table 5.6. Comparison of diffusion time constants (D_c/r_P^2) from pseudo-first order and interparticle model

	30 °C		45 °C		60 °C		75 °C	
Pressure (bar)	**Interparticle (10^{-4} s^{-1})**	**Pseudo-first order (10^{-4} s^{-1})**	**Interparticle (10^{-4} s^{-1})**	**Pseudo -first order (10^{-4} s^{-1})**	**Interparticle (10^{-4} s^{-1})**	**Pseudo-first order (10^{-4} s^{-1})**	**Interparticle (10^{-4} s^{-1})**	**Pseudo-first order (10^{-4} s^{-1})**
0.2	2.33	1.95	3.75	3.19	2.64	5.26	4.16	14.26
0.3	2.23	1.92	4.36	3.13	3.04	5.25	3.25	13.69
0.5	2.43	1.89	3.85	3.01	4.26	5.16	4.97	12.28
0.6	2.13	1.87	3.35	2.97	4.77	5.06	5.58	11.54
0.8	2.33	1.86	2.03	2.91	2.13	5.02	5.58	11.29
1	2.84	1.86	3.14	2.86	3.96	5.00	4.36	11.20
3	2.54	1.75	2.94	2.84	3.14	4.96	3.65	10.51
5	3.14	1.65	2.94	2.68	2.74	4.82	4.67	9.49
7	2.84	1.51	3.85	2.58	2.54	4.77	3.04	9.02
9	2.84	1.48	3.65	2.56	3.25	4.66	4.67	8.56
11	2.54	1.47	3.75	2.55	4.56	4.47	4.06	7.79

This result suggests that there could be another process that controlled the rate of CO_2 adsorption on MCM-41. To further investigate the mechanism of CO_2 adsorption, a model of intraparticle diffusion is considered. Fig. 5.4 shows the Weber-Morris plot for CO_2 adsorption on MCM-41 at 30, 45, 60 and 75 °C and pressure varying from 0.1 to 11 bar. It is clear that the plots are not linear over the whole time range. However, they exhibit tri-linearity revealing the existence of three successive steps for CO_2 adsorption on MCM-41. The initial portion, region 'I' is attributed to the diffusion of CO_2 through the bulk gas phase to the external surface of MCM-41. The first stage is correlated to the boundary layer diffusion of CO_2. The second portion, region 'II' describes the gradual adsorption stage, where intraparticle diffusion takes place. The third portion, region 'III' is attributed to the final equilibrium stage at which the intraparticle diffusion starts to slow down due to saturation of active sites. It is worth to note the fact from Fig. 5.4(a and b) that the linear plots corresponding to region 'II' did not pass through the origin. This deviation may be due to difference in mass transfer rate in the initial and subsequent stages of CO_2 adsorption at low temperature. If the pore diffusion would have been the only rate-controlling step, the plots would have passed through the origin. This is indicative of boundary layer effect over the adsorption of CO_2 on MCM-41 at 30 °C and also at 45 °C. For each CO_2 molecule, it can be deduced that there are three processes that control the rate of adsorption but only one is rate-controlling in any particular time range at a given temperature. During the early stage of adsorption, film diffusion controls the rate of adsorption as indicated by the first linear segment of Fig. 5.4(a). After the CO_2 molecule has diffused through the film, intraparticle diffusion will be the rate governing step shown by second linear portion. Finally, the rate controlled by surface reaction. However, there would be only one rate-controlling step in overall CO_2 adsorption process. The overall rate-controlling step governing the CO_2 uptake kinetics on MCM-41 can be deduced from the slope of the linear portions prior to equilibrium stage (region III). Among the linear portions attributed to region I and II, where CO_2 adsorption process is kinetically driven, it can be seen that the slope corresponding to the bulk diffusion is the least. This implies that the diffusion of CO_2 from bulk phase to the exterior surface of MCM-41, which

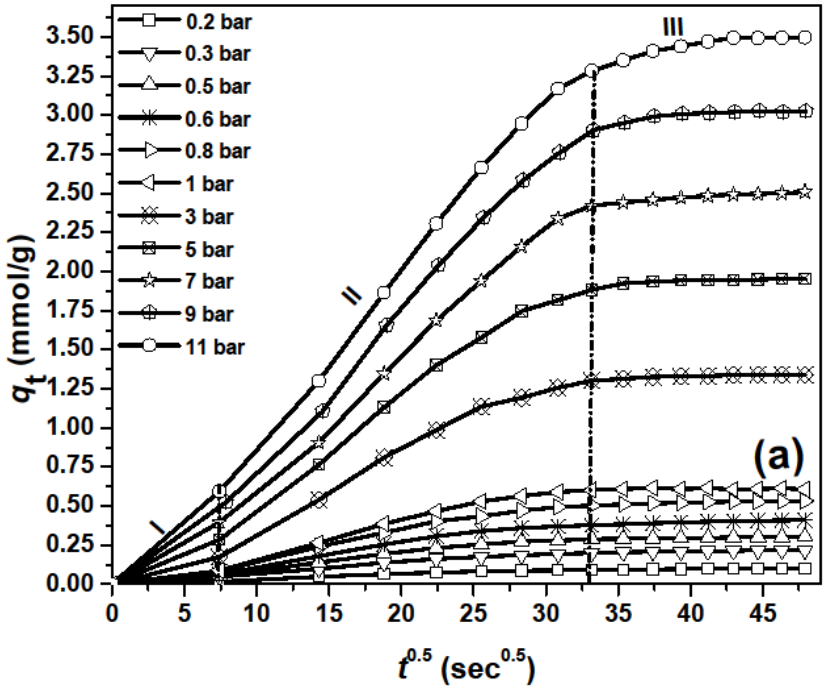

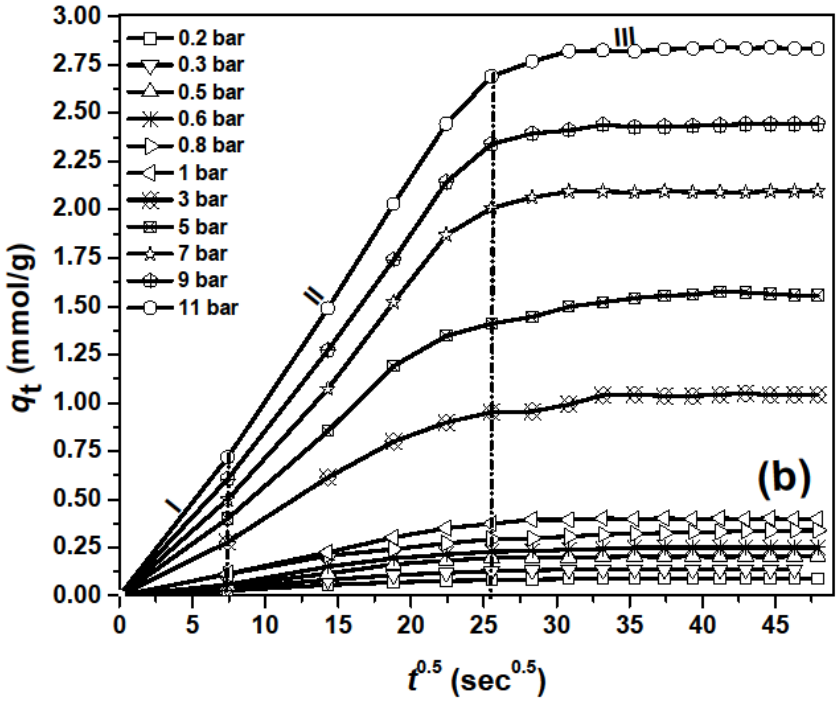

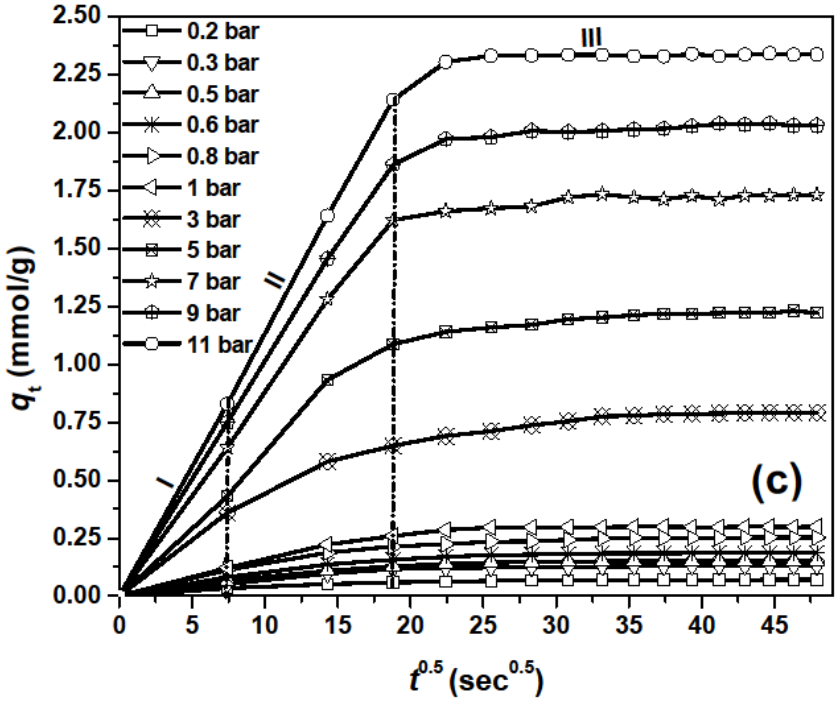

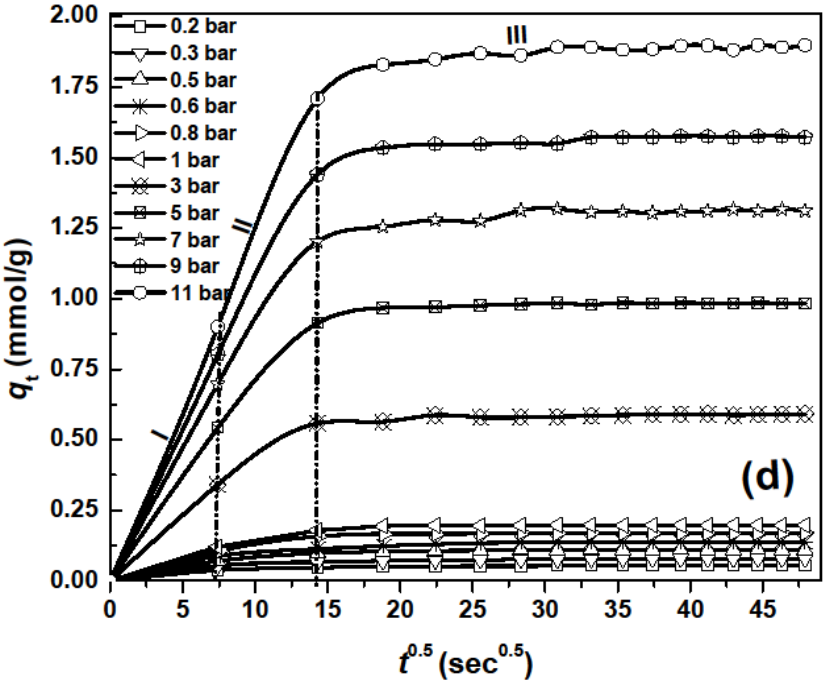

Figure 5.4. Prediction of Intraparticle diffusion model (a) 30 °C, (b) 45 °C, (c) 60 °C and (d) 75 °C

starts at the onset of the process, is the slowest and therefore the rate-controlling step. Interestingly, the slopes corresponding to first and second linear portion of the plot progressively increases with pressure (0.1 to 11 bar). A possible explanation for this phenomenon is that, with the rise in pressure, the film thickness will decrease and thereby the rate of film diffusion will increase. Similar phenomenon can be observed with respect to rise in temperature and it can be noticed from Fig. 5.4(b), (c) and (d) that both the slopes (corresponding to film and intraparticle diffusion) increase as pressure rises. In Fig. 5.4 (b), it can be noticed that, at 11 bar, the plot passes through the origin which suggests that the role of film diffusion becomes insignificant and pore diffusion is the only dominating factor in controlling the rate of CO_2 adsorption on MCM-41. For further progress in temperature (Fig. 5.4(c) and (d)), it can be seen that the plot passes through the origin even at lower pressure conditions (~7 bar for 60 °C and ~5 bar for 75 °C) indicating that intraparticle diffusion is the sole rate-controlling factor for overall CO_2 adsorption process on MCM-41 under the above mentioned conditions. In contrast, the plots (0.1 to 11 bar) obtained for 30 °C did not pass through the origin, which suggests that both film and pore diffusion processes controls the CO_2 uptake kinetics on MCM-41. However, the slope corresponding to film diffusion is the least for all the pressure conditions (0.1 to 11 bar) experimented at 30 °C indicating that film diffusion is highly involved in controlling the overall rate for CO_2 adsorption on MCM-41 at 30 °C.

A conclusion regarding mass transfer mechanism can be reached from the analysis of data by Boyd's model. The slopes and intercept of the Boyd model are given in Table 5.7 for all the pressure and temperature conditions. The presence of intercept values indicates that external mass transport mainly governs the rate-controlling process of adsorption of CO_2 onto MCM-41. However it seems that pore diffusion becomes more important at higher pressure, as the intercept approaches zero with increasing initial pressure for all the temperatures. This is in accordance with the result obtained from the intraparticle diffusion model.

Table 5.7. Boyd's model

	30 °C		45 °C		60 °C		75 °C	
P (bar)	**slope**	**Intercept**	**slope**	**Intercept**	**slope**	**Intercept**	**slope**	**Intercept**
0.2	0.002	-0.165	0.002	-0.037	0.003	-0.015	0.004	0.004
0.3	0.002	-0.151	0.002	-0.034	0.003	-0.014	0.003	-0.006
0.5	0.002	-0.149	0.003	-0.032	0.004	-0.012	0.005	-0.004
0.6	0.002	-0.134	0.002	-0.027	0.004	-0.011	0.004	-0.002
0.8	0.002	-0.125	0.002	-0.026	0.002	-0.010	0.006	-0.001
1	0.002	-0.118	0.002	-0.020	0.004	-0.010	0.004	-0.001
3	0.002	-0.112	0.002	-0.019	0.002	-0.009	0.004	-0.001
5	0.002	-0.109	0.002	-0.014	0.002	-0.003	0.005	0
7	0.001	-0.065	0.003	-0.012	0.001	0.001	0.004	-0.0001
9	0.001	0.041	0.002	-0.001	0.002	0.00003	0.005	-0.0001
11	0.001	-0.014	0.002	0.00004	0.003	-0.00001	0.004	-0.00008

5.5. Conclusions

Investigation on the CO_2 uptake kinetics on MCM-41 under wide range of pressure and temperature conditions is carried out. Pseudo-first order kinetic model successfully describes the adsorption kinetics of CO_2 on MCM-41 throughout the entire range of pressure and temperature regime suggesting that the adsorption process is controlled by physisorption. Information regarding CO_2 diffusion mechanism is obtained by further analyzing the kinetic data by intraparticle diffusion model. At 30 °C, for all the pressure conditions analyzed, it is found that film diffusion is highly involved in controlling the the CO_2 uptake kinetics on MCM-41. As the temperature progresses, with respect to rise in pressure, it is observed that film diffusion process becomes insignificant and pore diffusion process is the sole governing factor controlling the CO_2 adsorption kinetics on MCM-41. Boyd's model also corroborated the CO_2 diffusion mechanism elucidated by intraparticle diffusion model.

5.6. References

[1] Ding, L. P.; Bhatia, S. K.; and Liu, F. Kinetics of Adsorption on Activated carbon: Application of Heterogeneous Vacancy Solution Theory. *Chem. Eng. Sci.* **2002**, 57, 3909 - 3928.

[2] Shen, C.; Grande, C. A.; Li, P.; Yu, J.; and Rodrigues, A. E. Adsorption Equilibria and Kinetics of CO_2 and N_2 on Activated Carbon Beads. *Chem. Eng. J.* **2010**, 160, 398-407.

[3] Saha, D.; and Deng, S. Adsorption Equilibrium and Kinetics of CO_2, CH_4, N_2O, and NH_3 on Ordered Mesoporous Carbon. *J. Colloid Interface Sci.* **2010**, 345, 402-409.

[4] Grande, C. A.; and Rodrigues, A. E. Adsorption Kinetics of Propane and Propylene in Zeolite 4A. *Chem. Eng. Res. Des.* **2004**, 82, 1604-1612.

[5] Cheung, O.; Bacsik, Z.; Liu, Q.; Mace, A; and Hedin, N. Adsorption Kinetics For CO_2 On Highly Selective Zeolites NaKA and Nano-NaKA. *Applied Energy*, **2013**, 112, 1326-1336.

[6] Yi, H.; Deng, H.; Xiaolong, Q. Y.; Zhou, X.; and Liu, H. Adsorption Equilibrium and Kinetics for SO_2, NO, CO_2 on Zeolites FAU and LTA. *J. Hazard. Mater.* **2012**, 203, 111-117.

[7] Baoa, Z.; Alnemratc, S.; Yub, L.; Vasilievc, I.; Rena, Q.; Lua, X.; and Deng, S. Kinetic Separation of Carbon dioxide and Methane on a Copper Metal-organic framework. *J. Colloid Interface Sci.* **2011**, 357, 504-509.

[8] Sabouni, R.; Kazemian, H.; and Rohani, S. Carbon Dioxide Adsorption in Microwave-Synthesized Metal Organic Framework CPM-5: Equilibrium and Kinetics Study, *Microporous Mesoporous Mater.* **2013**, 175, 85-91.

[9] Nobar, S. N.; and Farooq, S. Experimental and Modeling Study of Adsorption and Diffusion of Gases in Cu-BTC. *Chem. Eng. Sci.* **2012**, 84, 801-813.

[10] Sayari, A.; and Guerrero, R.S. Modeling Adsorption of CO_2 on Amine-Functionalized Mesoporous silica. 2: Kinetics and Breakthrough Curves. *Chem. Eng. J.* **2010**, 161, 182-190.

[11] Sayari, A.; and Gorji, A.H. CO_2 Capture on Polyethyleneimine-Impregnated Hydrophobic Mesoporous silica: Experimental and Kinetic Modeling. *Chem. Eng. J.* **2011**, 173, 72-79.

[12] Ai, L.; Zhang, C.; and Meng, L. Adsorption of Methyl Orange from Aqueous Solution on Hydrothermal Synthesized Mg-Al Layered Double Hydroxide, *J. Chem. Eng. Data.* **2011**, 56, 4217-4225.

[13] Shokrollahi, A.; Alizadeh, A.; Malekhosseini, Z.; and Ranjbar, M. Removal of Bromocresol Green from Aqueous Solution via Adsorption on Ziziphus *nummularia* as a New, Natural, and Low-Cost Adsorbent: Kinetic and Thermodynamic Study of Removal Process, *J. Chem. Eng. Data*. **2011**, 56, 3738-3746.

[14] Ho, Y. S.; and McKay, G. Sorption of Dye from Aqueous Solution by Peat, *Chem. Eng. J.* **1998**, 70, 115-124.

[15] Borah, J. M.; Sarma, J.; and Mahiuddin, S. Adsorption Comparison at the Alumina/Water Interface: 3,4-Dihydroxybenzoic Acid vs. Catechol. *Colloids Surf., A.* **2011**, 387, 50-56.

[16] Cheung C. W.; Porter, J. F.; and McKay, G. Sorption Kinetic Analysis for the Removal of Cadmium Ions from Effluents using Bone Char. *Water Res.* **2001**, 35, 605-612.

[17] Gupta, S. S.; and Bhattacharyya, K. G. Kinetics of Adsorption of Metal ions on Inorganic Materials: A Review. *Adv. Colloid Interface Sci.* **2011**, 162, 39-58.

[18] Boyd, G. E.; Adamson, A. W.; and Meyers, L. S. The Exchange Adsorption of Ions from Aqueous Solutions by Organic Zeolites: Kinetics. *J. Am. Chem. Soc.* **1947**, 69, 2836-2848.

[19] Lopes, E.C.N.; Anjos, F.S.C.; Vieira, E.F.S.; and Cestari, A.R. An Alternative Avrami Equation to Evaluate Kinetic Parameters of the Interaction of Hg(II) with Thin Chitosan Membranes, *J. Colloid Interface Sci*. **2003**, 263, 542-547.

[20] Cestari, A.R.; Vieira, E.F.S.; Vieira, G.S.; and Almeida, L.E. The Removal of Anionic Dyes from Aqueous Solutions in the Presence of Anionic Surfactant using Aminopropylsilica - A Kinetic Study, *J. Hazard. Mater. B*. **2006**, 138, 133-141.

[21] Do, D.D.; and Do, H.D. Non-isothermal Effects on Adsorption Kinetics of Hydrocarbon Mixtures in Activated Carbon, *Sep. Purif. Technol.* **2000**, 20, 2049-65.

[22] Ruthven, D.M. Principles of Adsorption and Adsorption Processes, (Wiley, New York, ed., **1984**.

[23] Hameed, B.H.; Tan, I.A.W.; and Ahmad, A.L. Adsorption Isotherm, Kinetic Modeling and Mechanism of 2,4,6-trichlorophenol on Coconut husk-based Activated Carbon, *Chem. Eng. J.* **2008**,144, 235-244.

[24] Abramian, L.; and Rassy, H. Adsorption Kinetics and Thermodynamics of Azo-Dye Orange II onto Highly Porous Titania Aerogel, *Chem. Eng. J.* **2009**, 150, 403-410.

[25] Yousef, R.I.; Eswedb, B.; and Muhtasebc, A. H. Adsorption Characteristics of Natural Zeolites as Solid adsorbents for Phenol Removal from Aqueous Solutions: Kinetics, Mechanism, and Thermodynamics Studies, *Chem. Eng. J.* **2011**, 171, 1143-1149.

[26] Sharma, P.; and Das, M. R. Removal of a Cationic Dye from Aqueous Solution Using Graphene Oxide Nanosheets: Investigation of Adsorption Parameters, *J. Chem. Eng. Data*. **2013**, 58, 151-158.

[27] Ai, L.; Li, L. M.; and Li, L. Adsorption of Methylene Blue from Aqueous Solution with Activated Carbon/Cobalt Ferrite/Alginate Composite Beads: Kinetics, Isotherms and Thermodynamics. *J. Chem. Eng. Data*. **2011**, 56, 3475-3483.

[28] Campo, M.C.; Magalhães, F.D.; and Mendes, A. Comparative Study between a CMS Membrane and a CMS Adsorbent: Part I - Morphology, Adsorption Equilibrium and Kinetics, *J. Membr. Sci.* **2010,** 346, 15-25.

[29] Li, P.; and Tezel, H. Equilibrium and Kinetic Analysis of CO_2-N_2 Adsorption Separation by Concentration Pulse Chromatography, *J. Colloid Interface Sci.*, **2007,** 313, 12-17.

CHAPTER 6

SYNTHESIS, CHARACTERIZATION AND CO_2 ADSORPTION STUDIES FOR AMINE TETHERED MCM-41

The chapter highlights the importance for selection of suitable support for amine tethering. The optimization of synthesis procedure for fine tuning of the adsorbent's composition for its better CO_2 capture performance is discussed. Several characterization techniques used for structural, thermal, organic loading analyses and CO_2 adsorption performance of amine tethered MCM-41 is discussed.

6.1. Introduction

Dry grafting process is basically a reaction between surface silanol groups of mesoporous silica and alkoxy ligands of amino silane compounds, which leads to the formation of amine tethered functionalities on the pore walls of silica **[1]**. In dry grafting process, it is considered that ideally all the alkoxy ligands would react with surface silanol moieties through condensation reaction and liberate ethanol or methanol (depending on whether ethoxy or methoxy ligand is present in the amino silane compound selected). Hence, the final grafted structure is expected to be $(SiO)_3$ Si-R, where R represents the mono amine or tri amine chain (shown in Figure 6.1(a)) **[1]**. According to the assumption made for dry grafting process, stoichiometric ratio for SiOH-amino silane reaction should be 3:1 i.e., three Si-OH groups will be consumed per amino silane compound grafted, in order to achieve the above discussed structure. However, in practical conditions, one or two alkoxy groups may not react with Si-OH, such that always some free alkoxy ligands will be left in the reaction mixture (Figure 6.1(b)) **[1]**.

As the amine tethering process is dependent on the availability of surface silanol groups, the key to enhance silanol density and hence, amine loading is surface hydration of silica by wet grafting process. The benefit of wet grafting method is twofold (i) water would interact with the silica surface and thereby, help in enhancing the surface silanol density **[1, 2]** and (ii) water added could initiate the hydrolysis and condensation reaction between unreacted alkoxy ligands with free amino silane compound present in the reaction mixture leading to fully cross-linked and monolayer coverage of amino silane functionalities as proposed by Feng et al. shown in Figure 6.1(c)) **[3]**. However, achieving perfect monolayer coverage in reality is an ideal condition. This is due to the fact that all the aminosilane compounds may not be tethered directly with the surface silanol groups but linked to other grafted silane moieties through siloxane linkages as shown in Figure 6.1(d) **[1, 2]**. As the main objective of this doctoral work is to enhance the CO_2 uptake capacity in the low partial pressure regime (0.1-0.2 bar), increasing the surface coverage of accessible amine moieties without pore

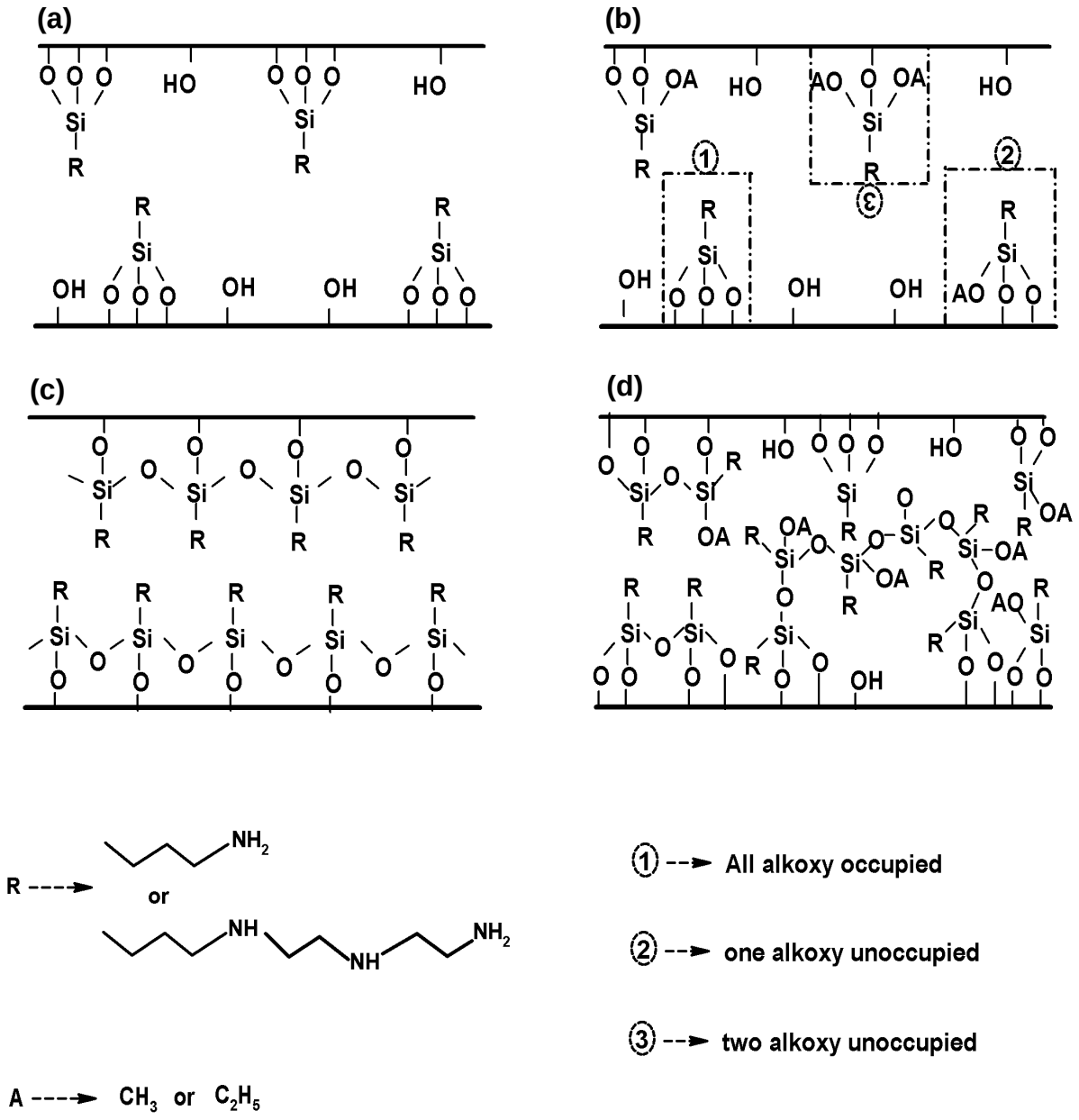

Figure 6.1. Hypothetical representation of pore wall surface under (a) and (b) dry grafting, (c) and (d) wet grafting conditions.

blockage becomes important. This can be achieved by optimizing the water-aminosilane ratio per gram of silica support and the temperature condition suitable for grafting reaction. Therefore, this part of work is devoted to the selection of suitable support for amine tethering process and optimization of adsorbent composition for its better CO_2 adsorption performance.

6.2. Experimental section

6.2.1. Materials

The details of materials used for synthesis of MCM-41 have been described in section 3.2.1. 3-aminopropyl triethoxy silane (hereafter will be referred to as 'mono amine' (AP)) and N-(3-trimethoxysilylpropyl) diethylenetriamine (hereafter will be referred to as 'tri amine' (TP)) obtained from Hi-media and Sigma Aldrich respectively were used as the amino-silane coupling agent. CO_2 and N_2 gas used for adsorption equilibrium measurements is 99% pure and was supplied by Assam Air Products, Guwahati, India.

6.2.2. Synthesis of amine grafted MCM-41

The synthesis procedure for MCM-41 has been described in section 3.2.2. Calcined MCM-41 (1 g) was weighed and transferred in to a dried 250 mL round bottomed flask. The support material was then dried at 120 °C for around 2 hours to desorb any adsorbed moisture. Anhydrous toluene (100 mL) and 0.3-0.7 mL water was added and the mixture was equilibrated. Then, 9 mmol of AP or TP was added to the above mixture and stirred at 75-90 °C under reflux condition for 24 hours. The obtained product was vacuum filtered, washed with copious amounts of anhydrous toluene and ethanol to remove any physisorbed aminosilanes from the sample. The as-synthesized AP and TP grafted MCM-41 was vacuum dried at 60 °C for 8 hours and stored in a dry sample box to carry out further characterization and CO_2 adsorption studies. The samples are named as MCM-41-PS-AG-X-Y-Z, where PS, AG, X, Y, and Z refers to the pore size (nm) of the MCM-41 support, type of amine, amount of amine added (mmol), temperature (°C) of the reaction mixture and amount of water (mL) added for wet grafting technique.

6.2.3. Material characterization

The details about characterization of MCM-41 have been elaborated in section 3.2.3. The characterization details for amine grafted MCM-41 samples are as follows: Nitrogen

physisorption measurements were conducted on a Beckman Coulter surface area analyzer (Coulter SA model 3100). The adsorbent was degassed at 125 °C for 3 h prior to N_2 adsorption-desorption measurements. The specific surface area was calculated from the BET (Brunauer, Emmett, and Teller) model. The pore size distribution was obtained through the BJH (Barrett, Joyner and Halenda) approach, and the total pore volume was estimated at a relative pressure of 0.99, assuming that full surface saturation had been achieved with nitrogen. Thermo gravimetric analysis (TGA) was performed on a Mettler Toledo thermo gravimetric analyzer (TGA/SDTA 851® model). The measurements were carried out under nitrogen atmosphere with a heating rate of 10 °C/min. FT-IR spectra were recorded between 4,000 and 450 cm^{-1} region using spectroscopic quality KBr powder with a Shimadzu IR affinity-1 model spectrometer. EDX spectra are pictoriated by scanning electron microscopy (SEM) (Make: Zeiss Model: LEO1430VP). The amine content of the samples was analyzed by an elemental analyser (Make: EuroEA Model: 3000).

6.2.4. CO_2 adsorption measurements

Adsorption equilibrium measurements of pure CO_2 on amine grafted MCM-41 samples at 30 °C and in the pressure range of (0-5 bar) were measured using a Rubotherm Magnetic Suspension balance. The measurements were carried out by using the similar procedure described in section 3.2.5. The amine grafted MCM-41 samples were activated by heating it at 125 °C under vacuum and then purging with helium.

6.3. Results & discussion

6.3.1. Selection of suitable support for amine tethering

In chapter 3, effect of aqueous ammonia on the pore size and pore volume of MCM-41 was investigated. From the outcome of the study, it was concluded that addition of 9 mL and 1 mL aqueous ammonia in the reaction mixture showed significant effect on the pore size (3 nm and 30 nm respectively) and pore volume (0.8 and 2.56 cc/g respectively). Hereafter, the MCM-41 samples characterized with pore size of 3 nm and 30 nm will be referred to as

MCM-41-3 and MCM-41-30 respectively. In order to investigate the influence of pore size and pore volume on the amine tethering, two different MCM-41 supports discussed above are selected.

6.3.1.1 Surface area analysis

Mono amine tethering on the MCM-41-3 as well as MCM-41-30 was carried out under dry conditions. The respective compositions of the adsorbents and their corresponding textural characteristics are provided in Table 6.1 (samples 1-12). The N_2 adsorption-desorption isotherms of the corresponding adsorbents are shown in Figure 6.2(a and b). The isotherms observed for the MCM-41-3 and MCM-41-30 samples depict a typical type IV adsorption-desorption isotherm and exhibit remarkably sharp capillary condensation steps, which is the characteristic feature of the mesoporous material **[4, 5]**. The adsorption isotherm for the MCM-41-30 features a narrow type 1 hysteresis loop with parallel adsorption and desorption branches, whereas adsorption isotherm for MCM-41-3 is found to be reversible as the adsorption curve almost coincided with the desorption curve. This indicates the more pronounced effect of capillary condensation in case of MCM-41-30 suggesting larger pore size and pore volume **[4, 5]**. The total adsorbed amount is also significantly high (62%) for MCM-41-30 in comparison to MCM-41-3, suggesting that the pore volumes are huge for larger size pores.

It can be seen from Table 6.1, with respect to increase in the monoamine concentration in the reaction mixture (for both MCM-41-3 and MCM-41-30 supports), the surface area, pore volume and volume adsorbed are found to exhibit decreasing trend. For MCM-41-3-AP-5-75, ~96%, 80% and 82% reduction in the surface area, pore volume and volume adsorbed respectively can be observed in comparison to MCM-41-3. Similarly, for MCM-41-30-AP-5-75 also exhibits ~70%, 36% and 35% reduction in the surface area, pore volume and volume adsorbed respectively comparison to MCM-41-30. This phenomenon confirms that silanol moieties of both the supports are utilized for covalent tethering of mono amino silane

moieties. However, with further increase in the amine concentration in the reaction mixture (for both the supports), significant reduction in the above mentioned textural properties are not observed. This indicates that amine tethering is solely dependent on the availability of silanol functionalities in the pore walls which is in contrast to amine

Table 6.1. Textural properties of MCM-41 samples

S:NO	*Sample Code	Surface Area (m^2/g)	Pore Volume (cc/g)	Volume Adsorbed (cc/g)
1	MCM-41-3	1204.13	0.7902	594.79
2	MCM-41-3-AP-5-75	48.37	0.1602	108.93
3	MCM-41-3-AP-7-75	42.12	0.1401	71.42
4	MCM-41-3-AP-9-75	40.15	0.1341	62.27
5	MCM-41-3-AP-11-75	38.14	0.1117	46.37
6	MCM-41-3-AP-13-75	37.61	0.1007	45.67
7	MCM-41-30	1045.21	2.58	1661.9
8	MCM-41-30-AP-5-75	314.58	1.6460	1080.37
9	MCM-41-30-AP-7-75	299.14	1.5360	986.39
10	MCM-41-30-AP-9-75	279.22	1.4190	908.15
11	MCM-41-30-AP-11-75	259.48	1.3703	890.29
12	MCM-41-30-AP-13-75	233.14	1.3672	854.23
13	MCM-41-30	1045.21	2.58	1661.9
14	MCM-41-30-TP-5-75	312.65	1.62	1078.57
15	MCM-41-30-TP-7-75	297.18	1.50	982.48
16	MCM-41-30-TP-9-75	274.32	1.39	904.68
17	MCM-41-30-TP-11-75	255.68	1.35	882.78
18	MCM-41-30-TP-13-75	230.51	1.33	850.31
19	MCM-41-30-AP-9-75	279.22	1.4190	908.15
20	MCM-41-30-AP-9-75-0.3	96.73	1.2330	797.05
21	MCM-41-30-AP-9-75-0.5	62.62	0.7614	492.25
22	MCM-41-30-AP-9-75-0.7	51.58	0.6033	400.78
23	MCM-41-30-AP-9-80-0.5	62.80	0.6864	443.74
24	MCM-41-30-AP-9-85-0.5	60.21	0.6784	440.04
25	MCM-41-30-AP-9-90-0.5	53.16	0.5457	352.78
26	MCM-41-30-TP-9-75	274.32	1.39	904.68
27	MCM-41-30-TP-9-75-0.3	38.75	0.4096	279.02
28	MCM-41-30-TP-9-75-0.5	8.91	0.0998	65.06
29	MCM-41-30-TP-9-75-0.7	8.42	0.0915	64.57
30	MCM-41-30-TP-9-80-0.3	37.17	0.399	274.28
31	MCM-41-30-TP-9-85-0.3	33.70	0.3498	243.28
32	MCM-41-30-TP-9-90-0.3	31.82	0.3439	242.53

* The samples are named as MCM-41-PS-AG-X-Y-Z, where PS, AG, X, Y, and Z refers to the pore size (nm) of the MCM-41 support, type of amine, amount of amine added (mmol), temperature (°C) of the reaction mixture and amount of water (mL) added for wet grafting technique.

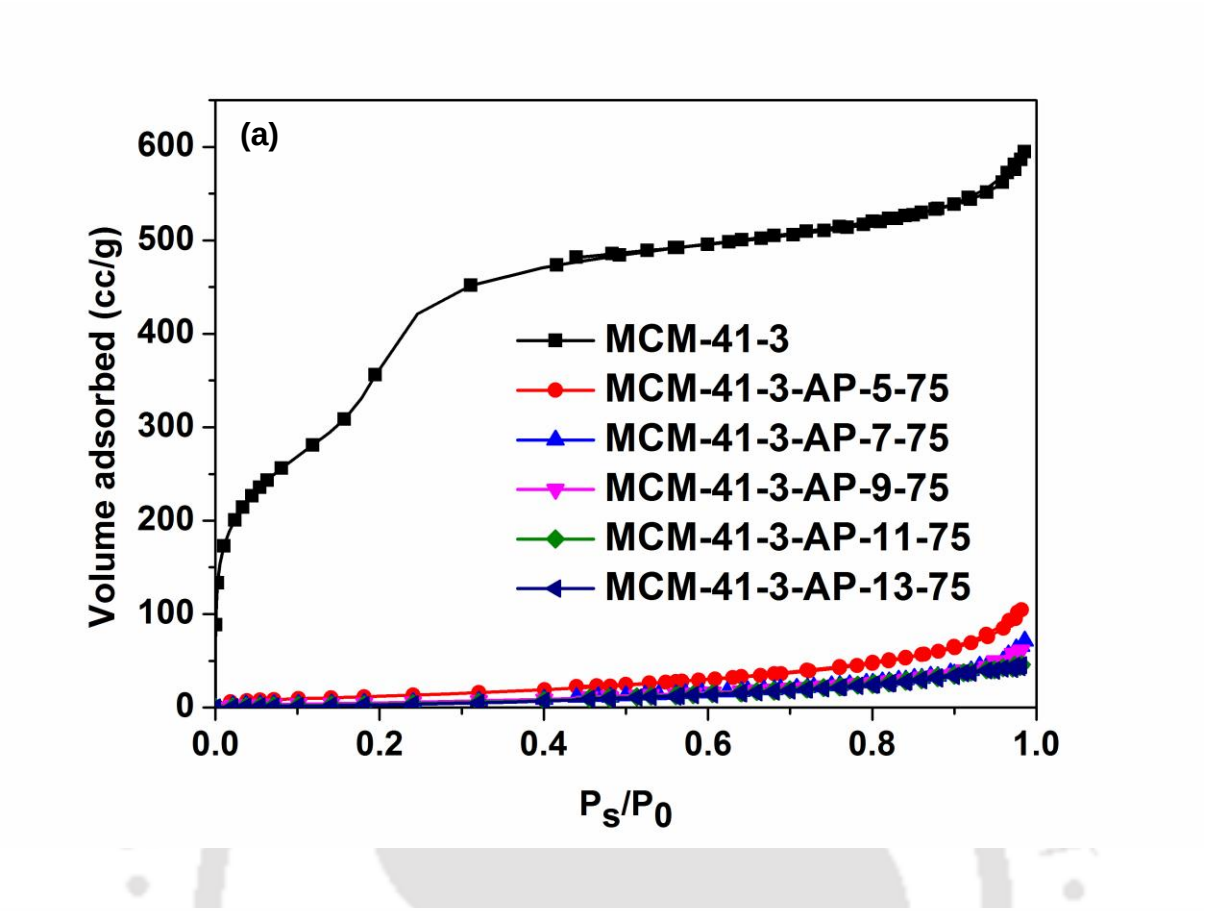

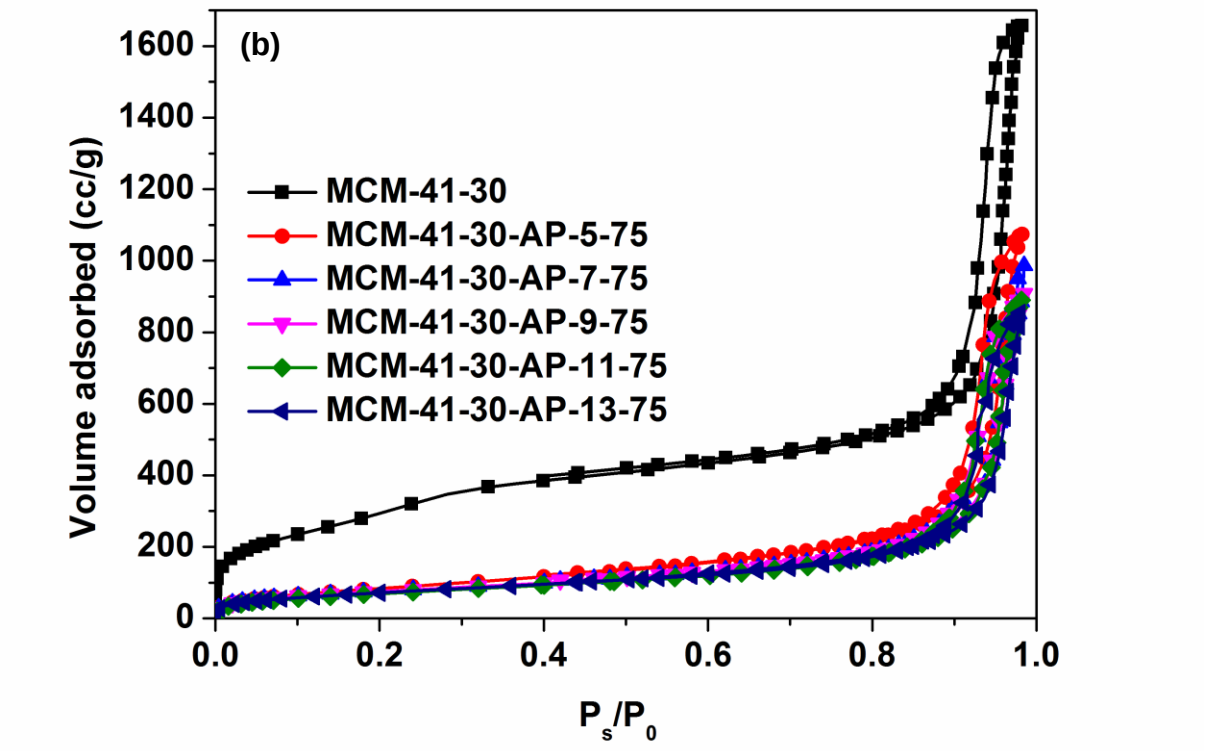

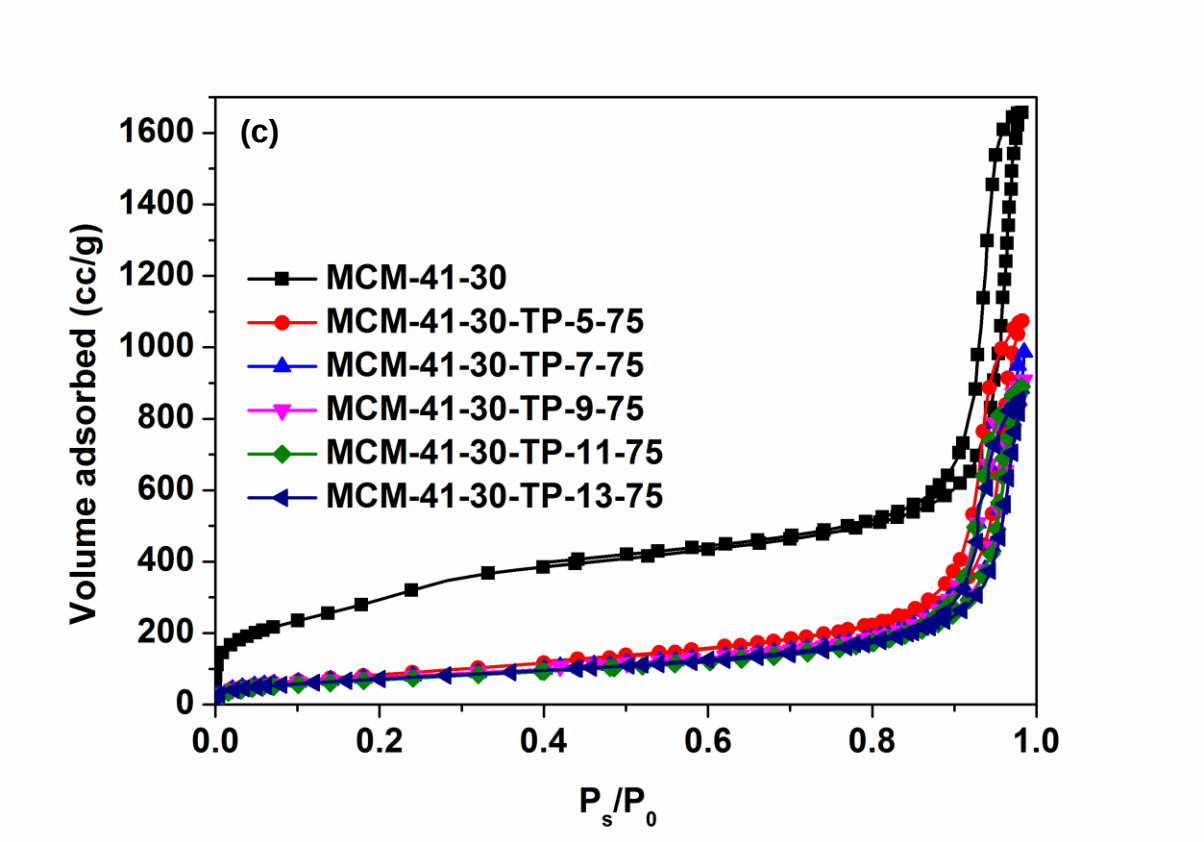

Figure 6.2. N_2 adsorption-desorption isotherms for (a) MCM-41-3-AP (b) MCM-41-30-AP and (c) MCM-41-30-TP series

impregnation process where the amine functionalization is totally dependent on the available vacant space inside the pores. From Figure 6.2 (a and b), it can be noticed that MCM-41-3-AP series exhibits type III isotherms indicative of pore blockage after mono amine tethering. However, MCM-41-30-AP series are found to exhibit type IV isotherms which indicate that mesoporosity is still maintained in the adsorbent system even after mono amino silane tethering. With respect to increase in the triamine concentration in the reaction mixture, similar phenomenon is observed for MCM-41-30-TP series (shown in Figure 6.2(c)). The significance of this behaviour is well reflected in terms of CO_2 adsorption capacity which is discussed in detail as follows.

6.3.1.2. CO_2 adsorption analysis

The CO_2 adsorption measurements on MCM-41-3-AP, MCM-41-30-AP and MCM-41-30-TP series adsorbents were carried out and their corresponding adsorption capacities ranging from 0-5 bar are shown in Figure 6.3. The comparison of CO_2 adsorption capacities for the above mentioned series (at 30 °C, 0.2 bar), amine loading and amine efficiency is tabulated in Table 6.2. It can be noticed from Table 6.2, MCM-41-30 series exhibits higher CO_2 adsorption capacity than MCM-41-3, irrespective of the amount of monoamino silane added. In case of MCM-41-3 series, CO_2 adsorption capacity, amine loading, amine efficiency decreased with respect to amount of amino silane added in the reaction mixture. In contrast, MCM-41-30 series exhibited a maximum CO_2 adsorption capacity, amine loading, amine efficiency for 9 mmol of amino silane (both mono and tri) addition in the reaction mixture. Further increase in amine concentration affected grafting efficiency and hence amine loading as well as CO_2 adsorption capacity exhibited downturn. These results indicate that MCM-41-30 serves as a promising support for amino silane tethering.

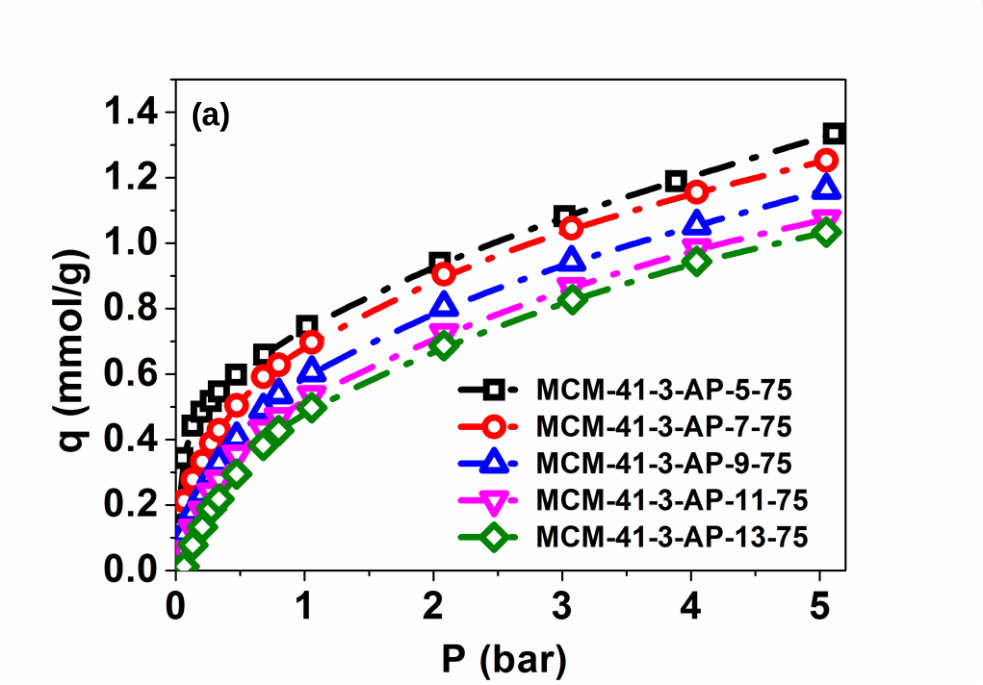

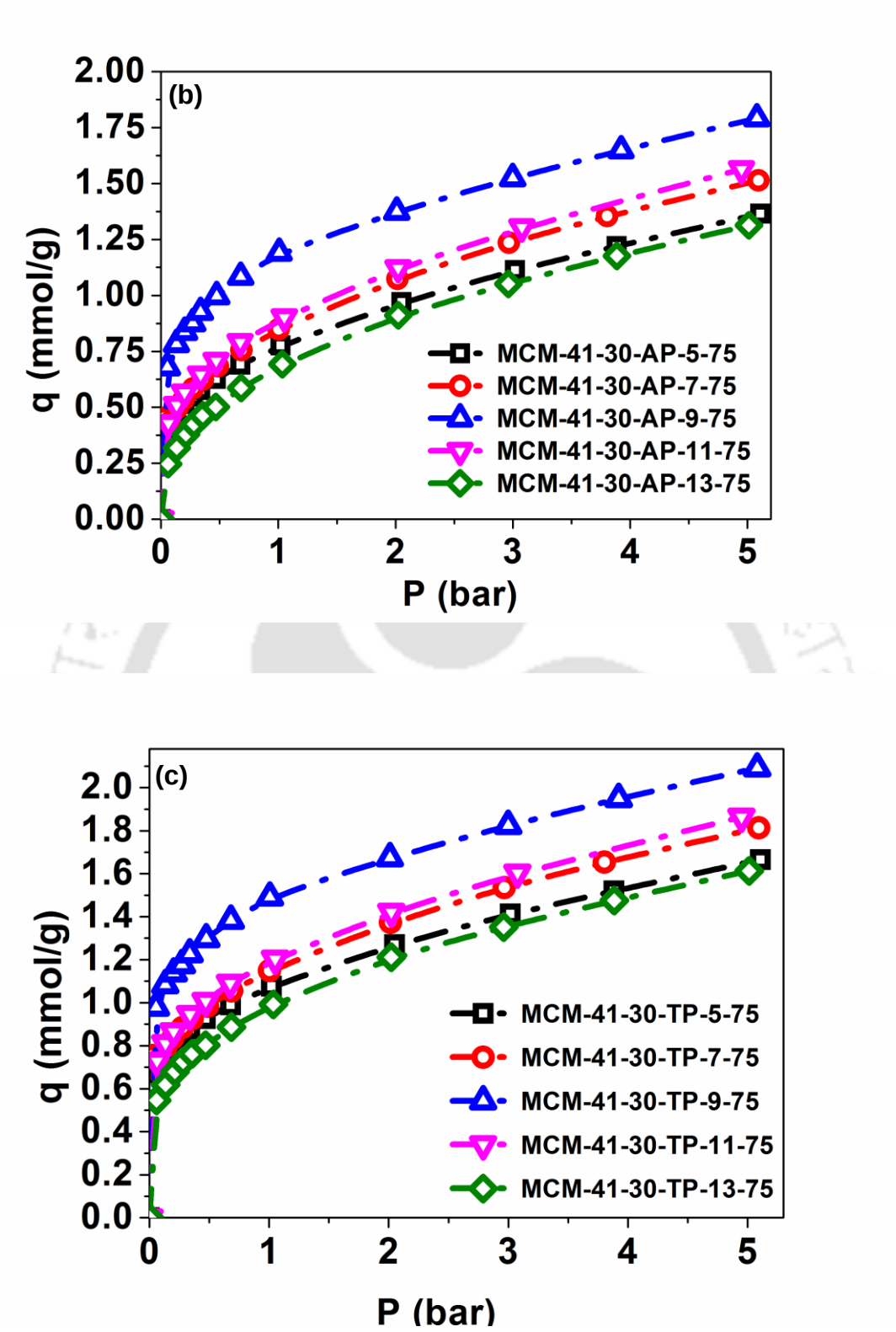

Figure 6.3. CO_2 adsorption isotherms at 30 °C for (a) MCM-41-3-AP (b) MCM-41-30-AP and (c) MCM-41-30-TP series.

Table 6.2. Comparison of CO_2 adsorption capacity, amine loading and amine efficiency

S:NO	Sample Code	CO_2 adsorption capacity (30 °C, 0.2 bar)	Amine loading (mmol (N)/g)	Amine efficiency (mmol (CO_2)/mmol (N))
1	MCM-41-3	0.12	-	-
2	MCM-41-3-AP-5-75	0.45	1.84	0.24
3	MCM-41-3-AP-7-75	0.33	1.52	0.22
4	MCM-41-3-AP-9-75	0.23	1.31	0.17
5	MCM-41-3-AP-11-75	0.20	1.24	0.16
6	MCM-41-3-AP-13-75	0.18	1.22	0.15
7	MCM-41-30	0.13	-	-
8	MCM-41-30-AP-5-75	0.50	1.81	0.28
9	MCM-41-30-AP-7-75	0.55	1.85	0.30
10	MCM-41-30-AP-9-75	0.83	2.21	0.38
11	MCM-41-30-AP-11-75	0.56	1.83	0.31
12	MCM-41-30-AP-13-75	0.37	1.40	0.26
13	MCM-41-30	0.13	-	-
14	MCM-41-30-TP-5-75	0.81	3.79	0.21
15	MCM-41-30-TP-7-75	0.85	3.85	0.22
16	MCM-41-30-TP-9-75	1.13	4.45	0.25
17	MCM-41-30-TP-11-75	0.86	3.83	0.22
18	MCM-41-30-TP-13-75	0.67	3.42	0.19
19	MCM-41-30-AP-9-75	0.83	1.80	0.46
20	MCM-41-30-AP-9-75-0.3	1.27	2.66	0.48
21	MCM-41-30-AP-9-75-0.5	1.40	2.98	0.47
22	MCM-41-30-AP-9-75-0.7	1.24	3.26	0.38
23	MCM-41-30-AP-9-80-0.5	1.44	2.99	0.48
24	MCM-41-30-AP-9-85-0.5	1.58	3.16	0.50
25	MCM-41-30-AP-9-90-0.5	1.19	3.06	0.39
26	MCM-41-30-TP-9-75	1.13	3.99	0.28
27	MCM-41-30-TP-9-75-0.3	1.75	6.39	0.27
28	MCM-41-30-TP-9-75-0.5	0.05	7.06	0.007
29	MCM-41-30-TP-9-75-0.7	0.05	8.34	0.006
30	MCM-41-30-TP-9-80-0.3	1.74	6.45	0.27
31	MCM-41-30-TP-9-85-0.3	1.66	6.27	0.26
32	MCM-41-30-TP-9-90-0.3	1.57	6.09	0.26

6.4. Optimization of the adsorbent composition and synthesis conditions for tethering of mono and tri amino silane compounds on suitable support

In order to increase the amine loading and further enhance the CO_2 uptake in the important low pressure regime (0.1-0.2 bar), wet grafting process is followed for amino silane tethering on MCM-41-30 support. Based on the dry grafting experiments, the optimum amount of amino silane that can be grafted per gram of support is determined as 9 mmol for both amino compounds. Hence, the amount of amino silane added in the reaction mixture is kept constant throughout for wet grafting process. Further, the effect of addition of water for optimization of the adsorbent composition and influence of temperature for optimizing efficient synthesis conditions for tethering of mono and tri amino silane compounds are investigated.

6.4.1. Surface area analysis

The textural properties of MCM-41-30-AP-9 and MCM-41-30-TP-9 series synthesized under wet grafting conditions together with respective control samples are presented in Table 6.1 (samples 13-26). For MCM-41-30-AP-9-75 series, significant percentage of reduction in the surface area, pore volume and volume of N_2 adsorbed of about ~ 65-82%, 13-57% and 12-56% is observed with respect to increase in amount of water added in the reaction mixture. This reveals that addition of water plays important role in enhancing the silanol densities of the respective samples which in turn has positive effect on the amine loading. However, for the same amount of water (0.5 mL) in the reaction mixture, significant difference in the textural properties is not noticed with respect to rise in reaction temperature. This might be due to the fact, that after an approximately optimum grafting temperature (75 °C) is reached, further increment in the heat energy did not provide much pronounced effect in the amine loading. MCM-41-30-TP-9 series adsorbents also follow similar phenomenon for increase in amount of water added as well as rise in temperature for same amount of water in the reaction mixture. This indicates that addition of water plays significant role in increasing the

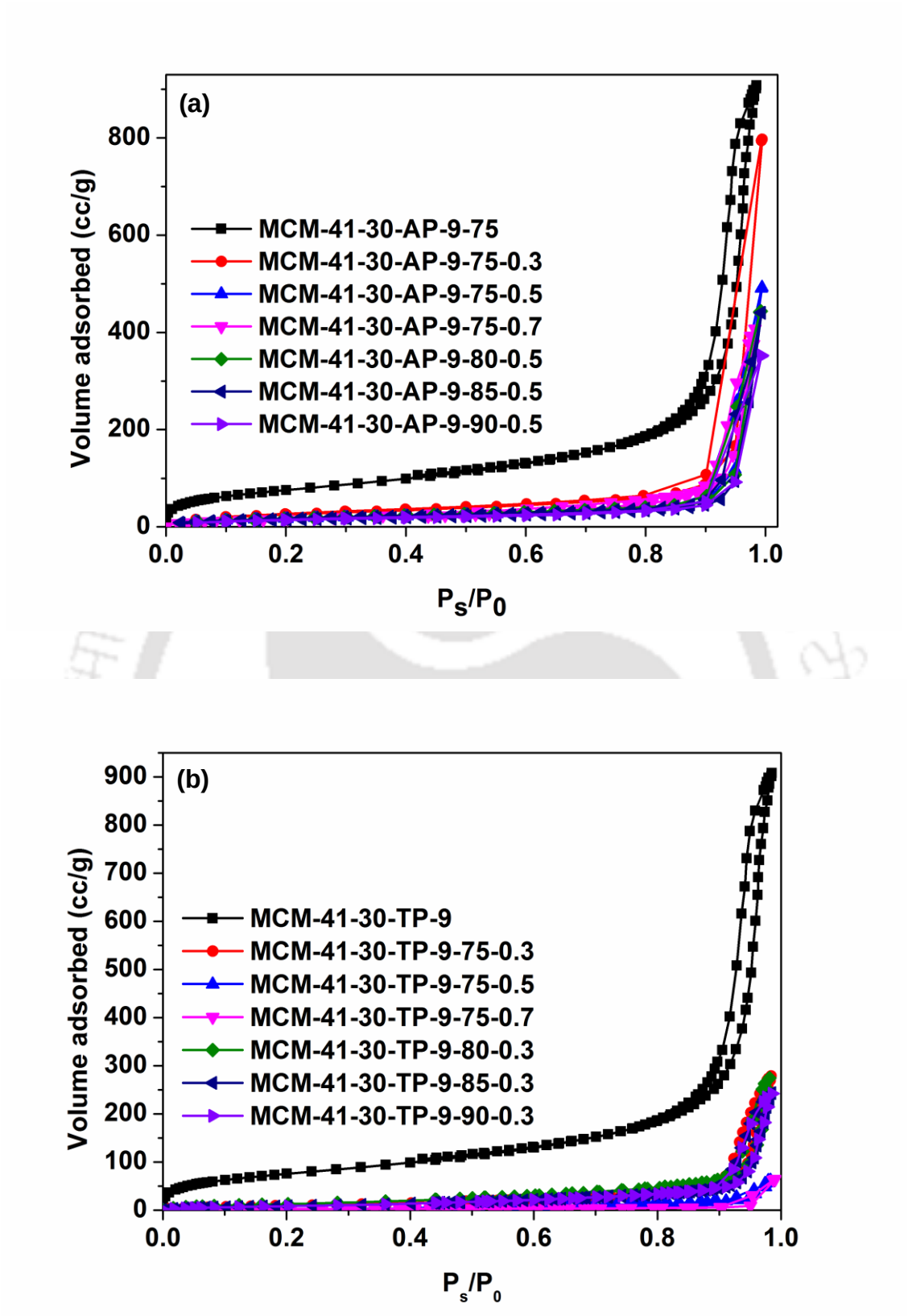

Figure 6.4. N_2 adsorption-desorption isotherms for (a) MCM-41-30-AP-9 and (b) MCM-41-30-TP-9 series

amine loading, whereas the effect is less pronounced in case of increase in reaction temperature for particular amount of water in the reaction mixture irrespective of type of amino silane compounds selected in the study. In case of N_2 adsorption-desorption isotherms (shown in Figure 6.4(a) and 6.4(b)), both MCM-41-30-AP-9 and MCM-41-30-TP-9 series exhibit type IV isotherms irrespective of the type of amino silane compounds tethered suggesting that MCM-41-30 support with large pore size (30 nm) and pore volume (2.58 cc/g) plays a role as promising support for amine tethering process.

6.4.2. Thermo-gravimetric analysis

Thermo-gravimetric analysis of MCM-41-30-AP-9 and MCM-41-30-TP-9 series samples is carried out to determine the amine loading of the respective samples (presented in Table 6.3) and the corresponding TGA profiles are shown in Figure 6. 5. The TGA thermographs of both MCM-41-30-AP-9 and MCM-41-30-TP-9 series exhibit two region of weight loss mainly. The first region of weight loss observed below the temperature range of ~110 °C is due to the physisorbed amino silane moieties **[1]**. The second region of weight loss can be divided into two temperature regions (below and above 250 °C). The weight loss that occurs below 250 °C may correspond to release of ethanol and methanol depending on the alkoxy groups present in mono amine and tri amino silane compound respectively **[1]**. This is because, all the alkoxy ligands are not consumed in the grafting reaction and always few of such groups are expected to be left unreacted **[1]**. When the temperature progresses, the alkoxy ligands may react with adjacent free-hydroxyl groups and liberate ethanol or methanol as discussed earlier. The decomposition of amine chains begins in the temperature range of above 250 °C and starts to reach a plateau by ~550 °C. All the samples exhibited similar TGA profiles and the organic loading is calculated based on the weight loss corresponding to the temperature range of 200 to 550 °C. Based on the weight loss results and considering tridentate grafting (mono and tri amino ligands grafted with three surface silanol groups) or bidentate grafting (mono and tri amino ligands grafted with two surface silanol groups with one dangling alkoxyl group), amine contents are estimated and tabulated in Table 6.3.

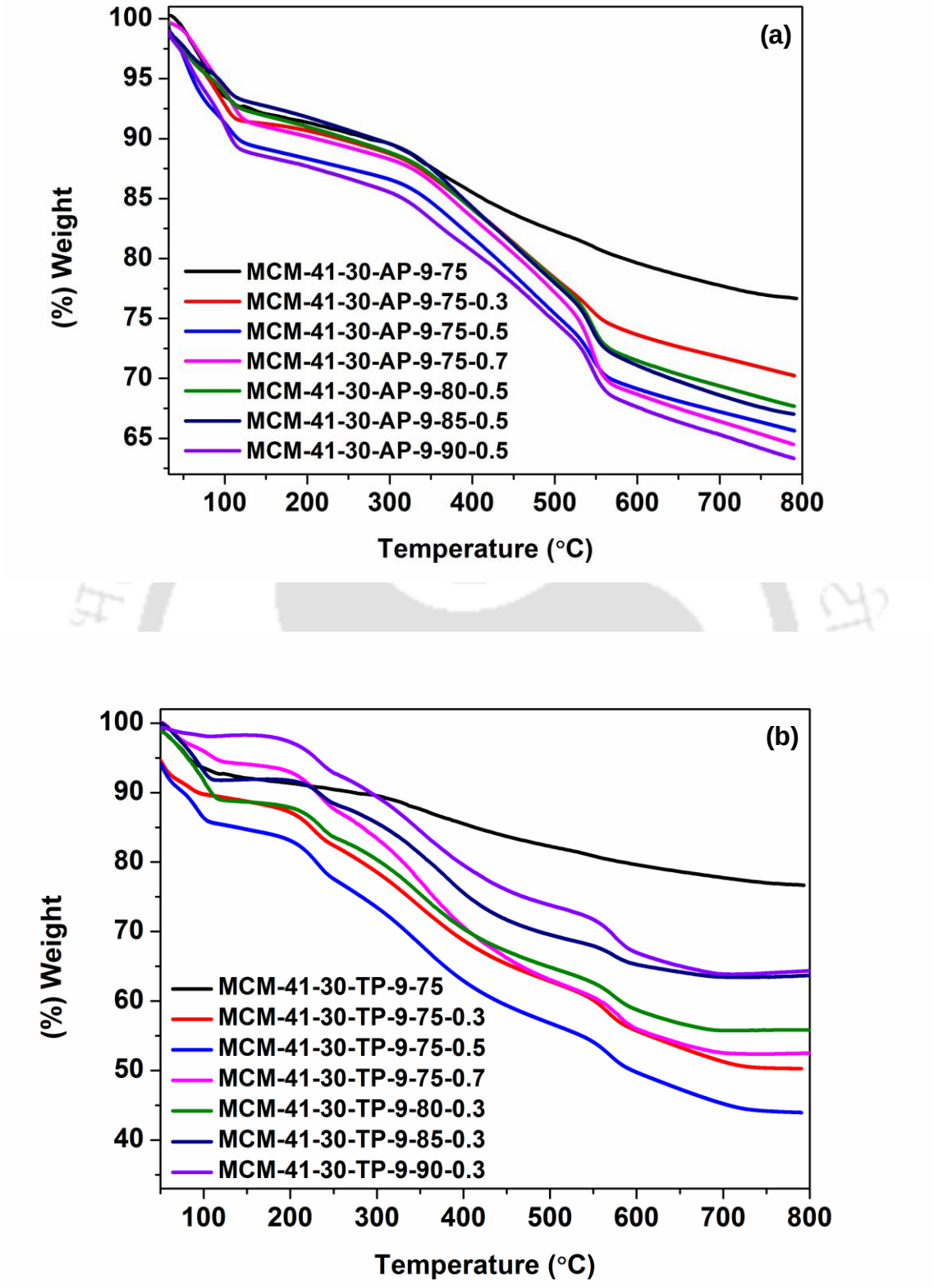

Figure 6.5. Thermo-gravimetric analysis for (a) MCM-41-30-AP-9 and (b) MCM-41-30-TP-9 series

Table 6.3. Comparison of organic loading and amine loading for MCM-41-30-AP-9 and MCM-41-30-TP-9 series

S:NO	Sample Code	Organic Loading						Amine Loading					
		mmol/g		μmol/m^2		molecules/nm^2		mmol(N)/g		μmol(N)/m^2		Molecules(N)/nm^2	
		TD	BD	TD	BD	TD	BD	TD	BD	TD	BD	TD	BD
19	MCM-41-30-AP-9-75	1.80	1.01	1.72	0.97	1.03	0.58	1.80	1.01	1.72	0.97	1.03	0.58
20	MCM-41-30-AP-9-75-0.3	2.66	1.50	2.54	1.43	1.53	0.86	2.66	1.50	2.54	1.43	1.53	0.86
21	MCM-41-30-AP-9-75-0.5	2.98	1.68	2.85	1.61	1.72	0.97	2.98	1.68	2.85	1.61	1.72	0.97
22	MCM-41-30-AP-9-75-0.7	3.26	1.83	3.12	1.75	1.88	1.05	3.26	1.83	3.12	1.75	1.88	1.05
23	MCM-41-30-AP-9-80-0.5	2.99	1.69	2.86	1.61	1.72	0.97	2.99	1.69	2.86	1.61	1.72	0.97
24	MCM-41-30-AP-9-85-0.5	3.16	1.78	3.03	1.70	1.82	1.02	3.16	1.78	3.03	1.70	1.82	1.02
25	MCM-41-30-AP-9-90-0.5	3.06	1.72	2.93	1.65	1.76	0.99	3.06	1.72	2.93	1.65	1.76	0.99
26	MCM-41-30-TP-9-75	1.33	1.09	1.27	1.04	0.76	0.63	3.99	3.27	3.81	3.12	2.28	1.89
27	MCM-41-30-TP-9-75-0.3	2.13	1.75	2.03	1.67	1.22	1.01	6.39	5.25	6.09	5.01	3.66	3.03
28	MCM-41-30-TP-9-75-0.5	2.36	1.94	2.25	1.86	1.36	1.12	7.06	5.82	6.75	5.58	4.08	3.36
29	MCM-41-30-TP-9-75-0.7	2.78	2.29	2.65	2.19	1.60	1.32	8.34	6.87	7.95	6.57	4.8	3.96
30	MCM-41-30-TP-9-80-0.3	2.15	1.78	2.05	1.69	1.23	1.02	6.45	5.34	6.15	5.07	3.69	3.06
31	MCM-41-30-TP-9-85-0.3	2.09	1.69	1.99	1.64	1.21	0.98	6.27	5.07	5.97	4.92	4.92	3.63
32	MCM-41-30-TP-9-90-0.3	2.01	1.66	1.92	1.58	1.16	0.95	6.09	4.98	5.76	4.74	3.48	2.85

6.4.3. DRIFTS analysis

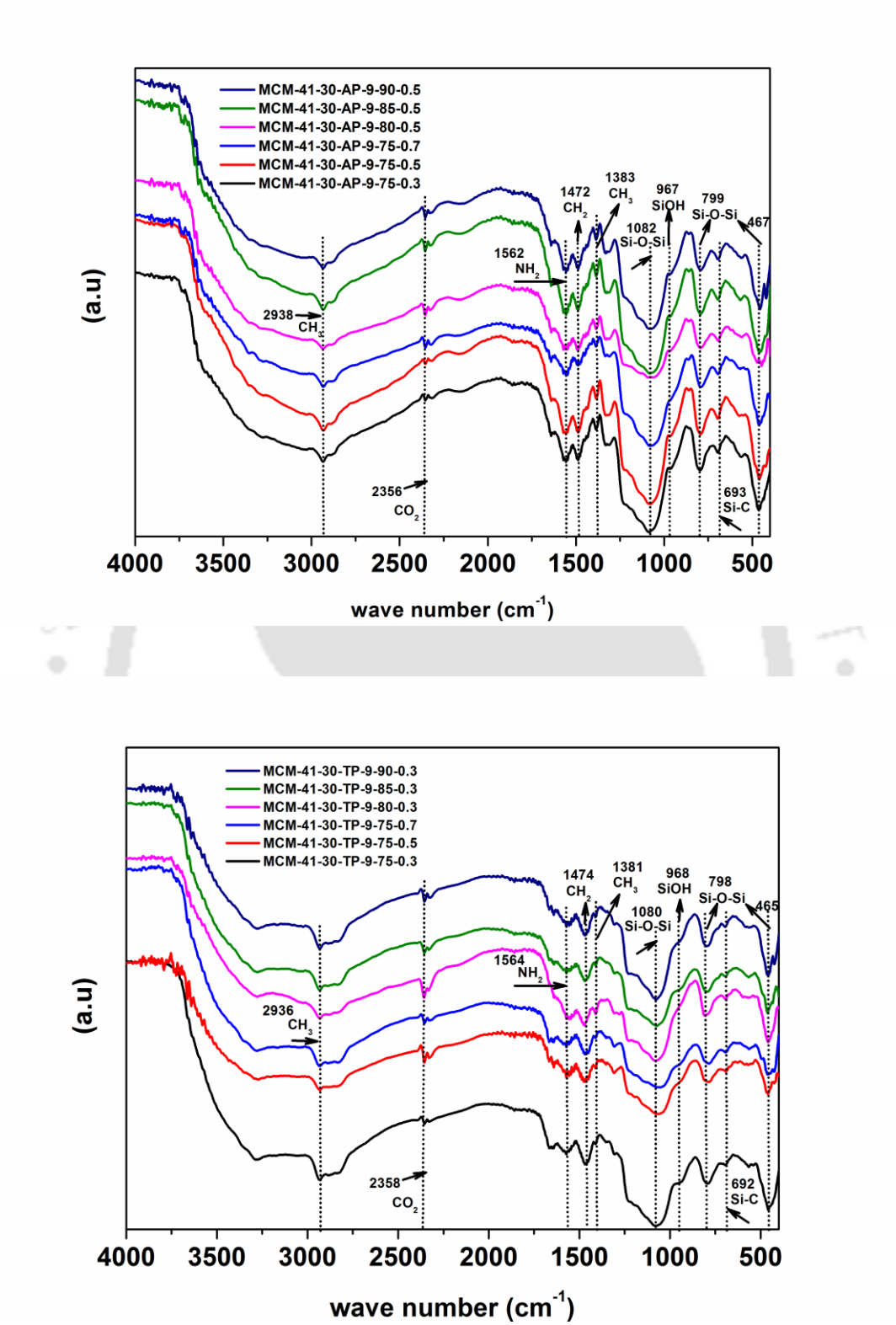

Figure 6.6. DRIFTS analysis for (a) MCM-41-30-AP-9 and (b) MCM-41-30-TP-9 series

The DRIFTS analysis for MCM-41-30-AP-9 and MCM-41-30-TP-9 series are portrayed in Figure 6.6(a) and (b) respectively. The DRIFT spectra obtained for both mono and tri amine tethered MCM-41 samples depict the effect of surface functionalization. The peak observed at ~2936 and 2937 cm^{-1} corresponds to the CH_2 vibrations of hydrocarbon chain of mono and tri amine tethered MCM-41 samples respectively **[6]**. The peak corresponding to Si–C vibrations is observed at 693 and 692 cm^{-1} for mono and tri amine samples respectively **[7]**. As amine moieties exhibit strong affinity towards CO_2, it is probable that CO_2 can be adsorbed on the amine tethered samples during storage or while exposed to atmosphere prior to analysis. The presence of peak at 2358 cm^{-1} confirms that CO_2 is adsorbed on amine tethered MCM-41 samples under the above mentioned conditions **[8]**. The appearance of peaks at ~1562 and 1564 cm^{-1} is attributed to NH_2 vibrations, which indicates the presence of amino groups in the mesoporous structure after functionalization **[6]**. In addition to this, the asymmetric stretching vibrations of Si-O-Si are also observed by the presence of bands at 1,066, 798 and 460 cm^{-1} **[9]**. The band noticed in the region of 967- 968 cm^{-1} is attributed to Si-OH vibrations indicating the presence of Si-OH groups that are not utilized for amine tethering **[10]**.

6.4.4. CO_2 adsorption analysis

MCM-41-30-AP-9 and MCM-41-30-TP-9 series samples are subjected to CO_2 adsorption measurements at 30 °C for screening of best adsorbent composition and the corresponding adsorption capacities of respective samples are shown in Figure 6.7 (a) and (b). It can be seen from Table 6.3, that organic loading increases with respect to increase in water content for constant grafting temperature (75 °C) for both mono and tri amino silane compounds. However, the similar trend in CO_2 adsorption capacity is not experienced indicating that inaccessible amine moieties increase with organic loading. From Figure 6.7, it is evident that the addition of water in the grafting solution for a particular temperature (75 °C) shows profound impact on the CO_2 uptake for both mono and triamine compound. The CO_2 adsorption capacity for mono and triamino silane grafted sample (75 °C grafting

temperature, 0.3 mL water) is enhanced by about two and 1.5 fold respectively in comparison to the respective control samples. For mono amino silane, with further increase in the addition of water, the adsorption capacity slightly increased from 1.27 to 1.4 mmol/g (0.5 mL water) and decreased to 1.24 mmol/g (0.7 mL water) at 0.2 bar. Therefore, 0.5 mL water is determined as optimum amount for mono aminosilane grafting and influence of temperature on the grafting efficiency is also investigated. For the constant amount of water (0.5 mL), increasing the grafting temperature does not show significant effect in the CO_2 adsorption capacity even though slight increase in the organic loading is observed at 85 °C.

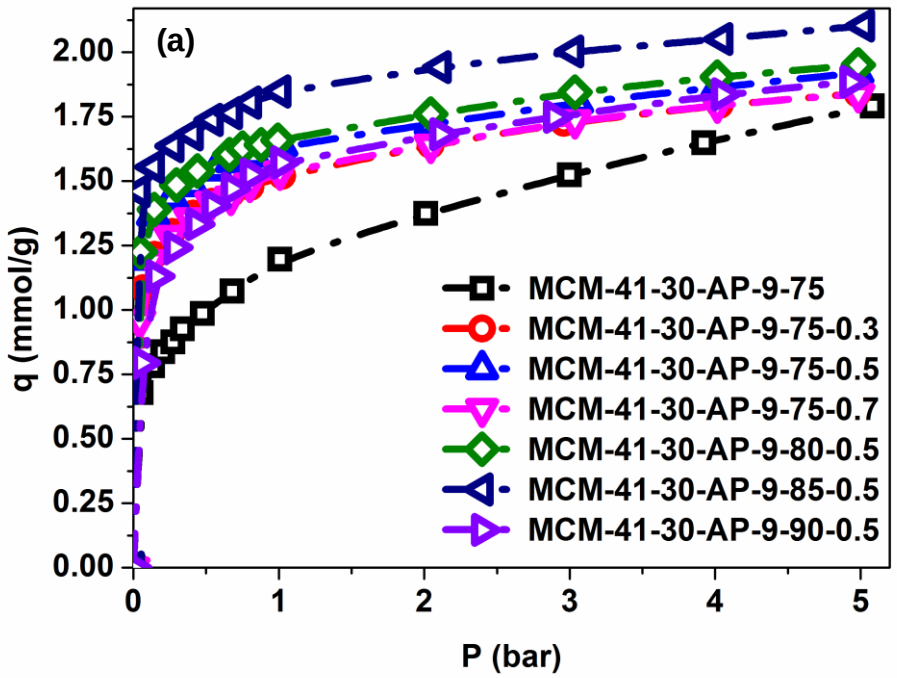

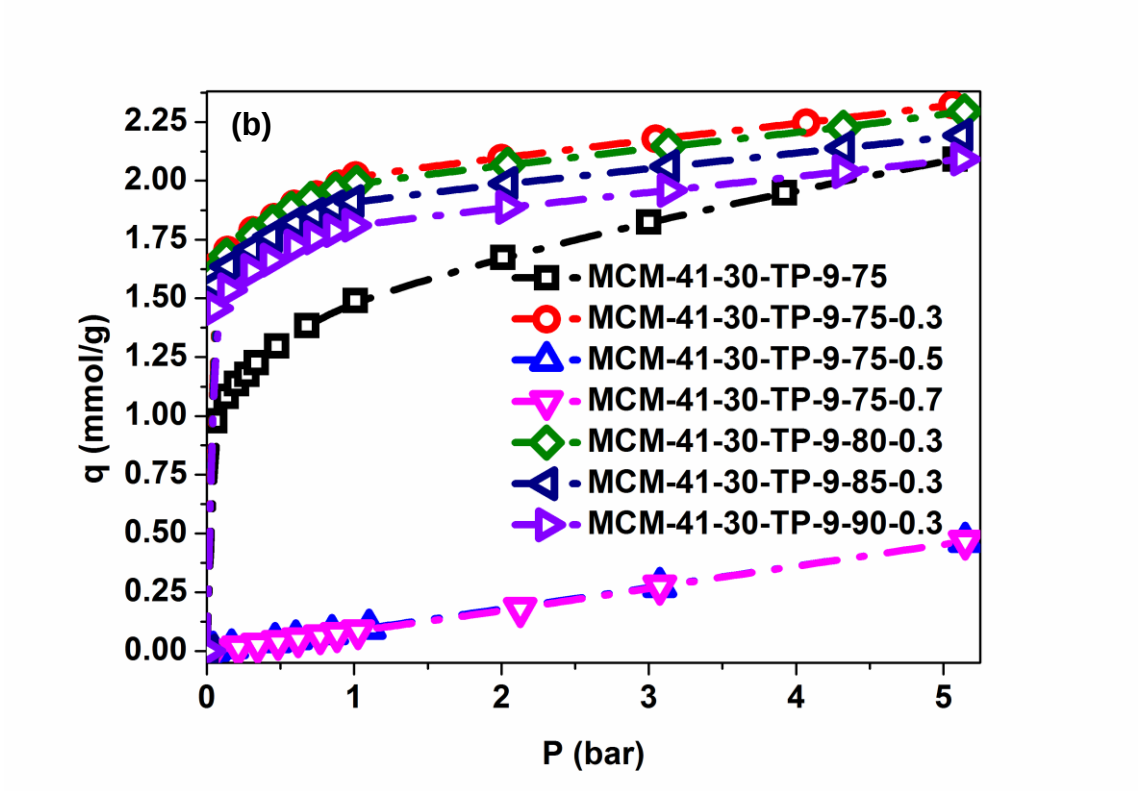

Figure 6.7. CO_2 adsorption isotherms at 30 °C for (a) MCM-41-30-AP-9 and (b) MCM-41-30-TP-9 series

In case of triamine, with further increase in the addition of water, the adsorption capacity exhibited dramatic downturn from 1.75 to about ~0.055 mmol/g for both 0.5 and 0.7 mL water at 0.2 bar, despite an increase in organic loading is noticed. By examining this result, it can be concluded that, for water additions above 0.3 mL in the reaction mixture, complete blockage of pores may occur (evidenced by pore volume data presented in Table 6.1). This phenomenon is attributed to the polymerization that takes place through methoxy ligand hydrolysis/condensation of the tri aminosilane in the bulk solution. This in turn, results in subsequent deposition of the same on the external surface of the support thereby leading to pore choking or clogging. For constant amount of water (0.3 mL), further increase in grafting temperature (except 80 °C) led to decrease in CO_2 adsorption capacity, because of decrease in organic loading experienced. Therefore, 75 °C and 0.3 mL water is considered

as an optimal condition under which MCM-41-30 can be grafted efficiently in order to achieve the targeted CO_2 capture application.

6.5. Conclusions

In summary, the amount of mono amino silane compound that can be used for grafting reaction on MCM-41-3 and MCM-41-30 support materials is optimized based on the outcome of preliminary CO_2 adsorption studies and elemental analysis. The CO_2 adsorption studies carried out on mono amine functionalized support materials under dry grafting conditions elucidated the importance of nature of support material to be selected for tethering application. Further, a suitable synthesis recipe is developed for mono and tri amine grafting on MCM-41-30 support under wet grafting conditions. Addition of water in the reaction mixture showed profound impact on the CO_2 adsorption characteristics of MCM-41-30-AP-9 and MCM-41-30-TP series samples. The MCM-41-30-AP-9-85-0.5 and MCM-41-30-TP-75-0.3 samples exhibited a maximum adsorption capacity of ~1.55 and ~1.75 mmol/g (30 °C, 0.2 bar) respectively, which indicates that MCM-41-30 support developed here in, acts as a promising support for amine tethering application.

6.6. References

[1] Harlick, P. J. E.; and Sayari, A. Applications of Pore-Expanded Mesoporous Silica. 5. Triamine Grafted Material with Exceptional CO_2 Dynamic and Equilibrium Adsorption Performance, *Ind. Eng. Chem. Res.* **2007**, 46, 446-458.

[2] Bollini, P.; Brunelli, N. A.; Didas, S.A.; and Jones, C. W. Dynamics of CO_2 Adsorption on Amine Adsorbents. 2. Insights into Adsorbent Design, *Ind. Eng. Chem. Res.* **2012**, 51, 15153-15162.

[3] Feng, X.; Fryxell, G. E.; Wang, L. Q.; Kim, A. Y.; Liu, J.; and Kemner, K. M. Functionalized Monolayers on Ordered Mesoporous Supports. *Science* **1997**, 276, 923-926.

[4] Kruk, M.; Jaroniec, M.; and Sayari, A. Application of Large Pore MCM-41 Molecular Sieves to Improve Pore Size Analysis Using Nitrogen Adsorption Measurements, *Langmuir*. **1997**, 13, 6267-6273.

[5] Huo, Q.; Margoleses, D. I.; and Stucky, G. D. Surfactant Control of Phases in the Synthesis of Mesoporous Silica-Based Materials, *Chem. Mater.* **1996**, 8, 1147-1160.

[6] Zheng, F.; Tran, D. N.; Busche, B. J.; Fryxell, G.E.; Addleman, R.S.; Zemanian, T. S.; and Aardahl, C. L. Ethylenediamine-Modified SBA-15 as Regenerable CO_2 Sorbent, *Ind. Eng. Chem. Res.* **2005**, 44, 3099-3105.

[7] Cui, S.; Cheng, W.; Shen, X.; Fan, M.; Russell, A.; Wu, Z.; and Yi, X. Mesoporous Amine-Modified SiO_2 Aerogel: A Potential CO_2 Sorbent, *Energy Environ. Sci.,* **2011**, 4, 2070-2074.

[8] Yu, J.; Le, Y.; and Cheng, B. Fabrication and CO_2 Adsorption Performance of Bimodal Porous Silica Hollow Spheres With Amine-Modified Surfaces, *RSC Advances*, **2012**, 2, 6784-6791.

[9] Monash, P.; and Pugazhenthi, G.; Investigation of Equilibrium and Kinetic Parameters of Methylene Blue Adsorption onto MCM-41, *Korean J. Chem. Eng*. **2010**, 27, 1184-1191.

[10] Hao, S.; Chang, H.; Xiao, Q.; Zhong, Y.; and Zhu, W. One-Pot Synthesis and CO_2 Adsorption Properties of Ordered Mesoporous SBA-15 Materials Functionalized with APTMS, *J. Phys. Chem. C* **2011**, 115, 12873-12882.

CHAPTER 7

EVALUATION OF AMINE TETHERED MCM-41 BASED ON POST COMBUSTION CO_2 CAPTURE METRICS

The chapter elucidates the performance of amine tethered MCM-41 in terms of post combustion CO_2 capture metrics such as (i) CO_2 adsorption capacity (ii) Amine efficiency (iii) Operating window (iv) CO_2 adsorption kinetics (v) Selectivity (vi) Cyclic adsorption-desorption studies and (vii) Cost. Comparative analysis of the same with other adsorbents such as activated carbon, zeolites, metal organic frameworks, amine impregnated, and amine tethered mesoporous silica adsorbents is highlighted to rank the performance of MCM-41 for the said application.

7.1. Introduction

For solid sorbents to be in fact competitive with alkanolamine solvents, certain R & D targets should be reached, as discussed in a study reported by U.S. DOE National Energy Laboratory (NETL). The said targets include (i) 90% capture efficiency by the solid sorbents (ii) added COE must be below 35% for post combustion in particular **[1]**. It was mentioned in the report that the amount of CO_2 projected to be captured per year according to the established targets could certainly have implications on the scale of capture materials required **[1]**. A separate study reports that, in order to achieve the first target, sorbents with capture capacity between 2-4 mmol/g are desirable **[2]**. In addition to adsorption capacity, kinetics of adsorption/desorption is also considered as main factor that decides the amount of solid sorbent required and fixed capital costs for achieving such astonishing capture targets **[3]**. Apart from the scale of materials required to capture CO_2, another challenge lies in the quantification of commercial-scale cost savings for any given change in the materials properties **[1]**. Hence, it is clear that once the adsorbent is developed in view of ultra-large-scale separation process like carbon capture from flue gas, the same should be evaluated on the basis of certain performance criteria such as (i) CO_2 adsorption capacity (ii) amine efficiency (iii) operating window (iv) CO_2 adsorption kinetics (v) CO_2 selectivity (vi) cyclic adsorption-desorption studies and (vii) cost. In view of this, the best adsorbents i.e. MCM-41-30-AP-9-85-0.5 and MCM-41-30-AP-75-0.3 screened in the present work (Chapter 6) based on the effective CO_2 adsorption characteristics are evaluated following the above mentioned post-combustion carbon capture metrics.

7.2. Experimental section

7.2.1. Materials

The details of materials used for synthesis of MCM-41 and amine grafted MCM-41 samples have been described in section 3.2.1 and 6.2.1 respectively. CO_2 and N_2 gas used for

adsorption equilibrium measurements is 99% pure and was supplied by Assam Air Products, Guwahati, India.

7.2.2. Synthesis of amine grafted MCM-41

The synthesis procedure for MCM-41 has been described in section 3.2.2 and 6.2.2 respectively.

7.2.3. Materials characterization

The details about characterization of MCM-41 and amine grafted MCM-41 samples have been elaborated in section 3.2.3 and 6.2.3 respectively.

7.2.4. CO_2 adsorption measurements

Adsorption equilibrium measurements of pure CO_2 and N_2 on amine grafted MCM-41 samples at four different temperatures (30, 45, 60 and 75 °C) and in the pressure range of (0-1 bar) were measured using a Rubotherm Magnetic Suspension balance. The measurements were carried out by using the similar procedure described in section 3.2.5. The amine grafted MCM-41 samples were activated by heating it at 125 °C under vacuum (and then purging with helium).

7.3. Results & discussion

7.3.1. Evaluation of the adsorbent based on CO_2 adsorption metrics

7.3.1.1. CO_2 adsorption capacity

CO_2 adsorption capacity is defined as a measure of an adsorbent's capability or potential to adsorb CO_2. It is expressed in terms of number of moles of CO_2 that a unit mass of an adsorbent adsorbs under equilibrium conditions **[4]**. The CO_2 adsorption isotherms for MCM-41-30, MCM-41-30-AP-9-85-0.5 and MCM-41-30-TP-9-75-0.3 at 30 °C are presented in Figure 7.1(a). The CO_2 adsorption isotherms for amine tethered samples exhibit a steep nonlinear isotherm due to the strong interactions between CO_2 molecules and amine

moieties. In contrast, MCM-41-30 exhibits a less steep isotherm indicating that pure silica interacts with CO_2 only by physisorption and hence lacks sufficient strong affinity towards CO_2. Therefore, it is clear that the adsorption of CO_2 on pure MCM-41 approaching the maximum adsorption with subsequent increase in pressure is a mere consequence of the large surface area and pore volume of this support. The CO_2 adsorption capacity of amine grafted samples dramatically depends on the amount of accessible amine ligands. MCM-41-30-AP-9-85-0.5 and MCM-41-30-TP-9-75-0.3 samples, that are characterized by the maximum surface density of mono and tri amine ligands shows the steepest CO_2 isotherm and the highest CO_2 adsorption capacity attaining 1.58 and 1.75 mmol/g respectively at 0.2 bar and 30 °C. This underlines the fact that CO_2 adsorption capacity increases with increasing surface density of accessible amine moieties although the surface area (S_{BET}) of

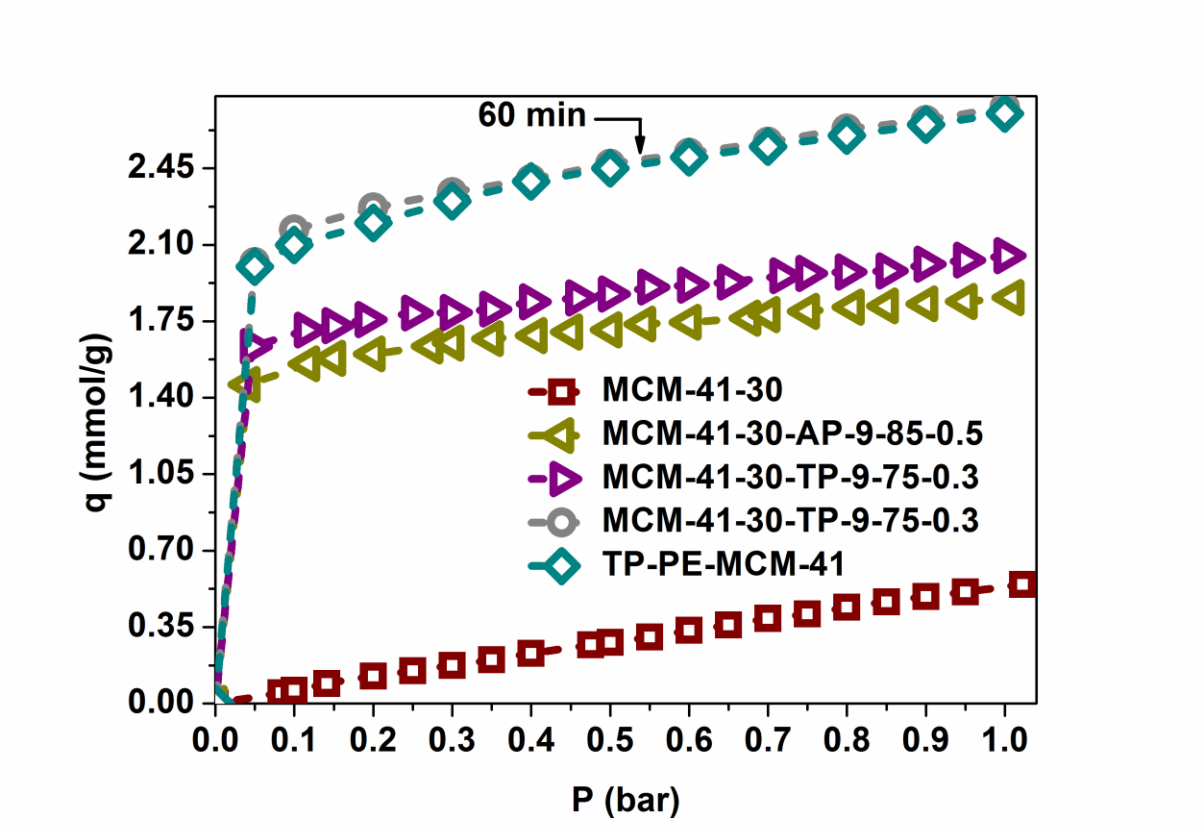

Figure 7.1. Comparison of CO_2 adsorption capacity for different adsorbents at 30 °C

amine tethered samples tend to decrease. Therefore, the surface density of amine ligands is the key parameter that influences the CO_2 adsorption. The dramatically high CO_2 adsorption capacity achieved at partial pressures (0.1-0.2 bar) relevant to flue gas conditions indicates that amine tethered functionalities act as effective adsorption sites through formation of carbamate, in which two nitrogen atoms are involved, as explained in Chapter 2.

7.3.1.2. Amine efficiency

Amine efficiency is another important metric that should be considered for amine tethered adsorbents while assessing CO_2 capture performance. The amine efficiency of an adsorbent is defined as the number of moles of CO_2 adsorbed per mole of amine functional groups **[5]**. Amine efficiency provides a measure of the fraction of amine groups present in an adsorbent that actively participate in adsorbing CO_2 by chemisorption **[5]**. It is reported that the theoretical maximum value for amine efficiency that an ideal adsorbent should exhibit under dry CO_2 adsorption conditions is 0.5 (p_{co_2} = 0.1-0.2 bar) i.e., in the absence of significant physisorption at non-functionalized sites **[6]**. The amine efficiency values for MCM-41-30-AP-9 series and MCM-41-30-TP-9 series are presented in Table 6.2, from which the variation in amine efficiency with respect to amine loading can be noticed. From Table 6.2, it is evident that, as amine loading increases, at first amine efficiency increases, then reaches a maximum at a critical value of amount of water added in the reaction mixture and then finally drops off at water levels higher than the critical value for both mono and tri aminosilane addition. The similar trend in amine efficiency is observed with respect to increase in grafting temperature for constant amount of water, in case of both mono and tri amino silane compounds. MCM-41-30-AP-9-85-0.5 sample exhibited the maximum amine efficiency of ~0.5, which is close to theoretical maximum value. This proves that MCM-41-30 serves as an ideal support for amine tethering process, where the CO_2 adsorption process is not hindered due to transport/diffusion limitation. However, in case of tri amine, despite an increase in amine loading on MCM-41-30 is experienced, amine efficiency is affected and MCM-41-30-TP-9-75-0.3 sample exhibited maximum amine efficiency of 0.28. This can be

explained by the concurrent occurrence of two processes that imposes opposite effects on the amine efficiency. The first reason is increasing the amine proximity by increasing amine loading leads to larger fraction of amines pairs that are reactive to CO_2 and a smaller fraction of amines that do not possess another amine group in close proximity to capture CO_2 for carbamate formation **[7]**. The second is increase in inaccessibility to active amine groups to the extent that even the increasing amine proximity cannot compensate for the amine sites located inside the pores due to diffusion limitation **[8]**. To confirm whether kinetic effect corresponds to a diffusion rate limitation or lead to inaccessibility scenario, the CO_2 uptake curve is analysed carefully. Interestingly, the CO_2 uptake curve does not reach a plateau when 10 min is considered as equilibrium time for each pressure point in the CO_2 adsorption isotherm. On the other hand, the CO_2 adsorption capacity and amine efficiency increased from 1.75 to 2.1 mmol/g and 0.28 to 0.33 respectively at 30 °C and 0.2 bar pressure, when 60 min is considered as equilibrium time. The CO_2 adsorption isotherm of MCM-41-30-TP-9-75-0.3, for which 60 min is considered as equilibration time for each pressure point in the isotherm curve is presented in Figure 7.1(a). However, the CO_2 uptake curve did not reach plateau for even 60 min equilibration time suggesting that the effect experienced in terms of CO_2 adsorption capacity and amine efficiency is most likely a diffusion rate limiting one. Since the rate of weight change is negligibly small when compared to 10 min equilibration time, quasi-equilibrium time of 10 min is followed throughout the study for constructing CO_2 adsorption isotherms. Hence, the adsorption capacity reported here for tri amine grafted samples are to be considered essentially as “working capacities” and not “equilibrium capacities”.

7.3.1.3. Operating window

Operating window or temperature dependency of adsorption capacities is another important metric that should be given paramount significance while assessing post combustion CO_2 capture performance. This is because, flue gas, in general will be cooled down to temperature ranging from ~ 45 to 75 °C, in order to allow appropriate conditions for SO_2 and

NO_X abatement **[2]**. Therefore, any adsorbent developed exhibiting potential CO_2 capture performance not only at ambient temperature conditions but mainly in the temperature and pressure conditions of ~45-75 °C and 0.1-0.2 bar, respectively, that are relevant to flue gas

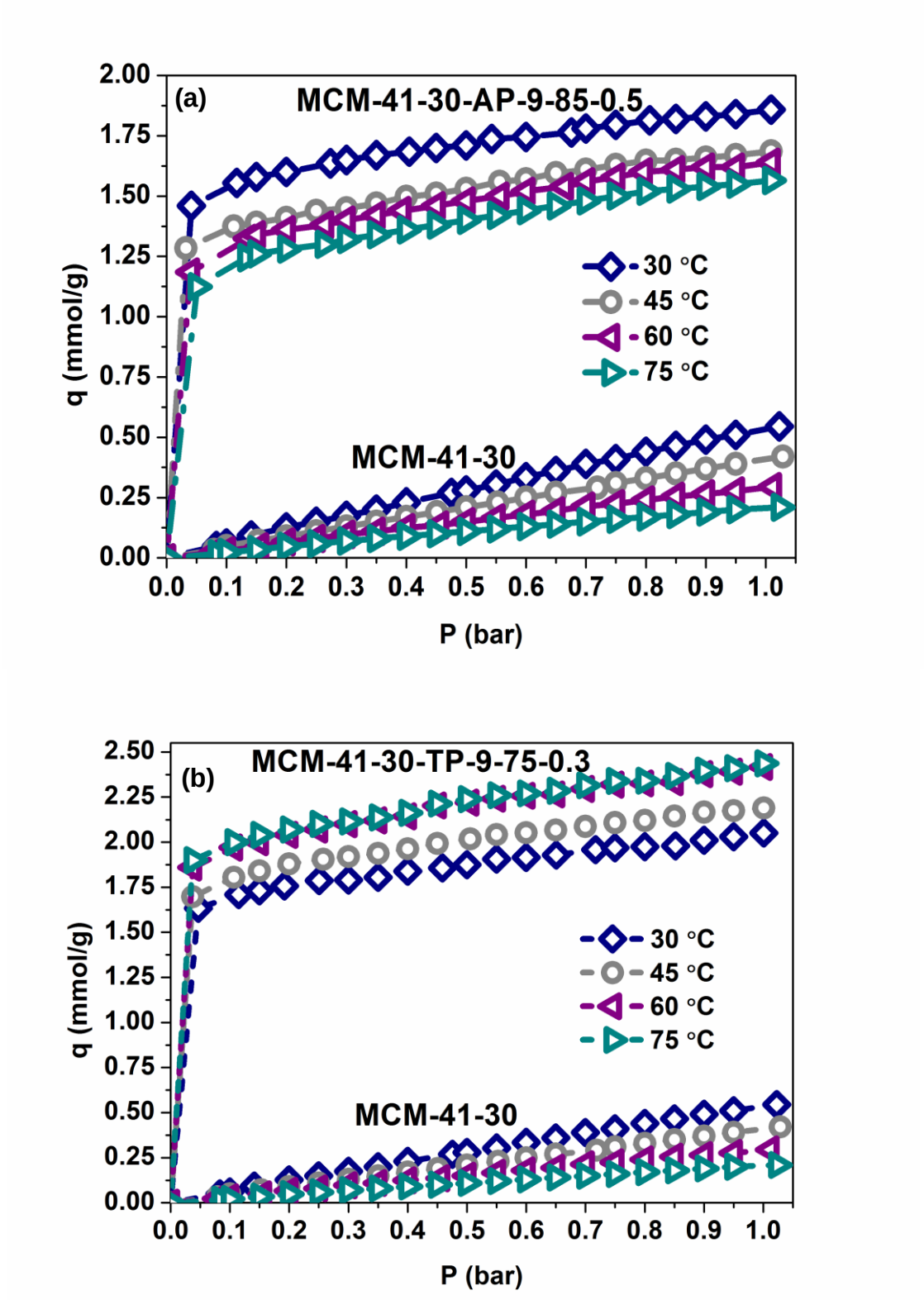

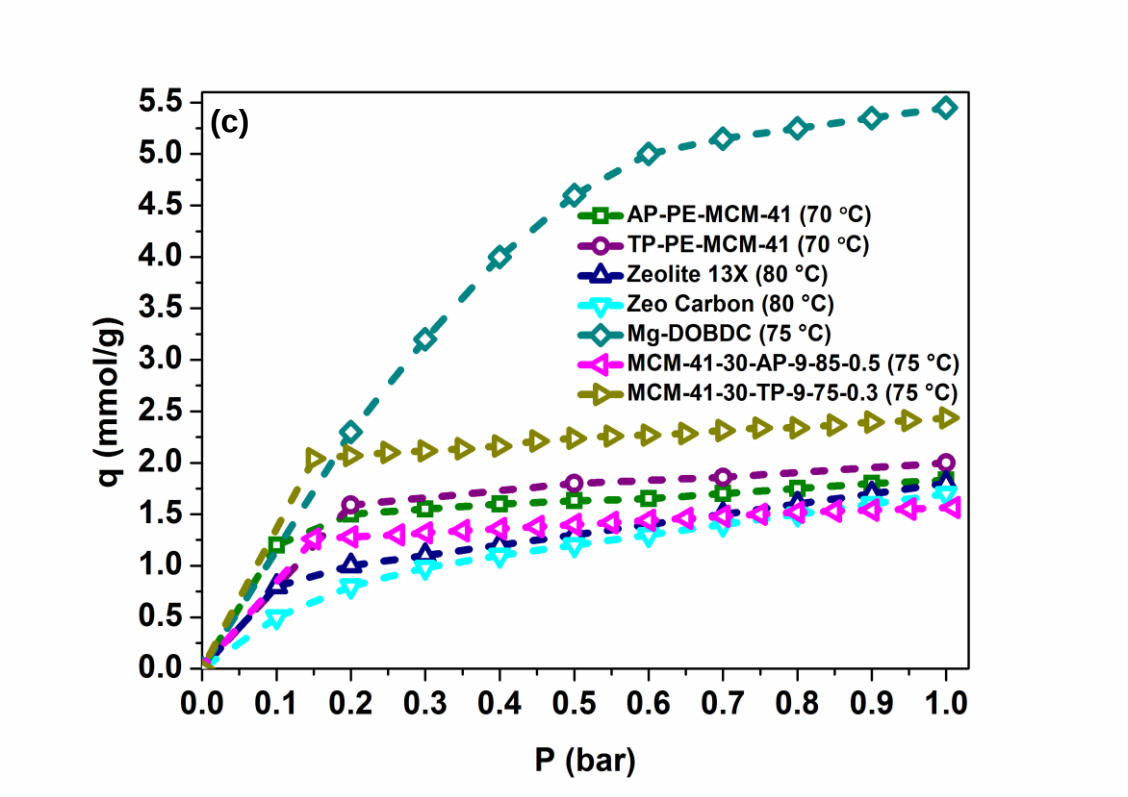

Figure 7.2. CO_2 adsorption isotherms at different temperatures for (a) MCM-41-30-AP-9-85-0.5 vs MCM-41-30 (b) MCM-41-30-TP-9-75-0.3 vs MCM-41-30 and (c) comparison of CO_2 adsorption capacities at 70-75 °C for different adsorbents

conditions becomes essential. This underlines the fact that the real success of developing an adsorbent for post combustion CO_2 capture applications lies in its potential to exhibit excellent uptake performance even under flexible operating conditions. The CO_2 adsorption isotherms for MCM-41-30-AP-9-85-0.5 and MCM-41-30-TP-9-75-0.3 samples in the temperature conditions ranging from 30-75 °C are portrayed in Figure 7.2(a) and (b) respectively. It can be seen from Figure 7.2(a) that the CO_2 adsorption capacity decreases for MCM-41-30-AP-9-85-0.5 with respect to rise in capture temperature, which is evident from the decrease in steepness exhibited by non-linear isotherm curves. The CO_2 adsorption capacity of MCM-41-30-AP-9-85-0.5 dropped down from 1.58 (30 °C) to 1.2 (75 °C) mmol/g at 0.2 bar, which corresponds to 24% decrease in capture efficiency. As the CO_2-amine reaction is exothermic in nature, the CO_2 adsorption capacity would be always expected to decrease with rise in capture temperature. Owing to this fact, MCM-41-30-AP-9-85-0.5

sample exhibited decreasing trend in the adsorption capacity with respect to increase in temperature. Interestingly, it can be observed from Figure 7.2(b), that the CO_2 adsorption capacity increases for MCM-41-30-TP-9-75-0.3 with respect to rise in capture temperature, which is further evident from slight increment in steepness exhibited by non-linear isotherm curves. The CO_2 adsorption capacity of MCM-41-30-TP-9-75-0.3 shooted up to 2.1 (75 °C) from 1.75 (30 °C) mmol/g (0.2 bar), which corresponds to 16.7% increase in capture efficiency. Similar behaviour is reported for higher molecular weight amine (polyethylene imine) functionalized silica adsorbents **[8]**. The adsorption capacities of these PEI functionalized adsorbents increased with in the temperature range of 50-100 °C and the maximum adsorption capacity has been achieved at 75 °C. This peculiar behaviour has been explained in the literature to be due to diffusion effects associated with the dense polymer grafted in the pores. As the capture temperature progresses, the polymeric chains are said to have more mobility which allows CO_2 to attain better access to the interior space of the silica support **[8]**. In the present case, as the tri amine used for grafting is more sensitive towards moisture in the reaction mixture, the hydrolysis and condensation polymerization is more intense when compared to mono amine. This in turn, results in the formation of dense coverage of polyamino siloxane amine moieties in the pores. Hence, in the present work also, with respect to rise in adsorption temperature, capture efficiency for MCM-41-30-TP-9-75-0.3 is enhanced, indicating that CO_2 molecules overcome the diffusion limitation due to better accessibility to the interior pore space. This is further evident from the enhancement in the amine efficiency observed at 75 °C (0.2 bar) for 10 min equilibration time allowed for adsorption run in comparison to 30 °C which proves that transport limitations affect the CO_2 uptake at lower temperature (30 °C). However, this phenomenon is an added advantage for MCM-41-30-TP-9-75-0.3, as it exhibits highest CO_2 adsorption capacity of ~2.1 mmol/g when compared to tri amino silane grafted on PE-MCM-41 support (1.55 mmol/g) developed by Sayari et al. at temperature and pressure conditions (70 °C, 0.2 bar respectively) relevant to flue gas **[9]** and several other adsorbents reported in Table A.1 (in annexure section).

7.3.1.4. CO_2 adsorption kinetics

Half time in adsorption kinetics is defined as the time required by the adsorbent to reach half of its maximum equilibrium adsorption capacity **[4]**. The kinetics of CO_2 adsorption is an extremely important measure of performance like equilibrium adsorption capacity from a practical perspective. In a large scale operation like CO_2 capture from a post combustion flue gas stream, the adsorption-desorption cycles are desired to be completed on the order of minutes. The faster, an adsorbent in kinetics and exhibit high adsorption capacity, likely less will be the amount of same required for the capture of targeted amount of CO_2 **[1]**. As the rate of adsorption determines the amount of adsorbent required and size of the equipment as well as process economics, it is important to investigate the kinetic performance for any developed adsorbent.

The kinetic uptake curves for CO_2 adsorption on MCM-41-30-AP-9-85-0.5 and MCM-41-30-TP-9-75-0.3 are measured by gravimetric method and the same are presented in Figure 7.3(a) and (b) respectively (0.2 bar and temperature ranging from 30 to 75 °C). Despite, gravimetric method allows for the direct interpretation of an adsorption rate for CO_2 uptake, the calculated rates are not ideal representative of adsorption kinetics in a packed bed or other practical configurations, because of the dissimilarity in flow pattern amongst gravimetric balance and other configurations **[4]**. At this stage, as there is overall lack of kinetic data in the literature for amine tethered adsorbents, comparison of any kinetic analysis performed by similar method will be indeed helpful to assess the kinetic performance of different adsorbents. In this regard, kinetic analysis of MCM-41-30-AP-9-85-0.5 and MCM-41-30-TP-9-75-0.3 is carried out and compared with available literature data. It can be observed from the CO_2 uptake curves that the adsorption half time ($t_{1/2}$) decreases from 0.8 min to 0.5 min for MCM-41-30-AP-9-85-0.5 when the capture temperature is increased from 30 to 75 °C. This is because, when the temperature progresses, kinetic energy of the CO_2 molecules increases resulting in faster migration of CO_2 inside the pores which in turn enhances the rate of adsorption. However, decrease in adsorbed amount is

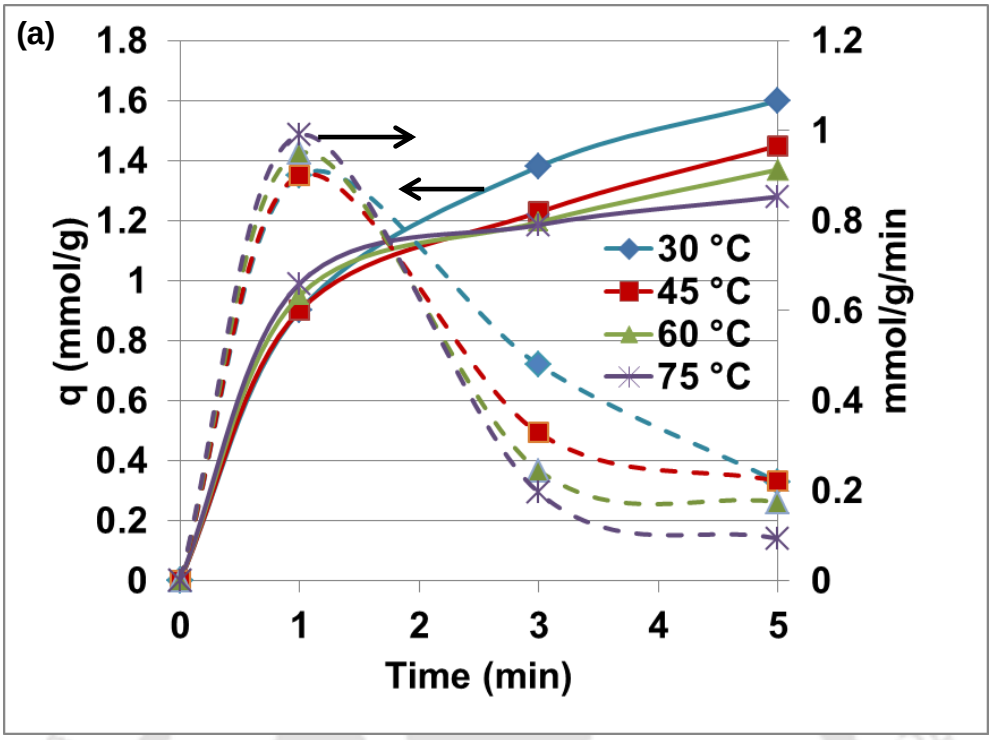

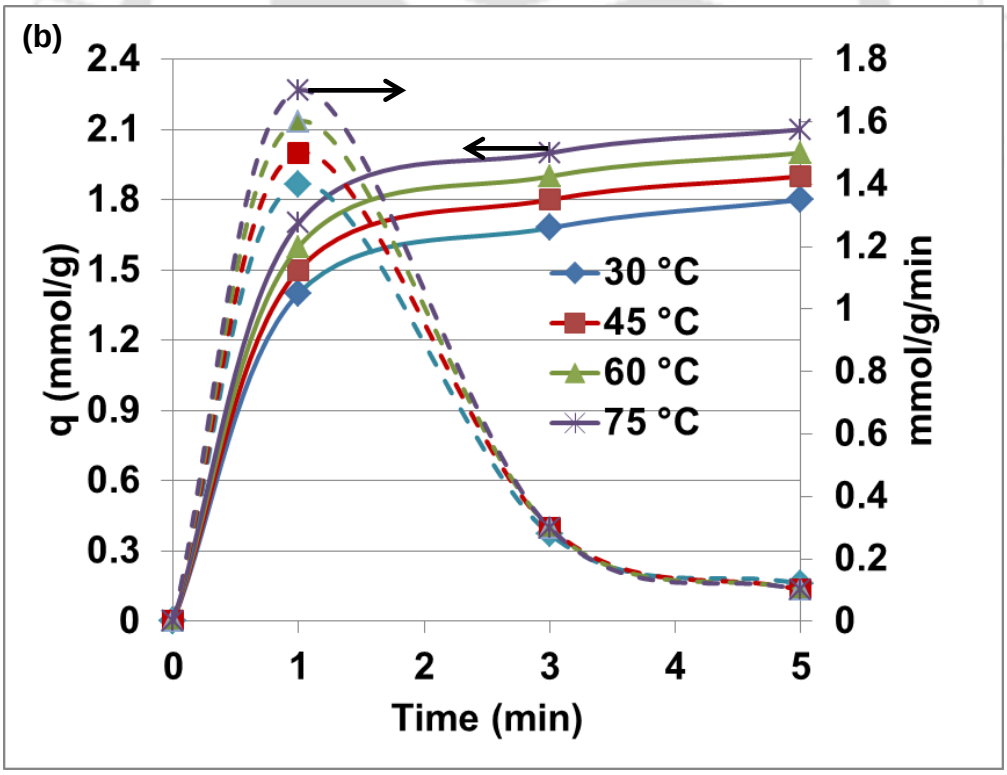

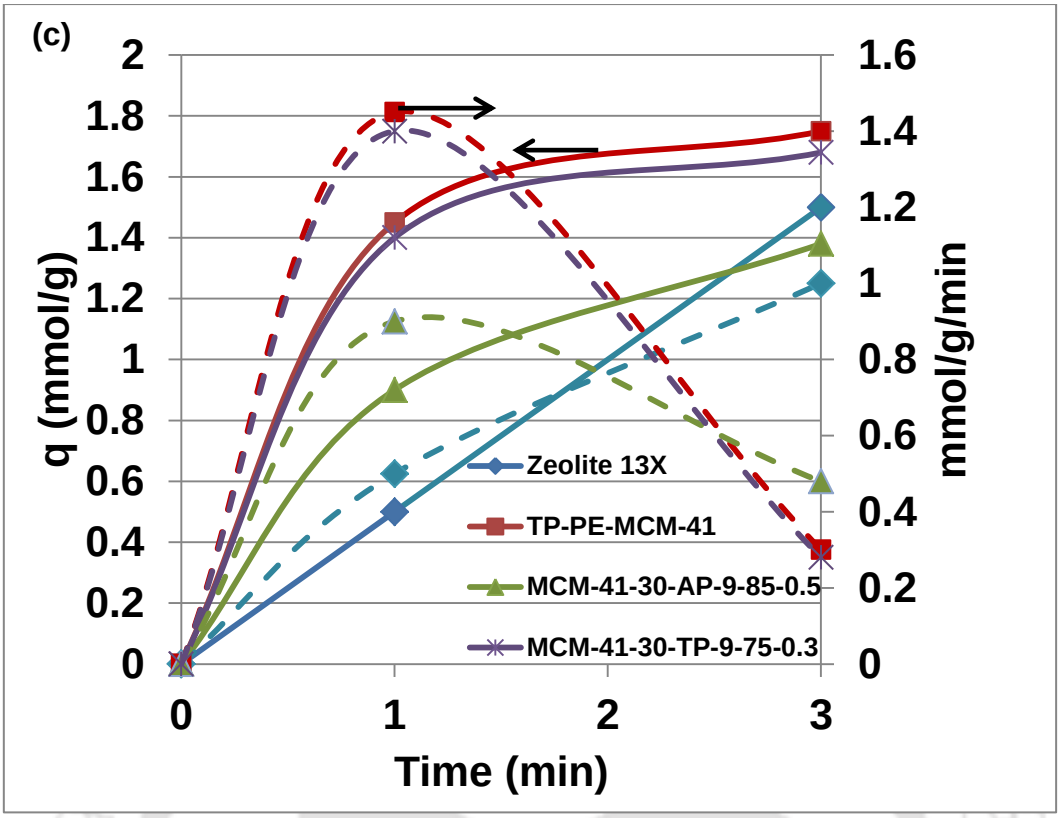

Figure 7.3. Kinetic profiles for CO_2 uptake at different temperatures for (a) MCM-41-30-AP-9-85-0.5 (b) MCM-41-30-TP-9-75-0.3 and (c) Comparison of kinetic profiles for CO_2 uptake at 25-30 °C for different adsorbents

exhibited after 1 min with rise in temperature, as adsorption is an exothermic process. MCM-41-30-TP-9-75-0.3 also exhibited enhanced rate of adsorption when the temperature progressed from 30 to 75 °C, for which $t_{1/2}$ is achieved within 0.5 min. In this case, the adsorbed amount also increased with rise in temperature, due to the better accessibility of polyamino siloxane proximities by the CO_2 molecules as mentioned in details in section 7.3.1.3. For both MCM-41-30-AP-9-85-0.5 and MCM-41-30-TP-9-75-0.3 samples, around 80% of the CO_2 uptake is achieved within 2 min for all the temperature conditions studied indicating the faster adsorption kinetics due to enhanced pore size of the support. In case of MCM-41-30-TP-9-75-0.3, ~1.4-1.7 mmol/g (for 30-75 °C) of CO_2 is adsorbed for 1 min equilibration time in 35-42% is higher in comparison to ~0.9-1 mmol/g adsorbed on MCM-41-30-AP-9-85-0.5 for the same equilibration time. This in fact is due to the three fold lower

loadings of amine moieties (mmol(N)/g) possessed by mono amino silane tethered adsorbent. Several authors have also discussed kinetics of amine tethered adsorbents by thermo-gravimetric analysis **[5, 10-12]**. An almost complete CO_2 uptake for mono amino silane functionalized HMS (pore size: ~12-14 nm) was reported by Chaffee et al. after 10 min of adsorption run, with an adsorption half time of ~1.5 min **[10]**. In a separate study carried out by Yang et al. 80 % of CO_2 equilibrium adsorption capacity was achieved for mono amine functionalized MCM-48 (pore size: ~3-4 nm) after 30 min of adsorption run and an adsorption halftime was calculated to be around 5 min **[11]**. A slower uptake rate of 0.24 mmol/g for 1 min equilibrium time is measured for monoamine SBA-12 (pore size: 6 nm) **[12]**. Sayari et al. measured CO_2 adsorption kinetics on tri-amine grafted pore-expanded MCM-41 and 80% of equilibrium adsorption capacity is reached within 2 min (shown in Figure 7.3(c)) **[5]**. The same adsorbent exhibited an uptake capacity of ~1.4 mmol/g for 1 min equilibration time in comparison to 0.45 mmol/g of CO_2 adsorbed on zeolite 13X (shown in Figure 8(c)) **[5]**. Hence, the results obtained in the present study indicate that the developed adsorbents (MCM-41-30-AP-9-85-0.5 and MCM-41-30-TP-9-75-0.3) exhibit faster adsorption kinetics comparable to PE-MCM-41 adsorbent indicating the importance of the type of silica support utilized for amine tethering.

7.3.1.5. CO_2 Selectivity

For any adsorbent to be considered as suitable candidate for CO_2 separation application, it's selectivity for CO_2 over other major components in the flue gas mixture should be assessed. The major components that are present in flue gas include nitrogen, water vapour and oxygen **[1-4]**. In the present study, nitrogen (N_2) adsorption on MCM-41-30-AP-9-85-0.5 and MCM-41-30-TP-9-75-0.3 is carried out at different temperatures (30, 45, 60, 75 °C) and the corresponding N_2 isotherms are presented in Figure 7.4(a) and (b) respectively. It can be observed from the figure that both the samples exhibited negligible N_2 adsorption for all the temperature and pressure conditions studied. The CO_2/N_2 selectivity is calculated according to the composition of CO_2 and N_2 in the flue gas mixture by the following relationship

$$Selectivity = \frac{q_{CO_2} / p_{CO_2}}{q_{N_2} / p_{N_2}} \quad (1)$$

where, q_{CO_2} and q_{N_2} refers to the adsorption capacity of CO_2 and N_2, respectively. p_{CO_2} and p_{N_2} refers to the partial pressure of CO_2 (0.2 bar) and N_2 (0.8 bar), respectively. Both the samples provided very high selectivity for CO_2 over N_2 for all the temperatures investigated. Amine-tethered adsorbents are already shown to provide very high selectivity to adsorb CO_2 over both oxygen and nitrogen in a number of literatures **[5, 13-15]**. The effect of water vapour on CO_2 adsorption is also discussed in details in several other literatures **[5, 16-21]**.

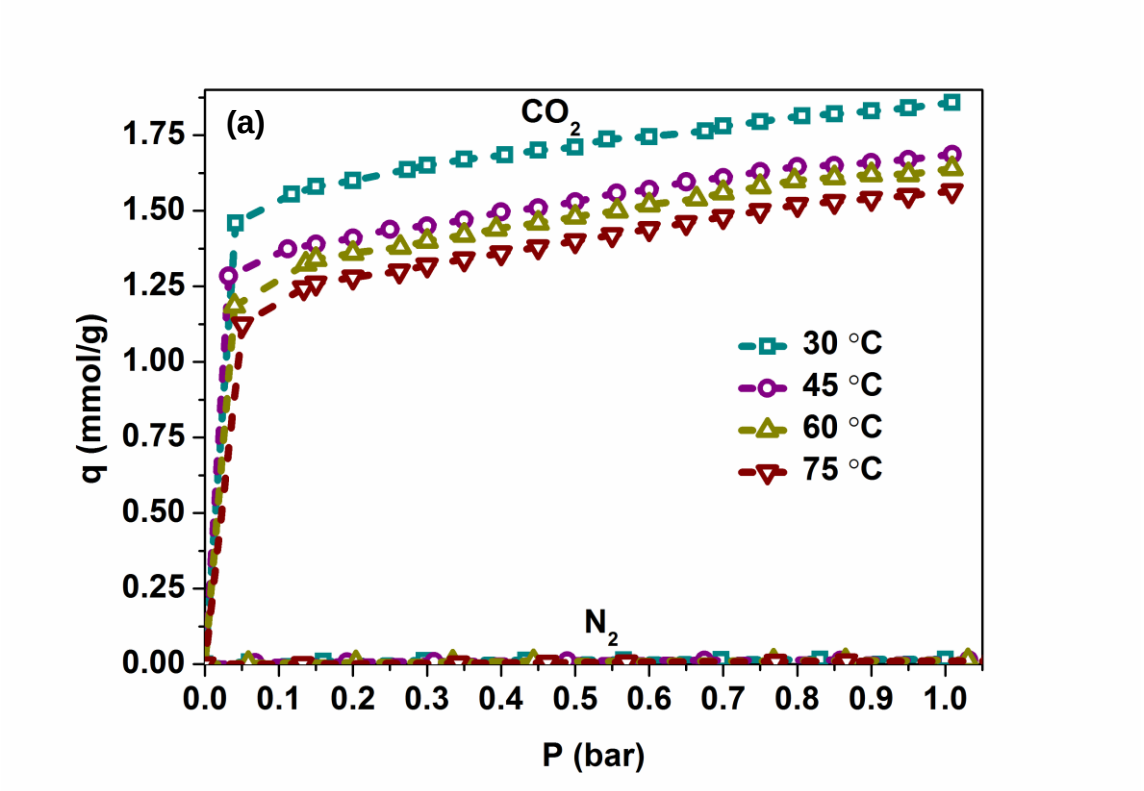

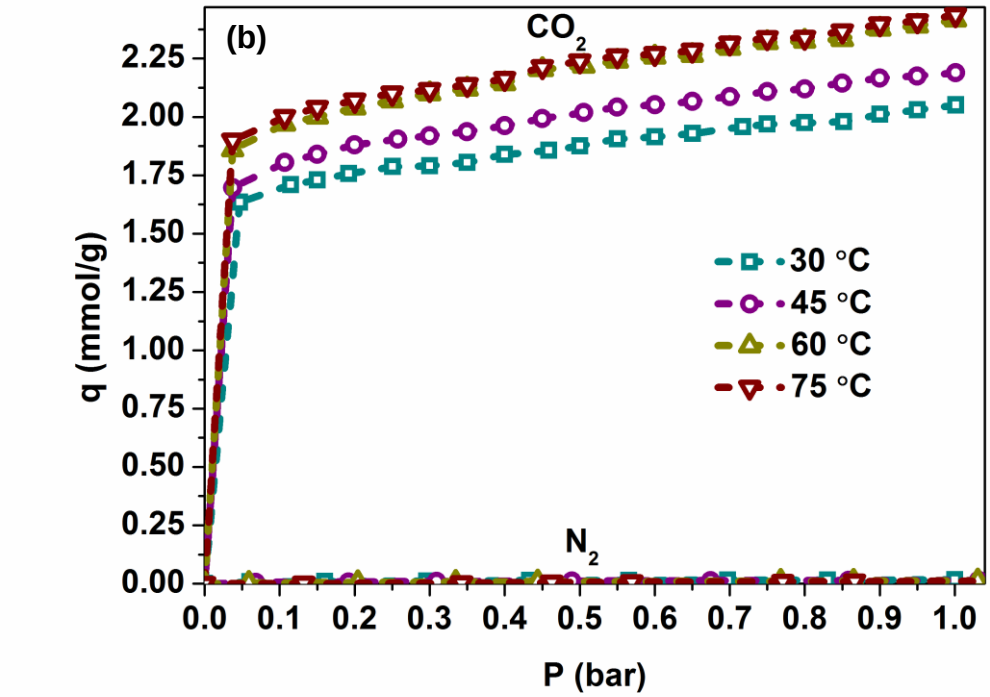

Figure 7.4. CO_2 and N_2 adsorption isotherms at different temperatures for (a) MCM-41-30-AP-9-85-0.5 and (b) MCM-41-30-TP-75-0.3

The presence of water vapour in the gas mixture led to improved amine efficiency, i.e. the number of moles of CO_2 adsorbed per mole of nitrogen in the adsorbent, thus providing an added advantage for enhancing the CO_2 capture performance. CO_2/N_2 selectivity for several other physisorbents is also calculated according to the available literature data relevant to flue gas conditions and presented in Table A1. It can be observed from the Table, porous solids such as zeolites and activated carbons appear to be good candidates for capturing CO_2 from flue gas through physical adsorption. High porosities of activated carbon as well as zeolites bestow them with CO_2 capture capacities of 2-3.5 mmol/g. However, the CO_2/N_2 selectivity of several activated carbon adsorbents is reported to be comparatively low (~10), which makes carbon-based systems suitable only for the gas streams enriched with CO_2 **[22]**. Despite zeolites and MOFs are reported to offer better CO_2/N_2 selectivities in comparison to carbon materials at ambient temperature conditions, their CO_2 selectivies are

experienced to degrade significantly with respect to rise in capture temperature (Table A1) and in the presence of water vapour present in the flue gas mixture for zeolites **[2-4]**. However, the exploration of the influence of water on CO_2 separations by MOF materials is rare in the literature. Based on the limited and available data, it is generally accepted that the CO_2 adsorption as well as selectivity decrease in the presence of water for MOFs since water molecules contend with CO_2 for the adsorption sites **[23]**. Investigation on the effect of water on CO_2 adsorption in Mg-MOF-74 is carried out by Yu et al. **[23]**. The CO_2 adsorption capacity exhibited downturn by two fold (~3 mmol/g at 0.2 bar and 21°C) in the presence of 13 wt% moisture **[23]**. Therefore, as pointed out by Keskin et al. for indeed Mg-MOF-74 to be a potential adsorbent for post-combustion CO_2 capture, the co-adsorption issue of CO_2 with water is vital to be resolved **[24]**. Unlike zeolites and MOFs, amine tethered adsorbents have been proved to be tolerant and exhibit positive response to moisture in feed gas during CO_2 adsorption **[2, 3]** and thus eliminates the necessity for strict control of humidity prior to carbon capture. The experimental results for CO_2/O_2 and CO_2/H_2O selectivity for MCM-41-30-AP-9-85-0.5 and MCM-41-30-TP-9-75-0.3 will be addressed in our future work. However, based on the literature information **[2, 3]**, it can be concluded that MCM-41-30-TP-9-75-0.3 might also serve as a potential candidate for carbon capture from flue gas by exhibiting very high selectivity for CO_2 over O_2 and positive effect on CO_2 capture performance in the presence of moisture.

7.3.1.6. Regeneration and Multi-cycle Stability

In addition to high CO_2 adsorption capacity and selectivity, an adsorbent should also possess long term stability and be easily regenerated under mild conditions for practical applications. Hence, the assessment of MCM-41-30-AP-9-85-0.5 and MCM-41-30-TP-9-75-0.3 is carried out based on regeneration conditions and multi-cycle stability. Industrial regeneration processes are usually accomplished by (i) isothermal regeneration i.e. pressure swing (PS) process which further includes vacuum swing (VS) or concentration swing (CS) (ii) non isothermal regeneration i.e. temperature swing process (TS) or a combination of

temperature and pressure gradients (TPS or TVS) **[4]**. In general, the nature of adsorbent-adsorbate interaction plays a major role in determining the type of regeneration process to be used. For amine tethered adsorbents, owing to chemical interactions between CO_2 and amine functionalities, heat driven regeneration modes (TS or TVS) are found to be appropriate as evidenced in several literatures **[2-4]**.

In the present part, prior to adsorption experiments, all the samples are activated at 125 °C under vacuum for 1.5 h. Hence, multi-cycle stability of MCM-41-30-AP-9-85-0.5 and MCM-41-30-TP-9-75-0.3 under TVS mode (regeneration is carried out at 125 °C under vacuum) is tested for both the adsorbents and the CO_2 adsorption measurements are carried out on both the samples (0.2 bar and 75 °C). No loss in the adsorption capacity is exhibited by both the samples for even 100 cycles of adsorption-desorption indicating that the adsorbents are stable when operated under TVS mode (shown in Figure 7.5(a)). However, the regeneration carried out at temperatures 125 °C which is higher than that of adsorption temperature (75 °C) led to lengthy adsorption and desorption procedures which is not suitable for maintaining rapid cycle times. Hence, the feasibility of heat free regeneration mode i.e vacuum swing process to regenerate both the adsorbents is investigated, where the adsorption and desorption temperature as well as time for both the samples is fixed to be 75 °C and 30 min respectively. The MCM-41-30-AP-9-85-0.5 and MCM-41-30-TP-9-75-0.3 samples that are already regenerated under TVS mode at 125 °C for 100 cycles are subjected to VS process. The corresponding adsorption-desorption profiles of both the samples are shown in Figure 7.5(b) respectively. It can be seen from the figures that the adsorption capacity of MCM-41-30-AP-9-85-0.5 and MCM-41-30-TP-9-75-0.3 drops down to 0.92 from 1.36 and 1.9 from 2.2 respectively, after first cycle. This corresponds to 32 % and 13.6% loss in adsorption capacity respectively, which is attributed to the incomplete regeneration, resulted from insufficient regeneration time provided at 75 °C. Thereafter, negligible change in the working capacity for both MCM-41-30-AP-9-85-0.5 and MCM-41-30-

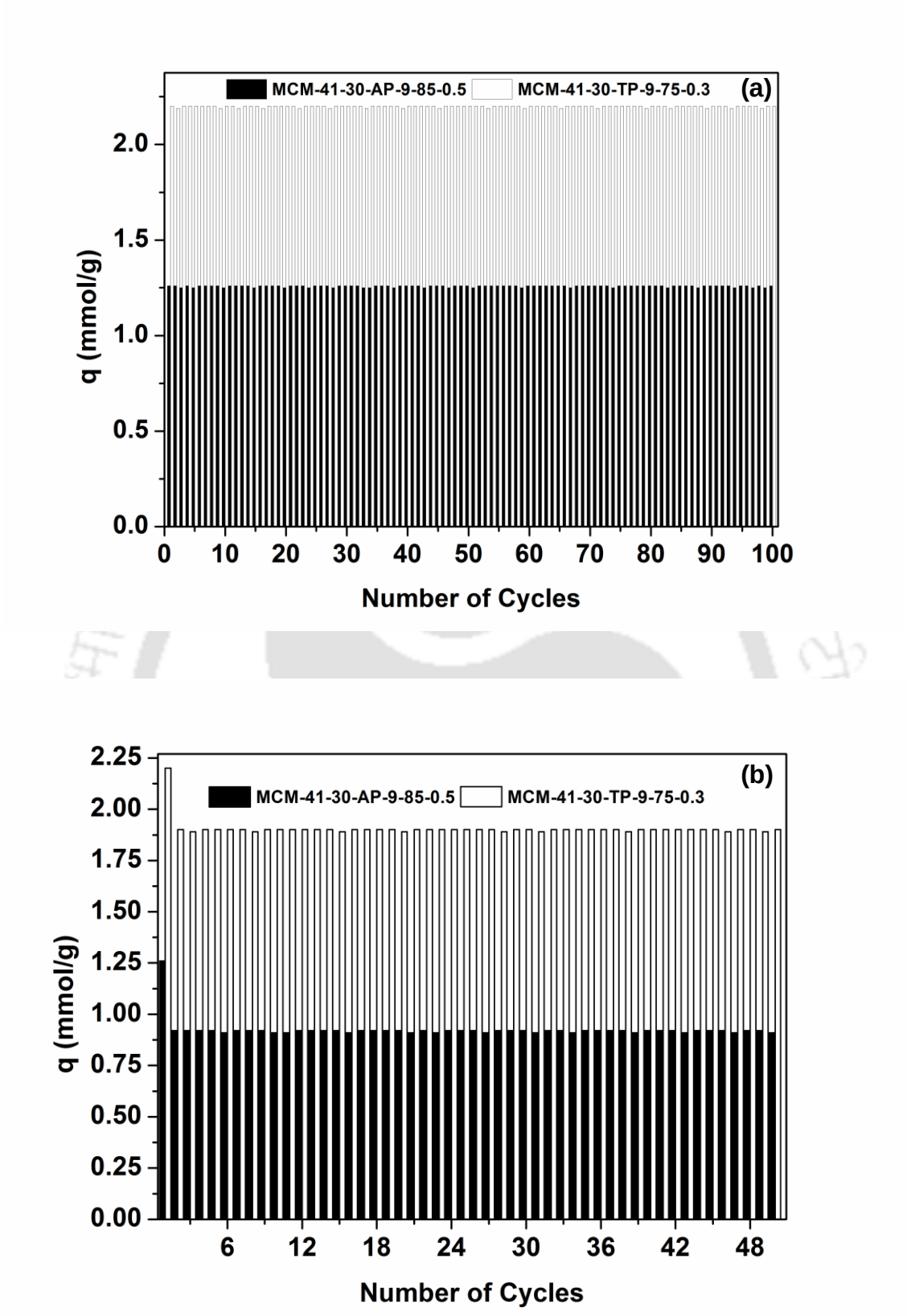

Figure 7.5. Cyclic adsorption-desorption studies (a) TVS mode and (b) VS mode

TP-9-75-0.3 respectively is exhibited by both the samples even for 50 cycles. The studies indicate that both the adsorbents exhibit multi-cycle stability irrespective of TVS or VS mode for desorption.

7.1.3.7. Cost

Majority of the cost for synthesis of amine tethered mesoporous silica adsorbents comes from the type of support used for grafting process. In the present work, the cost for synthesis of several mesoporous supports such as MCM-41-30, MCM-41-3, MCM-48, PE-MCM-41, SBA-15, and KIT-6 are estimated based on the amount of raw materials required for synthesis of one gram of the respective supports in laboratory scale. The costs of raw materials (Pluronic P123, DMDA, Cab-O-sil-M5 fumed silica, TEOS) are considered according to Sigma aldrich and for chemicals (TTAB, Cetyl trimethyl ammonium bromide (CTAB), 1-butanol, 25% aqueous ammonia, ethanol, HCl) as per Merck chemicals price list. The mesoporous silica supports namely MCM-41-30 **[25]**, MCM-41-3 **[25]**, MCM-48 **[26]**, SBA-15 **[27]**, and KIT-6 **[28]** are synthesized according to the procedure described in cited literatures. Thereafter, the yield of silica is calculated after calcination process and the same is obtained to be ~4, 3, 1, 2, and 2 gram for the corresponding mesoporous supports. In case of PE-MCM-41, the cost is estimated according to the amount of raw materials used for synthesis procedure described in **[29]** and the yield of silica is assumed to be ~4 g. The detailed cost calculation is shown in Table A.2 (in appendix section). The cost calculated for all the supports are portrayed in Figure 7.6. It can be noticed from the figure, that the cost of the support (MCM-41-30) developed in the current work is comparatively cheaper to other mesoporous supports reported in the literature **[25-27]**. Therefore, it becomes clear that the support synthesized herein, is promising in terms of amine tethering and demonstrates potential carbon capture characteristics. It becomes important to understand here that the estimated cost for adsorbents based on the price values of chemicals provided by Sigma Aldrich and other sources does not represent the true cost of manufacturing of the adsorbents at bulk scale. As the information about the cost for synthesis of mesoporous

silica adsorbents is scarce in the literature, the estimated cost based on laboratory scale might be helpful at this stage.

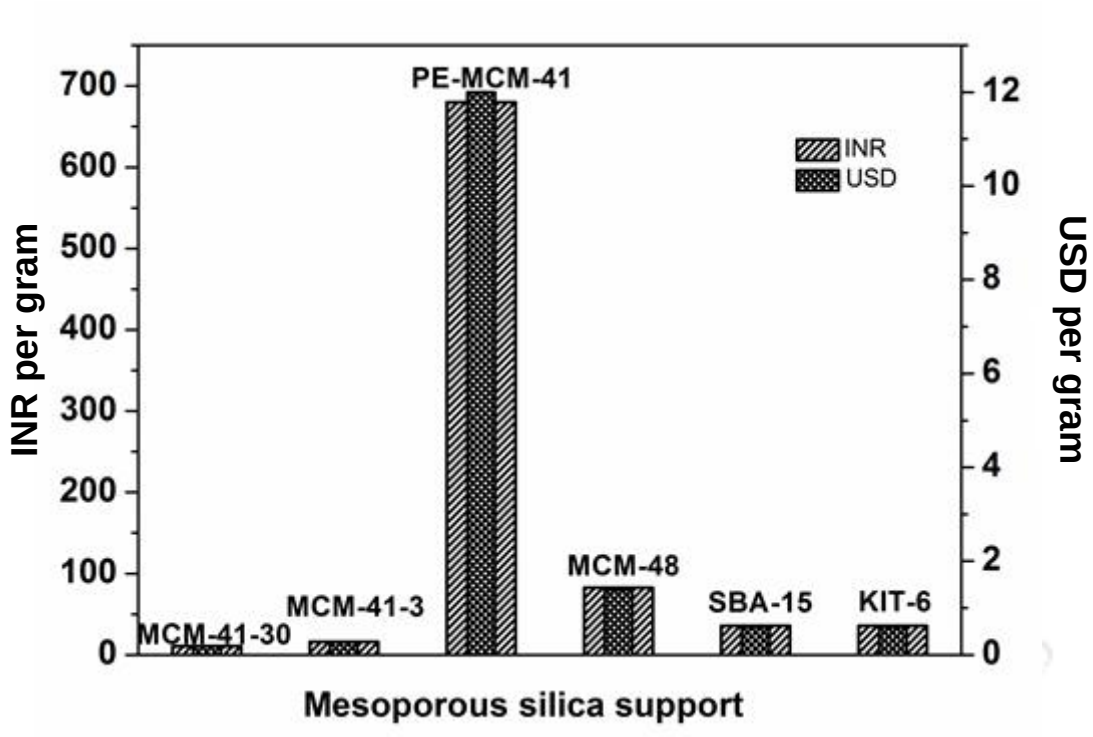

Figure 7.6. Cost estimation for different mesoporous silica supports.

7.5. Conclusions

The performance evaluation of adsorbents MCM-41-30-AP-9-85-0.5 and MCM-41-30-TP-9-75-0.3 based on post-combustion CO_2 capture metrics is carried out. The MCM-41-30-TP-9-75-0.3 exhibited an excellent CO_2 adsorption capacity of ~2.1 mmol/g at flue gas conditions (0.2 bar and 75 °C). The same adsorbent also demonstrated excellent performance in terms of CO_2 adsorption capacity, amine efficiency, selectivity, operating window, CO_2 uptake kinetics, multi-cycle stability and cost with other reported benchmark adsorbents. This study indicates that MCM-41-30-TP-9-75-0.3 shows implications that it can be utilized as a promising adsorbent for post-combustion CO_2 capture.

7.6. References

[1] Bhown, A. S.; and Freeman, B. C. Analysis and Status of Post-Combustion Carbon Dioxide Capture Technologies, *Environ. Sci. Technol.* **2011**, *45*, 8624-8632.

[2] Sayari, A.; Belmabkhout, Y.; and Guerrero, R.S. Flue Gas Treatment via CO_2 Adsorption, *Chem. Eng. J*. **2011**, 171, 760-764.

[3] Choi, S.; Drese, J. H.; and Jones, C. W. Adsorbent Materials for Carbon dioxide Capture from Large Anthropogenic Point Sources, *ChemSusChem.* 10.1002/cssc.200900036.

[4] Bollini, P.; Didas, S. A.; and Jones, C. W. Amine-oxide Hybrid Materials for Acid Gas Separations, *J. Mater. Chem.* **2011**, 21, 15100-15120.

[5] Harlick, P. J. E.; and Sayari, A. Applications of Pore-Expanded Mesoporous Silica. 5. Triamine Grafted Material with Exceptional CO_2 Dynamic and Equilibrium Adsorption Performance, *Ind. Eng. Chem. Res.* **2007,** 46*,* 446-458.

[6] Caplow, M.; Kinetics of Carbamate Formation and Breakdown, *J. Am. Chem. Soc.* **1968**, 90, 6795-6803.

[7] Fadhel, B.; Hearn, M.; and Chaffee, A. CO_2 Adsorption by PAMAM Dendrimers: Significant Effect of Impregnation into SBA-15, *Micropor. Mesopor. Mater.* **2009**, *123*, 140-149.

[8] Ma, X.; Wang, X.; and Song, C. “Molecular Basket” Sorbent for Separation of CO_2 and H_2S from Various Gas Streams, *J. Am. Chem. Soc.* **2009**, 131, 5777-5783.

[9] Belmabkhout, Y.; and Sayari, A. Isothermal versus Non-isothermal Adsorption-Desorption Cycling of Triamine-Grafted Pore-Expanded MCM-41 Mesoporous Silica for CO_2 Capture from Flue Gas*, Energy Fuels* **2010**, 24, 5273-5280.

[10] Knowles, G. P.; Graham, J. V.; Delaney, S. W.; and Chaffee, A. L. Aminopropyl-Functionalized Mesoporous Silicas as CO_2 Adsorbents, *Fuel Process.Technol.* **2005**, 86, 1435-1448.

[11 Huang, H. Y.; R. T. Yang, D. and Chinn, C. L. Munson, Amine-Grafted MCM-48 and Silica Xerogel as Superior Sorbents for Acidic Gas Removal from Natural Gas, *Ind. Eng. Chem. Res.* **2003**, 42, 2427-2433.

[12] Zelenak, V.; Halamova, D.; Gaberova, L.; Bloch, E.; and Llewellyn, P. Amine-Modified SBA-12 Mesoporous Silica for Carbon Dioxide Capture: Effect of Amine Basicity on Sorption Properties, *Microporous Mesoporous Mater*. **2008**, 116, 358-364.

[13] Belmabkhout, Y.; and Sayari, A. Effect of Pore Expansion and Amine Functionalization of Mesoporous Silica on CO_2 Adsorption Over a Wide Range of Conditions, *Adsorption*, **2009**, 15, 318-328.

[14] Belmabkhout, Y.; Serna-Guerrero, R.; and Sayari, A. Amine-bearing Mesoporous Silica for CO_2 Removal from Dry and Humid Air, *Chem. Eng. Sci*. **2010**, 65, 3695-3698.

[15] Belmabkhout, Y.; Serna-Guerrero, R.; and Sayari, A. Adsorption of CO_2 - Containing Gas Mixtures over Amine-Bearing Pore-Expanded MCM-41 Silica: Application for Gas Purification, *Ind. Eng. Chem. Res.* **2010**, 49, 359-365.

[16] Serna-Guerrero, R.; Da'na, E.; and Sayari, A. New Insights into the Interactions of CO_2 with Amine-Functionalized Silica, *Ind. Eng. Chem. Res.* **2008**, 47, 9406-9412.

[17] Tsuda, T.; Fujiwara, T.; Taketani, Y.; and Saegusa, T. Amino Silicagels Acting as Carbon Dioxide Absorbent, *Chem. Lett.* **1992**, 11, 2161-2164.

[18] Hicks, J. C.; Drese, J. H.; Fauth, D. J.; Gray, M. L.; Qi, G. G.; and Jones, C. W. Designing Adsorbents for CO_2 Capture from Flue Gas-Hyperbranched Aminosilicas Capable of Capturing CO_2 Reversibly, *J. Am. Chem. Soc.* **2008**, 130, 2902-2903.

[19] Zheng, F.; Tran, D. N.; Busche, B. J.; Fryxell, G. E.; Addleman, R. S.; Zemanian, T. S. and Aardahl, C. L. Ethylenediamine-Modified SBA-15 as Regenerable CO_2 Sorbent, *Ind. Eng. Chem. Res.* **2005**, 44, 3099-3105.

[20] Hiyoshi, N.; Yogo, K.; and Yashima, T. Adsorption Characteristics of Carbon Dioxide on Organically Functionalized SBA-15, *Microporous Mesoporous Mater.* **2005**, 84, 357-365.

[21] Hiyoshi, N.; Yogo, K.; and Yashima, T. Adsorption of Carbon Dioxide on Amine Modified SBA-15 in the Presence of Water Vapour, *Chem. Lett.* **2004**, 33, 510-511.

[22] Radosz, M.; Hu, X. D.; Krutkramelis, K.; and Shen, Y. Q. Flue-Gas Carbon Capture on Carbonaceous Sorbents: Toward a Low-Cost Multifunctional Carbon Filter for "Green" Energy Producers, *Ind. Eng. Chem. Res*. **2008**, 47, 3783-3794.

[23] Yu, J.; and Balbuena, P. B. Water Effects on Post-Combustion CO_2 Capture in Mg-MOF-74, *J. Phys. Chem.* C **2013**, 117, 3383-3388.

[24] Keskin, S.; van Heest, T. M.; and Sholl, D. S. Can Metal−Organic Framework Materials Play a Useful Role in Large-Scale Carbon Dioxide Separations, *ChemSusChem* **2010**, 3, 879-891.

[25] Loganathan, S.; Tikmani, M.; and Ghoshal, A. K. Novel Pore-Expanded MCM-41 for CO_2 Capture: Synthesis and Characterization, *Langmuir* **2013**, 29, 3491-3499.

[26] Zhao, D.; Rodriguez, A.; Dimitrijevic, N. M.; Rajh, T.; and Koodali, R. T. Synthesis, Structural Characterization and Photocatalytic Performance of Mesoporous W-MCM-48, *J. Phys. Chem. C* **2010**, 114, 15728-15734.

[27] Wang, L.; and Yang, R. T. Increasing Selective CO_2 Adsorption on Amine-Grafted SBA-15 by Increasing Silanol Density, *J. Phys. Chem. C*, **2011**, 115, 21264-21272.

[28] Pirez, C.; Caderon, J. M.; Dacquin, J. P.; Lee, A. F.; and Wilson, K. Tunable KIT-6 Mesoporous Sulfonic Acid Catalysis for Fatty Acid Esterification, *ACS Catal.* **2012**, 2, 1607-1614.

[29] Belmabkhout, Y.; and Sayari, A. Materials, Methods and Systems for Selective Capture of CO_2 at High Pressure, US patent No: US 12/579936.

[30] Bae, T. H.; Hudson, M. R.; Mason, J. A.; Queen, W. L.; Dutton, J. J.; Sumida, K.; Micklash, K. J.; Kaye, S. S.; Brown, C. M.; and Long, J. R. Evaluation of Cation-Exchanged Zeolite Adsorbents for Post-Combustion carbon Dioxide Capture, *Energy Environ. Sci.* **2013**, 6, 128-138.

[31] Barthomeuf, D. Conjugate Acid-Base Pairs in Zeolites, *J. Phys. Chem.* **1984**, 88, 42-45.

[32] Harlick, P.; and Tezel, F. H. An Experimental Adsorbent Screening Study for CO_2 Removal from N_2, *Microporous Mesoporous Mater.* **2004**, 76, 71-79.

[33] Cavenati, S.; Grande, C. A.; and Rodrigues, A. E. Adsorption Equilibrium of Methane, Carbon Dioxide and Nitrogen on Zeolite 13X at High Pressure, *J. Chem. Eng. Data* **2004**, 49, 1095-1101.

[34] Harlick, P. J. E.; and Tezel, F. H. Equilibrium Analysis of Cyclic Adsorption Processes: CO_2 Working Capacities with NaY, *Separ Sci and Technol* **2006**, 40, 2569-2591.

[35] McEwen, J.; Hayman, J. D.; and Yazaydin, A. O. A Comparative Study of CO_2, CH_4 and N_2 Adsorption in ZIF-8, Zeolite-13X and BPL Activated Carbon, *Chem Phys* **2013**, 412, 72-76.

[36] Himeno, S.; Komatsu, T.; and Fujita, S. High-Pressure Adsorption Equilibria of Methane and Carbon Dioxide on Several Activated Carbons, *J. Chem. Eng. Data* **2005**, 50, 369-376.

[37] Na, B. K.; Koo, K. K.; Eum, H. M.; Lee, H.; and Song, H. K. CO_2 Recovery from Flue Gas by PSA Process using Activated Carbon, *Korean J. Chem. Eng.* **2001**, 18, 220-227.

[38] Lu, C. Y.; Bai, H. L.; Wu, B. L.; Su, F. S.; and Fen-Hwang, J. Comparative Study of CO_2 Capture by Carbon Nanotubes, Activated Carbons and Zeolites, *Energy Fuels* **2008**, 22, 3050-3056.

[39] Lee, J. S.; Kim, J. H.; Kim, J. T.; Suh, J. K.; Lee, J. M.; and Lee, C. H. Adsorption Equilibria of CO_2 on Zeolite 13X and Zeolite X/Activated Carbon Composite, *J. Chem. Eng. Data* **2002**, 47, 1237-1242.

[40] Mason, J. A.; Sumida, K.; Herm, Z. R.; Krishna, R.; and Long, J. Evaluating Metal-Organic Frameworks for Post-Combustion Carbon Dioxide Capture via Temperature Swing Adsorption, *Energy Environ. Sci.* **2011**, 4, 3030-3040.

[41] Mishra, P.; Edubilli, S.; Uppara, H. P.; Mandal, B. P.; and Gumma, S. Effect of Adsorbent History on Adsorption Characteristics of MIL-53(Al) Metal Organic Framework, *Langmuir* **2013**, 29, 12162-12167.

[42] Chowdhury, P.; Bikkina, C.; and Gumma, S. Gas Adsorption Properties of the Chromium-Based Metal Organic Framework MIL-101, *J. Phys. Chem. C* **2009**, 113, 6616-6621.

[43] Mishra, P.; Edubilli, S.; Mandal, B. P.; and Gumma, S. Adsorption Characteristics of Metal-Organic Frameworks Containing Coordinatively Unsaturated Metal Sites: Effect of Metal Cations and Adsorbate Properties, *J. Phys. Chem. C*, **2014**, 118, 6847-6855.

[44] Mishra, P.; Edubilli, S.; Mandal, B. P.; and Gumma, S. Adsorption of CO_2, CO, CH_4 and N_2 on DABCO Based Metal Organic Frameworks, *Microporous Mesoporous Mater.* **2013**, 169, 75-80.

[45] Chowdhury, P.; Mekala, S.; Dreisbach, F.; and Gumma, S. Adsorption of CO, CO_2 and CH_4 on Cu-BTC and MIL-101 Metal Organic Frameworks: Effect of Open Metal Sites and Adsorbate Polarity, *Microporous Mesoporous Mater.* **2012**, 152, 246-252.

[46]. Xu, X.; Song, C.; Andersen, J. M.; Miller, B. G.; and Scaroni, A. W. Novel Polyethylenimine-Modified Mesoporous Molecular Sieve of MCM-41 Type as High-Capacity Adsorbent for CO_2 Capture, *Energy Fuels* **2002**, 16, 1463-1469.

[47] Son, W. J.; Choi, J. S.; and Ahn, W. S. Adsorptive Removal of Carbon Dioxide using Polyethylenimine-Loaded Mesoporous Materials, *Micropor. Mesopor. Mater.* **2008**, 113, 31-40.

[48] Chen, C.; Yang, S. T.; Ahn, W. S.; and Ryoo, R. Amine-Impregnated Silica Monolith with a Hierarchical Pore Structure: Enhancement of CO_2 Capture Capacity, *Chem. Commun.* **2009**, 24, 3627-3629.

[49] Yue, M. B.; Chun, Y.; Cao, Y.; Dong, X.; and Zhu, J. H. CO_2 Capture by As-prepared SBA-15 with an Occluded Organic Template, *Adv. Funct. Mater.* **2006**, 16, 1717-1722.

[50] Yue, M .B.; Sun, L. B.; Cao, Y.; Wang, Y.; Wang, Z. J.; and Zhu, J. H. Efficient CO_2 Capturer Derived from As-synthesized MCM-41 Modified with Amine, *Chem. Eur. J.* **2008**, 14, 3442-3451.

[51] Yue, M. B.; Sun, L. B.; Cao, Y.; Wang, Z. J.; Wang, Y.; Yu, Q.; and Zhu, J. H. Promoting the CO_2 Adsorption in the Amine-containing SBA-15 by Hydroxyl Group, *Micropor.Mesopor.Mater.* **2008**, 114, 74-81.

[52] Franchi, R. S.; Harlick, P. J. E.; and Sayari, A. Applications of Pore-Expanded Mesoporous Silica. 2. Development of a High-Capacity, Water-Tolerant Adsorbent for CO_2, *Ind. Eng. Chem. Res.* **2005**, 44, 8007-8013.

[53] Plaza, M. G.; Pevida, C.; Arias, B.; Fermoso, J.; Arenillas, A.; Rubiera, F.; and Pis, J. J. Application of Thermo Gravimetric Analysis to the Evaluation of Aminated Solid Sorbents for CO_2 Capture, *J. Therm. Anal. Calorim.* **2008**, 92, 601-606.

[54] Chen, Z.; Deng, S.; Wei, H.; Wang, B.; Huang, J.; and Yu, G. Polyethylenimine-Impregnated Resin for High CO_2 Adsorption: An Efficient Adsorbent for CO_2 Capture from Simulated Flue Gas and Ambient Air, *ACS Appl. Mater. Interfaces* **2013**, 5, 6937-6945.

[55] Pinto, M. L.; Mafra, L.; Guil, J. M.; Pires, J.; and Rocha, J. Adsorption and Activation of CO_2 by Amine-Modified Nanoporous Materials Studied by Solid-State NMR and $^{13}CO_2$ Adsorption, Chem. Mater. **2011**, 23, 1387-1395.

[56] Belmabkhout, Y.; Heymans, N.; Weireld, G. D.; and Sayari, A. Simultaneous Adsorption of H_2S and CO_2 on Triamine-Grafted Pore-Expanded Mesoporous MCM-41 Silica, *Energy Fuels* **2011**, 25, 1310-1315.

[57] Lee, D.; Jin, Y.; Jung, N.; Lee, J.; Lee, J.; Jeong, Y. S.; and Jeon, S. Gravimetric Analysis of the Adsorption and Desorption of CO_2 on Amine-Functionalized Mesoporous Silica Mounted on a Microcantilever Array, *Environ. Sci. Technol.* **2011**, 45, 5704-5709.

[58] Bollini, P.; Brunelli, N. A.; Didas, S. A.; and Jones, C. W. Dynamics of CO_2 Adsorption on Amine Adsorbents. 1. Impact of Heat Effects, *Ind. Eng. Chem. Res.* **2012**, 51, 15145-15152.

[59] Bollini, P.; Brunelli, N. A.; Didas, S. A.; and Jones, C. W. Dynamics of CO_2 Adsorption on Amine Adsorbents. 2. Insights Into Adsorbent Design, *Ind. Eng. Chem. Res.* **2012**, 51, 15153-15162.

[60] Sayari, A.; Belmabkhout, Y.; and Da'na, E.; CO_2 Deactivation of Supported Amines: Does the Nature of Amine Matter? *Langmuir* **2012**, 28, 4241-4247.

[61] Kim, S.; Ida, J.; Guliants, V. V.; and Lin, J. Y. S. Tailoring Pore Properties of MCM-48 Silica for Selective Adsorption of CO_2, *J. Phys. Chem. B* **2005**, 109, 6287-6293.

[62] Leal, O; Bolı´var, C.; Ovalles, C.; Garcı´a, J. J.; and Espidel, Y. Reversible Adsorption of Carbon Dioxide on Amine Surface-Bonded Silica Gel, *Inorg. Chim. Acta* **1995**, 240, 183-189.

[63] Knowles, G. P.; Delaney, S. W.; and Chaffee, A. L. Diethylenetriamine-[propyl(silyl)]-Functionalized (DT) Mesoporous Silicas as CO_2 Adsorbents, *Ind. Eng. Chem. Res.* **2006**, 45, 2626-2633.

[64] Harlick, P. J. E.; and Sayari, A. Applications of Pore-Expanded Mesoporous Silica. 3. Triamine Silane Grafting for Enhanced CO_2 Adsorption, *Ind. Eng. Chem. Res.* **2006**, 45, 3248-3255.

CHAPTER 8

MODELING OF CO_2 ADSORPTION ON AMINE TETHERED MCM-41: EQUILIBRIUM AND KINETIC STUDIES

The chapter elucidates the investigation of experimental equilibrium and kinetic data by several isotherm and kinetic models. The theory for both isotherm (Langmuir and Langmuir dual-site models) and kinetic models (Pseudo first order, Pseudo second order, Double-exponential models) are discussed.

8.1. Introduction

Prior to the design of an adsorption process, investigation of performance of solid sorbent in both equilibria and kinetics becomes critical. Equilibrium sorption studies are important in determining the effectiveness of adsorption where as the kinetic analyses allow understanding the dynamics and determination of the residence time required for completion of an adsorption process **[1]**. In view of this, in the present chapter, the experimental adsorption isotherm data obtained for MCM-41-30-AP-9-85-0.5 and MCM-41-30-TP-75-0.3 in the pressure range of 0-5 bar and at four different temperature conditions (30, 45, 60 and 75 °C) are analysed by isotherm models such as Langmuir and Langmuir dual-site models. Further, kinetic data obtained for CO_2 adsorption on MCM-41-30-AP-9-85-0.5 and MCM-41-30-TP-75-0.3 adsorbents under ambient pressure condition (1 bar) and at four different temperature conditions (30, 45, 60 and 75 °C) are analysed by kinetic models such as pseudo-first order, pseudo-second order and double-exponential model.

8.2. Experimental section

8.2.1. Materials

The details of materials used for synthesis of MCM-41 have been described in section 3.2.1.

8.2.2. Synthesis of amine grafted MCM-41

The synthesis procedure for MCM-41-30-AP-9-85-0.5 and MCM-41-30-TP-75-0.3 has been described in section 6.2.2.

8.2.3. Material characterization

The detailed characterization of MCM-41-30-AP-9-85-0.5 and MCM-41-30-TP-75-0.3 is discussed in section 6.2.3.

8.2.4. CO_2 adsorption isotherm and kinetic measurements

The CO_2 adsorption isotherm measurements for MCM-41-30-AP-9-85-0.5 and MCM-41-30-TP-75-0.3 adsorbents are described in section in 7.2.4. The CO_2 adsorption kinetic measurements for the same are carried out under ambient pressure conditions (1 bar) and at four different temperatures (30, 45, 60, 75 °C). Similar procedure described in section 5.2.4 is followed to obtain the kinetic data.

8.2.5. Determination of isotherm and kinetic model parameters

The methodology used for determination of isotherm and kinetic model parameters is similar as discussed in earlier in section 4.2.5 and 5.2.5 respectively.

8.3. Theory

8.3.1. Mathematical models of adsorption isotherms and kinetics

For isotherm modeling studies, Langmuir and Langmuir dual-site models are considered and theory for the same is described in section 4.3.1. For prediction of kinetic behavior, apart from pseudo-first order and pseudo-second order models, double-exponential model is introduced in this study. The theory for pseudo-first order and pseudo-second order model is described in sections 5.3.1.1 and 5.3.1.2 respectively.

The double exponential model is given by:

$$q_t = q_e - A_1 \exp(-k_1 t) - A_2 \exp(-k_2 t) \quad (1)$$

where, q_t and q_e represents the amount of CO_2 adsorbed at a given point of time and at equilibrium respectively. The factors A_1 and A_2 are similar to $q_{m,\,A}$ and $q_{m,\,B}$ in Langmuir dual site model whereas, k_1 and k_2 represent the kinetics rate constant of the two adsorption sites **[2]**. This model is considered in this study because of its feasibility in explaining the adsorption kinetics for adsorbent that possesses two different adsorption sites. This model also offers an advantage of explaining kinetic mechanisms which involve two steps, namely

a rapid phase controlled by strong surface reactions and intra-particle diffusion controlled slow phase **[2]**. The major merit of this model is that it takes into account the surface heterogeneity in the same way as Langmuir dual site.

8.3.2. Error calculation

The method used for error calculation is described in section 4.3.2.

8.3.3. Heat of adsorption

The method used for calculation of heat of adsorption is described in section 4.3.3.

8.4. Results and discussion

8.4.1. Comparison of isotherm models

The experimental equilibrium data obtained for both MCM-41-30-AP-9-85-0.5 and MCM-41-30-TP-9-75-0.3 adsorbents obtained in the pressure range of 0-5 bar and four different temperatures (30, 45, 60 and 75 °C) are fitted to Langmuir and Langmuir dual-site model. Comparative plots of experimental isotherm data with above mentioned models for MCM-41-30-AP-9-85-0.5 and MCM-41-30-TP-9-75-0.3 adsorbents are presented in Figure 8.1 and Figure 8.2 respectively. The estimated isotherm model parameters for MCM-41-30-AP-9-85-0.5 and MCM-41-30-TP-9-75-0.3 adsorbents are listed in the Table 8.1 and Table 8.2 respectively, along with the deviation of the predicted q values from the experimental q values (in terms of error %). From the listed error values and the plot, it can be seen that Langmuir dual-site isotherm model closely follows the experimental data throughout the entire range of pressure for different temperatures analyzed indicating the heterogeneous nature of the surface. Langmuir isotherm model, on the other hand, shows significant deviations from the experimental results. This is because, the model doesn't take into account the surface heterogeneity phenomenon **[3]**.

The plots of various models for all the temperatures analyzed show an initial steep rise in the CO_2 adsorption capacity on both MCM-41-30-AP-9-85-0.5 and MCM-41-30-TP-9-75-0.3 samples. This behaviour is different from that of MCM-41-30, where the adsorption capacity rises gradually, which can be explained on the basis of difference in the adsorption

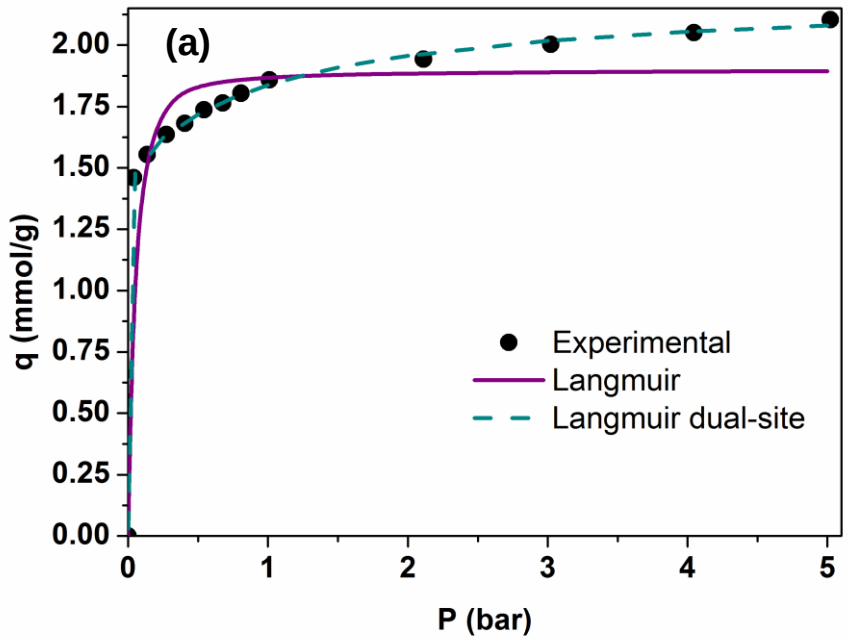

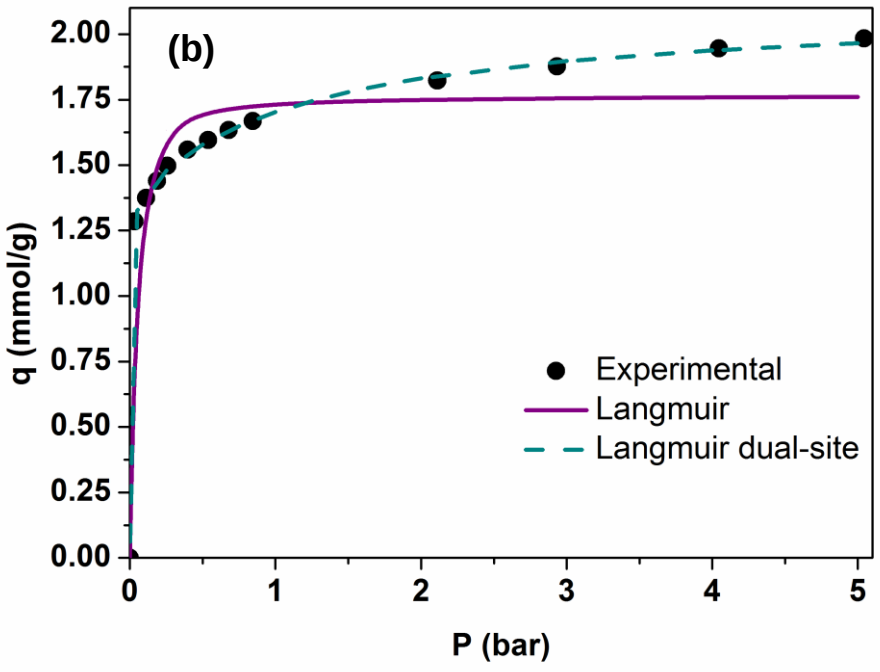

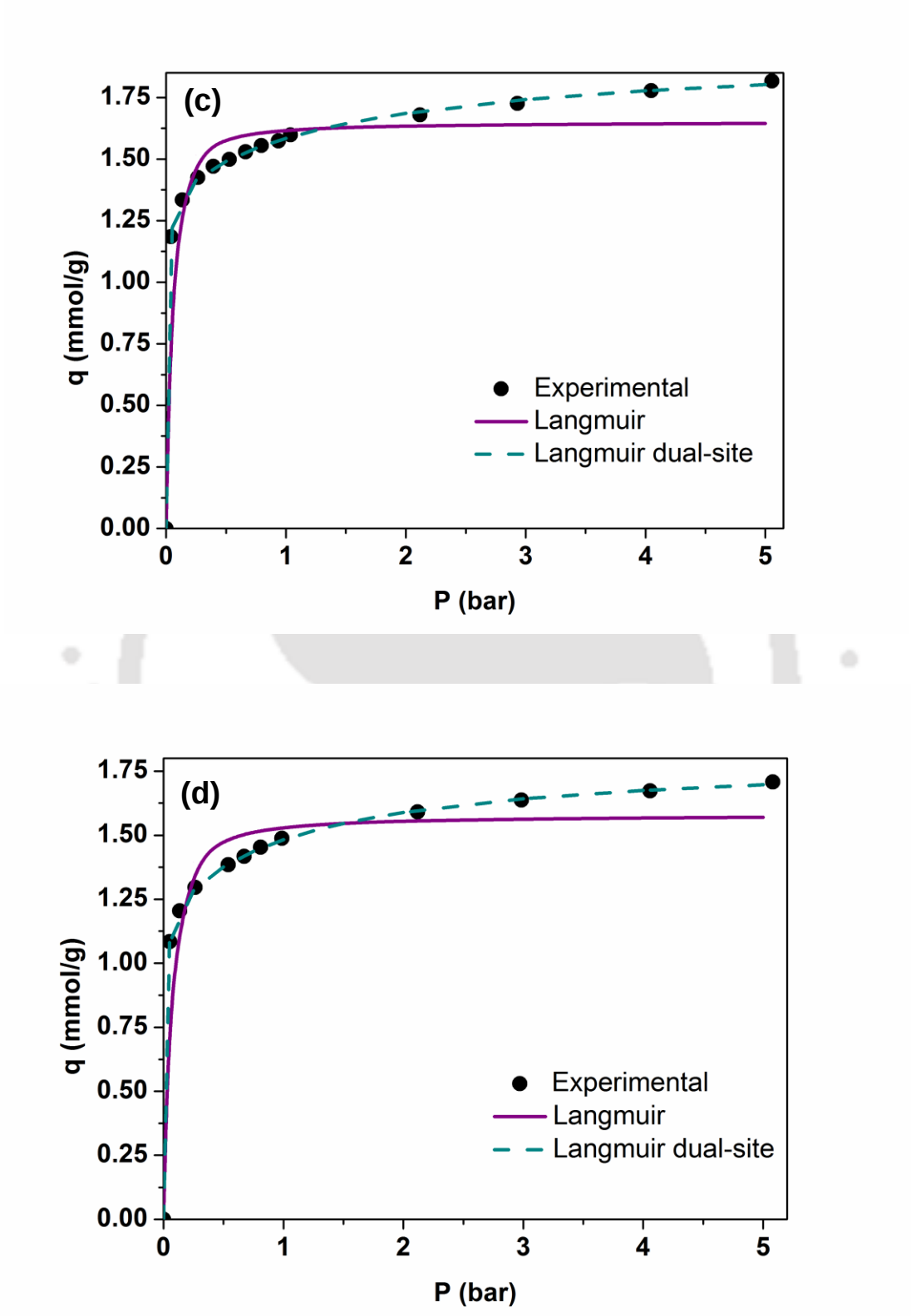

Figure 8.1. Comparison of different isotherm models with experimental data generated for adsorption of CO_2 on MCM-41-30-AP-9-85-0.5 (a) 30 °C (b) 45 °C (c) 60 °C and (d) 75 °C.

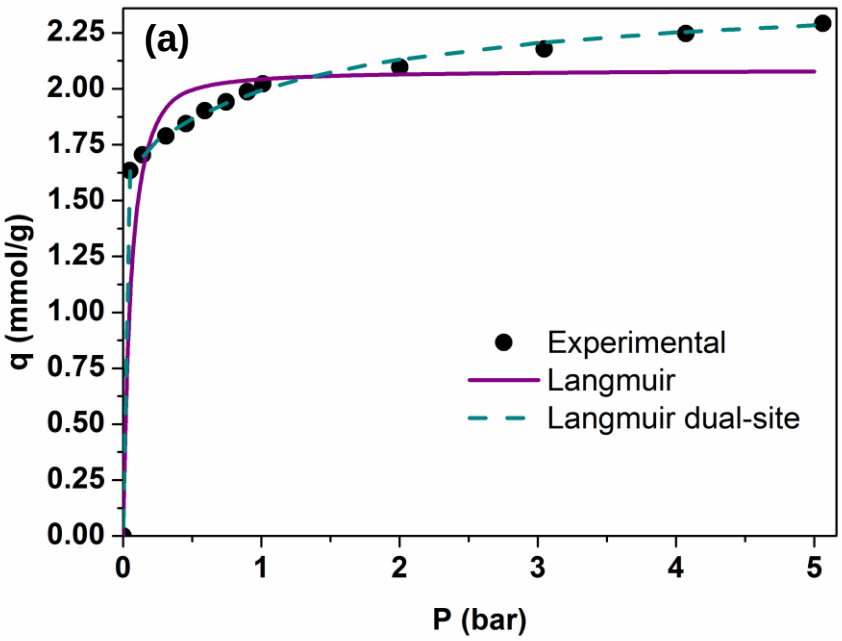

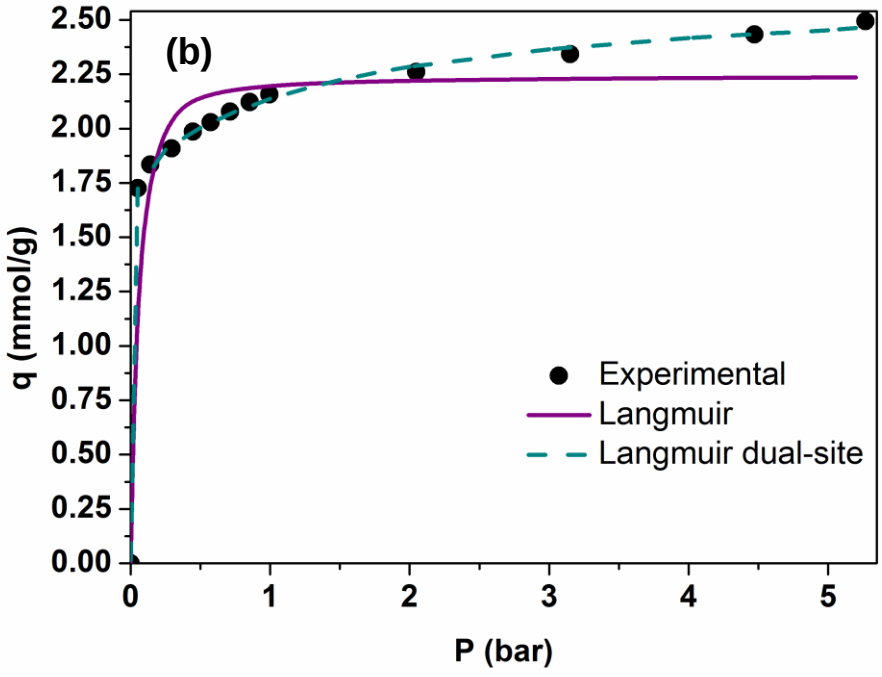

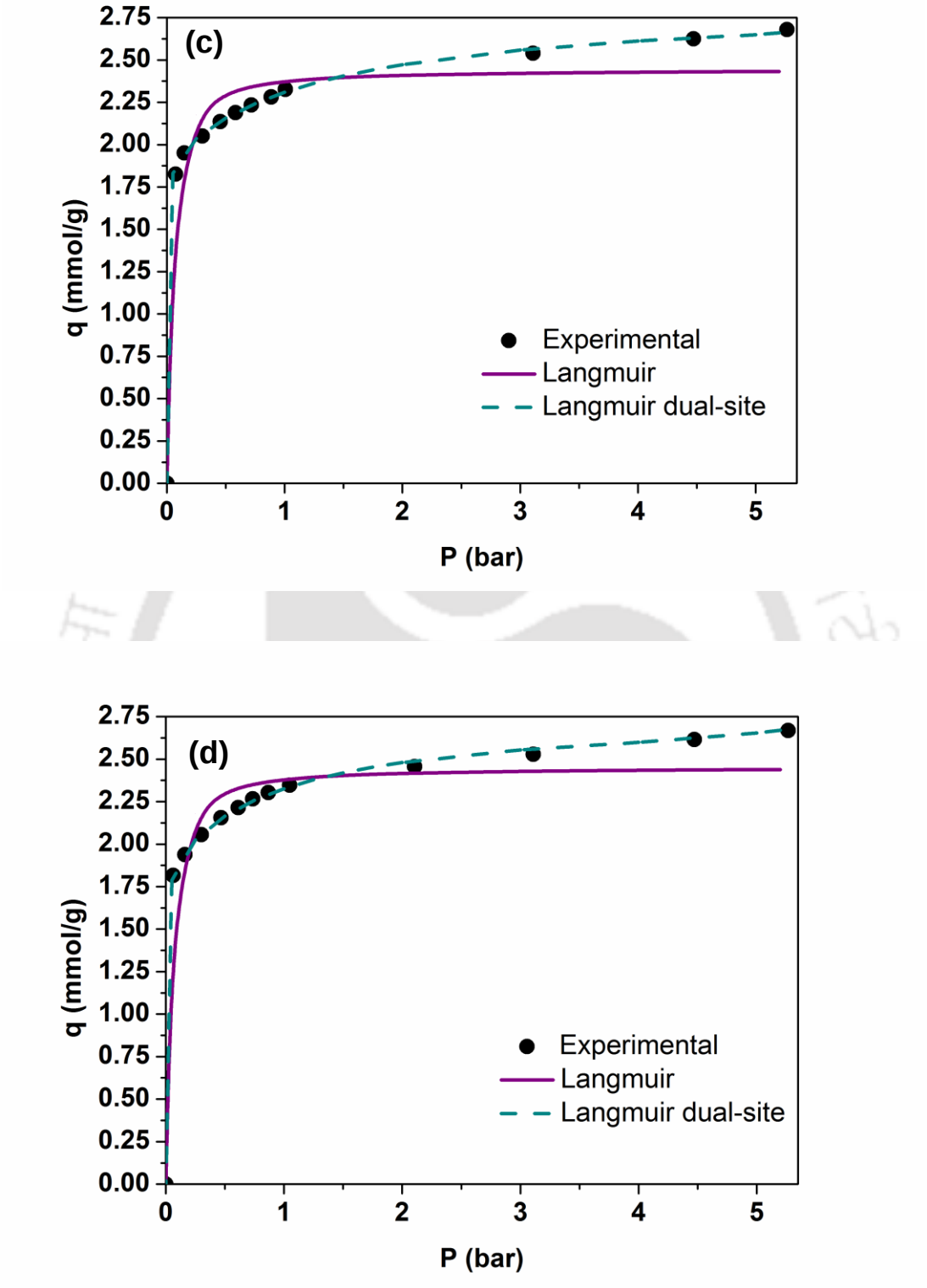

Figure 8.2. Comparison of different isotherm models with experimental data generated for adsorption of CO_2 on MCM-41-30-TP-9-75-0.3 (a) 30 °C (b) 45 °C (c) 60 °C and (d) 75 °C.

phenomena. In case of both MCM-41-30-AP-9-85-0.5 and MCM-41-30-TP-9-75-0.3 samples, chemisorption controls the initial stages of adsorption, hence a steep slope, whereas, physisorption is the adsorption process for the latter. Langmuir plot shows significant deviation from the experimental data at all temperatures for higher loading. This is so because the adsorption capacity keeps on increasing on account of coupled effect of physisorption and chemisorption rather than becoming constant as per the Langmuir model. In the initial stages, adsorption comes mainly from chemisorption whereas in the later stages, adsorption capacity keeps on increasing because of physisorption. As Langmuir dual-site model takes into account the two main adsorption sites, i.e., both physisorption and chemisorption and hence provides the correct fit to the experimental data.

8.4.2. Analysis of isotherm model parameters

From the values of the model parameters listed in the Table 8.1, it can be seen that these model parameters are function of temperature. For MCM-41-30-AP-9-85-0.5, the value of q_m for Langmuir and Langmuir dual site model decreases with increase in temperature confirming the exothermic nature of the adsorption process **[1, 4]**. As the temperature increases, desorption becomes significant resulting in lower q_m values. The affinity constant '*b'* for Langmuir model and Langmuir dual-site model decreases with increase in temperature for both MCM-41-30-AP-9-85-0.5 and MCM-41-30-TP-9-75-0.3 samples. In contrast, for MCM-41-30-TP-9-75-0.3, the maximum adsorption capacity (q_m) show an increasing trend with increase in temperature, which is different from that of previous case (Table 8.2). This variation from usual behaviour has been explained in a separate section (8.4.3). The model parameters of the Langmuir dual-site isotherm indicate that there are two different sites that are responsible for adsorption of CO_2 on both MCM-41-30-AP-9-85-0.5 and MCM-41-30-TP-9-75-0.3 samples. This includes siloxane sites and amine sites which correspond to physisorption and chemisorption respectively. The typical values of the model parameters q_m and *b* obtained for two sites demonstrate that CO_2 adsorption process is

predominated by chemisorption. The higher values of $q_{m,A}$ and b_A correspond to chemisorption site, whereas, the lower values of $q_{m,B}$ and b_B account for physisorption site.

Table 8.1. CO_2 isotherm model parameters and Error (%) for MCM-41-30-AP-9-85-0.5.

	Langmuir			Langmuir dual-site				
Temperature (°C)	q_m	b	**Error (%)**	$q_{m,A}$	b_A	$q_{m,B}$	b_B	**Error (%)**
30	1.9	55.76	6.99	1.51	503.9	0.76	0.91	0.64
45	1.76	49.13	6.91	1.36	384.9	0.74	0.85	0.61
60	1.65	45.16	6.66	1.30	139.2	0.59	0.83	0.58
75	1.58	30.26	6.13	1.21	136.3	0.56	0.76	0.35

Table 8.2. CO_2 isotherm model parameters and Error (%) for MCM-41-30-TP-9-75-0.3.

	Langmuir			Langmuir dual-site				
Temperature (°C)	q_m	b	**Error (%)**	$q_{m,A}$	b_A	$q_{m,B}$	b_B	**Error (%)**
30	2.08	48.13	7.01	1.66	566	0.79	0.72	0.60
45	2.24	45.14	6.94	1.81	311	0.84	0.69	0.59
60	2.44	32.03	6.74	1.91	176	0.90	0.62	0.57
75	2.45	31.89	6.36	1.97	143	0.92	0.58	0.32

8.4.3. Heat of adsorption

Based on the Clausius Clapeyron equation, the isosteric heat of adsorption for both MCM-41-30-AP-9-85-0.5 and MCM-41-30-TP-9-75-0.3 samples is calculated using the experimental CO_2 adsorption isotherms obtained at four different temperatures (30, 45, 60 and 75 °C) and in the pressure range of 0-5 bar. The obtained value of heat of adsorption for MCM-41-30-AP-9-85-0.5 sample is significantly higher than 40 kJ/mol which confirm that CO_2 adsorption on amine grafted adsorbent is dominated by chemisorption **[5, 6]**. A plot of isosteric heat of adsorption (ΔH_{iso}) vs q for MCM-41-30-AP-9-85-0.5 is shown in Figure 8.3(a). It can be inferred from the plot that ΔH_{iso} is a function of adsorbate loading and decreases non-linearly with an increase in loading. This can be explained by the fact that at

low surface coverage CO_2 opts for sites having strong interaction resulting in higher ΔH_{iso} values at lower loadings. However as the surface coverage increases, vertical interaction between the surface and CO_2 decreases, whereas, lateral interaction between CO_2 molecules in the adsorbed phase increases, resulting in lower heat of adsorption values **[7, 8]**. Here also, MCM-41-30-TP-9-75-0.3 sample shows peculiar behaviour i.e. increasing heat of adsorption with respect to loading (Figure 8.3(b)).

The experimental data for CO_2 adsorption on MCM-41-30-TP-9-75-0.3 showed an increasing trend in adsorption capacity with respect to progress in temperature (Figure. 7.2(b)). Because of this behaviour, the model parameter i.e. q_m for Langmuir and Langmuir dual site model as well as isosteric heat of adsorption values show increasing trend with temperature. The possible reason for this peculiarity exhibited by MCM-41-30-TP-9-75-0.3 adsorbent can be explained as follows: During amine tethering process, hydrolysis and condensation polymerization of the free silane groups occur in the pore space available in the support material. As tri amine is more sensitive to moisture as compared to mono amine,

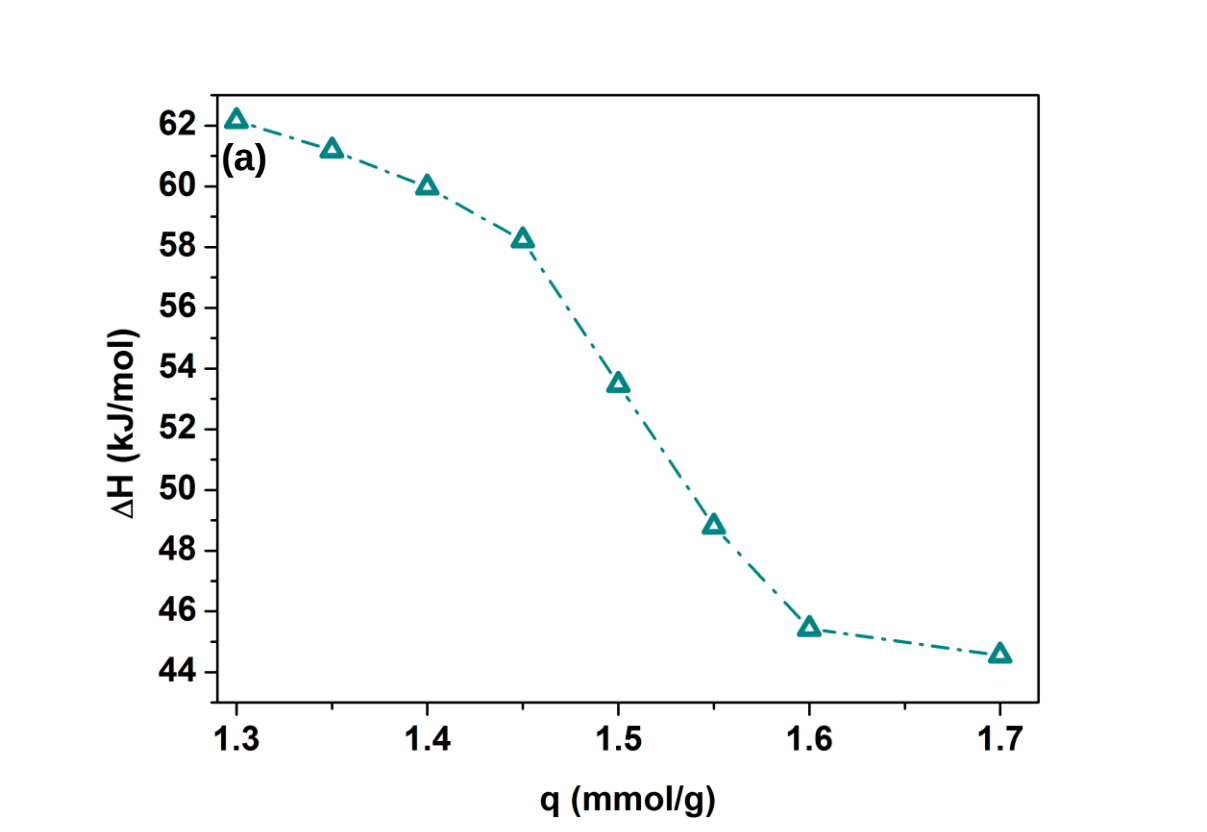

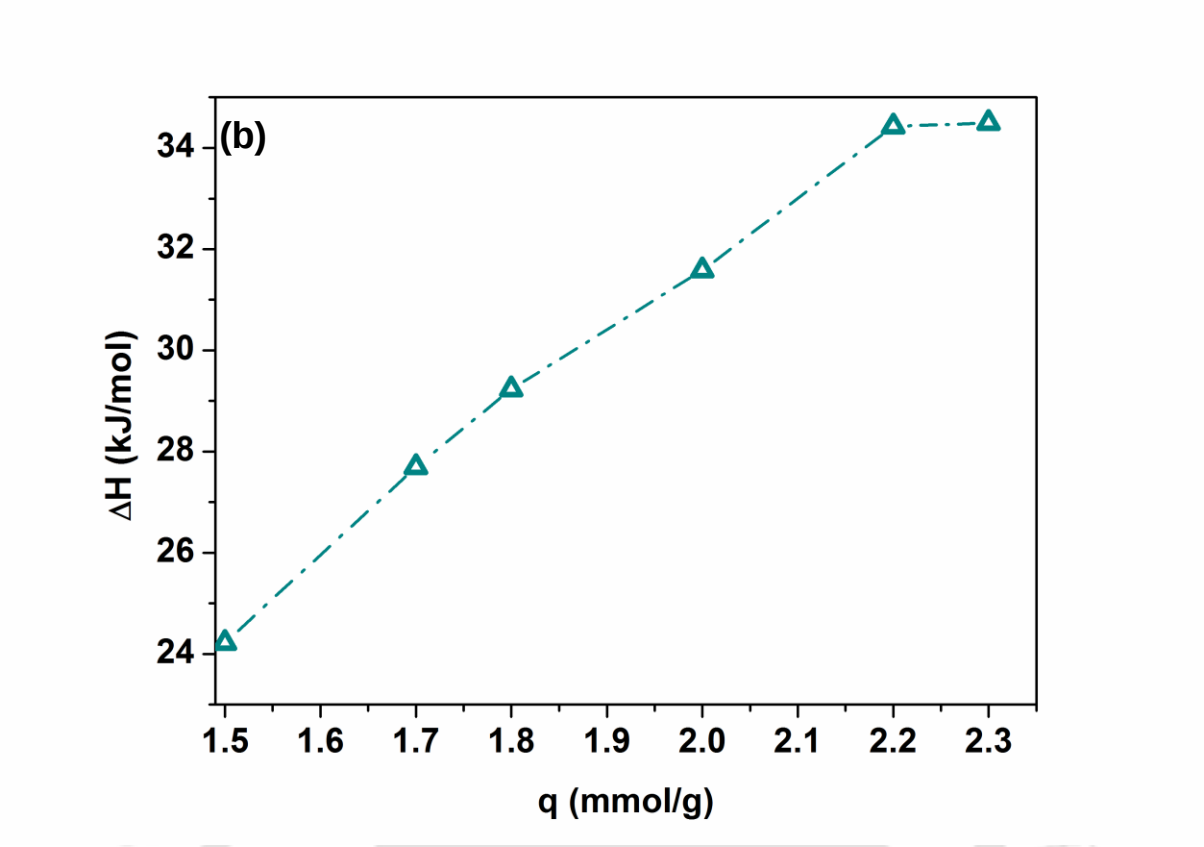

Figure 8.3. Isosteric heat of adsorption for as a function of loading for (a) MCM-41-30-AP-9-85-0.5 and (b) MCM-41-30-TP-9-75-0.3

the polymerization reaction is more intense leading to bulky polyamino siloxane moieties in the latter case. Due to this phenomenon, the adsorption sites get shielded and adsorption to full capacity doesn't take place in the tri amine case. With respect to increase in the temperature for adsorption process, the polymerized amine moieties may become accessible to CO_2 due to enhancement in the diffusion rate of CO_2 molecules, which in turn, leads to an increase in the adsorption capacity **[9]**. As heat of adsorption is a function of adsorbate loading, the same is observed to shoot up with increase in adsorbate loading with increase in temperature.

As compared to MCM-41-30-AP-9-85-0.5, lower values of heat of adsorption for MCM-41-30-TP-9-75-0.3 adsorbent can be noticed. The heat of absorption for MEA –CO_2, DEA-CO_2 and TEA-CO_2 interaction is reported to be 88.91, 70.44 and 44.72 kJ/mol CO_2 respectively in

a CO_2 absorption study carried out by Nam et al. **[10]**. The amine group in MEA is the primary one, where as in case of DEA and TEA, it is secondary and tertiary amine respectively. It is inferred from this literature that primary amine interacts more strongly with CO_2 and forms stable carbamate as compared to secondary and tertiary amine. This is because, secondary and tertiary amines provide more steric hindrance towards interaction with CO_2. In case of tri amino silane compound used for grafting on MCM-41-30, there are three amine sites present per chain: one primary amine (NH_2) site and two secondary amine (NH) sites. Therefore, it is probable that more secondary amine sites are available for interacting with CO_2 effectively than the primary amine site leading to lower heat lower heat of adsorption for MCM-41-30-TP-9-75-0.3.

8.4.4. Comparison of kinetic models

The experimental kinetic uptake data obtained at four different temperatures (30, 45, 60 and 75 °C) and ambient pressure condition (1 bar) are analyzed by using various kinetic models discussed above. Comparative plots of experimental kinetic data with above mentioned models for both MCM-41-30-AP-9-85-0.5 and MCM-41-30-TP-9-75-0.3 are presented in Figure 8.4 and Figure 8.5 respectively. The corresponding model parameters obtained for the various models are listed in Table 8.3 and Table 8.4. The deviation of predicted kinetic data from the experimental results in terms of error (%) for both MCM-41-30-AP-9-85-0.5 and MCM-41-30-TP-9-75-0.3 are tabulated in Table 8.5. From the Figures 8.4 and 8.5, it can be seen that pseudo first order model fails to provide a good fit for the experimental data. This is because, pseudo first order better explains adsorption under low surface coverage **[11]**. Pseudo second order model provides a comparatively good fit since this model explains adsorption at high adsorbate loadings or adsorption involving chemical reactions **[12]**. However, the best kinetic fit in the present study comes from the double exponential model. It predicts the kinetics of CO_2 adsorption on MCM-41-30-AP-9-85-0.5 and MCM-41-30-TP-9-75-0.3 adsorbents at all the four temperatures most adequately. This can be

explained on the basis that this model accounts for the surface heterogeneity of the adsorbent and best explains the adsorption mechanism involving two different sites for

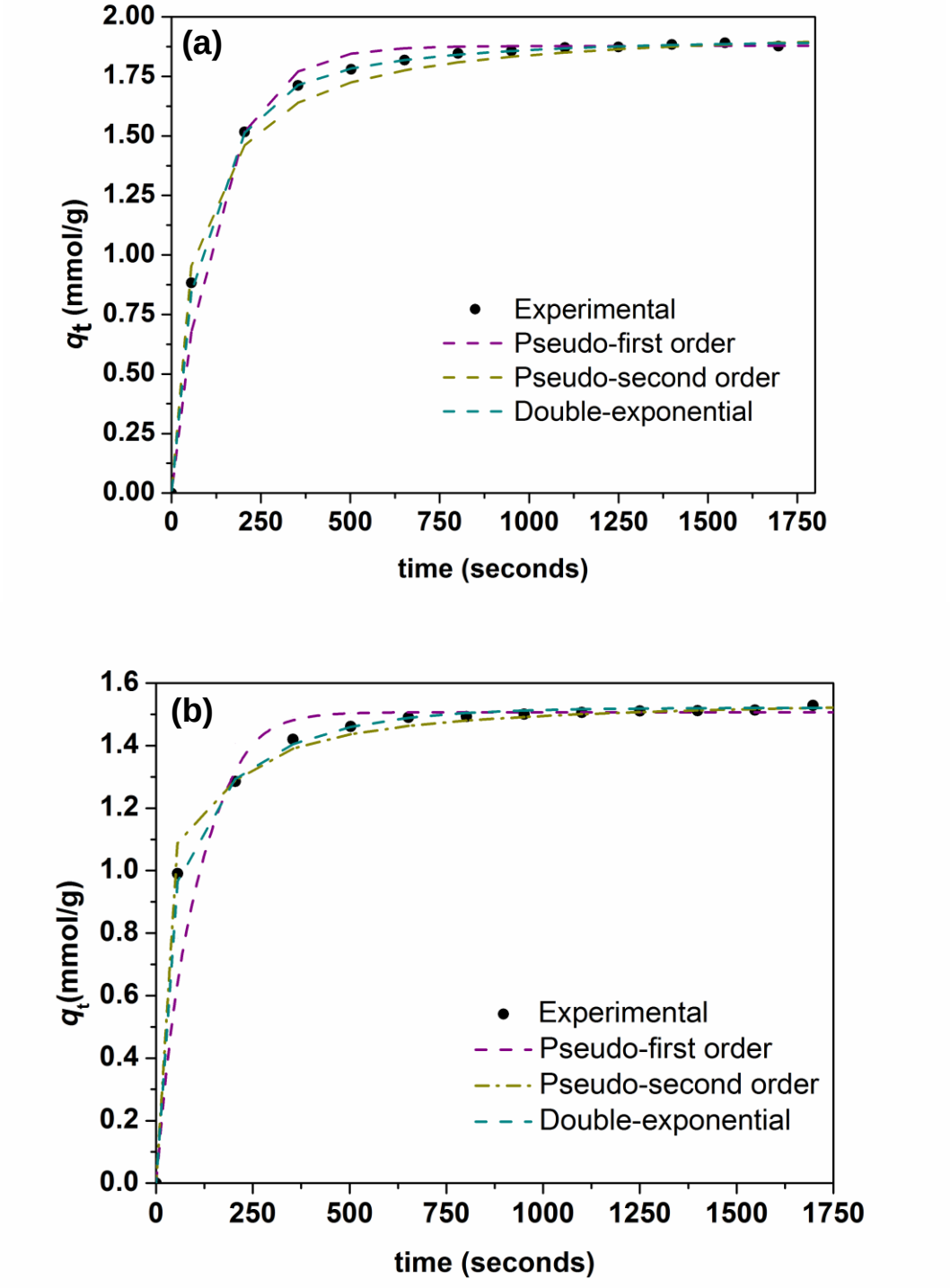

Figure 8.4. Comparison of different kinetic models with experimental data generated for adsorption kinetics of CO_2 on MCM-41-30-AP-9-85-0.5 (a) 30 °C and (b) 75 °C.

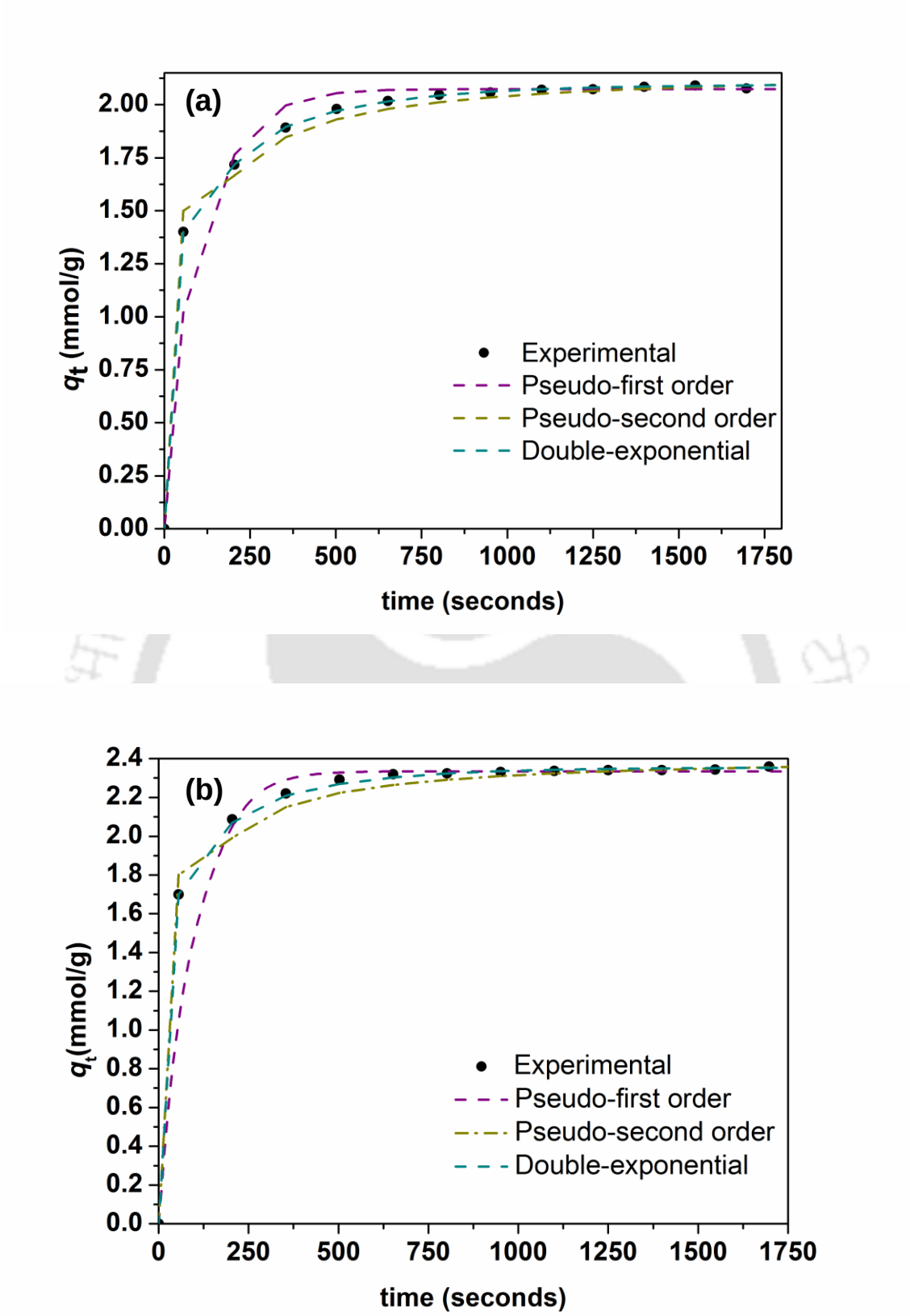

Figure 8.5. Comparison of different kinetic models with experimental data generated for adsorption kinetics of CO_2 on MCM-41-30-TP-9-75-0.3 (a) 30 °C and (b) 75 °C.

adsorption **[2]**. Further, this model takes into account the complexity of the reaction mechanism or the occurrence of more than one reaction pathway **[2]**. Hence, it is possible that the excellent fit obtained using this model resulted from its capacity to account for both physisorption and chemisorption of CO_2 on both the adsorbents.

8.4.5. Analysis of kinetic model parameters

The kinetic rate constant values (k_s, k_f, k_1& k_2) for the four kinetic models used show an increasing trend with temperature as can be observed from the values listed in Table 8.3 and Table 8.4. This is because, as temperature increases, kinetic energy of diffusing CO_2 molecules also increases which translates into a faster adsorption kinetics. The equilibrium adsorption capacity (q_e) for MCM-41-30-AP-9-85-0.5 decreases with temperature for all the

Table 8.3. CO_2 Kinetic model parameters for MCM-41-30-AP-9-85-0.5

		Pseudo-first order		Pseudo-second order		Double-exponential model				
Temperature (°C)	$q_{e,exp}$	$q_{e,model}$	k_f	$q_{e,model}$	k_s	$q_{e,model}$	A_1	k_1	A_2	k_2
30	1.89	1.87	0.008	1.97	0.008	1.89	1.58	0.010	0.03	0.002
45	1.74	1.71	0.009	1.79	0.010	1.73	1.23	0.015	0.04	0.002
60	1.63	1.62	0.010	1.68	0.012	1.63	1.16	0.018	0.4	0.003
75	1.52	1.50	0.013	1.55	0.015	1.52	0.97	0.025	0.5	0.004

Table 8.4. CO_2 Kinetic model parameters for MCM-41-30-TP-9-75-0.3

		Pseudo-first order		Pseudo-second order		Double-exponential model				
Temperature (°C)	$q_{e,exp}$	$q_{e,model}$	k_f	$q_{e,model}$	k_s	$q_{e,model}$	A_1	k_1	A_2	k_2
30	2.10	2.07	0.009	2.16	0.007	2.09	0.52	0.003	1.56	0.014
45	2.13	2.11	0.010	2.20	0.008	2.14	0.31	0.003	1.94	0.015
60	2.31	2.32	0.011	2.41	0.008	2.33	0.28	0.004	2.06	0.016
75	2.33	2.33	0.013	2.42	0.009	2.35	0.20	0.005	2.14	0.017

Table 8.5. Error (%) for kinetic models

	MCM-41-30-AP-9-85-0.5			MCM-41-30-TP-9-75-0.3		
Temperature (°C)	**Pseudo-first order**	**Pseudo-second order**	**Double-exponential Model**	**Pseudo-first order**	**Pseudo-second order**	**Double-exponential model**
30	2.47	1.99	0.20	2.29	2.11	0.19
45	3.15	1.77	0.44	3.51	1.97	0.24
60	2.50	2.01	0.22	2.65	2.22	0.25
75	3.06	0.98	0.47	3.15	1.45	0.30

three models used following the exothermic nature of CO_2 adsorption on amine-grafted adsorbent. However, the q_e values for the three models show an increasing trend with temperature for MCM-41-30-TP-9-75-0.3 (Table 8.4). The possible reason for this behaviour is explained previously in the section 8.4.3.

8.5. Conclusions

Langmuir dual-site isotherm model closely followed the experimental data for both mono and tri amine grafted MCM-41-30 for entire range of temperature conditions analyzed. The parameters (q_m and k) obtained from Langmuir dual-site isotherm model indicated that CO_2 is adsorbed on both the adsorbents through coupled effect of both chemisorption and physisorption. As double-exponential models provided good fit for the CO_2 uptake kinetics on both the adsorbents, it is inferred that CO_2 adsorption takes place via complex mechanism i.e. a rapid and slow phase controlled by chemisorptive and physisorptive interactions, respectively.

8.6. References

[1] Do, D. D. Adsorption Analysis: Equilibria and Kinetics, Imperial College Press, London, **1998**.

[2] Sciascia, L.; Liveri, M. L. T.; and Merli, M. Kinetic and Equilibrium Studies for the Adsorption of Acid Nucleic Bases onto K10 Montmorillonite, *Appl. Clay Sci.* **2011**, 53, 657-668.

[3] Rudzinski, W.; Lee, S. L.; Yan, C. C. S.; and Panczyk, T. A Fractal Approach to Adsorption on Heterogeneous Solid Surfaces. 1. The Relationship between Geometric and Energetic Surface Heterogeneities, *J. Phys. Chem. B* **2001**, 105, 10847-10856.

[4] Serna-Guerrero, R.; Belmabkhout, Y.; and Sayari, A. Modeling CO_2 Adsorption on Amine-functionalized Mesoporous Silica: 1. A Semi-empirical Equilibrium Model, *Chem. Eng. J.* **2010**, 161,173-181.

[5] Hoang, T. K. A.; Webb, M. I.; Mai, H. V.; Hamaed, A.; Walsby, C. J.; Trudeau, M.; and Antonelli, D. M. Design and Synthesis of Vanadium Hydrazide Gels for Kubas-Type Hydrogen Adsorption: A New Class of Hydrogen Storage Materials, *J. Am. Chem. Soc.* **2010**, 132, 11792-11798.

[6] Soubeyrand-Lenoir, E.; Vagner, C.; Yoon, J. W.; Bazin, P.; Ragon, F.; Hwang, Y. K.; Serre, C.; Chang, J. S.; and Llewellyn, P. L. How Water Fosters a Remarkable 5-Fold Increase in Low-Pressure CO_2 Uptake within Mesoporous MIL-100(Fe), *J. Am. Chem. Soc.* **2012**, 134, 10174-10181.

[7] Jiang, J.; and Sandler, S. I. Separation of CO_2 and N_2 by Adsorption in C_{168} Schwarzite: A Combination of Quantum Mechanics and Molecular Simulation Study, *J. Am. Chem. Soc.* **2005**, 127,11989-11997.

[8] Sillar, K.; and Sauer, J. Ab Initio Prediction of Adsorption Isotherms for Small Molecules in Metal-Organic Frameworks: The Effect of Lateral Interactions for Methane/CPO-27-Mg, *J. Am. Chem. Soc.* **2012**, 134, 18354-18365.

[9] Fadhel, B.; Hearn, M.; and Chaffee, A. CO2 Adsorption by PAMAM Dendrimers: Significant Effect of Impregnation into SBA-15, *Micropor. Mesopor. Mater.* **2009**, *123*, 140-149.

[10] Kim, Y. E.; Lim, J. A.; Jeong. S. K.; Yoon, Y.; Bae, S. T.; and Nam, S. C. Comparison of Carbon Dioxide Absorption in Aqueous MEA, DEA, TEA, and AMP Solutions, *Korean Chem. Soc.* **2013** , *34*, 783-787.

[11] Sayari, A.; and Guerrero, R.S. Modeling Adsorption of CO_2 on Amine-Functionalized Mesoporous silica. 2: Kinetics and Breakthrough Curves. *Chem. Eng. J.* **2010**, 161, 182-190.

[12] Borah, J. M.; Sarma, J.; and Mahiuddin, S. Adsorption Comparison at the Alumina/Water Interface: 3,4-Dihydroxybenzoic Acid vs. Catechol. *Colloids Surf., A.* **2011**, 387, 50-56.

CHAPTER 9

CONCLUSIONS AND FUTURE DIRECTIONS

The chapter elucidates the major inferences drawn from the doctoral work and an outlook for future studies.

9.1. Conclusions

The major conclusions drawn on the overall observation and main findings of the research work are as follows.

- A suitable protocol for synthesis of MCM-41 with enlarged pore size (~30 nm) and high pore volume (~2.5 cc/g) without the application of any swelling agent was developed. It was inferred that controlled addition of aqueous ammonia in the reaction mixture showed profound effect on the pore size and pore volume of the mesoporous silica MCM-41 support.
- The existence of various surface groups on MCM-41-30 is confirmed by DRIFTS analysis. Patch-wise topography hypothesis together with Langmuir multi-site model enlightened the potential surface groups through which CO_2 interacts with the silica surface. Heat of adsorption calculations demonstrated the heterogeneous nature of the surface and the same allowed for understanding that the CO_2 molecules interact with silanol groups through hydrogen bonding and siloxanes through dispersive forces.
- Investigation of CO_2 adsorption kinetics on MCM-41 under wide range of pressure (0-11 bar) and temperature conditions (30, 45, 60 and 75 °C) revealed that film diffusion predominantly controlled the CO_2 uptake kinetics on MCM-41 at 30 °C for all the pressure conditions analyzed. It was observed that, as the temperature progressed, with rise in pressure, pore diffusion becomes dominant in controlling the CO_2 uptake kinetics on MCM-41-30. As pseudo-first order model followed the experimental uptake date closely, it was inferred that CO_2 adsorption on MCM-41-30 is governed by physisorption.
- A potential MCM-41 support suitable for amine tethering is screened based on the amine loading and CO_2 adsorption characteristics exhibited by mono amine tethered MCM-41-3 and MCM-41-30 under dry grafting conditions. It was observed that mono amine tethered MCM-41-30 support showed promising outcome in terms of CO_2 adsorption capacity, amine loading and amine efficiency in comparison to MCM-41-3,

from which, the nature of mesoporous silica support to be selected for grafting process was inferred. It was determined that the optimum amount of mono and tri aminosilane compounds that can be used for grafting is 9 mmol, in case of MCM-41-30 support.

- Further, a suitable synthesis recipe and temperature conditions for mono and tri amine tethering on the novel support (MCM-41-30) under wet grafting conditions is developed. The optimum amount of water that can be used for grafting reaction was determined to be 0.5 and 0.3 mL, for mono and tri amine, respectively. The best suitable temperature condition for grafting process was determined to be 85 and 75 °C, for mono and tri amine, respectively.
- An excellent CO_2 adsorption capacity of ~2.1 mmol/g at flue gas conditions (0.2 bar and 75 °C) is demonstrated by the tri amine grafted MCM-41-30. In addition to this, tri amine grafted MCM-41-30 exhibited comparable performance in terms of CO_2 adsorption capacity, amine efficiency, selectivity, operating window, CO_2 uptake kinetics, multi-cycle stability and cost with other reported bench mark adsorbents.
- Langmuir dual-site isotherm model best fitted the experimental CO_2 adsorption isotherm data obtained for mono and tri amine tethered MCM-41-30 adsorbents at different temperature (30, 45, 60 and 75 °C) and pressure conditions ranging from 0-5 bar. From which, it was inferred that CO_2 adsorption on amine tethered MCM-41-30 adsorbents is governed by combined effect of chemisorption and physisorption processes.
- Double-exponential model provided an excellent fit to the experimental CO_2 uptake kinetics data obtained for mono and tri amine tethered MCM-41-30 adsorbents at different temperatures (30, 45, 60 and 75 °C) and ambient pressure conditions. This revealed that CO_2 adsorption kinetics on amine grafted MCM-41-30 adsorbents is controlled by a rapid phase which involves chemisorptive interactions followed by a slow phase accounting for physisorptive interactions.

9.2. Scope for future work

Future recommendations on the present work are as follows:

- The utilization of amine bearing species remains as one of the typical variable in the design of amine tethered mesoporous materials. Therefore, apart from mono and tri amino silane compounds used in the doctoral work, synthesis recipe as well as optimum reaction conditions for tethering of other amino compounds can be investigated.
- The CO_2 adsorption characteristics of the tri-amine grafted adsorbent can be investigated in the presence of other components such as O_2, SO_x, H_2O etc. present in the flue gas.
- Performance analysis of the adsorbent developed herein, can be investigated using column studies.
- The MCM-41-30 support developed in the doctoral work can be tested for its potential in other applications such as drug delivery and catalysis.

Table A.1. Comparison of dry CO_2 adsorption capacity, N_2 adsorption capacity, amine loading, amine efficiency and CO_2/N_2 selectivity for different adsorbents.

S:No	Adsorbent	Temperature (°C)	Dry CO_2 adsorption capacity (mmol/g)	N_2 adsorption capacity (mmol/g)	Amine Loading (mmol(N)/g)	Amine Efficiency (mmol(CO_2)/mmol(N))	CO_2/N_2 Selectivity	Reference
1	PS-MFI	25 40 55	0.52 0.45 0.25	0.15 0.12 0.12	- - -	- - -	6 6 3	**[30]**
2	Ca-A	25 40 55	4.2 3.8 3.4	0.48 0.45 0.45	- - -	- - -	14 13 12	**[30]**
3	Mg-A	25 40 55	2.6 1.8 1.25	0.35 0.3 0.3	- - -	- - -	12 9 7	**[30]**
4	Na-A	25 40 55	1.9 1.45 1.1	0.16 0.15 0.15	- - -	- - -	19 15 12	**[30]**
5	Na-X	25 40 55	4.4 3.5 2.7	0.16 0.15 0.15	- - -	- - -	43 37 28	**[30]**
6	Mg-X	25 40 55	3.1 2.3 1.4	0.14 0.13 0.13	- - -	- - -	35 28 17	**[30]**
7	Ca-X	25 40 55	3.7 2.7 2.0	0.17 0.17 0.17	- - -	- - -	34 25 18	**[30]**
8	H-ZSM-5	40	0.6	0.05	-	-	19	**[31]**
9	H-ZSM-5-30	22	0.9	-	-	-	-	**[32]**
10	HiSiv	22	0.6	-	-	-	-	**[32]**
11	HY-5	22	0.4	-	-	-	-	**[32]**

S:No	Adsorbent	Temperature (°C)	Dry CO_2 adsorption capacity (mmol/g)	N_2 adsorption capacity (mmol/g)	Amine Loading (mmol(N)/g)	Amine Efficiency (mmol(CO_2)/mmol(N))	CO_2/N_2 Selectivity	Reference
12	Zeolite 13X	20 40 60 80	2.5 2 1.5 1	0.42	- - - -	- - - -	9	**[33]**
13	NaY	23 45 65 75	3.0 2.0 1.4 1.1	0.28 0.17 0.14 0.12	- - - -	- - - -	17 18 16 14	**[34]**
14	BPL	25 50	0.7 0.4	0.25 -	- -	- -	4 -	**[35]** **[36]**
15	CAC	25 35 45 55	1 0.7 0.5 0.3	- - - -	- - - -	- - - -	- - - -	**[37]**
16	GAC	25	0.06	-	-	-	-	**[38]**
17	GAC-MEA	25	0.06	-	-	-	-	**[38]**
18	GAC-NH3	25	0.06	-	-	-	-	**[38]**
19	GAC-APTS	25	0.06	-	-	-	-	**[38]**
20	Zeo Carbon	20 40 60 80	2.1 1.8 1.4 0.9	- - - -	- - - -	- - - -	- - - -	**[39]**
21	Norit R1	25 50	0.6 0.3	- -	- -	- -	- -	**[36]**
22	A10	25 50	1.5 0.7	- -	- -	- -	- -	**[36]**

S:No	Adsorbent	Temperature (°C)	Dry CO_2 adsorption capacity (mmol/g)	N_2 adsorption capacity (mmol/g)	Amine Loading (mmol(N)/g)	Amine Efficiency (mmol(CO_2)/mmol(N))	CO_2/N_2 Selectivity	Reference
23	Maxsorb	25 50	1.8 0.8	- -	- -	- -	- -	**[36]**
24	Activated Carbon A	25 50	1.0 0.4	- -	- -	- -	- -	**[36]**
25	ZIF 8	25	0.2	0.06	-	-	5	**[35]**
26	Mg/DOBDC	30 40 50 60 70 75	6 5.4 4.9 4.0 3.2 2.4	0.73 0.5 0.38 0.33 0.30 0.25	- - - - - -	- - - - - -	13 17 20 19 17 15	**[40]**
27	MOF 177	30 40 50 60 70 75	0.16 0.15 0.14 0.11 0.09 0.07	0.14 0.10 0.09 0.08 0.075 0.06	- - - - - -	- - - - - -	2 2 2 2 2 2	**[40]**
29	MIL 53	20	0.6	0.2	-	-	5	**[41]**
30	MIL 101	46 78	0.03 0.015	- -	- -	- -	- -	**[42]**
31	Mn/DOBDC	21 42 79	3.8 2.28 0.89	0.34 0.28 0.16			18 13 9	**[43]**
32	CO/DOBDC	21 42 79	5.15 3.19 1.21	0.7 0.4 0.21			12 12 9	**[43]**

S:No	Adsorbent	Temperature (°C)	Dry CO_2 adsorption capacity (mmol/g)	N_2 adsorption capacity (mmol/g)	Amine Loading (mmol(N)/g)	Amine Efficiency (mmol(CO_2)/mmol(N))	CO_2/N_2 Selectivity	Reference
33	Ni/DOBDC	21 42 79	4.55 2.58 0.97	0.7 0.4 0.2			10 10 8	**[43]**
34	Cu/DABCO	21 41 77	0.45 0.20 0.09	0.7 0.4 -			1 1 -	**[44]**
35	Ni/DABCO	21 41 77	0.66 0.37 0.17	- 0.16 -			- 4 -	**[44]**
36	Zn/DABCO	21 41 77	0.42 0.21 0.10	0.2 0.14 0.08			3 2 2	**[44]**
37	CuBTC	22 45 80	0.86 0.46 0.18	0.4 0.28 -			3 3 -	**[45]**
38	PEI-MCM-41	75	2.1		11.66	0.18		**[46]**
39	PEI-SBA-15	75	3.18		11.77	0.27		**[8]**
40	PEI-KIT-6	75	2.27		11.47	0.20		**[47]**
41	PEI-Monolith	75	3.86		15	0.26		**[48]**
42	TEPA-SBA-15	75	3.35		11.60	0.29		**[49]**
43	TEPA-MCM-41	75	4.5		13.23	0.34		**[50]**
44	TEPA-DEA-SBA-15	75	3.85		9.92	0.39		**[51]**
45	DEA-PE-MCM-41	25	3.0		6.34	0.47		**[52]**
46	PEI-MS	70	2.4		9.23	0.26		**[53]**

S:No	Adsorbent	Temperature (°C)	Dry CO_2 adsorption capacity (mmol/g)	N_2 adsorption capacity (mmol/g)	Amine Loading (mmol(N)/g)	Amine Efficiency (mmol(CO_2)/mmol(N))	CO_2/N_2 Selectivity	Reference
47	PEI-HP20	75	2.95					**[54]**
48	PEI-MHS	75	4.90					**[54]**
49	PEI-MCF	75	3.45					**[54]**
50	PEI-Alumina	75	1.13					**[55]**
51	AP-PCH	25 35 45	0.3 0.2 0.1		1.86 1.86 1.86	0.16 0.11 0.05		**[55]**
52	TP-PE-MCM-41 (60 min)	25 35 45 70	2.2 2.0 1.7 1.55		6.11 6.11 6.11 6.11	0.36 0.33 0.28 0.25		**[56]**
53	AP-MSUF	30 45 60 75	0.3 0.28 0.27 0.25		2.4 2.4 2.4 2.4	0.13 0.12 0.11 0.10		**[57]**
54	DP-MSUF	30 45 60 75	0.75 1 0.77 0.56		4.3 4.3 4.3 4.3	0.17 0.23 0.18 0.13		**[57]**
55	TP-MSUF	30 45 60 75	1.29 1.52 1.47 1.09		7.6 7.6 7.6 7.6	0.16 0.20 0.19 0.14		**[57]**
56	AP-SBA-15	25 45	0.7 0.5		2.1 2.1	0.33 0.24		**[58]**
57	AP-SBA-15(W)	25 45	1.1 0.8		4.4 4.4	0.25 0.18		**[59]**

S:No	Adsorbent	Temperature (°C)	Dry CO_2 adsorption capacity (mmol/g)	N_2 adsorption capacity (mmol/g)	Amine Loading (mmol(N)/g)	Amine Efficiency (mmol(CO_2)/mmol(N))	CO_2/N_2 Selectivity	Reference
58	AP-PE-MCM-41 (16 h)	25 40 55 70	2.1 1.9 1.7 1.4		4.3 4.3 4.3 4.3	0.49 0.44 0.40 0.33		**[16, 60]**
59	AP-MCM-48	25	0.2		2.45	0.08		**[61]**
60	AP-silica gel	25 50	0.22 0.13		1.2 1.2	0.18 0.11		**[62]**
61	AP-Xerogel	25	0.66		1.0	0.65		**[11]**
62	AP-SBA-15	60	0.52		2.6	0.20		**[21]**
63	TP-SBA15	60	1.10		4.84	0.23		**[21]**
64	TP-HMS	18	0.9		2.88	0.31		**[63]**
66	TP-MCM-41	25	1.01		5.94	0.17		**[64]**
67	MCM-41-3-AP-9-75	30	0.23		1.31	0.17		Present study
68	MCM-41-30-AP-9-75	30	0.83		2.21	0.38		Present study
69	MCM-41-30-TP-9-75	30	1.13		4.45	0.25		Present study
70	MCM-41-30-AP-9-85-0.5	30 45 60 75	1.58 1.45 1.36 1.26		3.16 3.16 3.16 3.16	0.50 0.46 0.43 0.40		Present study
71	MCM-41-30-TP-9-75-0.3	30 45 60 75	1.78 1.9 2.0 2.1		6.39 6.39 6.39 6.39	0.27 0.30 0.31 0.33		Present study

*As amine functionalized mesoporous silica adsorbents are reported to exhibit infinite selectivity towards CO_2 over N_2, the selectivity for the same is not mentioned in Table A1

Table A.2. Cost estimation for different mesoporous silica supports

S:No	Name of the support	Raw materials	Amount of raw materials used (in g)	Cost of raw materials used (in Rs)	Total cost of the support per g (in Rs)
1	MCM-41-30	TTAB 25% aqueous ammonia TEOS Water	2 1 10 120	8.2 0.42 35 -	11
2	MCM-41-3	TTAB 25% aqueous ammonia TEOS Water	2 9 10 120	8.2 3.78 35 -	16
3	MCM-48	CTAB Water Ethanol 25% aqueous ammonia TEOS	1.2 50 25 6 1.8	4.52 - 70 2.52 6.3	83
4	SBA-15	P123 Water HCl TEOS	4 - 125 8.5	35.12 - 6.75 29.75	36
5	KIT-6	P123 Water HCl TEOS 1-Butanol	4 144 7.5 8.6 4	35.12 - 4.05 30.1 3.6	36
6	PE-MCM-41	TMAOH Water CTAB Cab-O-Sil DMDA	1.76 72 5.1 4 0.6	88.18 - 19.25 121.92 622.56	680

* The cost of water is not considered for synthesis of mesoporous silica supports.

RESEARCH PUBLICATIONS

JOURNALS

1. Sravanthi, L.; Tikmani, M.; and Ghoshal, A.K. Novel Pore-Expanded MCM-41 for CO_2 Capture, *Langmuir*, **2013**, 29, 3491-3499.

2. Sravanthi, L.; Tikmani, M.; Edubilli, S.; Mishra, A.; and Ghoshal, A. K. CO_2 Adsorption Kinetics on Mesoporous Silica Under Wide Range of Pressure and Temperature, *Chemical Engineering Journal,* **2014,** 258, 1-8.

CONFERENCE PROCCEDINGS

1. Sravanthi, L.; and Ghoshal, A.K. Synthesis and Characterization of Pore-expanded MCM-41 for CO_2 Capture, *Advanced Nano Materials* (ANM), **2012**, Indian Institute of Technology Chennai, India.

2. Sravanthi, L.; and Ghoshal, A.K. Amine Functionalized Mesoporous Silica for CO_2 Capture, *International Conference on Nanoscience and Technology* (ICONSAT), **2012**, Hyderabad, India.